ศิลาเคมีของหินที่มีคอรันดัมจากแหล่งมอนเตปวยซ์ ประเทศโมซัมบิก

นายอลงกต ฝั้นกา

วิทยานิพนธ์นี้เป็นส่วนหนึ่งของการศึกษาตามหลักสูตรปริญญาวิทยาศาสตรมหาบัณฑิต

สาขาวิชาธรณีวิทยา ภาควิชาธรณีวิทยา

คณะวิทยาศาสตร์ จุฬาลงกรณ์มหาวิทยาลัย

ปีการศึกษา 2556

PETROCHEMISTRY OF CORUNDUM-BEARING ROCKS FROM MONTEPUEZ DEPOSITS, MOZAMBIQUE

Mr. Alongkot Fanka

A Thesis Submitted in Partial Fulfillment of the Requirements
for the Degree of Master of Science Program in Geology
Department of Geology
Faculty of Science
Chulalongkorn University
Academic Year 2013

Thesis Title	PETROCHEMISTRY OF CORUNDUM-BEARING ROCKS FROM MONTEPUEZ DEPOSITS, MOZAMBIQUE
By	Mr. Alongkot Fanka
Field of Study	Geology
Thesis Advisor	Associate Professor Chakkaphan Sutthirat, Ph.D.

Accepted by the Faculty of Science, Chulalongkorn University in Partial Fulfillment of the Requirements for the Master's Degree

....Dean of the Faculty of Science

(Professor Supot Hannongbua, Dr. rer. nat.)

THESIS COMMITTEE

....Chairman

(Associate Professor Montri Choowong, Ph.D.)

....Thesis Advisor

(Associate Professor Chakkaphan Sutthirat, Ph.D.)

....Examiner

(Associate Professor Visut Pisutha-Arnond, Ph.D.)

....Examiner

(Assistant Professor Pitsanupong Kanjanapayont, Dr. rer. nat.)

....External Examiner

(Bhuwadol Wanthanachaisaeng, Dr. rer. nat.)

อลงกต ฝั้นกา : ศิลาเคมีของหินที่มีคอรันดัมจากแหล่งมอนเตปวยซ์ ประเทศโมซัมบิก (PETROCHEMISTRY OF CORUNDUM-BEARING ROCKS FROM MONTEPUEZ DEPOSITS, MOZAMBIQUE) อ.ที่ปรึกษาวิทยานิพนธ์หลัก: รศ.ดร.จักรพันธ์ สุทธิรัตน์ , 154 หน้า.

บริเวณแหล่งพลอยคอรันดัมมอนเตปวยซ์ทางภาคตะวันออกเฉียงเหนือของประเทศโมซัมบิก จัดอยู่ใน ชุดหินซับซ้อน มอนเตปวยซ์ เป็นส่วนหนึ่งของแนวเทือกเขา แปรสภาพ โมซัมบิก ซึ่งประกอบด้วยชุดหินแปรสภาพแอมฟิโบไลต์ ส่วนใหญ่พบหินแอมฟิโบไลต์และหินไนส์ หินแอมฟิโบไลต์ ประกอบด้วยหินแอมฟิโบไลต์ ที่มีคอรันดัม และหินแอมฟิโบไลต์ ที่ไม่มีคอรันดัมแร่องค์ประกอบส่วนใหญ่ ประกอบด้วย แอมฟิโบล สปิเนล แพลจิโอเคลส อาจพบการ์เนตและไมการ่วมด้วย โดยจะแตกต่างกันเฉพาะที่พบแร่คอรันดัมในหินแอมฟิโบไลต์ที่มีคอรันดัม นอกจากนั้นยังพบหินแอมฟิโบไลต์ที่มีคอรันดัมถูกแปรเปลี่ยน ซึ่งจะมีแร่ไมกาและแร่ดิน เพิ่มมากขึ้นและ สัมพันธ์กับหินเพกมาไทต์ ส่วนหินไนส์ประกอบด้วยแร่ แพลจิโอเคลส อัลคาไลเฟลด์สปาร์ ควอตซ์ แอมฟิโบล ไบโอไทต์ และการ์เนต ลักษณะธรณีเคมีบ่งชี้ว่าหินแอมฟิโบไลต์แปรสภาพจากหินเริ่มต้นชนิดหินเบสิค และหินไนส์แปรสภาพจากหินควอรตโซเฟลด์สปาร์ติกและตะกอนบก จากข้อมูลอุณหพลศาสตร์บ่งชี้ว่าหินแปร ในแหล่งมอนเตปวยซ์เกิดจากการแปรสภาพระดับสูงขั้นแอมฟิโบไลต์ โดยการคำนวณอุณหภูมิและความดันของการแปรสภาพหินแอมฟิโบไลต์ที่มีคอรันดัมประมาณ 550–600 องศาเซลเซียส 10.5-11 กิโลบาร์ หินแอมฟิโบไลต์ที่ไม่มีคอรันดัมประมาณ 450-550 องศาเซลเซียส 10.5-11.5 กิโลบาร์ และหินไนส์ประมาณ 550-600 องศาเซลเซียสและ 9-9.5 กิโลบาร์

ภาควิชา ธรณีวิทยา ลายมือชื่อนิสิต..........................

สาขาวิชา ธรณีวิทยา ลายมือชื่อ อ.ที่ปรึกษาวิทยานิพนธ์หลัก..........................

ปีการศึกษา 2556

5372386823: MAJOR GEOLOGY

KEYWORDS: CORUNDUM; RUBY; MOZAMBIQUE BELT; METAMORPHIC ROCK

ALONGKOT FANKA: PETROCHEMISTRY OF CORUNDUM-BEARING ROCKS FROM MONTEPUEZ DEPOSITS, MOZAMBIQUE. ADVISOR: ASSOC. PROF. CHAKKAPHAN SUTTHIRAT, Ph.D., 154 pp.

Montepuez corundum deposits situated in the northeastern Mozambique is geologically occupied by parts of Neoproterozoic Mozambique Belt in which is classified as Montepuez Complex. It is composed of high grade metamorphic rocks belonging to amphibolite facies that is mainly characterized by amphibolite and gneiss. Amphibolite is distinctively divided into corundum-bearing amphibolite and corundum-barren amphibolite. Corundum-bearing amphibolite is composed essentially of amphibole, spinel and plagioclase with minor amounts of garnet, mica and corundum. Moreover, some corundum-bearing amphibolites have been altered to contain significant mica and clay minerals. These altered rocks are crucially associated with pegmatite. Apart from corundum absence and with/without garnet occurrence, the other mineral assemblages are similar. On the other hand, gneiss is composed of plagioclase, alkali-feldspar, quartz, amphibole, biotite and garnet. Geochemically, these rocks appear to have different protoliths such as basic rock origin of amphibolite and quartzo-feldsparthic to pelitic rocks for gneiss. Based on geothermobarometry, these rocks should have undertaken high-grade metamorphism belonging to amphibolite facies with P-T estimations of 10.5-11 kbar and~550– 600 ^{o}C for corundum-bearing amphibolite, 10.5-11.5 kbar and 450-550 ^{o}C for Corundum-barren amphibolite and 9-9.5 kbar and 550-600 ^{o}C for gneiss.

Department: Geology Student's Signature

Field of Study: Geology Advisor's Signature

Academic Year: 2013

ACKNOWLEDGEMENTS

The author would like to express his special gratitude to his advisor, Associate Professor Dr. Chakkaphan Sutthirat Department of Geology, Faculty of Science, Chulalongkorn University, for his invaluable supervision, suggestion, encouragement and contribution, especially to make this research well achieved. Thanks to Jensarin Vivatpinyo, Chidchanok Kasiban, Vanachawan Hanyek and all of geology students at Chulalongkorn University who have assisted in this research. Special thank is given to Tawatchai Chualaowanich from Department of Mineral Resources and Dr. Prayath Nantasin from Department of Earth Sciences, Faculty of Science, Kasetsart University for training on PT estimation. Sample preparation and laboratory were supported by Sopit Poompuang, Jiraprapa Neampan and Prajin Thongchum.

My MSc. study is financially supported by the 90th Anniversary of Chulalongkorn University Fund (Ratchadaphiseksomphot Endowment Fund), Graduate School, Chulalongkorn University and the Human Resources Development in Science Project (Science Achievement Scholarship of Thailand, SAST). Field investigation in Montepuez, Mozambique was supported by The Gem and Jewelry Institute of Thailand (Public Organization) with the permission Ministry of Mineral Resources of Mozambique. The author is grateful to Mr. Wirach Sriphathoorat, Mr. Somyot Sodsri, Mr.Thammanoon Jewpattanakul and Mr. Narong for their help during field investigation in Montepuez, Mozambique.

This research program has been carried out at Department of Geology, Faculty of Science, Chulalongkorn University.

Finally, the author is indebted to my parents for their stimulation and encouragement.

CONTENTS

Page

List of Table

List of Figure

Figure Page

Figure Page

Figure Page

Figure Page

Figure Page

Figure Page

Figure Page

CHAPTER I

INTRODUCTION

1.1 General Statement

Corundum is an important exported gemstone supporting economy of Thailand. Gem corundum deposits in Thailand have been mined continuously for a few decades; consequently, their reserves are decreased leading to low activity of gem mining within a few areas. Thai gem traders have imported corundum from many places around the world. The main sources are from Myanmar, Vietnam, Sri Lanka and African countries including Madagascar, Tanzania and Mozambique. Historical geology and gem formation of Sri Lanka and East African countries as mentioned above have related to Mozambique Metamorphic Belt.

Mozambique Belt is metamorphic mountain ranges located in the east of Africa (East Africa Orogen) extending widely from Egypt southward to Mozambique eastward to Indian Ocean (Figure 1.1). It mainly covers areas of Kenya, Tanzania, Mozambique and Madagascar. Mozambique Belt is essential sources of gem varieties, particularly corundum, tourmaline, spinel, aquamarine etc. (Malisa and Muhongo, 1990; Lehto and Goncalves, 2008). High quantity of gem corundum from Mozambique has been imported into Thailand, recently.

Montepuez, a small city located in the northeast Mozambique (Figure 1.1), has been recently produced ruby and pink sapphire since 2009. Corundum (mostly red to pink varieties) found in this area has various qualities from top to low qualities (Figure 1.2) being supplied into the world market. Although, huge amount of ruby and pink sapphire has been traded economically for some years; original source rock of these stones have never been investigated and reported in detail prior to initiation of this thesis.

Characteristics of corundum-bearing rocks and associated rocks in Montepuez, northeast Mozambique, may be used for further exploration of new ruby deposit in this country as well as regional Mozambique Belt. Initial rock (protolith) and temperature-pressure equilibrium of ruby-bearing assemblages carried out from this study can also be significant information for interpretation of metamorphism and tectonic setting of the area. Therefore, petrographic description, detail studies of whole-rock geochemistry and mineral chemistry have designed for this research project.

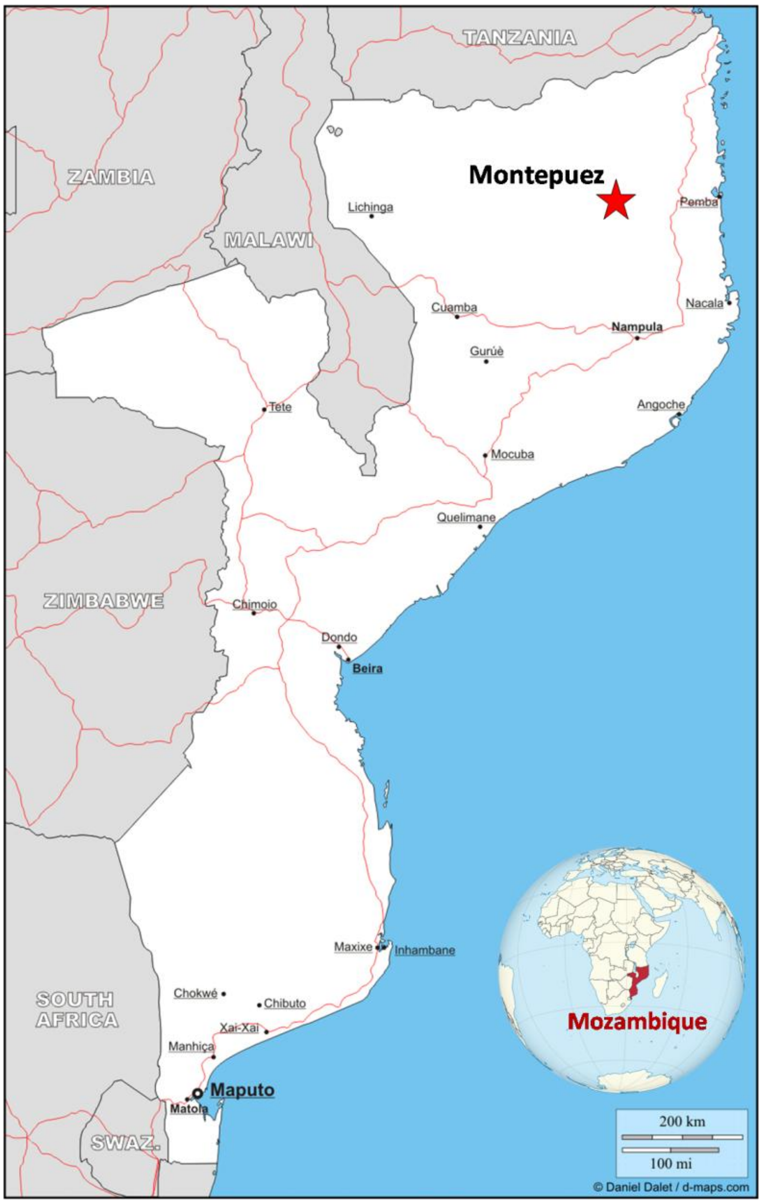

Figure 1.1 The map shows position of Mozambique in East Africa (from Dalet, 2007 and Marcos, 2011). Red star indicates Montepuez, the study area.

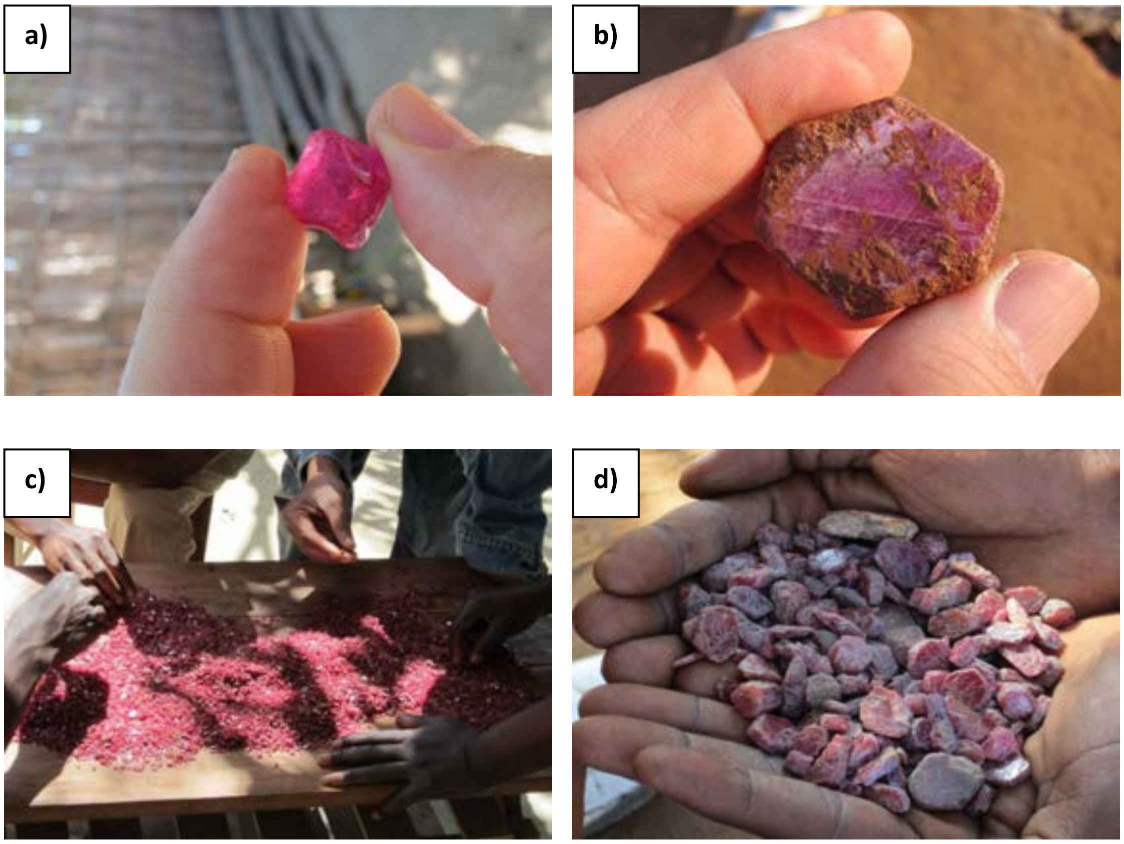

Figure 1.2 High quality ruby (a) and medium to low quality rubies (b, c, d) widely available in Montepuez markets.

1.2 Location and Accessibility

Mozambique is located along the Africa's southeastern coast. It is bound by Tanzania to the north, Malawi, Zambia and Zimbabwe to the west, and South Africa and Swaziland to the south (Figure 1.1). The study area is located on the northeastern part of Montepuez; a small town covers approximately 1,740 square kilometers between the latitude 12°56’ 7.7” - 13°12’ 24.3” S and longitude39° 0’ 0.0” - 39° 33’ 11.3” E or UTM grid reference 500000E-560000E and 8540000S-8570000S.

Accessibility to the area can take an airplane of Kenya Airline from Suvarnabhumi international airport, Bangkok, Thailand to Pemba international airport, Mozambique via Nairobi international airport, Kenya. The study area about 200 kilometers west of Pemba (Figure 1.3) can be accessed using the highway no. 106 and 242, respectively, from the Pemba international airport to the west.

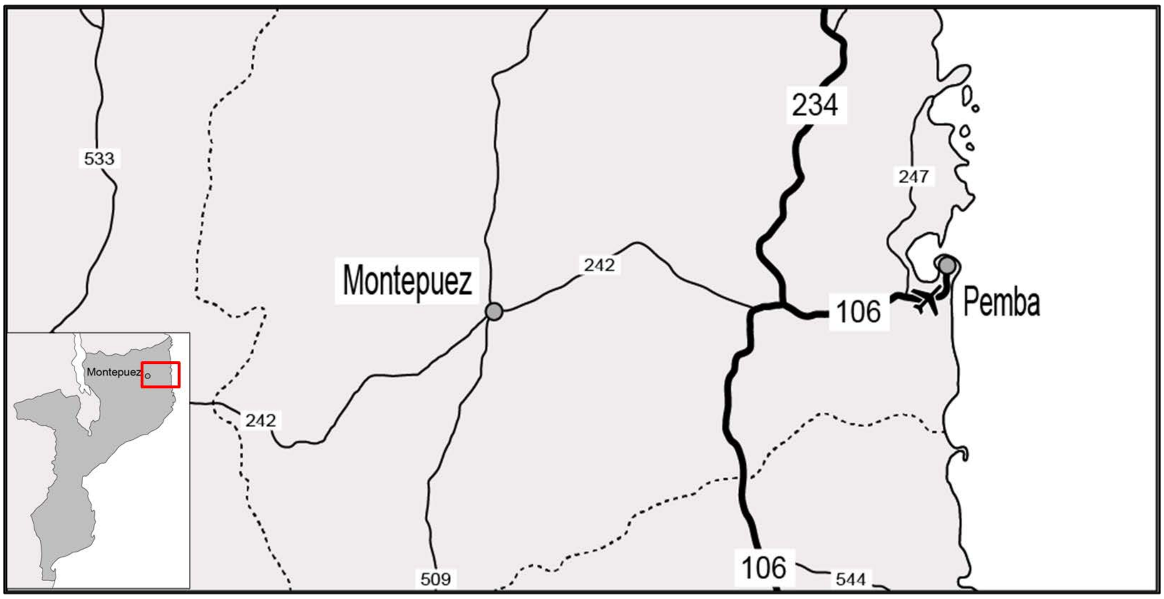

Figure 1.3 Map showing accessibility to the study area in Montepuez, Mozambique (after Accommodation Mozambique, 2013).

1.3 Climate and Physiography

Mozambique has a tropical climate with two main seasons, wet season from October to March and dry season from April to September. Climatic conditions, however, vary depending on altitude. Rainfall is quite heavy along the coastal and decreases in the north and south. Annual precipitation varies from 500 to 900 mm with an average of 590 mm. Cyclones has commonly occur during the wet season (Oliveira, 2005). Average temperature ranges in Northeast Mozambique (Pemba) are from 18 to 28 °C (65 to 82°F) in July to 23 to 31 °C (74 to 88 °F) in February (NordNordWest, 2012).

Physiography of the area contains small mountains in the rolling land and low plateaus (Figure 1.4). Their average elevation ranges from 400 to 450 m above the mean sea level (msl) (Figure 1.5). The highest mountain is about 850 m above msl.

Figure 1.4 General physiography of Montepuez area showing small mountains in the rolling land.

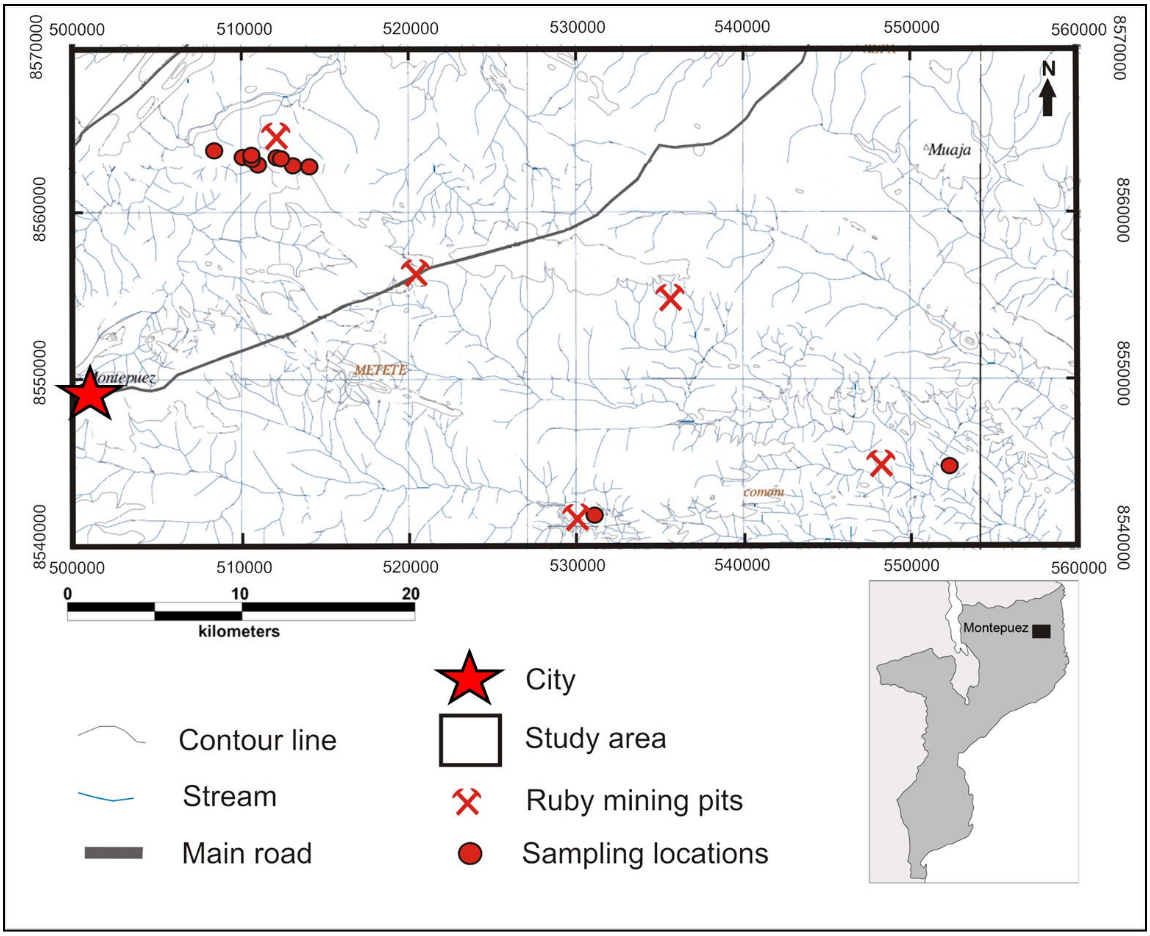

Figure 1.5 Topographic map of the study area showing 13 sample locations in Montepuez, Mozambique.

1.4 Objective

The main objective of this research is to study petrochemistry of corundum-bearing rocks and related rocks collected from Montepuez deposits, Northeastern Mozambique.

1.5 Methodology

All methods engaged in this study can be summarized in a flow chart (Figure 1.6). It consists of five main steps which details are reported below.

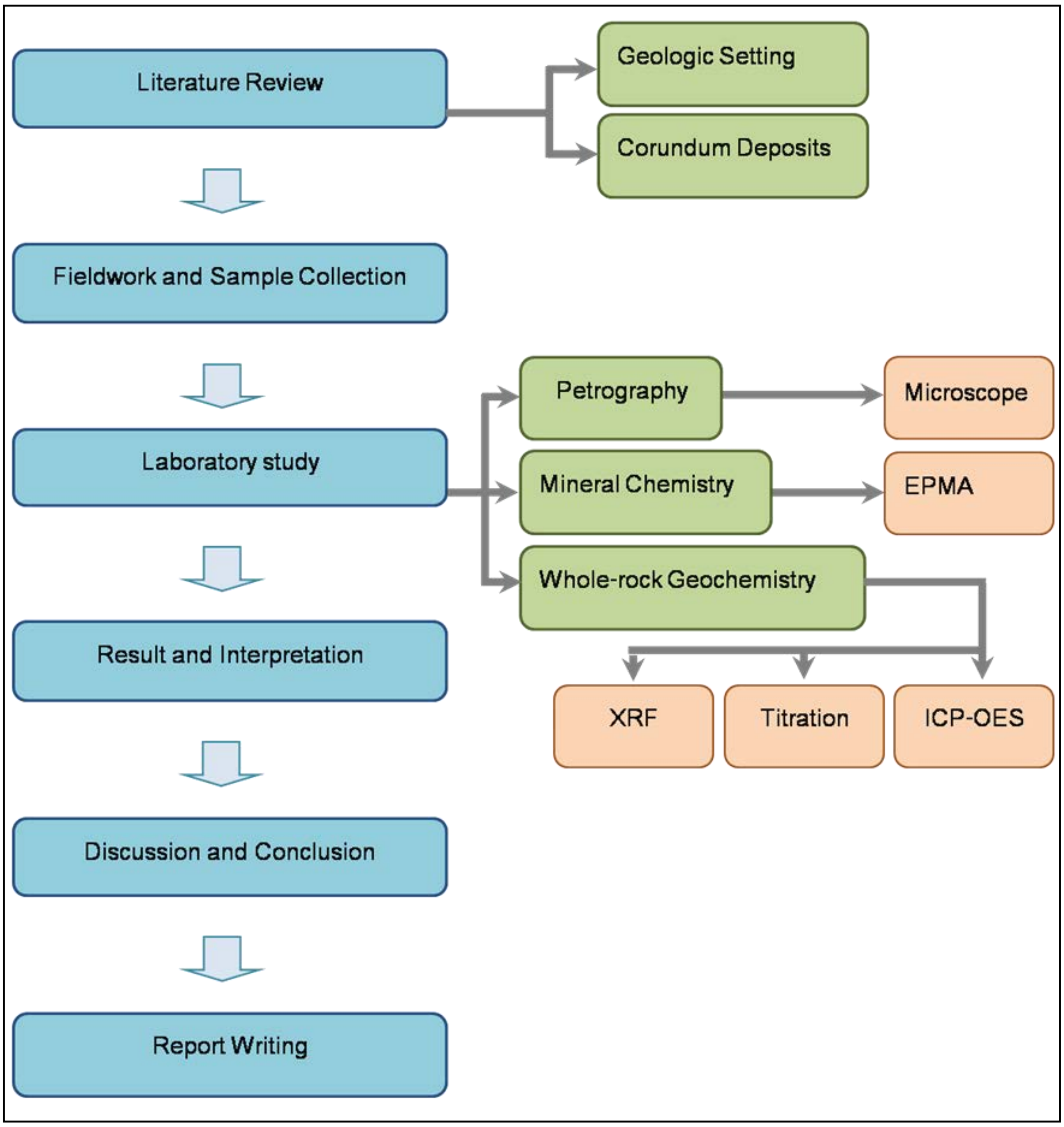

Figure 1.6 Flow chart showing a sequence of work under this study.

Literature Reviews: several previous works on regional geology, tectonic setting, corundum deposits, mineralization, metamorphism and tectonic setting of the study area and regional area were carried out prior to research planning. Information gained from this step is also used for discussion and interpretation in the final part of the report

Field Investigation and Sample Collection: Satellite image interpretation, geological structures, landforms, rock units and accessibility were prepared before fieldwork and sample collection were taken place. Thirteen localities around the area of Montepuez (Figure 1.5) were visited and collected rock and mineral samples.

Field investigation was focused on exposures of corundum-bearing rock around the Montepuez mining area and gem occurrences (Figure 1.7). Geologic map complied by Ministry of Mineral Resources of Mozambique (2005) was used during the field study and sample collection. Two groups of metamorphic rocks, amphibolite and gneiss can be classified based on field investigation. Corundum-bearing rocks are clearly characterized by amphibolite. Thirty-six rock samples were representatively selected for further investigations.

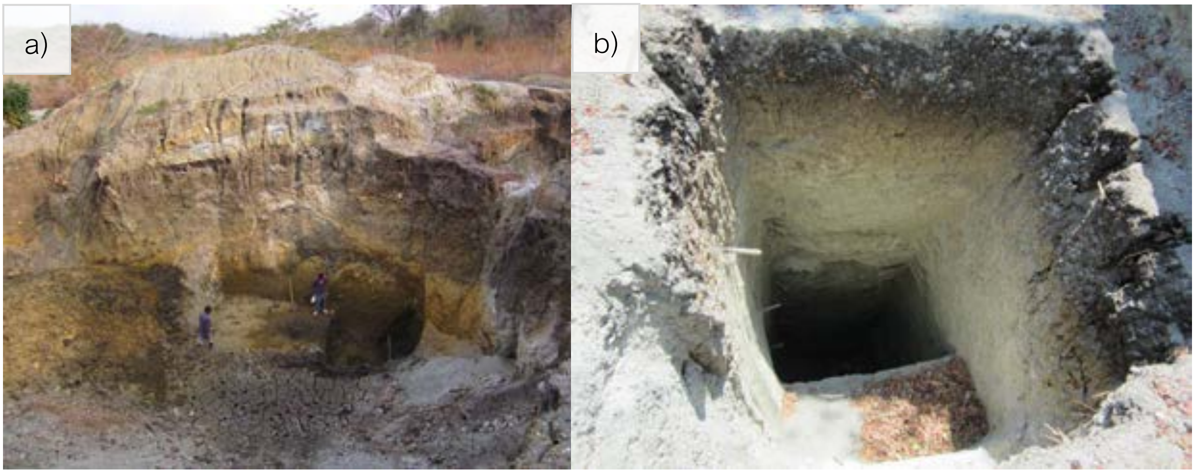

Figure 1.7 Photos taken during the field observation in mining area showing a ruby mine with heavy machinery (a) and small mining pits of local miners (b); these mines were operated within primary corundum deposits.

Petrographic Work: Sixteen rock samples were slab-cut and then prepared as thin sections. The polished thin sections were usually prepared at about 50 μm thick before polishing with 12, 6, 3, and 1 μm diamond pastes, respectively. After preparation, they were used for petrographic description for mineral assemblage and texture under a polarizing microscope. Subsequently, representative samples were selected, based on petrographic feature, for further analyses, e.g., whole-rock geochemistry and mineral chemistry.

Whole-rock Geochemistry: Nineteen rock samples were selected representatively and crushed by an iron jaw crusher prior to powdering by a tungsten carbide miller. Subsequently, powdered rock samples and binding agent (wax) were packed as pressed pellets before quantitative analysis using an X-ray Fluorescence (XRF) Spectrometer, Bruker Model AXS S4 PIONEER, based at Department of Geology, Faculty of Science, Chulalongkorn University. Analytical condition was set at 60 kV 50 mA range 0.2-20 A (60-0.6 keV) total resolutions 3-100 eV and typical measurement time 2-10 s per element. Nine major oxides (i.e., SiO_2, TiO_2, FeO_{total}, MnO, MgO, CaO, Na_2O, K_2O and P_2O_5) were measured in calibration of rock standards including JA-2, JG-2 and JR-1 provided by Geological Survey of Japan (GSJ) and DTS-2B, PCC-1, GSP-2 and BHVO-2 provided by United States Geological Survey (USGS). Moreover, loss on ignition (LOI) was also measured by weighting rock powders before and after ignition at 1000° C for 3 hrs in a RHF 14-3 220 V electric furnace and FeO determinate by titration with standard dichromate solution using diphynylamine sulfonic acid as the indicator (Shapiro 1975) based at Department of Geology, Faculty of Science, Chulalongkorn University.

Trace and rare earth element analyses were accomplished by an Inductively Coupled Plasma-Optical Emission Spectrometer (ICP-OES), model Perkin Elmer Optima 5300DV, and Inductively Coupled Plasma-Mass Spectrometry (ICP-MS), model Elan 6100 based at the SGS (Thailand) Limited. These samples were digested by sodium peroxide. Detection limits range from 0.01 ppm- 0.01% for trace elements that are 1 ppm Ag, 0.01 %Al, 5 ppm As, 0.5 ppm Ba, 5 ppm Be, 0.1 ppm Bi, 0.01 %Ca, 0.2 ppm Cd, 0.1 ppm Ce, 0.5 ppm Co, 10 ppm Cr, 0.1 ppm Cs, 5 ppm Cu, 0.05 ppm Dy, 0.05 ppm Er, 0.05 ppm Eu, 0.01 % Fe, 1 ppm Ga, 0.05 ppm Gd, 1 ppm Ge, 1 ppm Hf, 0.05 ppm Ho, 0.2 ppm In, 0.01 % K, 0.1 ppm La, 10 ppm Li, 0.05 ppm Lu, 0.01 % Mg, 10 ppm Mn, 2 ppm Mo, 1 ppm Nb, 0.1 ppm Nd, 5 ppm Ni, 0.01 % P, 5 ppm Pb, 0.05 ppm Pr, 0.2 ppm Rb, 0.1 ppm Sb, 5 ppm Sc, 0.1 ppm Sm, 1 ppm Sn, 0.1 ppm Sr, 0.5 ppm Ta, 0.05 ppm Tb, 0.1 ppm Th, 0.01 % Ti, 0.5 ppm Tl, 0.05 ppm Tm, 0.05 ppm U, 5 ppm V, 1 ppm W, 0.5 ppm Y, 0.1 ppm Yb, 5 ppm Zn, 0.5 ppm Zr.

Mineral Chemistry: All crucial minerals were subsequently analyzed using an Electron Probe Micro Analyzer (EPMA, model Jeol JXA-810) based at Department of Geology, Faculty of Science, Chulalongkorn University. These data led to detailed study of chemical compositions of minerals and appropriate environment of crystallization. Electron microprobe was operated under the principle that if a solid material is bombarded by an accelerated and focused electron beam, the incident electron beam has sufficient energy to liberate both matter and energy from the sample. These electron-sample interactions mainly liberate heat, but they also yield both derivative electrons and X-rays. This method is a non-destructive analytical technique. The primary importance of an EPMA is the ability to acquire precise, quantitative element analyses very small “spot” sizes on the surface of sample, so it is possible to re-analyze the same materials more than one time. For quantitative analyses, most of the standards used for calibration were pure oxide and mineral standards including corundum for Al, wollastonite for Si and Ca, periclase for Mg, fayalite for Fe, potassium titanium phosphate for K, Ti and P, jadeite for Na, barite for Ba, manganosite for Mn, eskolite for Cr, zinc oxide for Zn, strontium barium niobate for Nb, Hafnium for Hf, Zirconium for Zr. Operating condition was set at an accelerating voltage of 15.0 kV, about 24 nA sample current, with focused beam (smaller than 1μm). Measuring times were set at 30 seconds and 10 seconds for peak counts and background counts, respectively, for each element using suitable analytical crystals. The analytical results were then taken automatic ZAF correction before reported in form of present oxides. As EPMA cannot distinguish between Fe^{2+} and Fe^{3+}, Fe in mineral analyses must be given as Fe_{total}. For iron-bearing minerals that have variable of Fe^{2+} and Fe^{3+} ratios were recalculated using equation of Droop (1987).

Discussion and Conclusion: All results obtained from this study were collected and verified prior to interpretation on genesis of rock formation. P-T conditions of metamorphism. Corundum formations were discussed along with tectonic setting of the area. Crucial aspects were concluded and reported in the last part.

Report Writing: Finally, thesis report and presentation were carried out as well as manuscript for publication in international journals. This thesis report comprises 5 chapters which introduction of overall research background, objective and methodology are described herein this chapter (Chapter 1). Chapter 2 covers geologic setting which is composed of regional tectonic setting, general lithology and metamorphism of Mozambique Belt from literature reviews. Field investigation and petrography are described in Chapter 3 whereas whole-rock geochemistry and mineral chemistry are reported in Chapter 4. Discussion in Chapter 5 is focused on petrogenesis, P-T estimation for metamorphism, genesis of corundum before conclusions are made in the same chapter. Moreover, Appendices provide more detailed information which is not reported in the main chapters; they contain list of sample, petrographic data and EPMA data.

CHAPTER II

REGIONAL GEOLOGY OF THE MOZAMBIQUE BELT

2.1 Tectonic Setting

The Mozambique belt occurred along eastern margin of the African continent represents a zone of continent-continent collision (Meert, 2003; Muhongo, 1999; Maboko, 2000a) which has been related to east and west Gondwana collision (Murphy and Nance, 1991; Shackleton, 1996; Muhongo, 1999; Sacchi et al., 2000; Chen, 2001; Powell and Pisarevsky, 2002; Yoshida et al., 2003; Meert, 2003; Collins and Pisarevsky, 2005). It has been suggested to be a result of Himalaya-type collision (Maboko, 1997; Jacobs and Thomas, 2004; Vogt et al., 2006). Assembly of the eastern parts of Gondwana composing of East Africa, Arabian–Nubian Shield, Seychelles, India, Madagasgar, Sri Lanka, East Antarctica and Australia resulted from a complex series of orogenic events spanning the interval between ~750 and ~ 530 Ma (Kriegsman, 1994; Shibata et al., 1996; Nyamai et al., 1999; Maboko, 2001; Meert, 2003; Condie, 2003; Torsvik et al., 2008). Parallel assemble tectonic terranes is controlled by two main periods of orogenesis within the eastern Gondwana (Figure 2.1). The older orogen resulted from the amalgamation of arc terranes in the Arabian–Nubian shield region and oblique continent–continent collision (Maboko, 2000; Meert, 2003) between eastern Africa (Kenya–Tanzania and points northward) with an ill-defined collage of continental blocks including parts of Madagascar, Sri Lanka, Seychelles, India and East Antarctica during the interval from ~750 to 620 Ma. This is referred to as the East Africa Orogen. The second major episode of orogenesis took place between 570 and 530 Ma and resulted from the oblique collision between Australia plus an unknown portion of East Antarctica with the elements previously assembled during the East African Orogen (Suwa et al., 1996; Meert, 2003) (Figure 2.2).

The Pan-African Mozambique Belt is a part of the East African Orogen (Stern, 1994; Meert, 2003) that extends from northern Egypt to southern Mozambique, with continuation to Antarctica (Jacobs and Thomas, 2004) is classified into northern

Arabian–Nubian Shield (ANS) and the southern Mozambique Belt (MB)(Fritz et al., 2009)(Figure 2.3).

The northern Arabian Nubian Shield (ANS) is characterized by a predominance of Neoproterozoic juvenile crust, strike slip faulting and orogen-parallel extension. The Central Mozambique Belt (CMB) and Southern Mozambique Belt (SMB) show orthogonal collision tectonics. They differ in continental fragments incorporated: age domains within CMB are 2.6, 1.9, 0.8 Ga whereas those within SMB are 2.6, 1.9, 1.8, 1.1, 0.7 Ga. Regarding to ages of crustal consolidation, they are assigned as ca. 620 Ma for CMB and ca. 550 Ma for SMB (Fritz et al., 2009).

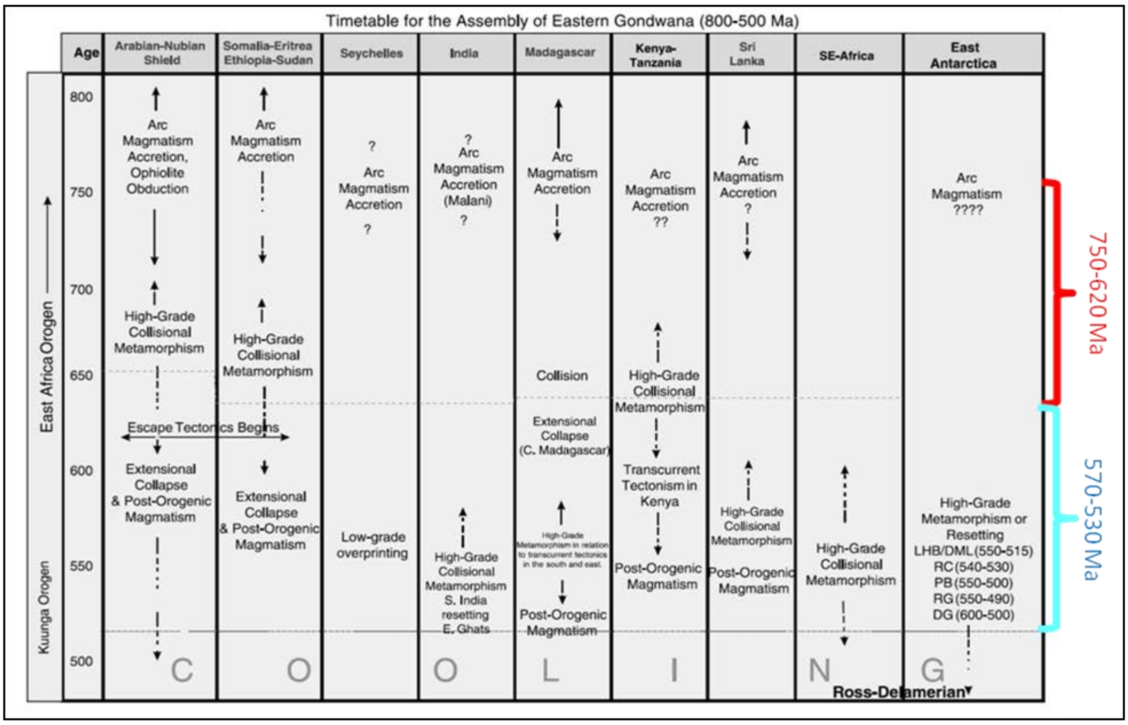

Figure 2.1 Summary of the tectonic events within different regions of eastern Gondwana (Meert, 2003).

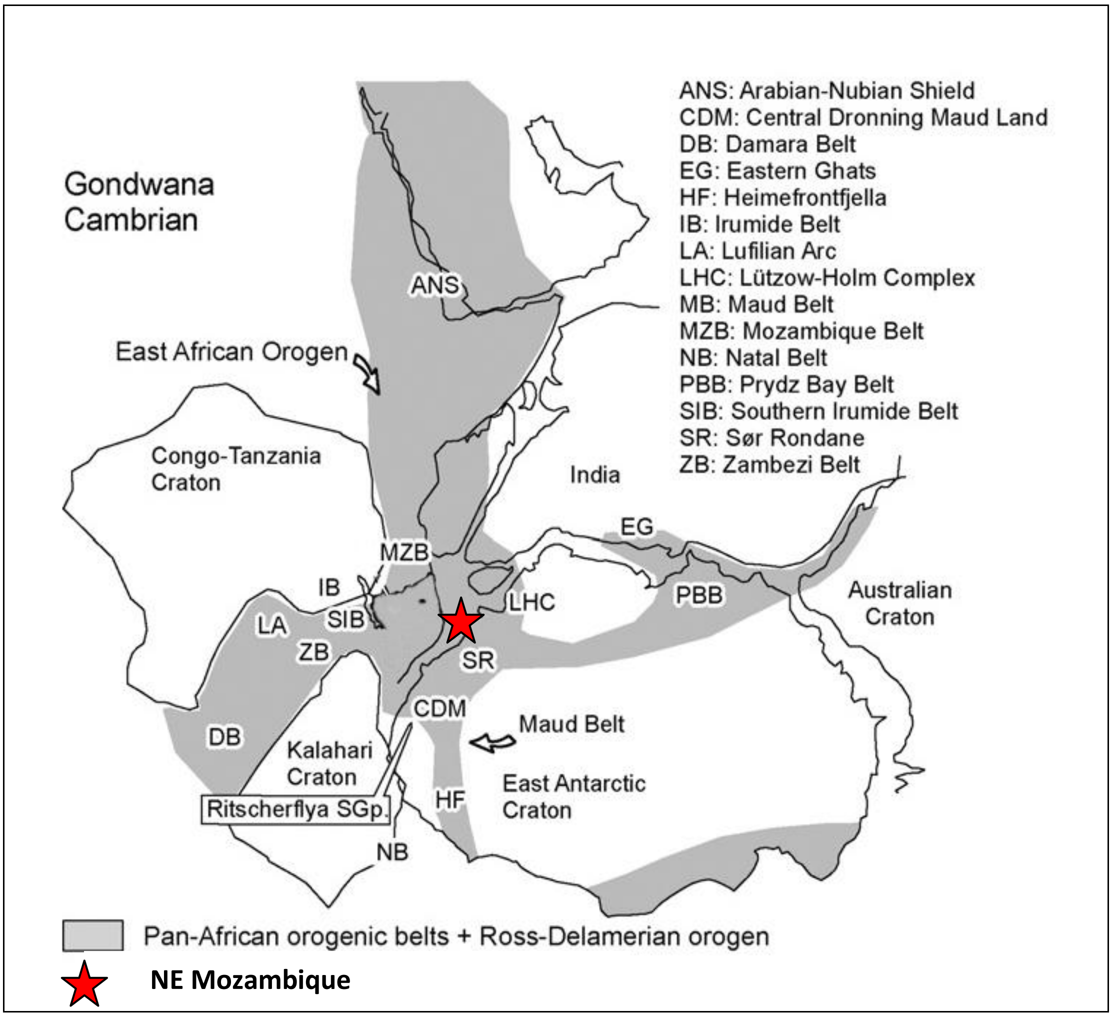

Figure 2.2 Schematic summary of Pan African Orogen from assembly of east Gondwana (after Meert, 2003; Bingen et al., 2009) red star indicates location of NE Mozambique.

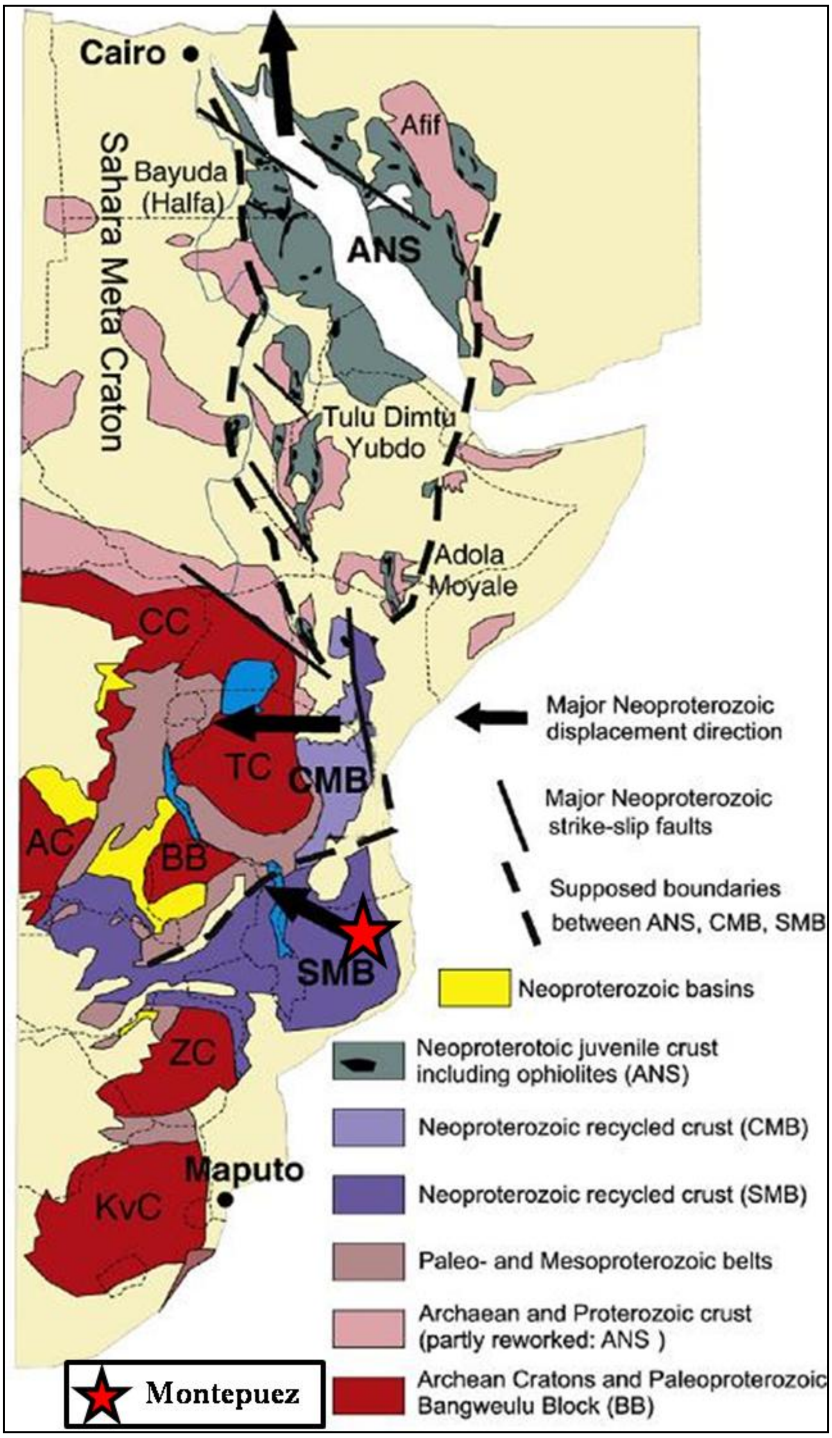

Figure 2.3 Distribution of crustal fragments along the East African Orogen including the northern Arabian Nubian Shield (ANS), Central Mozambique Belt (CMB) and Southern Mozambique Belt (SMB). Cratonic areas are Congo-Craton (CC), Tanzania Craton (TC), Angola–Kasai–Craton (AC), Bangweulu–Block (BB), Zimbabwe–Craton (ZB), Kapvaal–Craton (KvC) (Fritz et al., 2009).

Mozambique Belt was active during Paleoproterozoic and Neoproterozoic orogenies (Kartz, 1974; Stern, 1994; Vall, 1989; Maboko and Nkamura, 2002; Meert, 2003) with evidences from the Central Tanzania Shear Belt (CTSB) (Tenczer et al., 2007). It formed along the southern margin of the Archean Tanzania Craton that acted as rigid indenter during both orogenies which are Usagaran Belt and Mozambique Belt (Figure 2.4).

The Usagaran Belt was formed (Reddy et al., 2003) by strike-slip tectonics in an island arc regime (Fritz et al., 2005) whereas the Mozambique Belt was formed by westward thrust propagation during oblique collision of east and west Gondwana (Veevers, 2003; Fritz et al., 2005; Tenczer et al., 2007).

Mozambique Belt can be divided into 2 units, Western Granulite and Eastern Granulite (Figure 2.4). Both of them have formed during Neoproterozoic orogenies although the Western Granulite may have formed earlier (Fritz et al., 2005) (Figure 2.5).

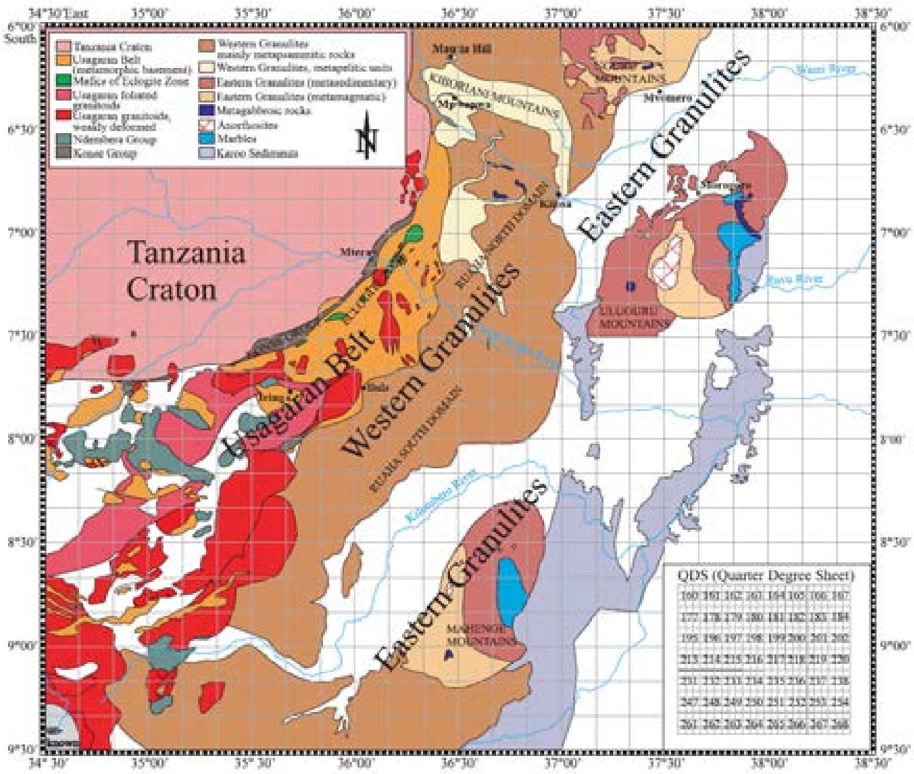

Figure 2.4 Lithological units of central Tanzania show the Western Granulite and Eastern Granulite of Mozambique Belt (Fritz et al., 2005).

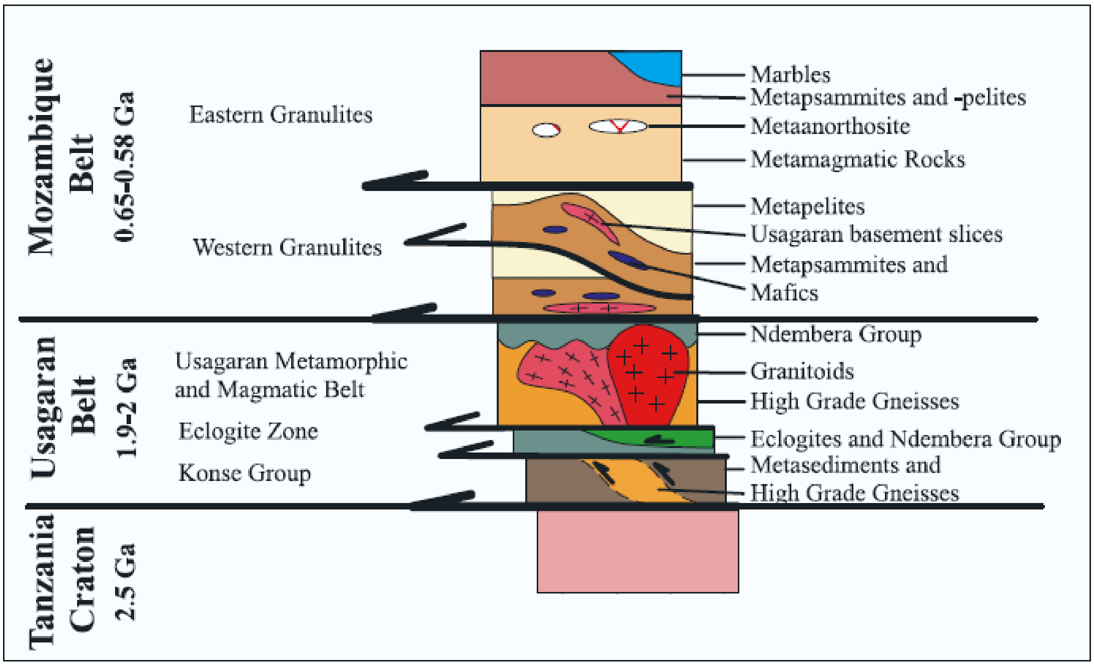

Figure 2.5 Tectono-stratigraphy of central Tanzania and its main lithologies. On the basis of prevailing metamorphic ages, three orogenic belts, the Archean Tanzanian Craton, the Paleoproterozoic Usagaran Belt, and the Neoproterozoic Pan-African Mozambique Belt are distinguished (Fritz et al., 2005).

Several episodes of deformation have been described throughout the Mozambique belt. The general N-S structural trend (Meert, 2003) has long been recognized to be the most prominent and crucial characteristic. However, E-W, NE-SW and NW-SE trending structures are also significant. Some of these structures appear to be related to high temperature ductile shear zones and are associated with granulite facies metamorphism (Muhongo, 2001). The E-W structures appear to be the oldest. NW-SE and NE-SW trending structures within the Mozambique belt are products of oblique collision (Muhongo, 1999).

The Northeastern Mozambique has been divided into a number of lithotectonic complexes (Figure 2.6) (Bingen et al., 2009), partly overlapping in definition and extent with the stratigraphic entities previously defined by Pinna et al. (1993). These complexes can be grouped into four distinct mega-units each with a distinct geological evolution (Figures 2.7 and 2.8) (Bingen et al., 2009; Thomas et al., 2010).

(1) The Palaeoproterozoic Ponta Messuli Complex is exposed to the NW of the Maniamba Graben.

(2) The Unango and Marrupa Complexes represent Stenian–Tonian felsic crust lying between the Maniamba Graben and the Lurio Belt. In the south, they are progressively reworked towards and into the Lurio Belt (Pinna, 1995; Engvik et al., 2007) and their southern boundary is defined by slivers of rocks of the Ocua Complex.

(3) The Nampula Complex (Macey et al., 2010; Ueda et al., 2012) represents Stenian felsic crust along the south Lurio Belt.

(4) The Stenian–Tonian basement is overlain by a set of Pan-African nappes (Bingen et al., 2009). To the north of the Lurio Belt, the Nairoto, Meluco, Muaquia, M'Sawize, Xixano, Lalamo and Montepuez Complexes, collectively referred to as the Cabo Delgado Nappe Complex (Viola et al., 2008; Bingen et al., 2009) that shares a number of similarities with the Eastern Granulite of Tanzania (Mohongo, 1984; Fritz et al., 2005; Bingen et al., 2009) and Vohibory Complex in Madagascar (Bingen et al., 2009)(see Figure 2.6), overlie the Marrupa Complex (Viola et al., 2008). To the south of the Lurio Belt, the Mugeba and Monapo klippen, overlie the Nampula Complex (Sacchi et al., 1984; 2000; Grantham et al., 2008; Boyd et al., 2010).

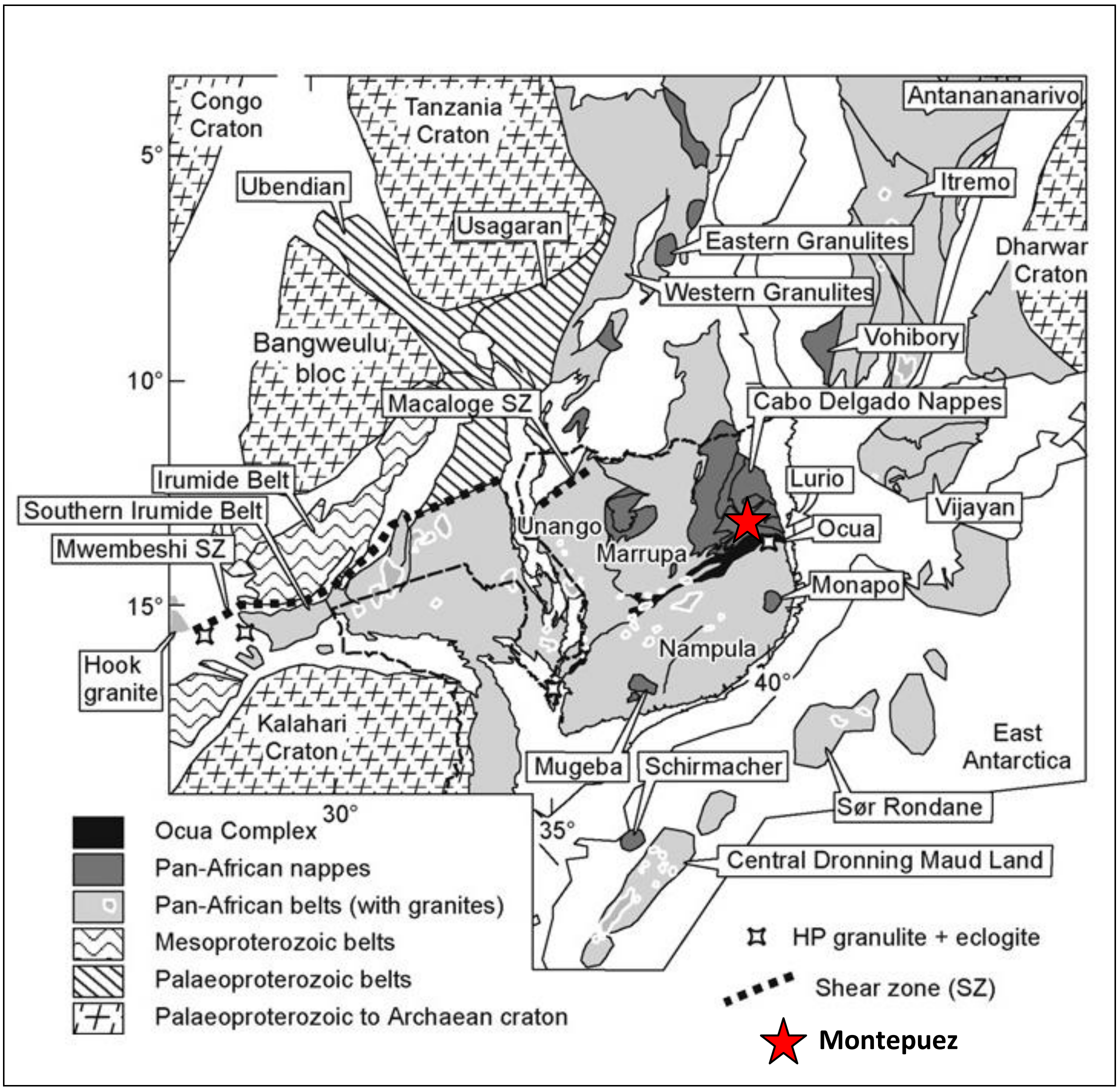

Figure 2.6 Sketch map of NE Mozambique (after Bingen et al., 2009) showing location of Montepuez.

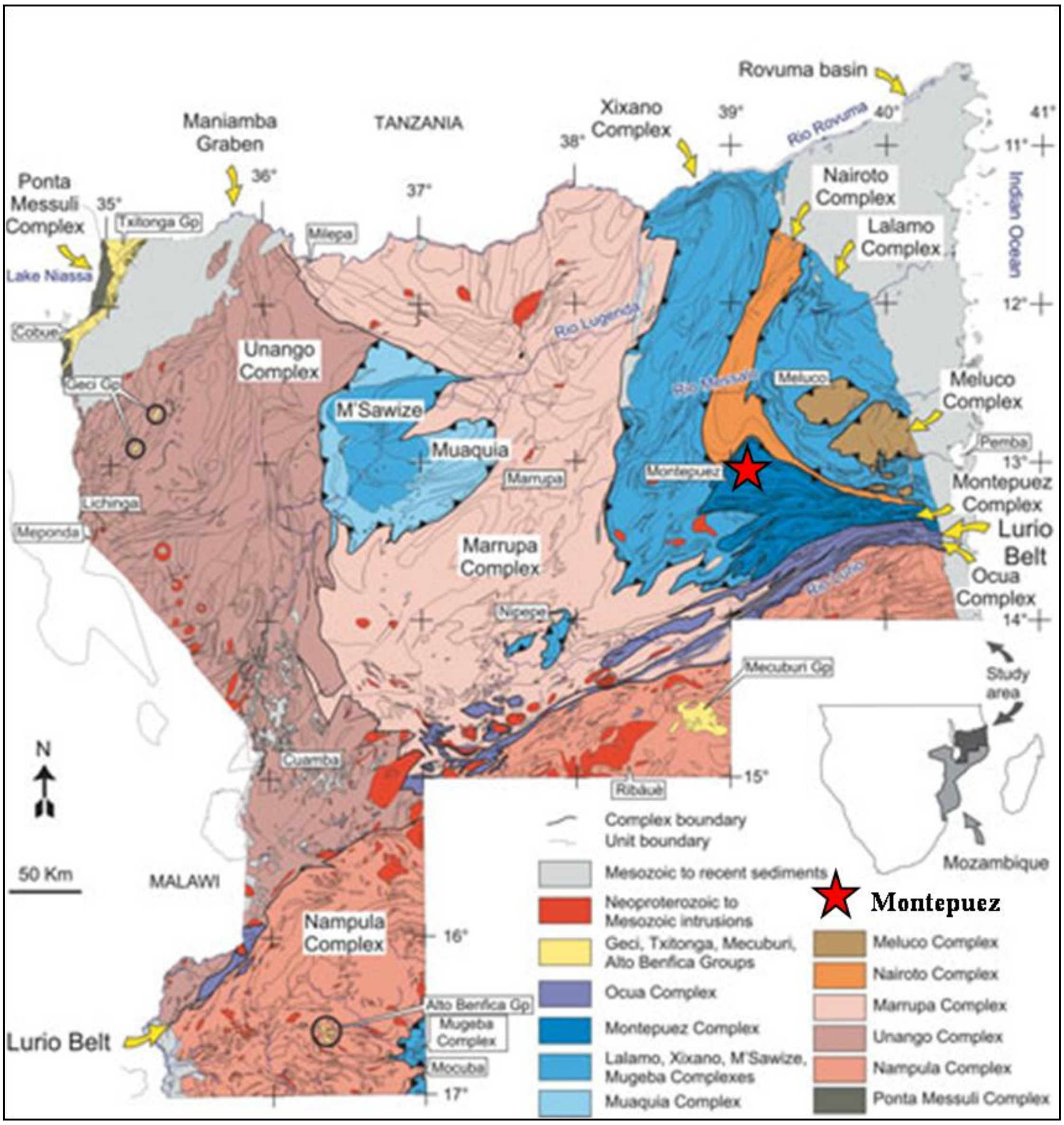

Figure 2.7 Geologic map showing the main rock units in northeast Mozambique based on compilations at 1:250 000 scale (by Boyd et al., 2010).

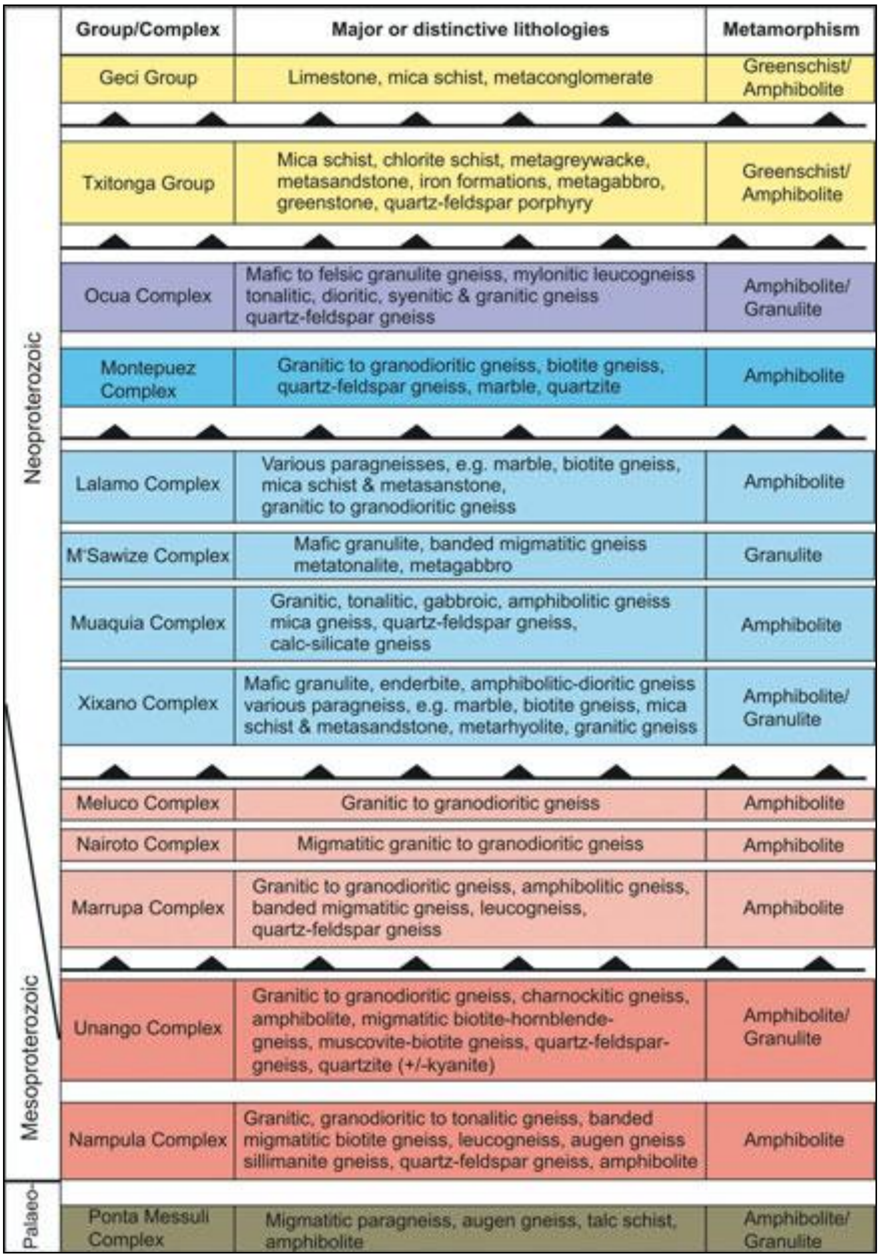

Figure 2.8 Overview of the main Proterozoic tectonostratigraphic units in the northeast Mozambique (Boyd et al., 2010).

2.2 General Lithology and Metamorphism

Lithology of Mozambique presents significantly high-grade metamorphic rocks (Muhongo et al., 1999; Muhongo, 2001; Tenczer et al., 2006; 2007) that are characterized by the occurrences of high P-T granulite facies rocks including enderbites and metaanorthosite, marbles and pegmatites; moreover, gem mineralization is also well pronounced (Munyanyiwa et al., 1997; Mercier et al., 1999; Muhongo, 1999; Schwarz et al., 2008).

Characteristics of the main rock units in the northeastern Mozambique can be presented by a continuous north to south series of the Lurio Belt (Viola et al., 2008) (Figure2.7). With complex nomenclatures (Pinna et al., 1993; Viola et al., 2008; Bingen et al., 2009), they can be subdivided spatially into a number of tectonostratigraphic units (Boyd et al., 2010) as presented in Figure 2.8.

The Montepuez Complex is lithologically similar to the adjoining Lalamo and Xixano Complexes, although the Montepuez and Lalamo Complexes are everywhere separated by a felsic gneiss unit attributed to the Nairoto Complex. The Montepuez Complex contains granitic gneiss, calcitic and dolomitic marbles, quartzitic gneiss, quartz-feldspar gneiss, biotite gneiss and migmatite (Boyd et al., 2010).

The Neoproterozoic Mozambique Belt is characterized by high-grade metamorphism belonging to granulite facies (Andreoli, 1984; Pinna et al., 1993; Grantham, 1994; Reeves and Wit, 2000; Kroner et al.1997; Kroner et al., 2001; Hauzenberger et al., 2004; Viola et al., 2008; Bingen et al., 2009; Boyd et al., 2010) that appear to have been formed during peak of metamorphism at 650-620 Ma (Appel et al., 1998). In central and southern Mozambique Belts (Figure 2.3) (Fritz et al., 2005; Tenczer et al., 2007), they can be divided into Western Granulite and Eastern Granulite (Hauzenberger et al., 2004; Fritz et al., 2005; Fritz et al., 2009).

Western Granulite Belt (Figure 2.9) presents peak metamorphic conditions of 760–800 °C and 13–14 kbar (Johnson et al., 2003; Fritz et al., 2005). Eastern Granulite

Belt (Figure 2.9) appears to have peak metamorphic conditions fairly homogenous with ca. 820 °C and 12 kbar (Fritz et al., 2005).

Northeast Mozambique offers an important transect across the southern part of the East African Orogen (Figure 2.7) (Boyd et al., 2010). The main rock units are represented by amphibolite facies (Figure 2.8) (Boyd et al., 2010) that may have formed during Proterozoic (Bingen et al., 2009). The Montepuez Complex in northeast Mozambique can be referred to Eastern Granulite (Hauzenberger et al., 2004; Fritz et al., 2005; Fritz et al., 2009) in Tanzania and Kenya (Bingen et al., 2009).

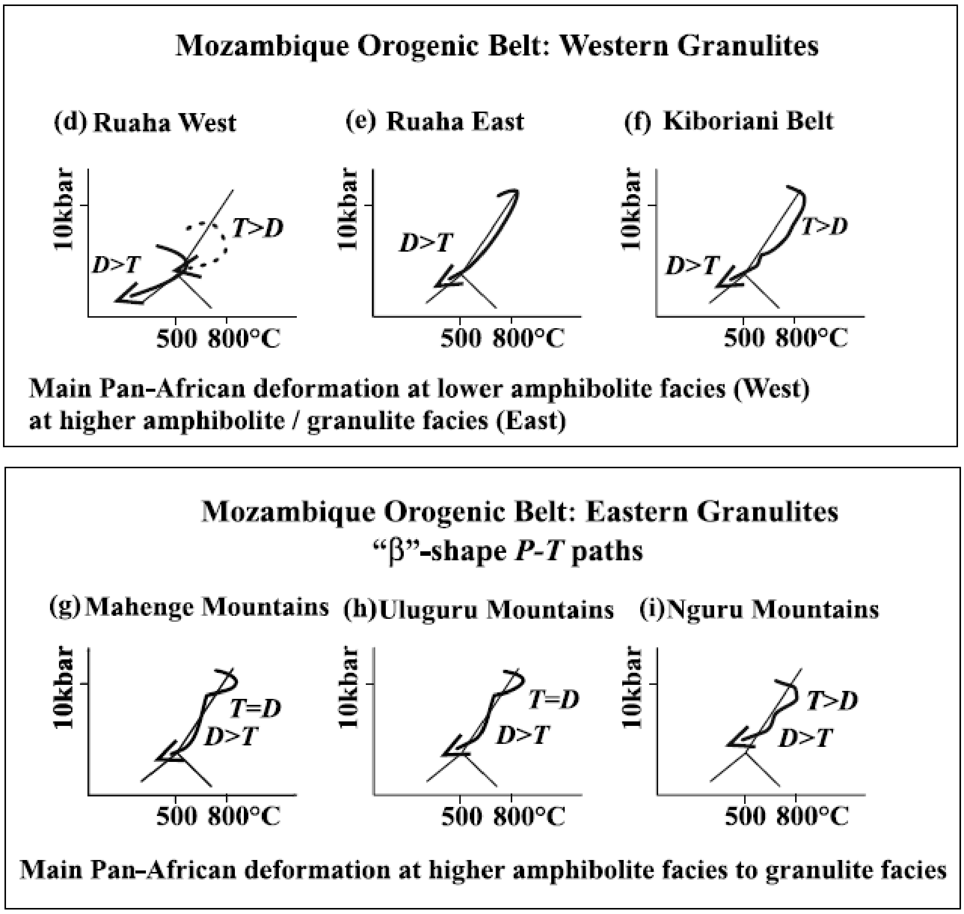

Figure 2.9 P-T-D paths from key areas for Neoproterozoic Pan-African (solid lines) and for Paleoproterozoic pre-Pan-African (dashed lines) events. D > T is deformation outlasting temperature, T > D is temperature outlasting deformation, and T = D is deformation at indicated temperatures (Fritz et al., 2005).

CHAPTER III

FIELD INVESTIGATION AND PETROGRAPHIC DESCRIPTION

3.1 Introduction

Field investigation was performed in order to collect information and relationship between corundum deposits and geologic setting within this area. Thirteen locations were visited for this study (Figure 3.1). Observation and finding of each location are summarized in Table 3.1. Most corundum occurrences and mining sites during this visit are located in the eastern part of Montepuez. Geologically, this area is composed of a variety of high grade metamorphic rocks; however, they are mainly characterized by gneiss, migmatite, marble, amphibolite and altered amphibolite which the later rock is significantly related to pegmatite intrusion. All of rocks in this area can be classified into two main types including amphibolites (Figures 3.2-3.7) (the main focus) and other metamorphic rock types (Figures 3.8).

Petrographic study was carried out with both macroscopic and microscopic descriptions (Figure 3.9). Subsequently, corundum-bearing amphibolite (Figures 3.10-3.12), corundum-barren amphibolite (Figures 3.13-3.15) and metamorphic rocks (gneiss) (Figures 3.16-3.18) are identified and described in details.

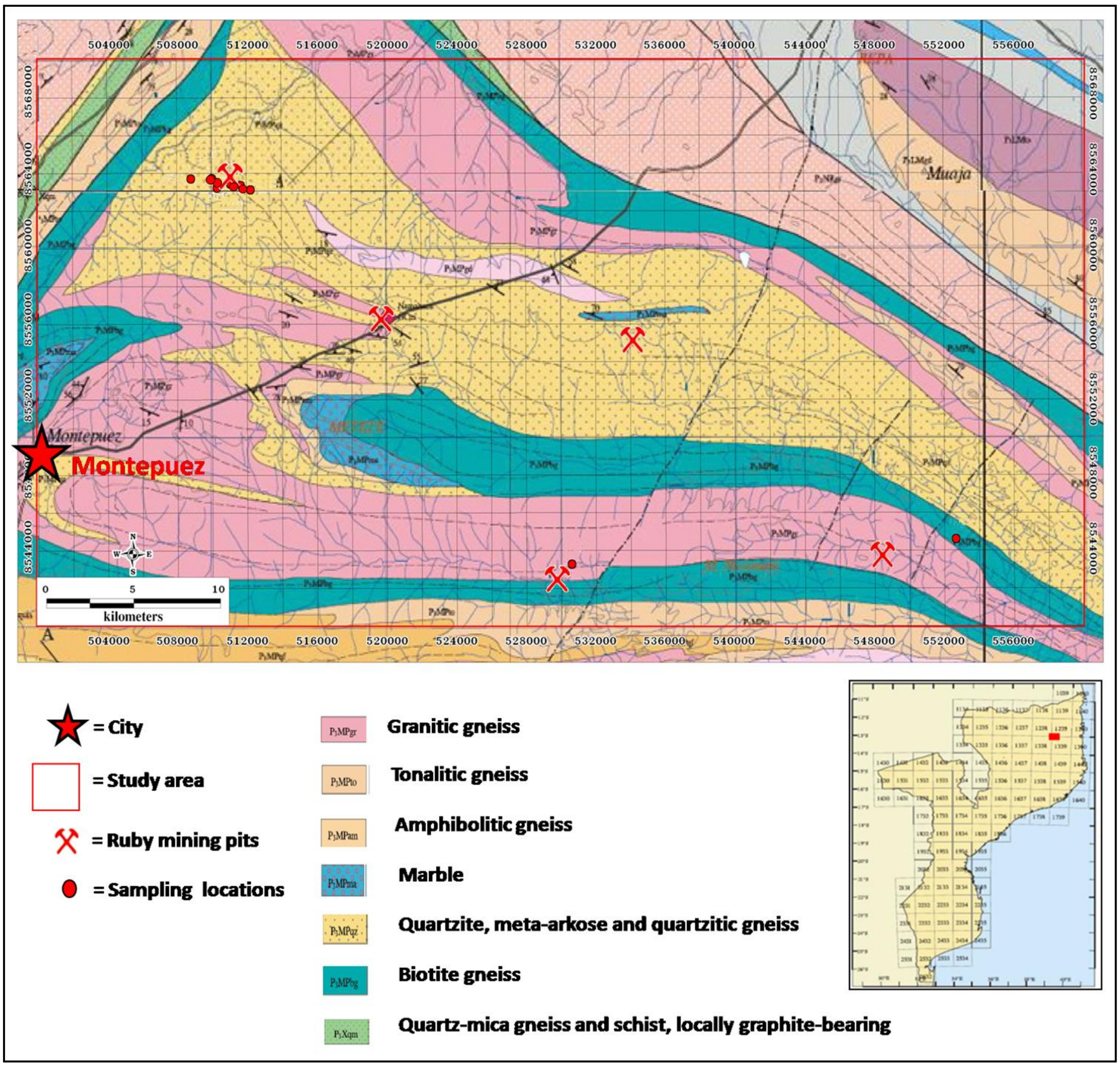

Figure 3.1. Geologic map of the Montepuez area (modified from Ministry of Mineral Resources of Mozambique, 2005) shows mining sites and sample locations of this study.

Table 3.1 Summary of sample collections during the fieldwork.

Map sheet 1239 and 1339.

Station No.	Easting	Northing	Rock Types
1	0552666	8544652	gneiss
2	0530596	8543321	gneiss
3	0529089	8542158	amphibolite
4	0508817	8563754	amphibolite
5	0508802	8563750	amphibolite
6	0508888	8563464	gneiss
7	0510010	8563755	amphibolite
8	0510028	8563770	altered ruby-bearing amphibolite
9	0510122	8563705	altered ruby-bearing amphibolite
10	0510314	8563270	gneiss
11	0511076	8563481	ruby-bearing amphibolite
12	0511666	8563398	amphibolite
13	0512234	8563177	amphibolite

3.2 Field Investigation

Amphibolite:

Amphibolite is commonly found as lens in the basement of migmatitic gneiss and marble within this area; in addition, amphibolite usually associates with corundum, mostly ruby and pink sapphire (Figure 3.2). Based on field investigation, amphibolite is divided into 2 main types, corundum-barren amphibolite and corundum-bearing amphibolite. Their details are reported below.

Corundum-Bearing Amphibolite: Corundum occurrences can be discovered in 2 types of amphibolites, primary deposits. They are fresh amphibolite and altered amphibolite. Both types of corundum-bearing amphibolites appear to have different characteristics that are present below.

Corundum-bearing amphibolite (Figure 3.3) is composed of amphibole, plagioclase, spinel and corundum (ruby). Most of rubies in this depositional type are deep red to red. However, these rock types lie along the Northwest-Southeast trend. It should be notified that rubies from both types of primary deposits usually contain a lot of fractures.

Ruby and pink sapphire relates to altered amphibolites (Figure 3.4). This altered corundum-bearing amphibolite is composed of amphibole, clay mineral and green mica (Figure 3.5) that appear to have related to coarse-grained quartz and feldspar pegmatite intrusion (Figure 3.6).

Corundum-Barren Amphibolite: is commonly found as loose blocks near corundum pit (Figure 3.7) and some locations are found as outcrop (Figure 3.7). The major assemblages contain abundant amphibole with variable proportions of plagioclase, garnet and mica. The general feature is foliation and folding. Green mica, clay minerals and other alteration minerals are sometimes discovered at the same places.

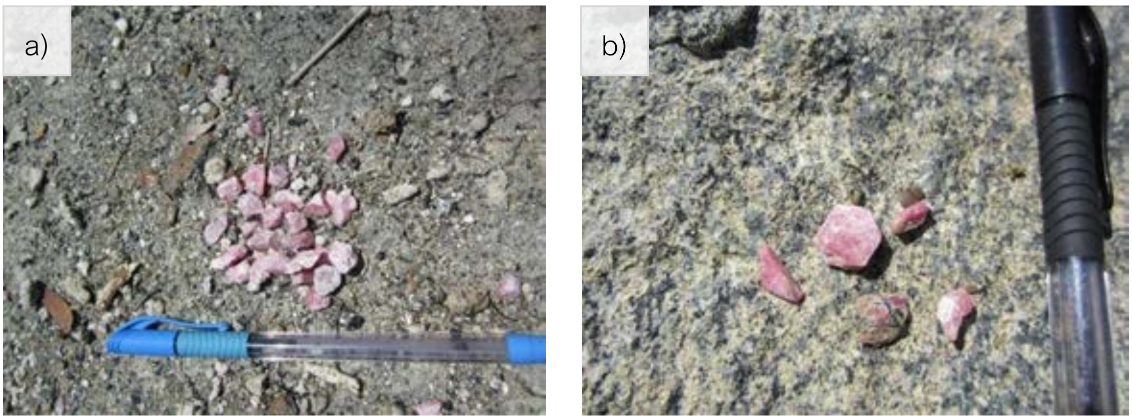

Figure 3.2 Ruby and pink sapphire (a, b) discovered in Montepuez deposits, Mozambique.

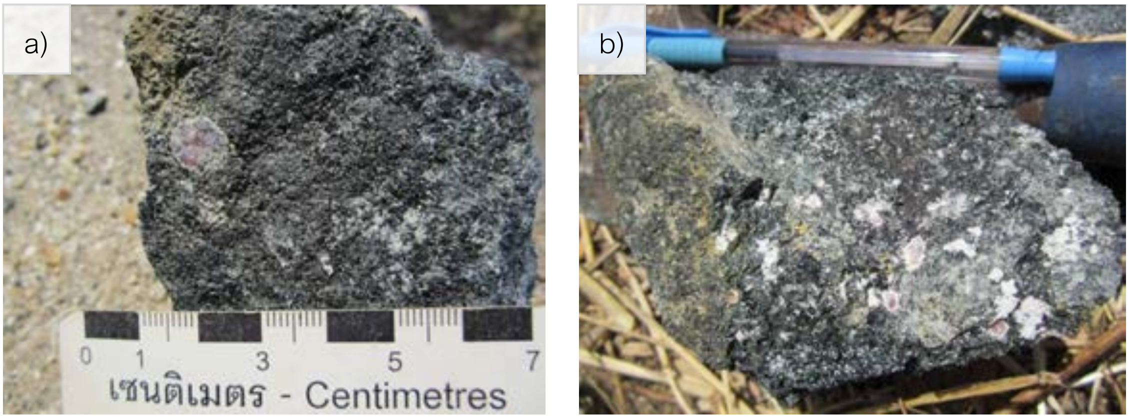

Figure 3.3 Corundum-bearing amphibolite (a, b) recognized as the main primary ruby deposits in Montepuez, Mozambique.

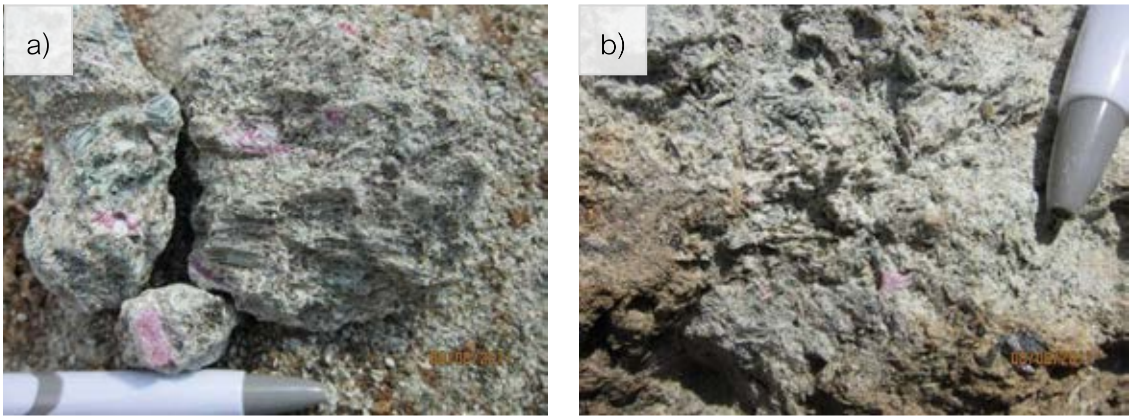

Figure 3.4 Altered corundum-bearing amphibolite (a, b) present primary ruby deposits in Montepuez, Mozambique.

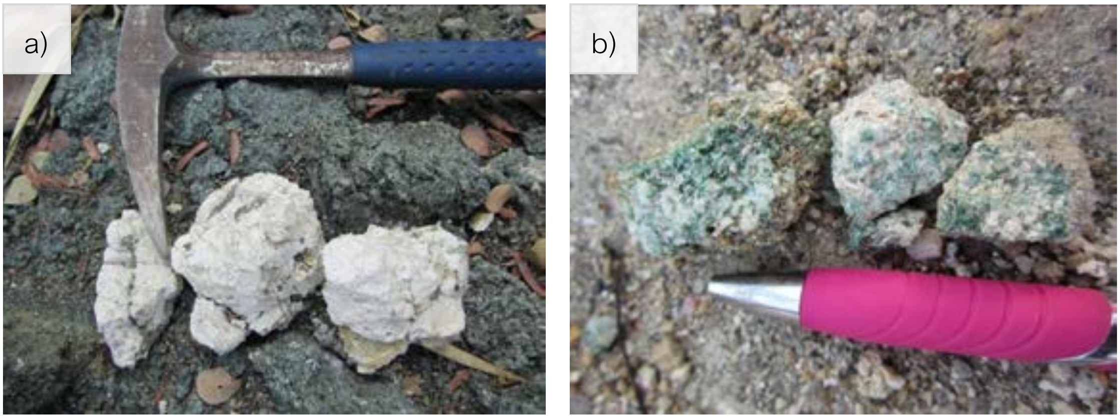

Figure 3.5 Altered amphibolite containing clay mineral (a) and green mica (b) are commonly related to ruby (pink sapphire) formation.

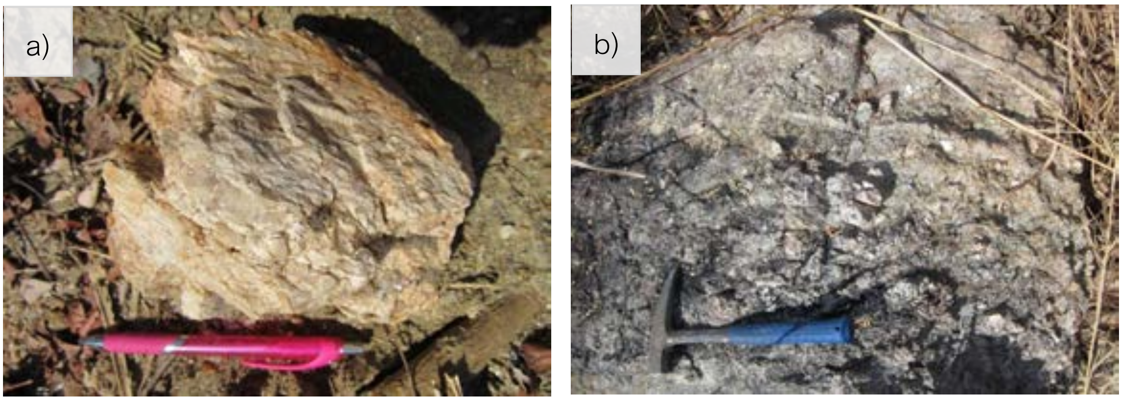

Figure 3.6 Coarse-grained quartz and feldspar pegmatite (a, b) are commonly associated with altered ruby-bearing amphibolite.

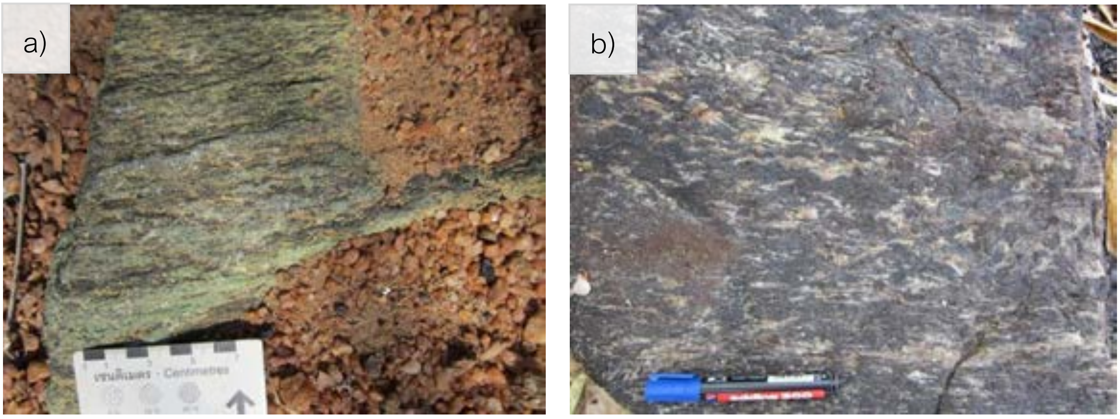

Figure 3.7 Corundum-barren amphibolite (a, b) found in the study area, Montepuez, Mozambique.

Other Metamorphic Rocks

Other metamorphic rocks consist of gneiss, migmatite and marble which formed as common basement rocks in this area. They are normally exposed as extensive outcrops over 30 meters (see Figures 3.8-3.11).

Gneiss is composed of 3 main units based on geologic map (Ministry of Mineral Resources of Mozambique, 2005) which can also be discovered in corundum mining area (Figure 3.1). They are characterized by biotite gneiss (Figure 3.8), quartzitic gneiss (Figure 3.9) and granitic gneiss (Figure 3.10).

Biotite gneiss is commonly characterized by coarse-grained plagioclase, biotite, quartz, K-feldspar and garnet. It shows clearly black and white layers. White layer contains mainly quartz, plagioclase, K-feldspar and garnet whereas black layer contains biotite, amphibole and garnet (Figure 3.8).

Quartzitic gneiss is characterized by coarse-grained K-feldspar, plagioclase, quartz and biotite. It shows white layer of K-feldspar, plagioclase, quartz and black layer of biotite (Figure 3.9).

Granitic gneiss is characterized by medium-grained K-feldspar, plagioclase, quartz, biotite and garnet. It shows clearly white layer of K-feldspar, plagioclase, quartz and black layer of biotite and garnet (Figure 3.10).

Most gneiss groups usually show folding indicating strong deformation. Moreover, some outcrops partly contain migmatite (Figure 3.11).

Marble is characterized significantly by coarse-grained calcite (Figure 3.11). It has exposed specifically in some locations.

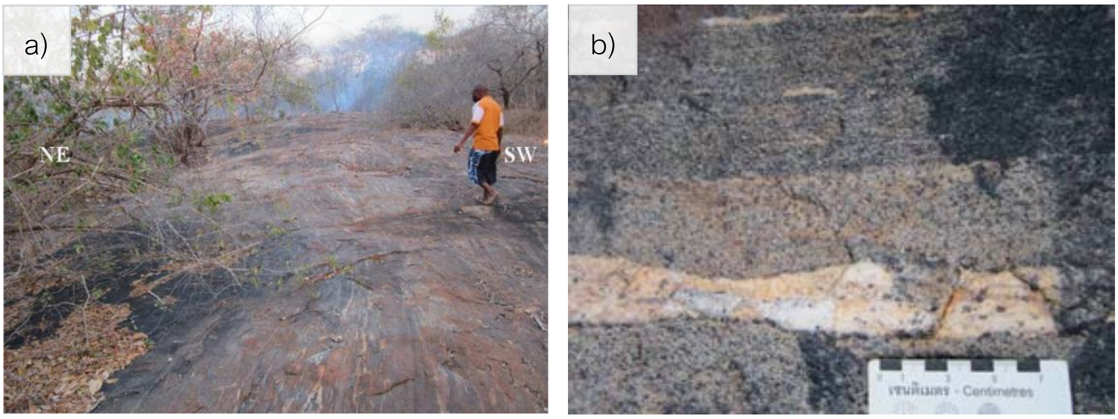

Figure 3.8 Outcrop exposures of biotite gneiss (a) showing foliation of biotite gneiss (b).

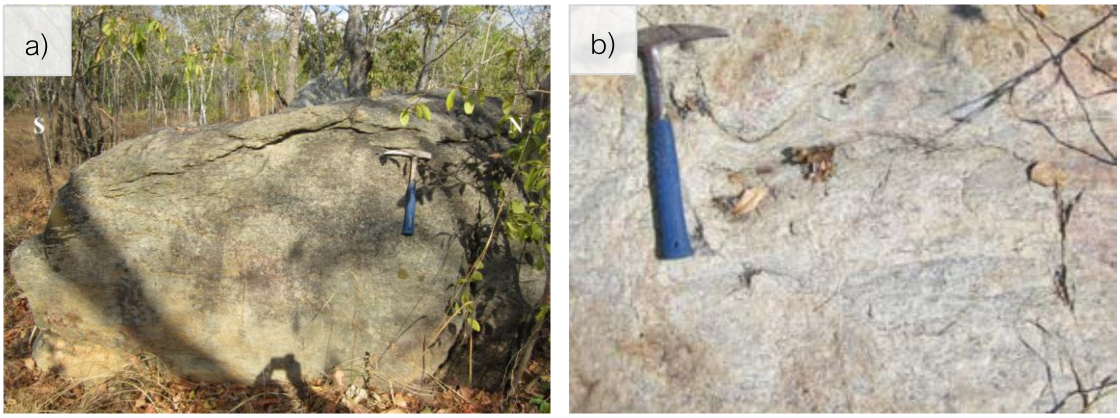

Figure 3.9 Outcrop exposures of quartzitic gneiss (a) showing foliation of quartzitic gneiss (b).

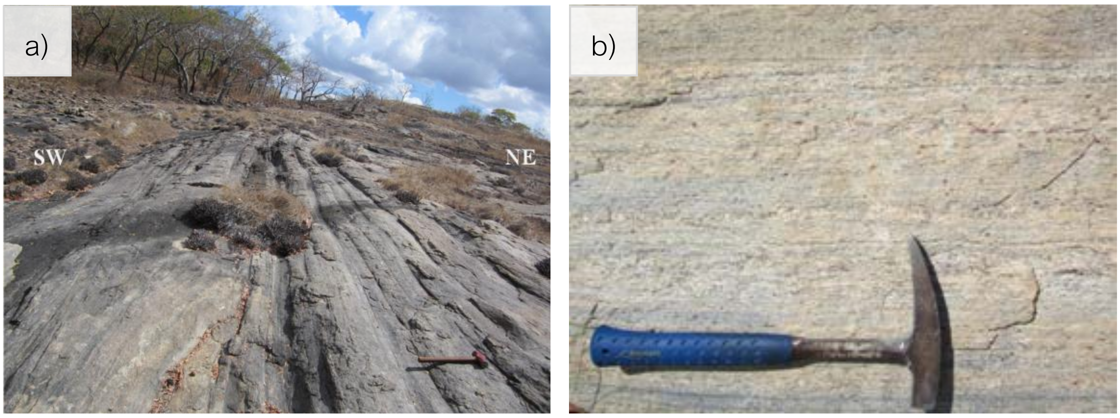

Figure 3.10 Outcrop exposures of granitic gneiss (a) showing foliation of granitic gneiss (b).

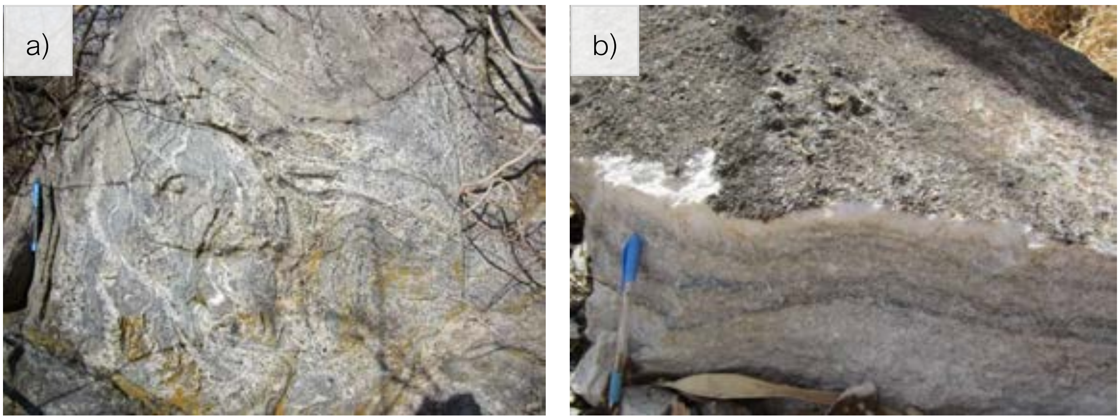

Figure 3.11 Outcrop exposures of other metamorphic rocks showing migmatite feature (a) and marble (b).

3.3 Petrographic Description

Corundum-bearing amphibolite, altered corundum-bearing amphibolite, corundum-barren amphibolite and gneiss are found in study area, as reported in section 3.2 (Figure 3.12). However, only four samples of corundum-bearing amphibolite (i.e., MBQ-8-8-1, MBQ-8-8-2, MBQ-9-1-3, MBQ-9-1-4), six samples of corundum-berren amphibolite (i.e., MBQ-8-1-1, MBQ-8-2-2, MBQ-8-4-4, MBQ-8-9-1, MBQ-8-9-3, MBQ-9-2-1), and six samples of gneiss including biotite gneiss (MBQ-5-2-3), quartzitic gneiss (MBQ-8-7-1 and MBQ-8-3-1) and granitic gneiss (MBQ-6-3-14, MBQ-6-3-13 and MBQ-6-3-5) were selected for this study and their photos are shown in Appendix A. Their representatives are shown in Figure 3.12. All samples were slab cut prior to rough classification. Subsequently, they were prepared as thin sections and polished thin sections. Petrographic descriptions of all rock samples are reported in Appendix B and summarized below.

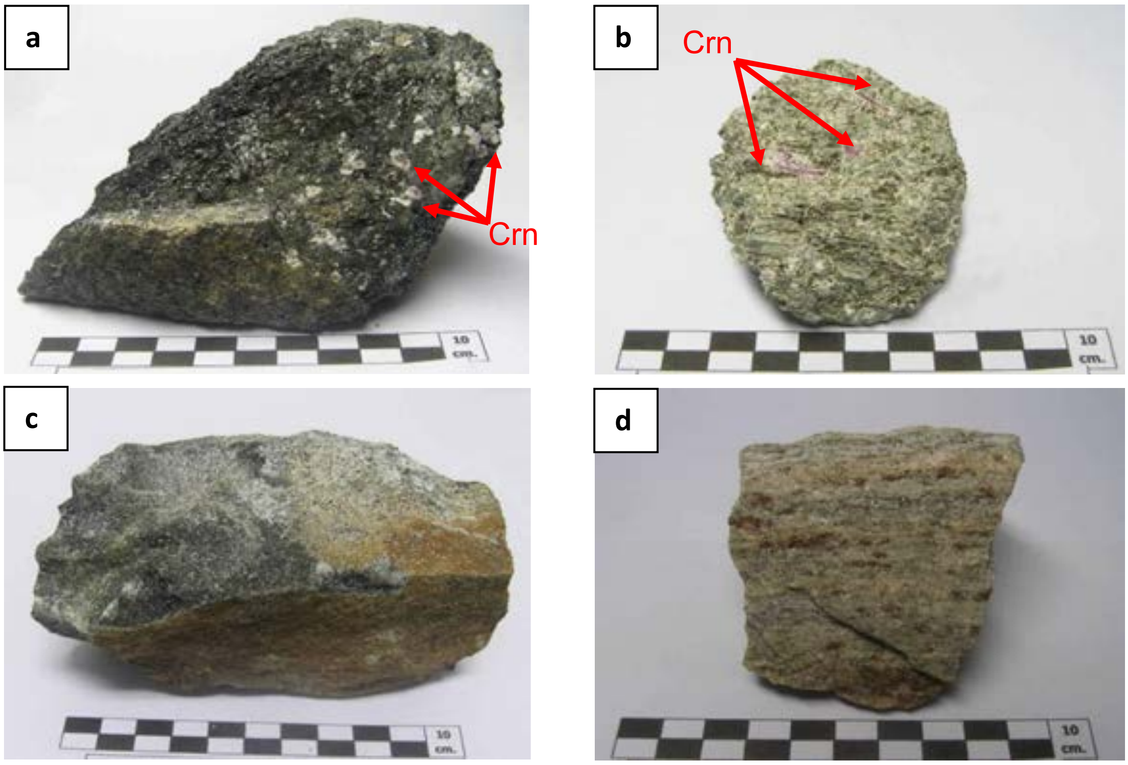

Figure 3.12 Representative specimens of corundum-bearing amphibolite (a), altered corundum-bearing amphibolite (b), corundum-barren amphibolite(c) and gneiss sample (d).

Corundum-bearing Amphibolite

Corundum-bearing amphibolite (Figure 3.12) is often exposed in Montepuez, northeastern Mozambique (Viola et al., 2008, Bingen et al., 2009, Boyd et al., 2010). They are associated with corundum formation (Muhongo, 1999, Schwarz et al., 2008) and composed of amphibole, plagioclase, spinel and corundum. They usually show foliations that approximately range from 0.5 to 1 cm across. The corundum-bearing amphibolite has various colors usually ranging from black to greenish black with pink or red spot of corundum (pink sapphire or ruby, respectively).

Microscopically, corundum-bearing amphibolite is normally characterized by coarse-grained granoblastic texture and typically exhibits 120^{O} triple junctions. The grain sizes of mineral assemblages generally range from 0.5-1 mm. These minerals are characterized essentially by amphibole, plagioclase and spinel with less abundance of garnet and mica (Figures 3.13 and 3.14). Corundum (about 5% mode) usually forms euhedral to subhedral crystals with various sizes of about 1 mm-1 cm. The bigger grains are typical porphyrotoblasts (see Figures 3.13). Amphibole (70-80% mode) is the most abundant phase of this rock type. It commonly forms euhedral to subhedral nematoblastic crystals with various sizes about 0.5-4 mm long (Figures 3.13 and 3.14). Plagioclase, approximate 10-15% mode, usually forms subhedral to anhedral granoblastic crystals with average grain size of about 0.5-1 mm. (Figures 3.13). Plagioclases are always surrounded by spinel that is a crucial feature observed in this rock. Spinel, mostly anhedral crystals, is generally found as fine grains with average sizes of about 0.2-0.5 mm surrounding granoblastic plagioclase (Figures 3.13). Its low proportion is approximate 5-10% mode.

Petrographic character of corundum-bearing amphibolite shows higher abundance of amphibole than those of corundum-barren amphibolite. On the other hand, low abundance of plagioclase and spinel is obviously recognized.

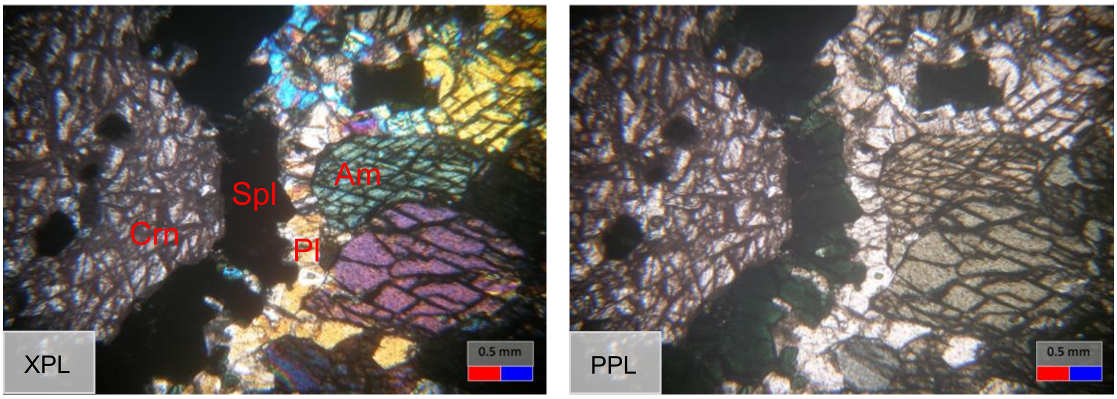

Figure 3.13 Photomicrographs (under cross-polarized light=XPL, under plane-polarized light=PPL) of corundum-bearing amphibolite (sample no. MBQ-9-1-4) showing a corundum (Crn) porphyroblast surrounded by tiny crystals of spinel (Spl) and plagioclase (Pl) with amphibole (Am) granoblasts.

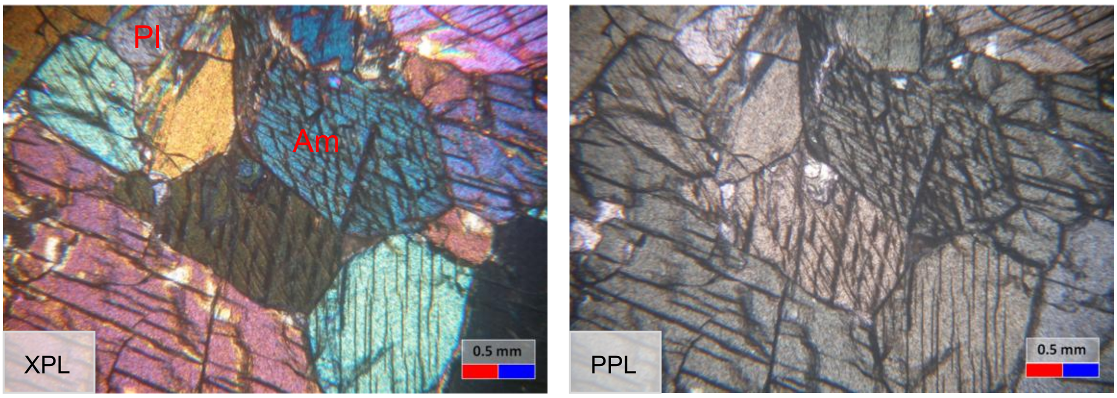

Figure 3.14 Photomicrographs (under cross-polarized light=XPL, under plane-polarized light=PPL) of corundum-bearing amphibolite (sample no. MBQ-8-8-2) showing granoblastic texture of amphibole (Am) and plagioclase (Pl) with typical triple junctions.

Corundum-barren Amphibolite

Corundum-barren amphibolite (Figure 3.12) is normally composed of amphibole, plagioclase and spinel ranging in sizes from 0.5 to 2 cm. Moreover, foliations are commonly observed in this rock type.

Microscopically, it is characterized by fine- to coarse-grained granoblastic texture exhibiting typical 120^{O} triple junctions. Mineral grain sizes generally range from 0.5-1 mm. The main mineral assemblages are mostly composed of amphibole, plagioclase and spinel (Figures 3.15, and 3.16). Amphibole (about 50 to 60% mode) commonly forms subhedral to anhedral nematoblasts with an average length of about 0.5-1 mm; besides, some amphibole porphyroblasts are also observed. Plagioclase (approximately 30-40% mode) is characterized by subhedral to anhedral granoblast with an average grain sizes of about 0.5-1 mm. Spinel (about 10% mode) generally forms anhedral granoblastic grains with an average grain size of about 0.2-0.5 mm (Figure 3.16).

Petrographic character of corundum-barren amphibolite shows higher abundance of plagioclase and spinel than those of corundum-barren amphibolite; on the other hand, lower abundance of amphibole is observed clearly.

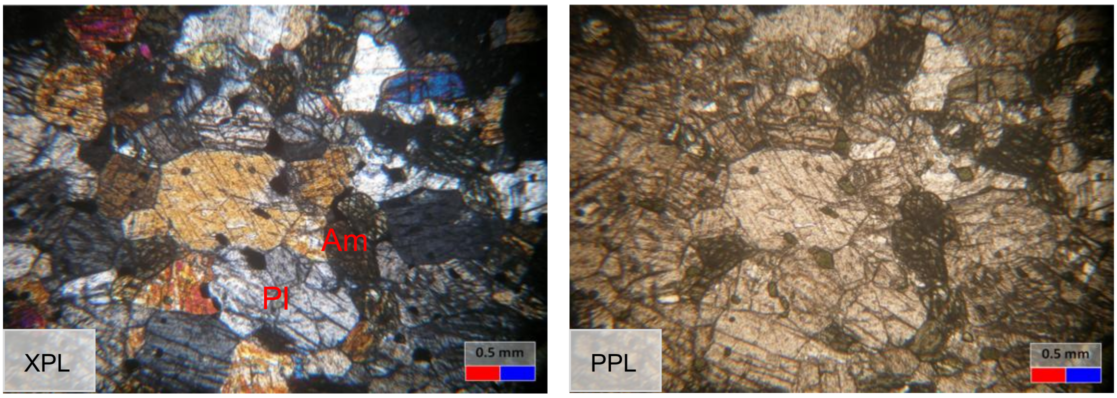

Figure 3.15 Photomicrographs (under cross-polarized light=XPL, under plane-polarized light=PPL) of corundum-barren amphibolite (sample no. MBQ-8-9-1) showing triple junction and granoblastic texture of amphibole (Am) and plagioclase (Pl).

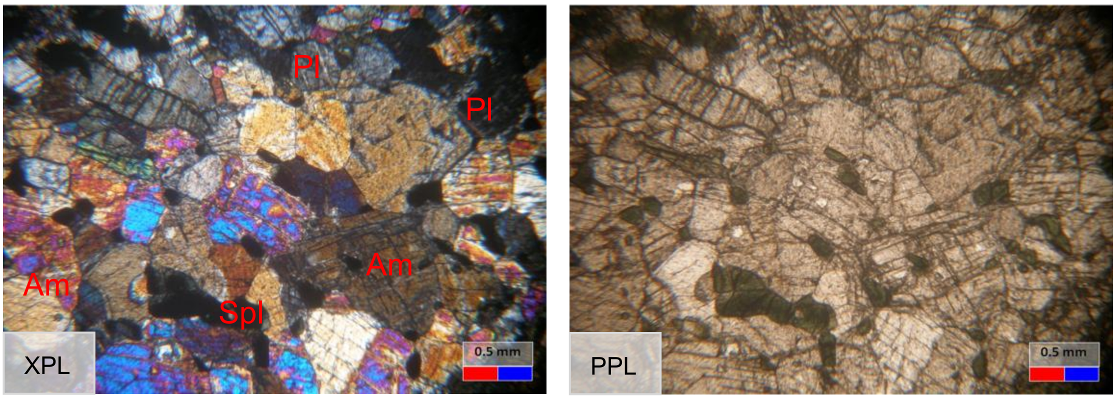

Figure 3.16 Photomicrographs (under cross-polarized light=XPL, under plane-polarized light=PPL) of corundum-barren amphibolite (sample no. MBQ-8-9-3) showing granoblastic texture of plagioclase (Pl) and amphibole (Am) with accessory of irregular anhedral spinel (Spl).

Gneiss

Gneiss is commonly found as the main part of Montepuez Complex (Viola et al., 2008, Bingen et al., 2009, Boyd et al., 2010). It is generally characterized by biotite gneiss, quartzitic gneiss and granitic gneiss. Foliations ranging between 0.5 and 30 cm thick (Figure 3.12) are commonly observed. Garnet porphyroblasts, up to 0.5 cm in diameter, associate with biotite, microcline and plagioclase.

Microscopically, gneiss is characterized by medium- to coarse-grained granoblastic texture comprising plagioclase, microcline, biotite, quartz, amphibole and opaque minerals (Figures 3.17, 3.18 and 3.19). Most samples usually exhibit 120° triple junctions of grain boundaries. These minerals generally range from 0.5-1 mm in size; on the other hand, garnet porphyroblasts may reach several centimeters in diameter. Plagioclase (about 10 to 15% mode) forms subhedral to anhedral grains and exhibits albite twins, generally less than 1 mm in diameter (Figures 3.17-3.18). K-feldspar, mainly microcline about 40 to 50% (Figures 3.17 and 3.19), always shows subhedral to anhedral grains usually exhibiting tartan twin. Its grain sizes are about 0.5-1.5 mm. Biotite usually forms lepidoblastic texture (Figures 3.17, 3.18 and 3.19) as subhedral grains. It contains about 10-20% mode and has average grain size of about 0.5-1 mm.

Quartz (about 5-10% mode) is present anhedral grain with size of about 0.1-0.5 mm forming granoblastic texture (Figures 3.17 and 3.18). Garnet (about 5 %) generally forms subhedral to anhedral porphyroblasts (Figure 3.18) with average size of 1-3 mm.

Amphibole (5-10 % mode) is rarely found related to garnet porphyroblast (Figure 3.18) in some samples. It presents as anhedral grain approximately ranging from 1-3 mm.

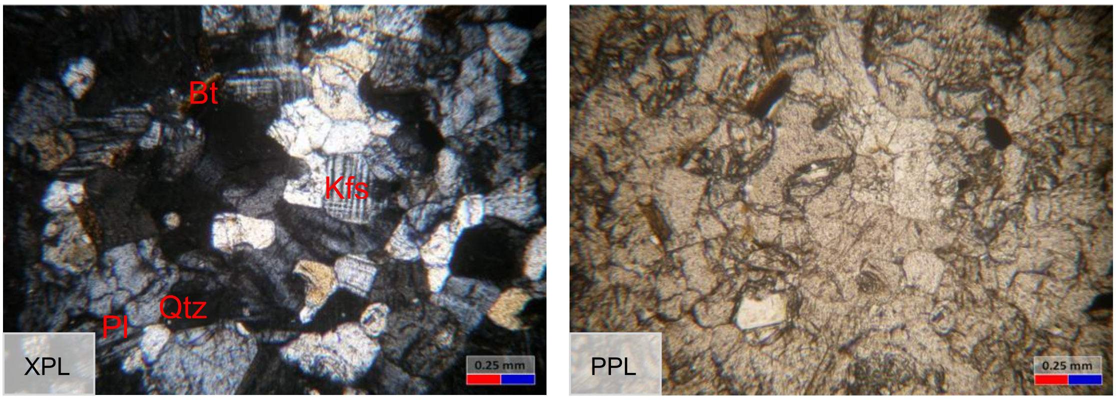

Figure 3.17 Photomicrographs (under cross-polarized light=XPL, under plane-polarized light=PPL) of granitic gneiss (sample no. MBQ-6-3-5) showing granoblastic texture and triple junction of plagioclase (Pl), K-feldspar (Kfs), Biotite (Bt), and Quartz (Qtz).

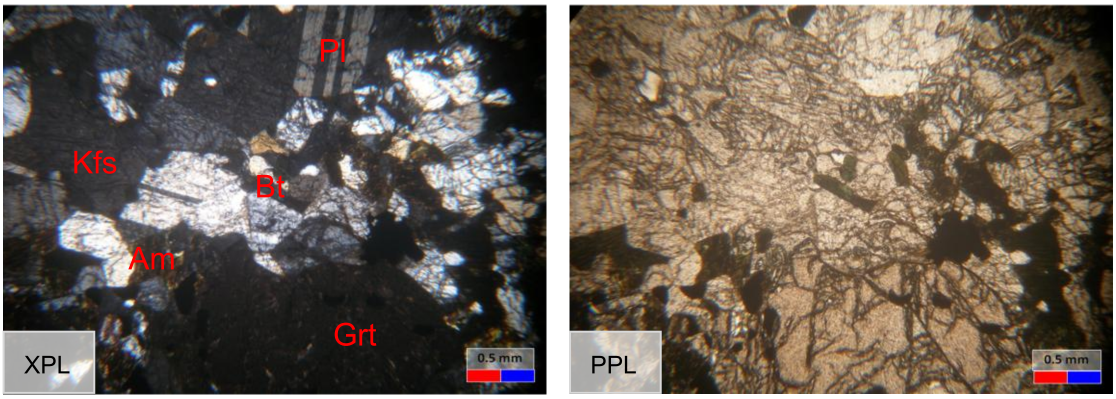

Figure 3.18 Photomicrographs (under cross-polarized light=XPL, under plane-polarized light=PPL) of biotite gneiss (sample no. MBQ-5-2-3) showing porphyroblastic texture of garnet (Grt), granoblastic texture of quartz (Qtz), K-feldspar (Kfs), plagioclase (Pl), amphibole (Am) and lepidoblastic texture of biotite (Bt).

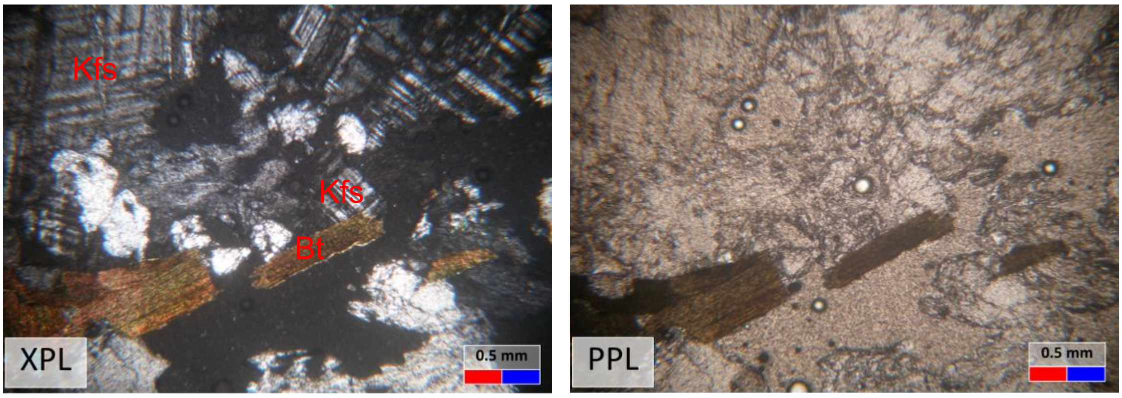

Figure 3.19 Photomicrographs (under cross-polarized light=XPL, under plane-polarized light=PPL) of quartzitic gneiss (sample no. MBQ-8-3-1) showing granoblastic texture of K-feldspar (Kfs) and lepidoblastic texture of biotite (Bt).

CHAPTER IV
WHOLE-ROCK GEOCHEMISTRY AND MINERAL CHEMISTRY

4.1 Introduction

Based on field evidences and petrographic features of sample collection under this study, three major rock units can be grouped as corundum-bearing amphibolite, corundum-barren amphibolite and gneissic rocks. Alteration has been recognized in some corundum-bearing amphibolite samples. That would affect significantly on their geochemistry. Total nineteen samples were selected and prepared for whole-rock analyses of major and minor oxides, trace and rare earth elements using XRF, ICP-OES and ICP-MS, respectively. Detail of these analytical techniques were reported in Chapter 1. Moreover, mineral chemistry of main assemblages including corundum, amphibole, feldspar, spinel, and garnet were carried out using thirty polished thin sections by Electron Probe Micro Analyzer (EPMA). Whole-rock geochemistry and mineral chemistry are then reported herein this chapter 4.

4.2 Whole-Rock Geochemistry

Nineteen rock samples including five corundum-bearing amphibolites, four altered corundum-bearing amphibolites, five corundum-barren amphibolites, and five gneisses were analyzed and summarized in Table 4.1.

4.2.1 Major and Minor Oxides

Corundum-Bearing Amphibolite: consists of samples MBQ-8-8-1, MBQ-8-8-2, MBQ-9-1-2, MBQ-9-1-3, and MBQ-9-1-4. These rocks vary in whole-rock chemical compositions between 41.32 – 44.62% SiO_2 (av. 43.23%), 0.24 – 0.35% TiO_2 (av. 0.29%), 14.99 – 17.92% Al_2O_3 (av. 16.23%), 4.82 – 7.45% Fe_2O_3 (av. 5.87%), 2.11 – 4.47% FeO (av. 3.25%), 0.15 – 0.39% MnO (av. 0.20%), 12.69 – 14.82% MgO (av. 13.83%), 11.84 – 14.57% CaO (av. 13.41%), 1.24 – 1.27% Na_2O (av. 1.25%), 0.40 – 0.51% K_2O (av. 0.44%), and $<$ 0.05% P_2O_5 (av. 0.03%).

Altered Corundum-Bearing Amphibolite: consists of samples MBQ-8-5-1, MBQ-8-5-2, MBQ-8-5-3, and MBQ-8-5-8. These rocks vary in compositions between 45.52 – 46.54% SiO_2 (av. 46.03%), 0.10 – 0.42% TiO_2 (av. 0.22%), 13.71 – 16.17% Al_2O_3 (av. 14.67%), 2.97 – 7.23% Fe_2O_3 (av. 5.42%), 0.75 – 1.59% FeO (av. 1.09%), 0.03 – 0.13% MnO (av. 0.08%), 14.50 – 19.08% MgO (av. 16.11%), 3.70 – 5.25% CaO (av. 4.62%), 0.22 – 0.85% Na_2O (av. 0.49%), 0.06 – 0.23% K_2O (av. 0.12%), and <0.2% P_2O_5 (av. 0.05%).

Corundum-Barren Amphibolite: samples include MBQ-8-1-1, MBQ-8-2-2, MBQ-8-4-4, MBQ-8-9-1, and MBQ-9-2-1. They vary in compositions between 43.45 – 49.53% SiO_2 (av. 45.00%), 0.15 – 0.33% TiO_2 (av. 0.23%), 5.15 – 25.98% Al_2O_3 (av. 18.00%), 2.73 – 3.82% Fe_2O_3 (av. 3.24%), 0.43 – 4.35% FeO (av. 1.91%), 0.04 – 0.14% MnO (av. 0.09%), 6.34 – 28.10% MgO (av. 14.70%), 5.47 – 19.05% CaO (av. 13.15%), 0.41 – 0.72% Na_2O (av. 0.58%), 0.07 – 0.54% K_2O (av. 0.25%),and <0.05% P_2O_5 (av. 0.02%).

Gneiss: samples, MBQ-5-2-3, MBQ-8-7-1, MBQ-8-3-1, MBQ-6-3-13, and MBQ-6-3-5 vary in compositions between 54.81 – 74.85% SiO_2 (av. 69.13%), 0.05 – 1.51% TiO_2 (av. 0.43%), 14.20 – 16.09% Al_2O_3 (av. 14.81%), 0.05 – 3.44% Fe_2O_3 (av. 1.18%), 0.11 – 7.27% FeO (av. 1.67%), 0.02 – 0.21% MnO (av. 0.08%), 0.56 – 2.56% MgO (av. 1.33%), 0.13 – 8.15% CaO (av. 2.39%), 2.25 – 5.36% Na_2O (av. 3.74%), 0.34 – 7.54% K_2O (av. 4.06%), and <1% P_2O_5 (av. 0.23%). In general, gneiss has different major oxides ranging within the compositional range of amphibolite.

Variation diagrams show plots of other major oxides against wt% of MgO/(MgO+FeO) (Figures 4.1 and 4.2) (as suggested by Rollinson, 1993). Each rock unit shows different trends. Amphibolite shows negative correlation between MgO/(MgO+FeO) and some major oxides particularly TiO_2, Fe_2O_3, MnO and K_2O whereas SiO_2 shows positive correlation. Al_2O_3, Na_2O and CaO show unclearly correlation (Figure 4.1).

Gneiss shows negative correlation between MgO/(MgO+FeO) against some major oxides particulalrly TiO_2, Al_2O_3, Fe_2O_3, MnO, MgO and CaO whereas SiO_2 and K_2O show positive correlation. Na_2O show unclearly correlation (Figure 4.2).

In general, major compositions of amphibolites have a narrow range of SiO_2 contents (41.32-49.53%). In general, however, corundum-bearing amphibolites appear to have high Al_2O_3, CaO and MgO contents which yield corundum occurrences within abundant amphibole, low amounts of plagioclase and spinel. On the other hand, main corundum-barren amphibolites appear to have higher Al_2O_3, CaO contents but lower MgO contents than those of corundum-bearing amphibolite that may be result of more abundance of plagioclase with less amount of spinel.

Table 4.1 Representative analyses of major oxides (weight %) trace and rare earth elements (ppm).

Lithology:	Corundum-bearing amphibolite					Altered corundum-bearing amphibolite			
Sample:	MBQ-8-8-1	MBQ-8-8-2	MBQ-9-1-2	MBQ-9-1-3	MBQ-9-1-4	MBQ-8-5-1	MBQ-8-5-2	MBQ-8-5-3	MBQ-8-5-8
SiO_2	42.71	44.14	43.34	44.62	41.32	46.42	45.65	45.52	46.54
TiO_2	0.25	0.24	0.33	0.35	0.27	0.42	0.10	0.24	0.12
Al_2O_3	17.92	17.32	14.99	15.24	15.68	14.36	13.71	14.42	16.17
Fe_2O_3	6.31	5.42	4.82	5.34	7.45	7.23	2.97	5.71	5.79
FeO	3.27	2.11	3.35	3.03	4.47	1.59	1.07	0.75	0.95
MnO	0.16	0.16	0.39	0.15	0.15	0.13	0.03	0.07	0.09
MgO	13.13	12.69	14.50	13.99	14.82	14.50	19.08	16.14	14.73
CaO	13.19	14.57	13.66	13.79	11.84	5.25	3.70	4.85	4.69
Na_2O	1.26	1.24	1.24	1.26	1.27	0.33	0.22	0.55	0.85
K_2O	0.43	0.44	0.43	0.40	0.51	0.23	0.06	0.07	0.10
P_2O_5	0.03	0.00	0.04	0.04	0.03	0.02	0.00	0.18	0.00
LOI	1.01	0.88	1.30	1.31	1.42	8.89	12.90	11.40	9.63
Total	**99.68**	**99.21**	**98.37**	**99.50**	**99.23**	**99.37**	**99.49**	**99.90**	**99.66**
Elements (ppm)									
Ba	33.10	30.60	32.60	32.30	36.30	70.60	43.40	23.10	21.10
Cr	630.00	370.00	510.00	270.00	1120.00	1170.00	3750.00	2140.00	2590.00
Cu	10.00	<5	<5	6.00	32.00	25.00	7.00	<5	<5
Li	20.00	10.00	20.00	20.00	20.00	30.00	40.00	30.00	40.00
Ni	261.00	226.00	264.00	311.00	243.00	609.00	502.00	448.00	429.00
Sc	8.00	7.00	9.00	7.00	8.00	8.00	<5	<5	<5
Sr	169.00	259.00	217.00	221.00	104.00	94.60	71.10	241.00	197.00
V	70.00	69.00	83.00	81.00	75.00	51.00	37.00	32.00	33.00
Zn	438.00	63.00	56.00	57.00	833.00	61.00	55.00	60.00	41.00
Bi	0.20	<0.1	0.20	0.30	0.40	0.20	0.10	0.10	0.10
Cd	0.30	0.20	0.30	0.30	0.20	0.20	0.30	<0.2	<0.2
Ce	8.60	5.50	10.10	11.00	13.00	23.70	7.80	15.60	10.20
Co	78.70	81.70	74.80	89.10	99.40	88.80	74.60	65.60	78.50
Cs	0.50	0.60	0.30	0.60	1.50	0.70	0.50	0.70	0.60
Dy	1.12	0.89	1.46	1.31	0.99	2.20	0.41	0.94	0.90
Er	0.57	0.51	0.76	0.69	0.57	1.20	0.23	0.53	0.45
Eu	1.54	0.56	0.81	0.81	1.48	0.73	0.52	0.65	0.79
Ga	16.00	13.00	14.00	14.00	18.00	14.00	11.00	13.00	12.00
Gd	1.19	1.04	1.84	1.46	1.16	2.33	0.45	1.06	0.84
Ge	1.00	1.00	2.00	2.00	2.00	1.00	1.00	1.00	2.00
Hf	<1	<1	<1	<1	<1	2.00	<1	<1	<1
Ho	0.20	0.18	0.28	0.25	0.19	0.45	0.07	0.17	0.17
In	<0.2	<0.2	<0.2	<0.2	<0.2	<0.2	<0.2	<0.2	<0.2
La	4.90	2.20	4.20	4.40	8.50	8.20	2.80	8.50	3.80
Lu	0.07	0.08	0.11	0.09	0.09	0.21	<0.05	0.08	0.08
Nb	1.00	<1	1.00	1.00	1.00	4.00	2.00	10.00	2.00
Nd	4.20	3.80	6.40	6.30	4.70	10.70	3.30	6.10	4.40
Pb	5.00	7.00	5.00	6.00	5.00	6.00	<5	7.00	6.00
Pr	0.99	0.85	1.39	1.46	1.31	2.67	0.98	1.80	1.20
Rb	5.20	4.90	3.90	4.50	9.70	13.00	2.60	4.80	3.40
Sb	0.30	<0.1	<0.1	0.20	0.30	0.10	0.20	4.50	0.20
Sm	1.00	1.00	1.60	1.50	1.00	2.10	0.50	1.10	0.90
Sn	3.00	2.00	2.00	3.00	4.00	2.00	2.00	2.00	3.00
Ta	<0.5	<0.5	<0.5	0.60	0.50	<0.5	<0.5	4.30	0.70
Tb	0.15	0.14	0.23	0.21	0.12	0.34	<0.05	0.13	0.11
Th	0.90	0.50	0.90	0.40	0.70	3.50	0.80	1.70	17.20
Tm	0.06	0.06	0.10	0.09	0.06	0.18	<0.05	0.07	0.07
U	0.61	0.23	0.67	0.61	1.20	0.67	0.42	0.58	2.30
W	203.00	175.00	203.00	310.00	270.00	115.00	42.00	88.00	154.00
Y	5.70	5.30	7.90	6.80	5.10	11.40	2.20	5.50	4.90
Yb	0.50	0.50	0.60	0.70	0.50	1.30	0.30	0.50	0.50
Zr	22.90	23.10	31.10	24.90	19.80	91.60	11.40	13.70	11.20

Table 4.1 Representative analyses of major oxides (weight %) trace and rare earth elements (ppm).

Lithology:	Corundum-barren amphibolite					Gneiss				
Sample:	MBQ-8-1-1	MBQ-8-2-2	MBQ-8-4-4	MBQ-8-9-1	MBQ-9-2-1	MBQ-5-2-3	MBQ-8-7-1	MBQ-8-3-1	MBQ-6-3-13	MBQ-6-3-5
SiO_2	43.92	44.06	44.04	43.45	49.53	54.81	74.85	74.09	73.88	68.03
TiO_2	0.33	0.24	0.24	0.15	0.19	1.51	0.09	0.05	0.13	0.35
Al_2O_3	22.63	25.98	10.61	25.64	5.15	16.09	14.20	14.39	14.58	14.77
Fe_2O_3	3.60	2.90	3.82	2.73	3.17	3.44	0.05	0.15	0.70	1.58
FeO	0.63	0.67	4.35	0.43	3.47	7.27	0.27	0.11	0.11	0.59
MnO	0.09	0.07	0.14	0.04	0.12	0.21	0.06	0.02	0.04	0.09
MgO	7.35	6.85	24.86	6.34	28.10	2.56	0.56	0.63	0.58	2.32
CaO	19.05	17.41	5.47	18.13	5.71	8.15	0.53	0.13	0.88	2.26
Na_2O	0.72	0.63	0.41	0.69	0.44	3.62	3.92	2.25	3.54	5.36
K_2O	0.29	0.27	0.09	0.54	0.07	0.34	4.49	7.54	4.65	3.27
P_2O_5	0.04	0.03	0.03	0.02	0.00	0.95	0.00	0.02	0.02	0.16
LOI	1.05	0.40	5.39	1.09	3.73	0.16	0.91	0.04	0.43	0.23
Total	99.68	99.49	99.46	99.25	99.68	99.10	99.93	99.42	99.53	99.02
Elements (ppm)										
Ba	140.00	87.20	77.80	157.00	0.50	105.00	654.00	4090.00	1090.00	708.00
Cr	1450.00	1900.00	1210.00	1340.00	1790.00	10.00	<10	<10	<10	<10
Cu	<5	<5	234.00	<5	44.00	25.00	<5	<5	<5	<5
Li	<10	<10	20.00	<10	<10	50.00	10.00	10.00	<10	<10
Ni	330.00	337.00	712.00	281.00	462.00	10.00	6.00	6.00	7.00	6.00
Sc	8.00	10.00	7.00	6.00	9.00	25.00	<5	<5	<5	<5
Sr	760.00	921.00	56.20	935.00	36.60	392.00	73.30	127.00	250.00	237.00
V	80.00	76.00	58.00	52.00	64.00	63.00	<5	<5	8.00	22.00
Zn	42.00	28.00	48.00	9.00	42.00	108.00	<5	<5	10.00	39.00
Bi	0.30	0.20	0.10	0.20	0.10	<0.1	<0.1	<0.1	<0.1	<0.1
Cd	0.30	0.30	<0.2	0.20	0.30	0.40	<0.2	<0.2	<0.2	0.30
Ce	8.80	5.20	5.10	4.20	6.80	33.60	85.50	69.70	43.60	84.40
Co	73.00	58.50	111.00	71.00	89.50	102.00	165.00	90.60	145.00	54.00
Cs	0.20	0.10	0.30	0.30	0.30	0.60	0.90	2.40	0.40	0.60
Dy	1.63	1.06	1.30	0.86	1.08	8.41	4.74	4.95	1.16	2.59
Er	0.94	0.60	0.67	0.50	0.63	4.93	2.25	2.81	0.46	1.23
Eu	0.74	0.53	0.44	0.55	0.19	2.11	1.53	0.92	1.04	1.12
Ga	17.00	16.00	11.00	18.00	7.00	23.00	18.00	18.00	16.00	19.00
Gd	1.62	1.27	1.59	0.97	1.13	7.95	5.12	5.42	2.12	3.99
Ge	2.00	1.00	1.00	2.00	1.00	2.00	2.00	2.00	1.00	1.00
Hf	<1	<1	<1	<1	1.00	5.00	3.00	2.00	4.00	6.00
Ho	0.34	0.21	0.25	0.16	0.23	1.83	0.82	0.99	0.17	0.51
In	<0.2	<0.2	<0.2	<0.2	<0.2	<0.2	<0.2	<0.2	<0.2	<0.2
La	4.50	2.40	5.40	2.00	2.80	15.70	41.30	50.50	23.80	43.70
Lu	0.14	0.10	0.09	0.06	0.09	0.73	0.39	0.43	0.06	0.18
Nb	<1	<1	<1	<1	1.00	25.00	10.00	9.00	3.00	5.00
Nd	5.90	3.70	5.80	3.00	3.90	21.80	32.50	29.80	17.60	32.00
Pb	18.00	18.00	<5	23.00	<5	5.00	22.00	46.00	18.00	16.00
Pr	1.42	0.79	1.36	0.67	0.94	4.74	9.72	9.24	5.06	9.31
Rb	5.50	3.10	2.50	9.20	2.00	16.10	192.00	404.00	77.20	60.20
Sb	0.20	<0.1	<0.1	<0.1	0.30	<0.1	0.10	<0.1	0.20	<0.1
Sm	1.40	0.90	1.30	0.80	1.00	6.10	7.00	5.50	2.90	5.10
Sn	1.00	<1	<1	<1	1.00	4.00	2.00	2.00	1.00	2.00
Ta	0.60	<0.5	<0.5	0.60	<0.5	5.60	2.70	1.80	2.00	0.90
Tb	0.25	0.14	0.19	0.11	0.16	1.27	0.87	0.83	0.21	0.49
Th	0.40	0.30	0.30	0.30	1.10	1.00	15.40	27.00	3.10	6.30
Tm	0.15	0.07	0.09	0.05	0.09	0.73	0.35	0.43	<0.05	0.19
U	0.10	0.06	0.15	0.17	1.18	0.55	1.61	3.23	0.25	0.44
W	287.00	180.00	72.00	330.00	100.00	666.00	1230.00	743.00	1040.00	421.00
Y	7.90	6.00	6.80	4.90	6.30	46.10	17.20	30.70	5.60	13.30
Yb	1.00	0.50	0.60	0.50	0.60	4.80	2.50	2.90	0.40	1.30
Zr	27.10	19.10	19.30	18.10	41.00	211.00	66.40	43.80	144.00	227.00

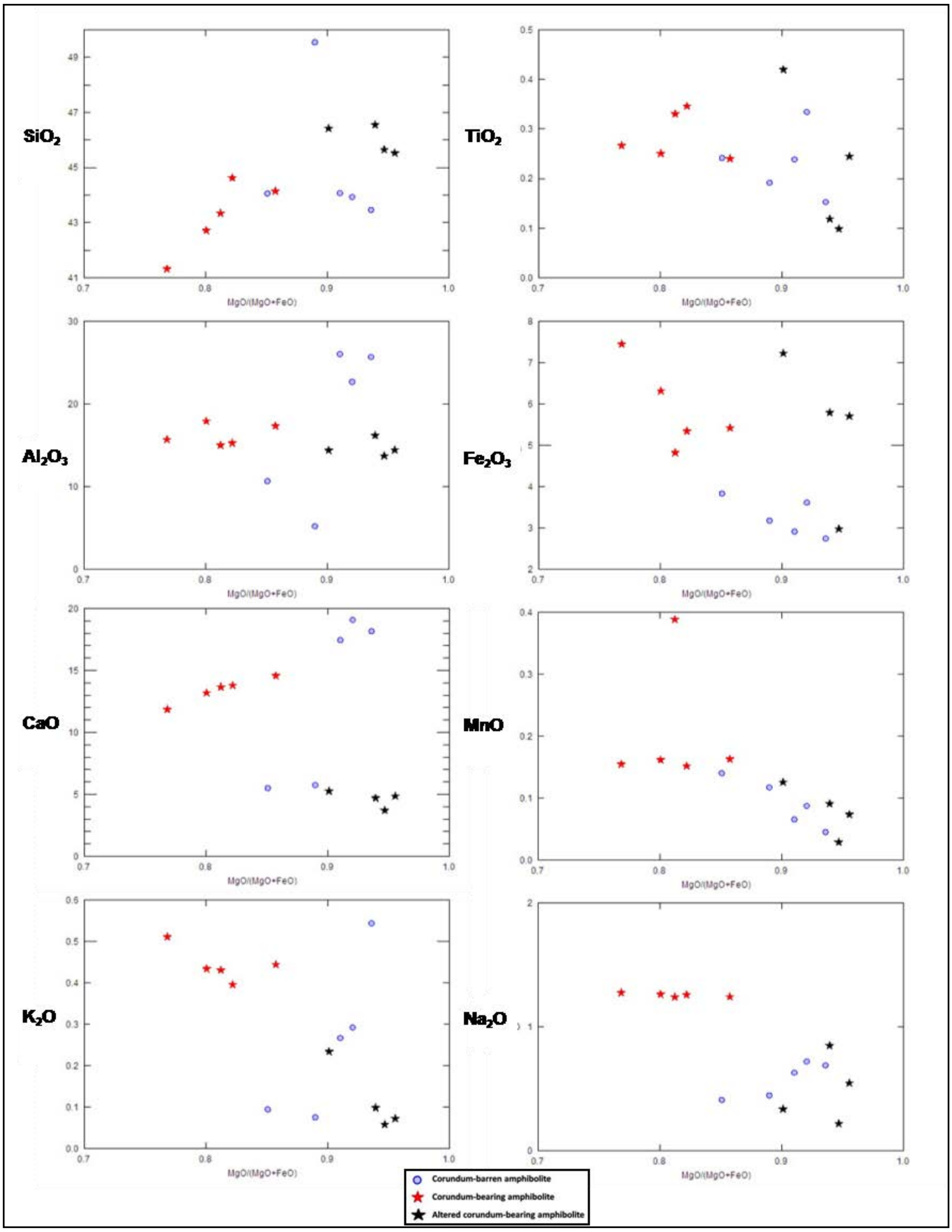

Figure 4.1 Variation diagram of major and minor oxides (wt %) versus MgO/(MgO+FeO) (wt %) of amphibolite.

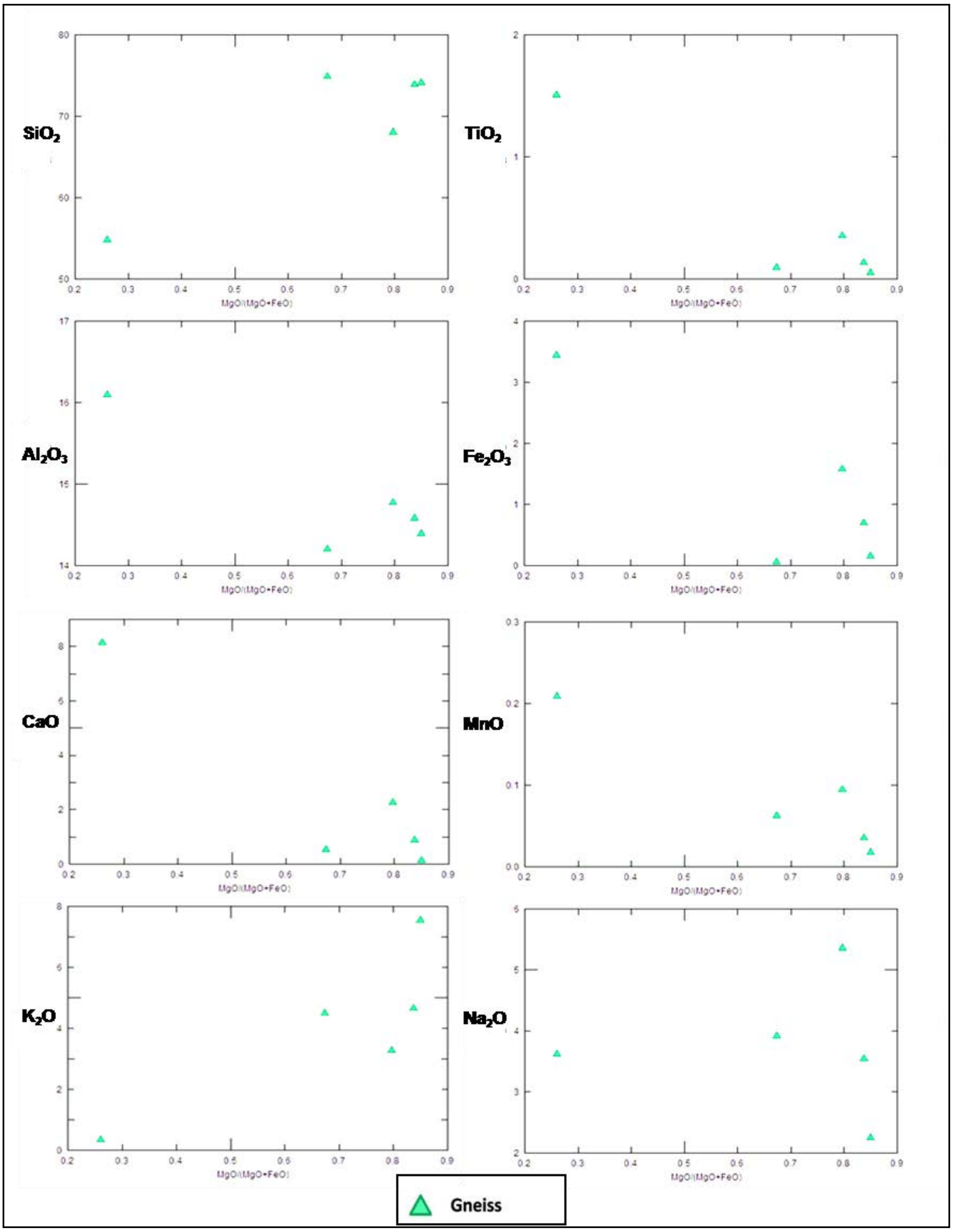

Figure 4.2 Variation diagram of major and minor oxides (wt %) versus MgO/(MgO+FeO) (wt %) of gneiss.

4.2.2 Trace Elements and Rare Earth Elements

Trace elements

Representative analyses of trace elements of high-grade metamorphic samples from Montepuez, northeastern Mozambique are summarized in Table 4.1 and all analyses are collected in Appendix A. The detailed descriptions of some crucial elements are given below.

Rubidium (Rb) contents vary from 3.90 to 9.70 ppm (av. 5.64 ppm) in corundum-bearing amphibolite, 2.60 to 13.00 ppm (av. 5.95 ppm) in altered corundum-bearing amphibolite, 2.00 to 9.20 ppm (av. 4.46 ppm) in corundum-barren amphibolite and 16.10 to 404.00 ppm (av. 149.90 ppm) in gneiss.

Strontium (Sr) contents vary from 104.00 to 259.00 ppm (av. 194.00 ppm) in corundum-bearing amphibolite, 71.10 to 241.00 ppm (av. 105.93 ppm) in altered corundum-bearing amphibolite, 36.60 to 935.00 ppm (av. 541.76 ppm) in corundum-barren amphibolite, and 73.30 to 392.00 ppm (av. 215.86 ppm) in gneiss.

Yttrium (Y) contents vary from 5.10 to 7.90 ppm (av. 6.16 ppm) in corundum-bearing amphibolite, 2.20 to 11.40 ppm (av. 6.00 ppm) in altered corundum-bearing amphibolite, 4.90 to 7.90 ppm (av. 6.38 ppm) in corundum-barren amphibolite and 5.60 to 46.10 ppm (av. 22.58 ppm) in gneiss.

Zircon (Zr) contents vary from 19.80 to 31.10 ppm (av. 24.36 ppm) in corundum-bearing amphibolite, 11.20 to 91.60 ppm (av. 31.98 ppm) in altered corundum-bearing amphibolite, 18.10 to 41.00 ppm (av. 24.92 ppm) in corundum-barren amphibolite and 43.80 to 227.00 ppm (av. 138.44 ppm) in gneiss.

Niobium (Nb) contents vary from <1.00 to 1.00 ppm (av. 1.00 ppm) in corundum-bearing amphibolite, 2.00 to 10.00 ppm (av. 4.50 ppm) in altered corundum-bearing amphibolite, <1.00 to 1.00 ppm (av. 1.00 ppm) in corundum-barren amphibolite and 3.00 to 25.00 ppm (av. 10.40 ppm) in gneiss.

Cesium (Cs) contents vary from 0.30 to 1.50 ppm (av. 0.70 ppm) in corundum-bearing amphibolite, 0.50 to 0.70 ppm (av. 0.63 ppm) in altered corundum-bearing amphibolite, 0.10 to 0.30 ppm (av. 0.24 ppm) in corundum-barren amphibolite and 0.40 to 2.40 ppm (av. 0.98 ppm) in gneiss.

Barium (Ba) contents vary from 30.60 to 36.30 ppm (av. 32.98 ppm) in corundum-bearing amphibolite, 21.10 to 70.60 ppm (av. 39.55 ppm) in altered corundum-bearing amphibolite, 0.50 to 157.00 ppm (av. 92.50 ppm) in corundum-barren amphibolite and 105.00 to 4090.00 ppm (av. 1329.40 ppm) in gneiss.

Hafnium (Hf) contents vary from <1.00 to <1.00 ppm (av. 0.00 ppm) in corundum-bearing amphibolite, <1.00 to 2.00 ppm (av. 2.00 ppm) in altered corundum-bearing amphibolite, <1.00 to 1.00 ppm (av. 1.00 ppm) in corundum-barren amphibolite and 2.00 to 6.00 ppm (av. 4.00 ppm) in gneiss.

Tantalum (Ta) contents vary from <0.50 to 0.60 ppm (av. 0.55 ppm) in corundum-bearing amphibolite, <0.50 to 4.30 ppm (av. 2.50 ppm) in altered corundum-bearing amphibolite, <0.50 to 0.60 ppm (av. 0.60 ppm) in corundum-barren amphibolite and 0.90 to 5.60 ppm (av. 2.60 ppm) in gneiss.

Lead (Pb) contents vary from 5.00 to 7.00 ppm (av. 5.60 ppm) in corundum-bearing amphibolite, <0.50 to 7.00 ppm (av. 6.33 ppm) in altered corundum-bearing amphibolite, <0.50 to 23.00 ppm (av. 19.67 ppm) in corundum-barren amphibolite and 5.00 to 46.00 ppm (av. 21.40 ppm) in gneiss.

Thorium (Th) contents vary from 1.00 to 27.00 ppm (av. 10.56 ppm) in gneiss, <0.30 to 1.10 ppm (av. 0.48 ppm) in corundum-barren amphibolite, 0.40 to 0.90 ppm (av. 0.68 ppm) in corundum-bearing amphibolite, and 0.80 to 17.20 ppm (av. 5.80 ppm) in altered corundum-bearing amphibolite.

Uranium (U) contents vary from 0.23 to 1.20 ppm (av. 0.66 ppm) in corundum-bearing amphibolite, 0.42 to 2.30 ppm (av. 0.99 ppm) in altered corundum-bearing amphibolite, 0.66 to 1.18 ppm (av. 0.33 ppm) in corundum-barren amphibolite and 0.25 to 3.23 ppm (av. 1.22 ppm) in gneiss.

The primitive mantle (composition by Sun and McDonough, 1989) normalized trace element patterns of corundum-bearing amphibolite, altered corundum-bearing amphibolite, corundum-barren amphibolite and gneiss are shown in Figure 4.3.

Chondrite (composition by Thompson, 1982) normalized trace element patterns of corundum-bearing amphibolite, altered corundum-bearing amphibolite, corundum-barren amphibolite and gneiss are shown in Figure 4.4.

MORB (Pearce, 1983) normalized incompatible element patterns of corundum-bearing amphibolite, altered corundum-bearing amphibolite, corundum-barren amphibolite and gneiss are shown in Figure 4.5.

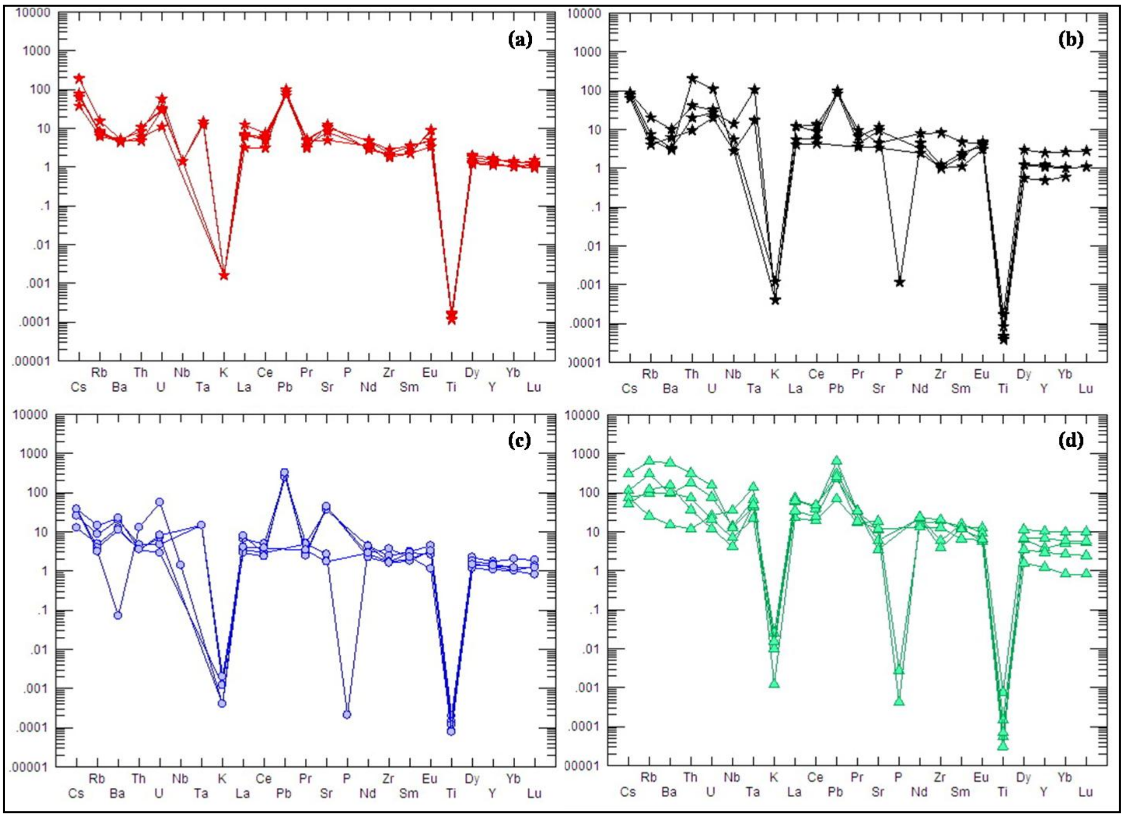

Figure 4.3 The primitive mantle-normalized incompatible element patterns of corundum-bearing amphibolite (a), altered corundum-bearing amphibolite (b), corundum-barren amphibolite (c) and gneiss (d) from Montepuez, NE Mozambique. The primitive mantle values are from Sun and McDonough (1989).

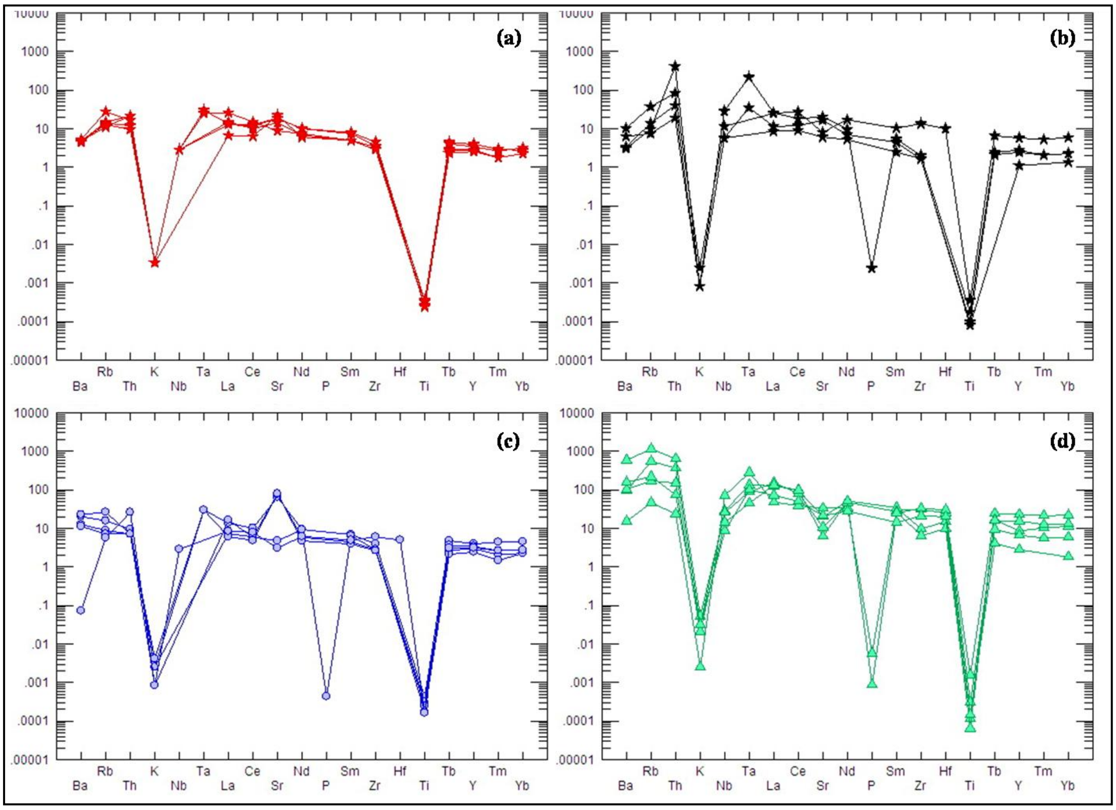

Figure 4.4 Chondrites-normalized incompatible element patterns of corundum-bearing amphibolite (a), altered corundum-bearing amphibolite (b), corundum-barren amphibolite (c) and gneiss (d) from Montepuez, NE Mozambique. The Chondrites values are from Thompson (1982).

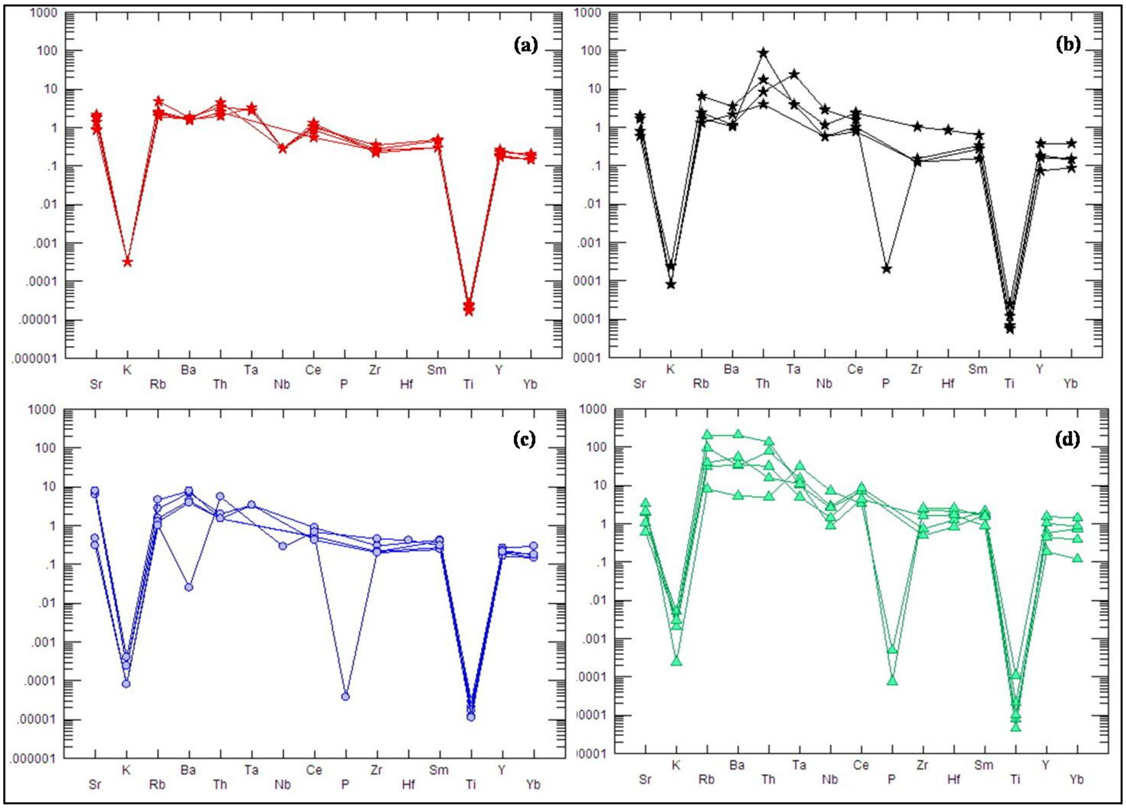

Figure 4.5 MORB-normalized incompatible element patterns of corundum-bearing amphibolite (a), altered corundum-bearing amphibolite (b), corundum-barren amphibolite (c) and gneiss (d) from Montepuez, NE Mozambique. The MORB values are from Pearce (1983).

Rare earth elements (REE) of samples are selectively present in Table 4.1. The detailed descriptions of some elements are given below.

Lanthanum (La) values range from 2.20 to 8.50 ppm (av. 4.84 ppm) in corundum-bearing amphibolite, 2.80 to 8.50 ppm (av. 5.83 ppm) in altered corundum-bearing amphibolite, 2.00 to 5.40 ppm (av. 3.42 ppm) in corundum-barren amphibolite and 15.70 to 50.50 ppm (av. 35.00 ppm) in gneiss.

Cerium (Ce) values range from 5.50 to 13.00 ppm (av. 9.64 ppm) in corundum-bearing amphibolite, 7.80 to 23.70 ppm (av. 14.33 ppm) in altered corundum-bearing amphibolite, 4.20 to 8.80 ppm (av. 6.02 ppm) in corundum-barren amphibolite and 33.60 to 85.50 ppm (av. 63.36 ppm) in gneiss.

Praseodymium (Pr) values range from 0.85 to 1.46 ppm (av. 1.20 ppm) in corundum-bearing amphibolite, 0.98 to 2.67 ppm (av. 1.66 ppm) in altered corundum-bearing amphibolite, 0.67 to 1.42 ppm (av. 1.04 ppm) in corundum-barren amphibolite and 4.74 to 9.72 ppm (av. 7.61 ppm) in gneiss.

Neodymium (Nd) values range from 3.80 to 6.40 ppm (av. 5.08 ppm) in corundum-bearing amphibolite, 3.30 to 10.70 ppm (av. 6.13 ppm) in altered corundum-bearing amphibolite, 3.00 to 5.90 ppm (av. 4.46 ppm) in corundum-barren amphibolite and 17.60 to 32.50 ppm (av. 26.74 ppm) in gneiss.

Samarium (Sm) values range from 1.00 to 1.60 ppm (av. 1.22 ppm) in corundum-bearing amphibolite, 0.50 to 2.10 ppm (av. 1.15 ppm) in altered corundum-bearing amphibolite, 8.80 to 1.40 ppm (av. 1.08 ppm) in corundum-barren amphibolite and 2.90 to 7.00 ppm (av. 5.32 ppm) in gneiss.

Europium (Eu) values range from 0.56 to 1.54 ppm (av. 1.04 ppm) in corundum-bearing amphibolite, 0.52 to 0.79 ppm (av. 0.67 ppm) in altered corundum-bearing amphibolite, 0.19 to 0.74 ppm (av. 0.49 ppm) in corundum-barren amphibolite and 0.92 to 2.11 ppm (av. 1.34 ppm) in gneiss.

Gadolinium (Gd) values range from 1.04 to 1.84 ppm (av. 1.34 ppm) in corundum-bearing amphibolite, 0.45 to 2.33 ppm (av. 1.17 ppm) in altered corundum-bearing amphibolite, 0.97 to 1.62 ppm (av. 1.32 ppm) in corundum-barren amphibolite and 2.12 to 7.95 ppm (av. 4.92 ppm) in gneiss.

Terbium (Tb) values range from 0.12 to 0.23 ppm (av. 0.17 ppm) in corundum-bearing amphibolite, <0.05 to 0.34 ppm (av. 0.19 ppm) in altered corundum-bearing amphibolite, 0.11 to 0.25 ppm (av. 0.17 ppm) in corundum-barren amphibolite and 0.21 to 1.27 ppm (av. 0.73 ppm) in gneiss.

Dysprosium (Dy) values range from 0.89 to 1.46 ppm (av. 1.15 ppm) in corundum-bearing amphibolite, 0.41 to 2.20 ppm (av. 1.11 ppm) in altered corundum-bearing amphibolite, 0.86 to 1.63 ppm (av. 1.19 ppm) in corundum-barren amphibolite and 1.16 to 8.41 ppm (av. 4.37 ppm) in gneiss.

Holmium (Ho) values range from 0.18 to 0.28 ppm (av. 0.22 ppm) in corundum-bearing amphibolite, 0.07 to 0.45 ppm (av. 0.22 ppm) in altered corundum-bearing amphibolite, 0.16 to 0.34 ppm (av. 0.24 ppm) in corundum-barren amphibolite and 0.17 to 1.83 ppm (av. 0.86 ppm) in gneiss.

Erbium (Er) values range from 0.51 to 0.76 ppm (av. 0.62 ppm) in corundum-bearing amphibolite, 0.23 to 1.20 ppm (av. 0.60 ppm) in altered corundum-bearing amphibolite, 0.50 to 0.94 ppm (av. 0.67 ppm) in corundum-barren amphibolite and 0.46 to 4.93 ppm (av. 2.34 ppm) in gneiss.

Thulium (Tm) values range from 0.06 to 0.10 ppm (av. 0.07 ppm) in corundum-bearing amphibolite, 0.07 to 0.18 ppm (av. 0.11 ppm) in altered corundum-bearing amphibolite, 0.05 to 0.15 ppm (av. 0.09 ppm) in corundum-barren amphibolite and 0.19 to 0.73 ppm (av. 0.43 ppm) in gneiss.

Ytterbium (Yb) values range from 0.50 to 0.70 ppm (av. 0.56 ppm) in corundum-bearing amphibolite, 0.30 to 1.30 ppm (av. 0.65 ppm) in altered corundum-bearing amphibolite, 0.50 to 1.00 ppm (av. 0.64 ppm) in corundum-barren amphibolite and 0.40 to 4.80 ppm (av. 2.38 ppm) in gneiss.

Lutetium (Lu) values range from 0.07 to 0.11 ppm (av. 0.09 ppm) in corundum-bearing amphibolite, 0.08 to 0.21 ppm (av. 0.12 ppm) in altered corundum-bearing amphibolite, 0.06 to 0.14 ppm (av. 0.10 ppm) in corundum-barren amphibolite and 0.06 to 0.73 ppm (av. 0.36 ppm) in gneiss.

These REE analyses are normalized by composition of chondrite (reported by Sun and McDonough, 1989) prior to pattern plots. The chondrite-normalized REE patterns of all rock types are present in Figure 4.6.

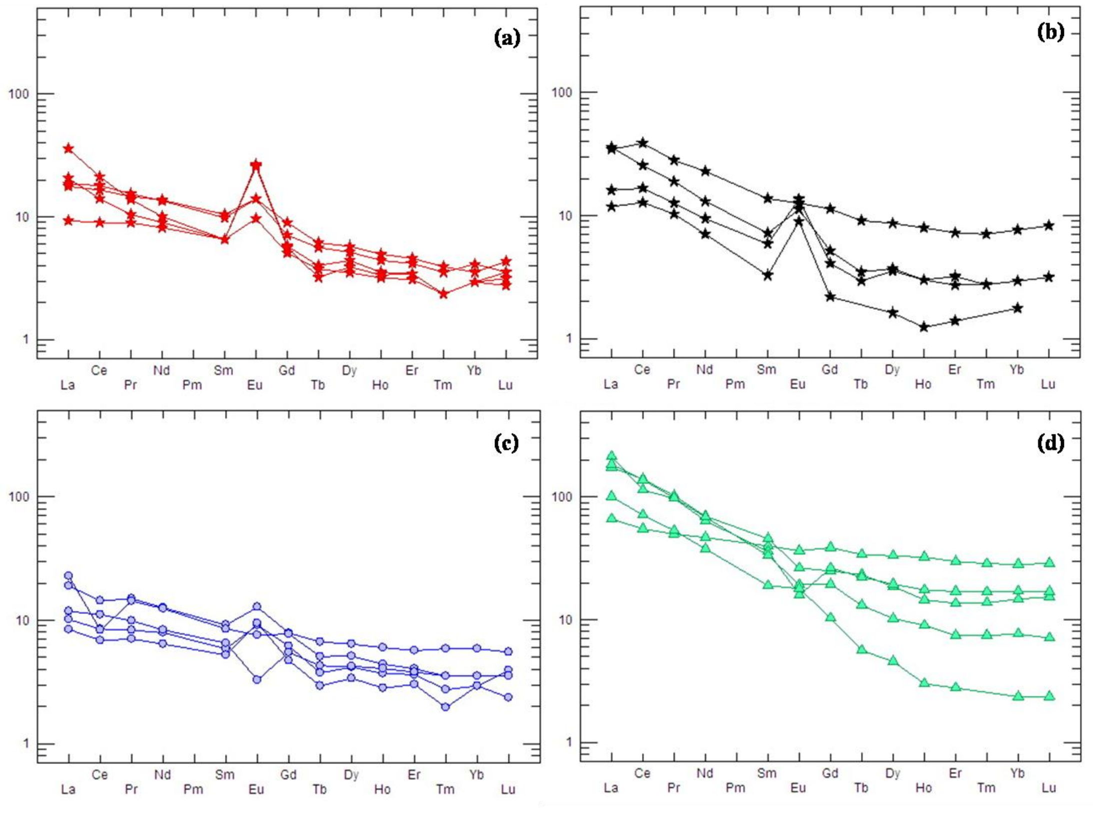

Figure 4.6 Chondrite-normalized REE patterns of corundum-bearing amphibolite (a), altered corundum-bearing amphibolite (b), corundum-barren amphibolite (c) and gneiss (d). The chondrite compositions are from Sun and McDonough (1989).

4.3 Mineral Chemistry

Mineral chemistry provides crucial information to understand the origin of corundum-bearing rocks and related rock units in Montepuez, Mozambique. As reported in sections 3.1, 3.2 and 4.1, many index minerals, particularly amphibole, feldspar, spinel, garnet, and corundum are often found in these rock units (Table 4.2). These minerals were also analyzed chemically for comparison. Mineral chemical analyses are then presented and described in this section.

Thirty two samples were selected and prepared as polished thin sections or polished sections for mineral chemical analyses using Electron Probe Analyzer (EPMA); detail procedure was reported in section 1.5. Seven polished thin sections of 6 gneiss samples, 6 polished thin sections of 5 corundum-barren amphibolite samples, 51 polished thin sections of 5 corundum-bearing amphibolite samples and 29 polished sections of 16 altered corundum-bearing amphibolite samples were analyzed. Representative analyses of mineral chemical compositions are summarized in Tables 4.3 to 4.9 and all selective data are collected in Appendix C.

Table 4.2 Major mineral assemblages found in various rock units. Note: XXX = significant found; XX = found; X = rarely found.

Rock units \ Mineral assemblages	Amphibole	Feldspar	Spinel	Garnet	Corundum
Corundum-bearing amphibolite	xxx	xx	xx	x	x
Altered Corundum-bearing amphibolite	xxx				x
Corundum-barren amphibolite	xxx	xxx	xxx	x	
Gneiss	x	xxx		x	

4.3.1 Amphibole

Amphibole is a common assemblage found in corundum-bearing amphibolite, altered corundum-bearing amphibolite and corundum-barren amphibolite; moreover, it is sometime found in gneiss. Amphiboles were analyzed prior to estimation of Fe^{3+} contents using equation of Doop (1987) as for calcic amphibole. Representatives of analytical data and their recalculated cations based on 23 oxygens are present in Table 4.3.

Amphiboles of corundum-bearing amphibolite comprise approximately 41% SiO_2, 17% Al_2O_3, 15-16% MgO, 14% CaO, 8-9% FeO_{total} and 2% Na_2O with atomic proportion of about 60-61% Mg and 39-40% Ca.

Amphiboles of altered corundum-bearing amphibolite contain about 44–45% SiO_2, 16–17% Al_2O_3, 14-16% MgO, 11% CaO, 9-10%FeO_{total} and <1% Na_2O. The main atomic proportions are about 63-66% Mg and 34-35% Ca.

Amphiboles of corundum-barren amphibolite mainly contain about 39% SiO_2, 17–18% Al_2O_3, 15% MgO, 13% CaO, 10-11% FeO_{total} and 2% Na_2O The main atomic proportions are very unique (61% Mg and 39% Ca).

Amphiboles of gneiss unit are composed mainly of about 39% SiO_2, 15% Al_2O_3, 8% MgO, 13% CaO, 20% FeO_{total} and 4% Na_2O. The main atomic proportions range within a narrow range of 47-48% Mg and 52-53% Ca.

In general, graphic Mg-Fe-Ca plots (Figure 4.7) indicate that most amphiboles found in all types of amphibolite are characterized chemically by Ca-amphibole composition (Figure 4.7). Although, gneissic amphiboles also fall within the similar composition, they appear to have higher Ca contents.

Table 4.3 Representative EPMA analyses of amphibole in each rock unit.

Oxide	Corundum-bearing amphibolite			Altered corundum-bearing amphibolite			Corundum-barren amphibolite			Gneiss		
	9-1-3_Am4-2c	9-1-3_Am4-1c	9-1-3_Fel5-2c	8-5-11-1_Am2-2	8-5-11-2_Am1-1	8-5-13-1_Am1-2	8-9-1_Am1-2b	8-9-1_Am4-2b	8-9-1_Am1-2b	5-2-3_Bt2-1b	5-2-3_Bt2-3b	5-2-3_Bt2-1b
SiO_2	41.25	40.84	40.82	44.87	44.64	44.35	38.91	39.17	38.91	38.64	38.64	38.64
TiO_2	0.39	0.33	0.45	0.07	0.18	0.12	0.44	0.41	0.44	1.00	0.98	1.00
Al_2O_3	16.96	17.33	17.21	16.25	17.09	17.24	17.54	18.13	17.54	14.51	14.93	14.51
Cr_2O_3	0.05	0.06	0.08	0.50	0.54	0.61	0.23	0.26	0.23	0.01	0.01	0.01
FeO *	8.24	8.77	8.76	9.21	9.79	8.67	10.85	10.55	10.85	19.74	19.64	19.74
MnO	0.16	0.15	0.17	0.20	0.18	0.15	0.08	0.08	0.08	0.08	0.11	0.08
MgO	15.95	15.71	15.28	15.70	14.64	16.00	14.87	14.80	14.87	8.34	8.28	8.34
CaO	14.32	14.10	14.22	11.62	11.48	11.61	13.25	12.86	13.25	12.59	12.78	12.59
Na_2O	2.23	2.27	2.37	0.47	0.48	0.39	2.00	2.06	2.00	3.77	3.79	3.77
K_2O	0.30	0.31	0.33	0.33	0.37	0.31	1.15	1.17	1.15	0.70	0.70	0.70
P_2O_5	0.00	0.00	0.00	0.02	0.03	0.04	0.00	0.00	0.00	0.00	0.02	0.00
F	0.00	0.00	0.00	0.00	0.00	0.00	0.00	0.00	0.00	0.00	0.00	0.00
Cl	0.00	0.00	0.00	0.00	0.00	0.01	0.01	0.01	0.01	0.02	0.04	0.02
Total	99.95	99.96	99.94	99.37	99.52	99.61	99.37	99.65	99.37	99.71	100.01	99.71
Formula 23(O)												
Si	5.866	5.821	5.832	6.305	6.272	6.201	5.666	5.671	5.666	5.874	5.849	5.874
Ti	0.041	0.036	0.048	0.007	0.019	0.013	0.049	0.045	0.049	0.114	0.112	0.114
Al	2.843	2.911	2.899	2.692	2.831	2.842	3.010	3.094	3.010	2.601	2.663	2.601
Cr	0.006	0.006	0.009	0.055	0.060	0.067	0.027	0.029	0.027	0.001	0.001	0.001
Fe^{3+}	0.980	0.980	1.039	1.082	1.06	1.01	1.234	1.258	1.322	2.510	2.486	2.546
Fe^{2+}	0.000	0.000	0.000	0.000	0.09	0.00	0.000	0.000	0.000	0.000	0.000	0.000
Mn	0.019	0.018	0.021	0.023	0.022	0.018	0.009	0.010	0.009	0.010	0.014	0.010
Mg	3.380	3.336	3.253	3.287	3.064	3.333	3.226	3.192	3.226	1.889	1.867	1.889
Ca	2.182	2.153	2.176	1.750	1.728	1.739	2.067	1.995	2.067	2.051	2.073	2.051
Na	0.614	0.627	0.656	0.129	0.130	0.107	0.565	0.578	0.565	1.112	1.113	1.112
K	0.054	0.055	0.060	0.059	0.067	0.055	0.213	0.216	0.213	0.135	0.135	0.135
P	0.000	0.000	0.000	0.002	0.003	0.005	0.000	0.000	0.000	0.000	0.002	0.000
F	0.000	0.000	0.000	0.000	0.000	0.000	0.000	0.000	0.000	0.000	0.000	0.000
Cl	0.000	0.000	0.000	0.000	0.000	0.002	0.003	0.001	0.003	0.005	0.009	0.005
Total (S)	15.999	16.019	16.020	15.405	15.355	15.404	16.155	16.117	16.155	16.322	16.324	16.322
Atomic%												
Fe	0.00	0.00	0.00	0.00	1.77	0.00	0.00	0.00	0.00	0.00	0.00	0.00
Mg	60.77	60.78	59.91	65.26	62.81	65.72	60.94	61.54	60.94	47.95	47.39	47.95
Ca	39.23	39.22	40.09	34.74	35.42	34.28	39.06	38.46	39.06	52.05	52.61	52.05

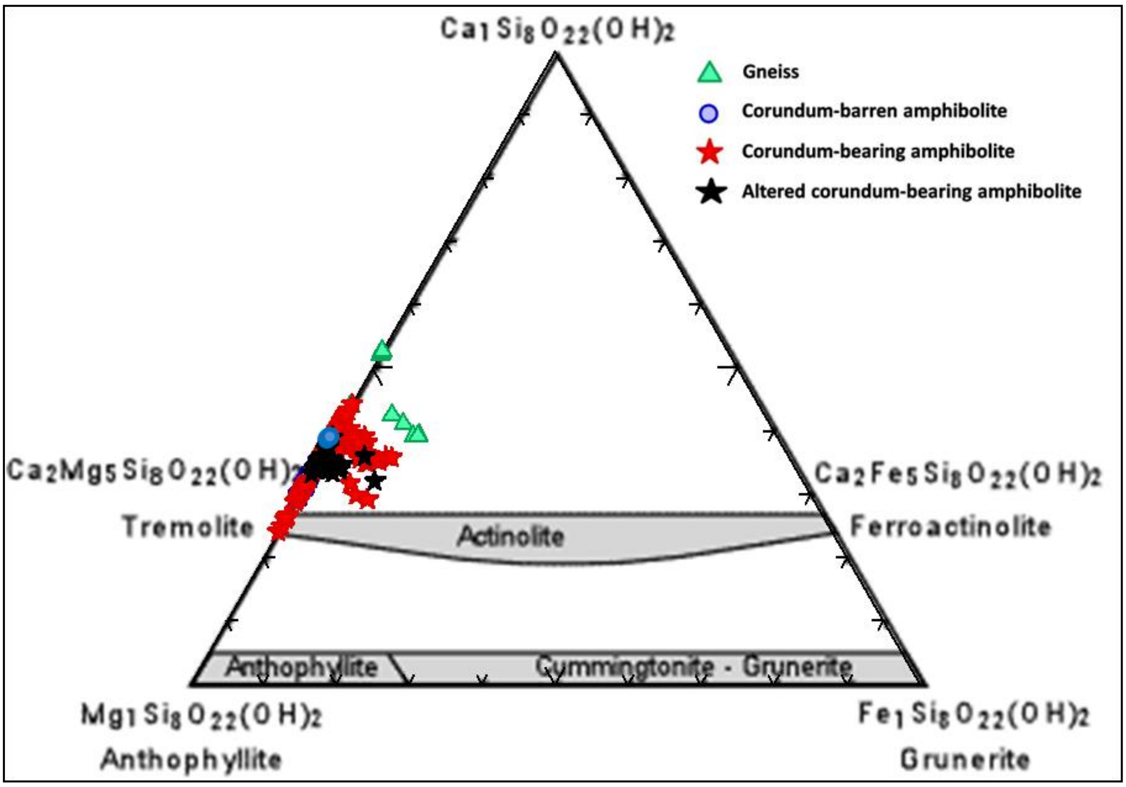

Figure 4.7 Atomic plots between Ca-Mg-Fe showing similar composition of amphiboles in all rock units.

4.3.2 Feldspar

Feldspar, mostly characterized by plagioclase composition, is mainly observed in both corundum-barren and corundum-bearing amphibolites. For the last unit, they always occur around corundum and spinel. Moreover, gneiss samples significantly show both plagioclase and alkali feldspars. For altered corundum-bearing amphibolite, all feldspars appear to have been altered to clay minerals. EPMA analyses of these feldspars and recalculated formula based on 8 oxygens are representatively present in Table 4.4.

Plagioclases found in corundum-bearing amphibolite mainly fall within ranges of about 42% SiO_2, 37–40% Al_2O_3, 18-20% CaO with very low Na_2O and K_2O contents. Atomic Ca-Na-K proportions fall within a narrow range of 99-99.5% An and 0.5-1% Ab.

Corundum-barren amphibolites contain lagioclases which are mainly composed of about 42% SiO_2, 37% Al_2O_3, and 20% CaO with very low Na_2O and K_2O contents. Atomic Ca-Na-K proportions indicate similar end-members ofhigher than 99.5% An with <0.5% Ab.

Gneissic feldspars, both alkali feldspar and plagioclase are described here. Alkali-feldspars are mainly composed of about 60.80-69.33% SiO_2, 19.05-20.99% Al_2O_3, 9.40-15.79% K_2O and 0.52-0.63% Na_2O with low CaO contents. Atomic Ca-Na-K proportions fall within 4.7-9.2% Ab and 90.8-95.3% Or, respectively. Plagioclases contain about 52–66% SiO_2, 18–22% Al_2O_3, 5-25% CaO and 1-8% Na_2O with very low K_2O contents. Atomic Ca-Na-K proportions present a range of about 25.7-91.26% An, 7.8-73.1% Ab and 0.4-1.3% Or, respectively.

Figure 4.8 shows plots of atomic Ca-Na-K proportions of feldspars observed in three rock types. They are chemically characterized by wide compositional ranges crucially from orthoclase to albite and anorthite. Feldspars in gneiss are characterized similarly by orthoclase for alkali feldspar but widely by albite to oligoclase andesine, bytownite and anorthite for plagioclase. Feldspars found in both corundum-barren and corundum-bearing amphibolites are mostly are anorthite.

Table 4.4 Representative EPMA analyses of feldspars.

	Corundum-bearing amphibolites			Corundum-barren amphibolites			Gneiss								
	Plagioclase												Alkali feldspar		
Oxide	8-8-2_Pl4-1c	8-8-2_Pl4-3c	9-1-3_Fel4-1c	8-9-1_Px1-1b	8-9-1_Px1-3b	8-9-1_Fel1-1b	6-3-14-2_Am2-2b	6-3-14-2_Fel3-1b	6-3-14-2_Fel3-3b	5-2-3_r2Grt2-1	6-3-14-2_Un3-2	6-3-14-2_Un2-2	6-3-14-2_Fel1-1b	6-3-14-2_Px1-1b	8-3-1_Fel4-1c
SiO_2	42.45	42.38	41.61	41.88	41.96	41.68	65.54	65.61	65.48	55.05	52.13	56.03	60.80	61.92	69.33
TiO_2	0.00	0.00	0.00	0.01	0.01	0.00	0.01	0.04	0.01	0.03	0.01	0.00	0.00	0.00	0.02
Al_2O_3	36.93	37.17	39.89	36.92	36.76	36.74	20.90	20.58	19.54	18.10	21.58	19.87	20.99	20.95	19.05
FeO *	0.03	0.04	0.25	0.12	0.04	0.09	0.06	0.06	0.09	0.03	0.15	0.00	0.31	0.04	0.00
MnO	0.02	0.00	0.01	0.02	0.00	0.02	0.04	0.01	0.00	0.03	0.00	0.02	0.00	0.00	0.00
MgO	0.00	0.00	0.19	0.01	0.00	0.00	0.01	0.00	0.00	0.00	0.00	0.00	0.00	0.00	0.01
CaO	19.45	19.62	17.78	19.92	20.39	20.48	5.08	5.08	5.77	24.52	24.50	22.02	0.02	0.00	0.00
Na_2O	0.07	0.05	0.09	0.04	0.04	0.05	7.99	7.92	7.82	1.67	1.16	1.30	0.59	0.52	0.63
K_2O	0.00	0.00	0.01	0.00	0.00	0.01	0.20	0.22	0.17	0.11	0.20	0.08	15.15	15.79	9.40
P_2O_5	0.01	0.00	0.10	0.01	0.00	0.00	0.01	0.00	0.02	0.01	0.00	0.00	0.00	0.00	0.04
Total	99.25	99.34	99.95	99.17	99.39	99.06	99.90	99.76	99.02	99.75	99.91	99.46	98.13	99.42	98.62
Formula 8(O)															
Si	1.982	1.975	1.917	1.962	1.963	1.957	2.888	2.897	2.917	2.586	2.450	2.603	2.872	2.887	3.095
Ti	0.000	0.000	0.000	0.000	0.000	0.000	0.000	0.001	0.000	0.001	0.000	0.000	0.000	0.000	0.001
Al	2.033	2.042	2.167	2.039	2.027	2.033	1.086	1.071	1.026	1.002	1.196	1.088	1.169	1.152	1.003
Fe	0.001	0.001	0.010	0.005	0.001	0.003	0.002	0.002	0.003	0.001	0.006	0.000	0.012	0.002	0.000
Mn	0.001	0.000	0.000	0.001	0.000	0.001	0.001	0.001	0.000	0.001	0.000	0.001	0.000	0.000	0.000
Mg	0.000	0.000	0.013	0.001	0.000	0.000	0.001	0.000	0.000	0.000	0.000	0.000	0.000	0.000	0.000
Ca	0.973	0.980	0.878	1.000	1.022	1.030	0.240	0.240	0.275	1.234	1.234	1.096	0.001	0.000	0.000
Na	0.006	0.004	0.008	0.004	0.004	0.005	0.682	0.678	0.676	0.152	0.106	0.117	0.054	0.047	0.054
K	0.000	0.000	0.001	0.000	0.000	0.000	0.011	0.012	0.009	0.006	0.012	0.005	0.913	0.939	0.535
P	0.000	0.000	0.004	0.000	0.000	0.000	0.000	0.000	0.001	0.000	0.000	0.000	0.000	0.000	0.001
Total (S)	5.002	5.005	4.998	5.016	5.023	5.029	4.914	4.908	4.910	4.989	5.008	4.912	5.026	5.030	4.693
Atomic%															
An	99.38	99.55	99.04	99.64	99.62	99.51	25.7	25.8	28.7	88.63	91.26	90.0	0.1	0.0	0.0
Ab	0.62	0.45	0.87	0.36	0.38	0.45	73.1	72.9	70.4	10.90	7.84	9.6	5.6	4.7	9.2
Or	0.00	0.00	0.09	0.00	0.00	0.04	1.2	1.3	1.0	0.46	0.90	0.4	94.3	95.3	90.8

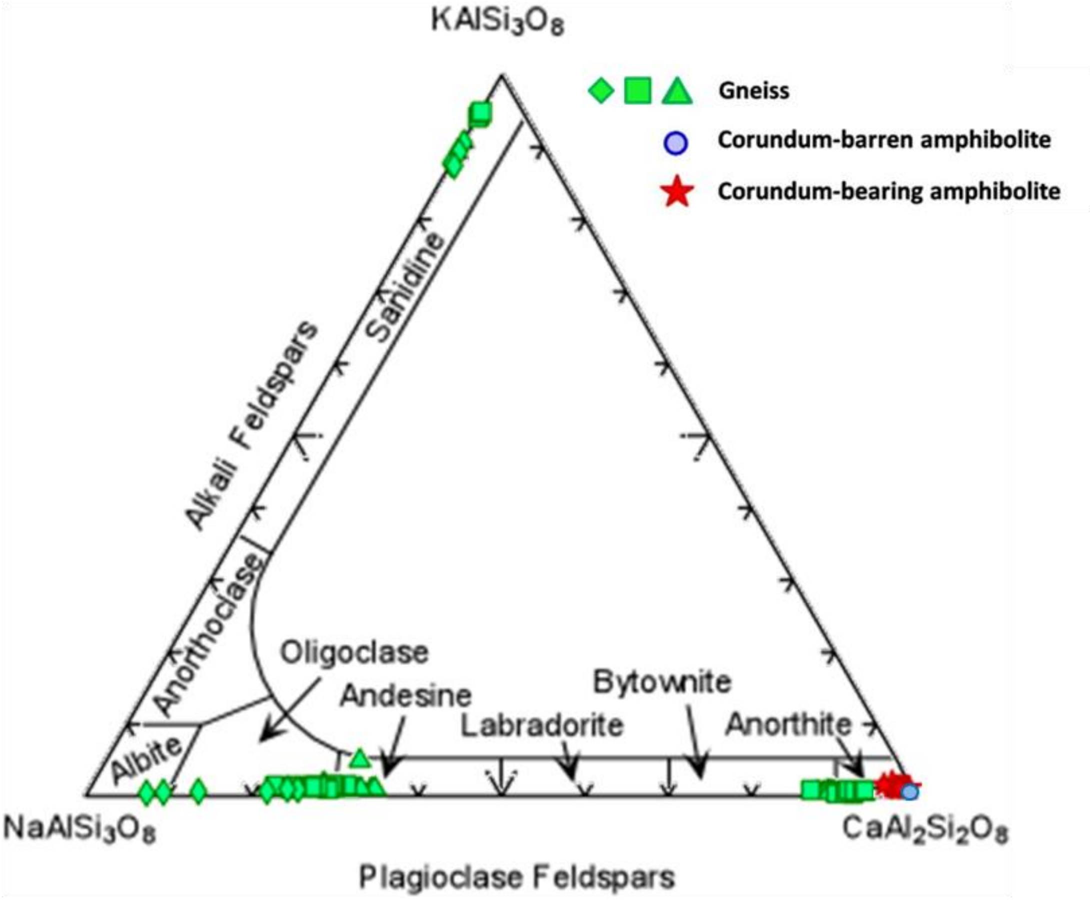

Figure 4.8 Atomic Ca-Na-K plots of feldspars in the ternary Or-Ab-An end-members and compositional ranges.

4.3.3 Spinel

Spinel is an important mineral found in both types of amphibolite. It usually occurs around corundum as a reaction edge ring. On the other hand, corundum-barren amphibolite usually shows spinel as a main assemblage.

The analytical data and their recalculated cations based on 4 oxygens are presented in Table 4.5. The whole range of analyses is collected in Appendix C.

Spinels found in corundum-bearing amphibolite are composed mainly of 63.18–67.09% Al_2O_3, 19.79-21.32% MgO, 12.09-14.69% FeO_{total} and less amounts of Cr_2O_3, MnO, and TiO_2.

Spinels in corundum-barren amphibolite are composed mainly of 65.22–65.89% Al_2O_3, 20.03-20.15% MgO, 12.01-12.25% FeO_{total} and less amounts of Cr_2O_3, MnO, and TiO_2.

Atomic Al-Fe^{3+}-Cr and Mg-Fe^{2+}-Mn proportions of spinels are plotted and presented in Figures 4.9 and 4.10, representatively, which clearly indicate almost pure spinel compositions.

Table 4.5 Representative EPMA of spinel.

Oxide	Corundum-bearing amphibolites					Corundum-barren amphibolites	
	9-1-4_6-Spl1-1	9-1-4_6-Spl1-2	9-1-4_6-Spl1-3	9-1-4_3-Spl1-3	9-1-4_2-Spl1-1	8-9-1_3-Spl1-1	8-9-1_3-Spl1-2
SiO_2	0.00	0.00	0.00	0.07	0.00	0.00	0.00
TiO_2	0.04	0.02	0.05	0.04	0.00	0.02	0.01
Al_2O_3	63.18	63.93	63.92	64.46	67.0	65.89	65.22
Cr_2O_3	0.04	0.07	0.04	0.00	0.06	0.01	0.01
FeO *	14.69	13.73	14.41	12.09	12.5	12.01	12.25
MnO	0.18	0.18	0.14	0.02	0.17	0.02	0.01
MgO	21.05	20.86	20.78	21.32	19.7	20.15	20.03
CaO	0.00	0.01	0.00	0.02	0.00	0.00	0.00
Na_2O	0.04	0.06	0.04	0.02	0.05	0.02	0.03
K_2O	0.00	0.00	0.00	0.80	0.02	0.02	0.00
P_2O_5	0.00	0.02	0.00	0.03	0.00	0.00	0.00
Total	99.35	99.02	99.54	99.04	99.9	98.30	97.67
Formula 4(O)							
Si	0.000	0.000	0.000	0.002	0.00	0.000	0.000
Ti	0.001	0.000	0.001	0.001	0.00	0.000	0.000
Al	1.913	1.931	1.926	1.939	1.98	1.982	1.977
Cr	0.001	0.001	0.001	0.000	0.00	0.000	0.000
Fe3+	0.113	0.087	0.093	0.104	0.01	0.021	0.030
Fe2+	0.202	0.208	0.215	0.153	0.25	0.235	0.233
Mn	0.004	0.004	0.003	0.000	0.00	0.000	0.000
Mg	0.806	0.797	0.792	0.810	0.74	0.766	0.768
Ca	0.000	0.000	0.000	0.000	0.00	0.000	0.000
Na	0.002	0.003	0.002	0.001	0.00	0.001	0.001
K	0.000	0.000	0.000	0.026	0.00	0.001	0.000
P	0.000	0.000	0.000	0.001	0.00	0.000	0.000
Total (S)	3.043	3.033	3.035	3.040	3.00	3.008	3.011
Atomic%							
Spinel	72.67	71.90	71.04	77.88	66.3	68.49	68.70
Hercynite	18.22	18.74	19.31	14.74	22.4	21.01	20.87
Magnetite	9.11	9.37	9.65	7.37	11.2	10.50	10.43

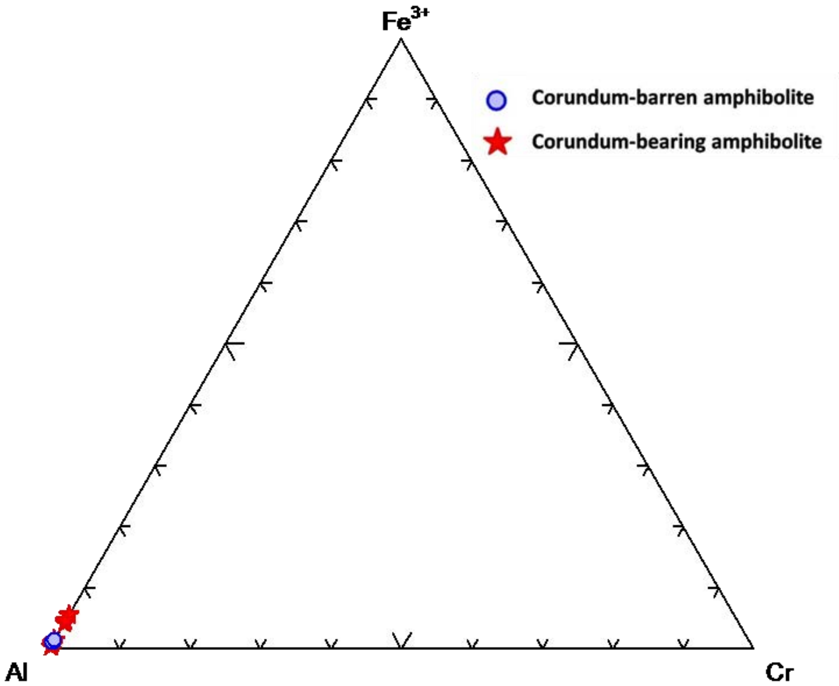

Figure 4.9 Ternary plots of atomic Al-Fe^{3+}-Cr proportion of spinels.

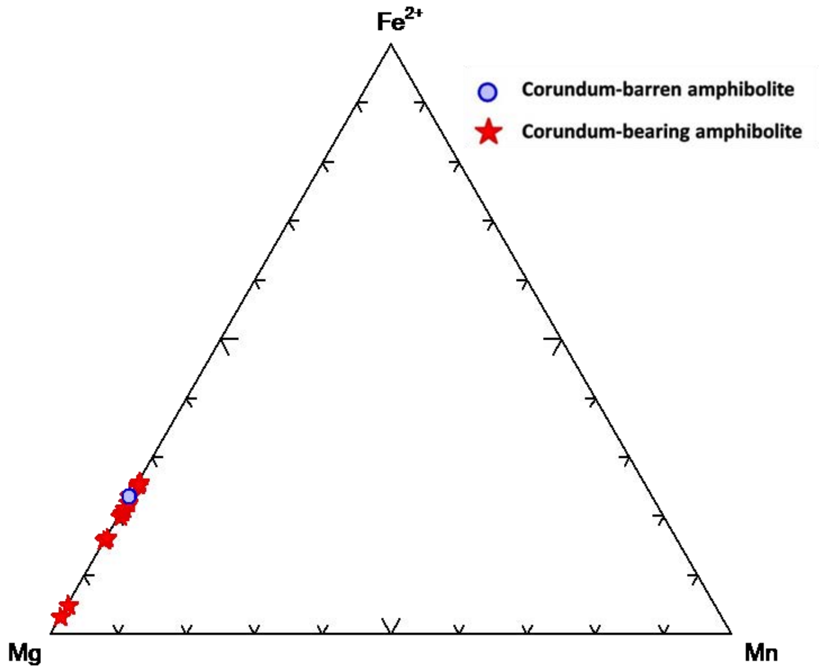

Figure 4.10 Ternary plot of atomic Mg-Fe^{2+}-Mn proportion of spinels.

4.3.4 Garnet

Garnet has been discovered significantlyin gneiss as porphyroblasts. Moreover, it is present as less abundance in some samples of corundum-bearing amphibolite and corundum-barren amphibolite.

All analytical data and their recalculated cations based on 12 oxygens are presented in Table 4.6. The whole range of analyses is collected in Appendix C.

Garnets found in corundum-bearing amphibolite are composed mainly of 37.67-38.14% SiO_2, 28.82-29.14% Al_2O_3, 6.65-6.83% FeO_{total}, 25.52-25.72% CaO, 0.23-0.27% MgO, 0.05-0.10% Cr_2O_3 with less abundance of MnO. Their chemical compositions are close to the ideal garnet formula ($X_3Y_2(SiO_4)_3$). Recalculated cations based on 12(O) show atomic proportions of about $Ca_{0.82}$, $Fe^{2+}{}_{0.17}$, and $Mg_{0.01}$ (Table 4.6) and classified as grossular garnet.

Garnets found in corundum-barren amphibolite are composed mainly of 37.76-38.15% SiO_2, 36.04-36.61% Al_2O_3, 1.99-2.14% FeO_{total}, 23.71-23.99% CaO, 0.08-0.10% MgO, 0.14-0.23% Cr_2O_3 with less abundance of MnO. Their chemical compositions are also close to the ideal garnet formula ($X_3Y_2(SiO_4)_3$). Recalculated cations based on 12(O) yield atomic proportions of about $Ca_{0.93}$, $Fe^{2+}{}_{0.06}$, and $Mg_{0.01}$ (Table 4.6) and classified as grossular garnet.

Gneissic garnets are composed mainly of 40.09-40.87% SiO_2, 18.86-20.38% Al_2O_3, 19.29-20.76% FeO_{total}, 12.84-13.29% MgO, 4.48-5.06% CaO with less abundances of MnO, and Cr_2O. Their chemical compositions are also close to the ideal garnet formula ($X_3Y_2(SiO_4)_3$). Recalculated cations based on 12(O) yield atomic proportions of $Ca_{0.12}$, $Fe^{2+}{}_{-0.39}$, and $Mg_{0.49}$ (Table 4.6) classified as pyrope-almandine garnet.

Table 4.6 Representative EPMA of garnet.

Oxide	Corundum-bearing amphibolite			Corundum-barren amphibolite			Gneiss		
	9-1-3_inPl4-1c	9-1-3_inPl4-2c	9-1-3_inPl4-3c	8-9-1_Am3-1b	8-9-1_Am3-2b	8-9-1_Am3-3b	5-2-3_Grt2-11	5-2-3_Grt2-14	5-2-3_Grt2-15
SiO_2	37.83	37.67	38.14	38.15	37.76	37.76	40.09	40.87	40.46
TiO_2	0.02	0.12	0.07	0.06	0.05	0.03	0.06	0.03	0.03
Al_2O_3	29.09	29.14	28.82	36.61	36.04	36.24	18.86	20.38	19.76
Cr_2O_3	0.06	0.05	0.10	0.14	0.15	0.23	0.00	0.01	0.01
FeO *	6.83	6.78	6.65	2.14	2.06	1.99	19.54	19.29	20.76
MnO	0.10	0.04	0.04	0.02	0.04	0.01	1.01	1.19	1.24
MgO	0.23	0.23	0.27	0.10	0.10	0.08	12.84	13.29	12.88
CaO	25.52	25.72	25.55	23.99	23.85	23.71	4.50	5.06	4.48
Na_2O	0.01	0.00	0.00	0.00	0.00	0.02	0.03	0.01	0.01
K_2O	0.00	0.01	0.00	0.00	0.00	0.00	0.00	0.00	0.01
P_2O_5	0.04	0.04	0.05	0.06	0.06	0.08	0.00	0.00	0.01
Total	99.98	99.97	99.96	101.33	100.25	100.39	97.12	100.26	99.76
Formula 12(O)									
Si	2.819	2.808	2.841	2.707	2.710	2.706	3.105	3.060	3.064
Ti	0.001	0.007	0.004	0.003	0.003	0.002	0.003	0.002	0.002
Al	2.556	2.561	2.531	3.062	3.049	3.063	1.721	1.798	1.764
Cr	0.003	0.003	0.006	0.008	0.008	0.013	0.000	0.001	0.001
Fe^{3+}	0.000	0.000	0.000	0.000	0.000	0.000	0.083	0.109	0.150
Fe^{2+}	0.426	0.423	0.414	0.127	0.124	0.119	1.182	1.099	1.165
Mn	0.006	0.003	0.003	0.001	0.002	0.000	0.067	0.076	0.079
Mg	0.026	0.025	0.030	0.011	0.010	0.008	1.482	1.483	1.454
Ca	2.038	2.054	2.039	1.824	1.834	1.821	0.373	0.406	0.364
Na	0.002	0.000	0.000	0.000	0.001	0.003	0.004	0.001	0.001
K	0.000	0.001	0.000	0.000	0.000	0.000	0.000	0.000	0.001
P	0.002	0.002	0.003	0.004	0.004	0.005	0.000	0.000	0.001
Total (S)	7.891	7.897	7.879	7.748	7.750	7.746	8.028	8.037	8.050
Atomic%									
Pyrope	1.04	1.01	1.20	0.56	0.52	0.42	48.79	49.64	48.74
Almandine	17.11	16.89	16.68	6.46	6.29	6.11	38.92	36.78	39.07
Grossular	81.85	82.10	82.12	92.98	93.20	93.46	12.29	13.58	12.19

Plots of atomic Ca-Fe^{2+}-Mg show different compositions between amphibolites garnets (grossular-rich composition) and gneissic garnets (pyrope-almandine composition) (Figure 4.11).

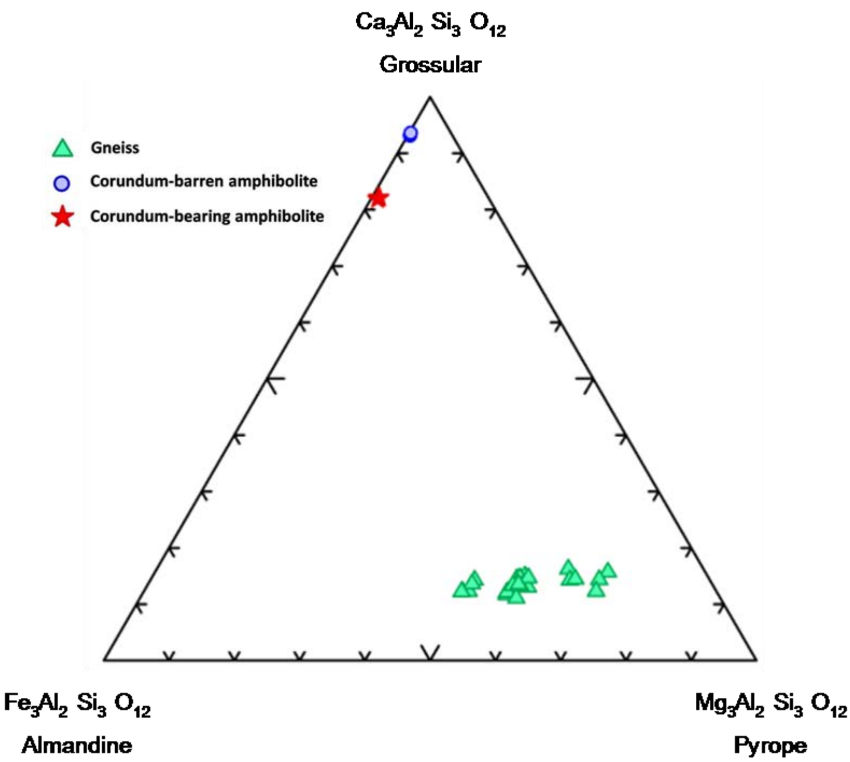

Figure 4.11 Plot of atomic Ca-Mg-Fe showing composition of garnet.

4.3.5 Corundum

Corundum in amphibolite samples, MBQ-8-8-1, MBQ-8-8-2, MBQ-9-1-2, MBQ-9-1-3 and MBQ-9-1-4, and altered amphibolite samples, MBQ-8-5-1, MBQ-8-5-2, MBQ-8-5-3, MBQ-8-5-4, MBQ-8-5-5, MBQ-8-5-6, MBQ-8-5-7, MBQ-8-5-8, MBQ-8-5-9, MBQ-8-5-10, MBQ-8-5-11, MBQ-8-5-12, MBQ-8-5-13, MBQ-8-5-14, MBQ-8-5-15 and MBQ-8-5-16 were analyzed. All corundum analyses yield >99.05% Al_2O_3, confirming optical identification.Their chemical compositions are close to the ideal corundum formula (Al_2O_3). Representative analytical data and their recalculated cations based on 3 oxygens are presented in Table 4.7. The whole range of analyses is collected in Appendix C.

Corundum in fresh samples of amphibolite are composed mainly of 98.70–99.38% Al_2O_3, 0.02-0.08% Cr_2O_3, 0.01-0.45 % FeO_{total} with less abundant Ga_2O_3. Similar compositions of corundum in altered amphibolites samples are also present including 98.55–99.05% Al_2O_3, 0.18-0.37% Cr_2O_3, 0.27-0.31% FeO_{total} and less abundant Ga_2O_3.

Table 4.7. Representative EPMA of corundum.

Oxide	Corundum-bearing amphibolite				Altered corundum-bearing amphibolite			
	9-1-4_6-Cor1-2	9-1-4_2-Cor1-2	9-1-4_Crn2-1c	8-8-1-16_Cor1-1	8-5-15-1_Cor1-1	8-5-15-1_Cor1-3	8-5-15-1_inCor1-2	8-5-8-2_Cor1-1
SiO_2	0.00	0.00	0.00	0.01	0.00	0.00	0.01	0.00
TiO_2	0.02	0.03	0.01	0.02	0.03	0.00	0.01	0.01
Al_2O_3	99.24	99.35	99.38	98.70	98.55	99.05	98.99	98.95
Cr_2O_3	0.05	0.04	0.08	0.02	0.19	0.21	0.18	0.37
FeO *	0.13	0.01	0.45	0.45	0.30	0.27	0.28	0.31
MnO	0.00	0.03	0.01	0.00	0.00	0.02	0.01	0.00
MgO	0.00	0.01	0.00	0.00	0.00	0.00	0.00	0.00
CaO	0.01	0.00	0.00	0.00	0.00	0.01	0.02	0.00
Na_2O	0.01	0.00	0.00	0.01	0.00	0.00	0.00	0.01
K_2O	0.00	0.00	0.01	0.01	0.00	0.00	0.00	0.00
V_2O_3	0.01	0.00	0.00	0.02	0.00	0.00	0.00	0.00
ZrO_2	0.00	0.00	0.05	0.00	0.04	0.01	0.00	0.00
P_2O_5	0.00	0.00	0.00	0.00	0.00	0.00	0.00	0.01
HfO_2	0.02	0.03	0.00	0.00	0.10	0.00	0.01	0.02
Ga_2O_3	0.00	0.01	0.00	0.09	0.05	0.00	0.09	0.04
NiO	0.00	0.00	0.00	0.00	0.00	0.02	0.01	0.00
Total	99.49	99.53	99.98	99.33	99.25	99.58	99.72	99.72
Formula 3(O)								
Si	0.000	0.000	0.000	0.000	0.000	0.000	0.000	0.000
Ti	0.000	0.000	0.000	0.000	0.000	0.000	0.000	0.000
Al	1.997	1.998	1.994	1.994	1.992	1.994	1.993	1.991
Cr	0.001	0.001	0.001	0.000	0.003	0.003	0.002	0.005
Fe	0.002	0.000	0.006	0.006	0.004	0.004	0.004	0.004
Mn	0.000	0.000	0.000	0.000	0.000	0.000	0.000	0.000
Mg	0.000	0.000	0.000	0.000	0.000	0.000	0.000	0.000
Ca	0.000	0.000	0.000	0.000	0.000	0.000	0.000	0.000
Na	0.000	0.000	0.000	0.000	0.000	0.000	0.000	0.000
K	0.000	0.000	0.000	0.000	0.000	0.000	0.000	0.000
V	0.000	0.000	0.000	0.000	0.000	0.000	0.000	0.000
Zr	0.000	0.000	0.000	0.000	0.000	0.000	0.000	0.000
P	0.000	0.000	0.000	0.000	0.000	0.000	0.000	0.000
Hf	0.000	0.000	0.000	0.000	0.000	0.000	0.000	0.000
Ga	0.000	0.000	0.000	0.001	0.001	0.000	0.001	0.000
Ni	0.000	0.000	0.000	0.000	0.000	0.000	0.000	0.000
Total(S)	2.001	2.000	2.002	2.003	2.001	2.001	2.002	2.001

4.3.6 Conclusion

According to mineral chemistry, gneiss contains two feldspars which vary from orthoclase, albite to anorthite ($<An_{20}$) and amphibole which is characterized by hornblende. They indicate high grade metamorphism in amphibolite facies condition (Vernon and Clarke, 2008). Moreover, gneissic garnet is characterized by pyrope-almandine is also commonly present.

All types of amphibolites contain mainly amphiboles (hornblende composition) and plagioclase (mostly anorthite composition). Hornblende, calc-amphibole (Leake et al., 1997), usually occurs in medium-grade metamorphic rocks (Klein and Hurlbut, 1993) such as amphibolite facies condition (Vernon and Clarke, 2008) which both hornblende and its associated plagioclase are major constituents (Vernon and Clarke, 2008). Less abundance of corundum, spinel and garnet are present in amphibolites. Garnets found in both corundum-bearing amphibolite and corundum-barren amphibolite is characterized similarly by grossular. Spinels with almost pure composition also presented in both corundum-bearing and corundum-barren amphibolites are high temperature mineral which is commonly found metamorphic rocks and igneous rocks (Klein and Hurlbut, 1993). It is also often associated with corundum (Klein and Hurlbut, 1993).

Therefore, it may be concluded, based on mineral chemistry, that all of rock units i.e. gneiss and amphibolite are high grad metamorphic rocks belonging to amphibolite facies.

CHAPTER V

DISCUSSION AND CONCLUSIONS

5.1 Petrogenesis

Montepuez Complex is related to Eastern granulite gneiss (Bingen et al., 2009) of Neoproterozoic Mozambique Belt (Pinna et al., 1993; Viola et al., 2008; Bingen et al., 2009; Boyd et al., 2010). Based on field observation and petrographic description, they indicate that high grade metamorphic rocks in Montepuez are mostly represented by amphibolite and gneiss. Apart from corundum occurrence, corundum-bearing amphibolite is composed of amphibole, spinel and plagioclase with minor amounts of garnet and mica. Two stages of metamorphism are recognized in corundum-bearing amphibolite. They appear to have been metamorphosed initially under the equilibrium condition represented by granoblastic texture with triple junction between amphibole and plagioclase. Subsequent metamorphic reaction may be essentially involving amphibole, corundum, spinel and plagioclase which seem to be break down reactions as described below.

2Hornblende + 9Corumdum = 8Spinel + 4Plagioclase + 4Silica + 2 Water + 1/2Oxigen .... (1)

$$(2Ca_2Mg_4Al_3Si_6O_{22}(OH)_2 + 9Al_2O_3 = 8MgAl_2O_4 + 4CaAl_2Si_2O_8 + 4SiO_2 + 2H_2O + 1/2O_2)$$

3Plagioclase = Garnet + 2 Corumdum + 3Silica .... (2)

$$(3CaAl_2Si_2O_8 = Ca_3Al_2Si_3O_{12} + 2Al_2O_3 + 3SiO_2)$$

Corundum-barren amphibolite is composed of amphibole, plagioclase, spinel with/without garnet. They appear to have been metamorphosed initially under equilibrium condition represented by granoblastic crystals of amphibole, plagioclase and spinel that can be described as equation below

2Hornblende + 3 Oxigen = 2Spinel + Plagioclase + Grossular + 11Silica + 2Water…..(3)

$2(Ca_2MgAl_4Si_8O_{22}(OH)_2)+3(O_2) = 2MgAl_2O_4+CaAl_2Si_2O_8+Ca_3Al_2Si_3O_{12}+11(S_2O)+2(H_2O)$

From (1), (2) and (3), silica is absent phase which may be caused by low melting point of silica and low SiO_2 content of amphibolites. Therefore, silica may occur as inherent tiny inclusion or glassy phases. Secondary corundum resulted by reaction (2) is also absent phase because it may appear as very tiny crystal (sub-micrometer scale) in plagioclase. They cannot be observed under microscope.

On the other hand, gneiss usually contains plagioclase, microcline, biotite, quartz, amphibole, garnet and opaque minerals.

These high-grad metamorphic rocks, amphibolite and gneiss, can be distinguished clearly by whole-rock geochemistry. ACF diagram (as proposed by Eskola, 1915) is used to indicate their protolith (initial rocks). As the results, their chemical assemblages are plotted into different fields of average rock compositions (see Figures 5.1 and 5.2). Corundum-bearing amphibolite and its altered counterpart are significantly plotted in the field basic rock composition whereas corundum-barren amphibolite falls outside basic composition. Gneiss is plotted between compositional fields of quartzo-feldspathic rocks and pelitic rocks (Figure 5.2) which may indicate wide ranges of protoliths before they were undergone metamorphism.

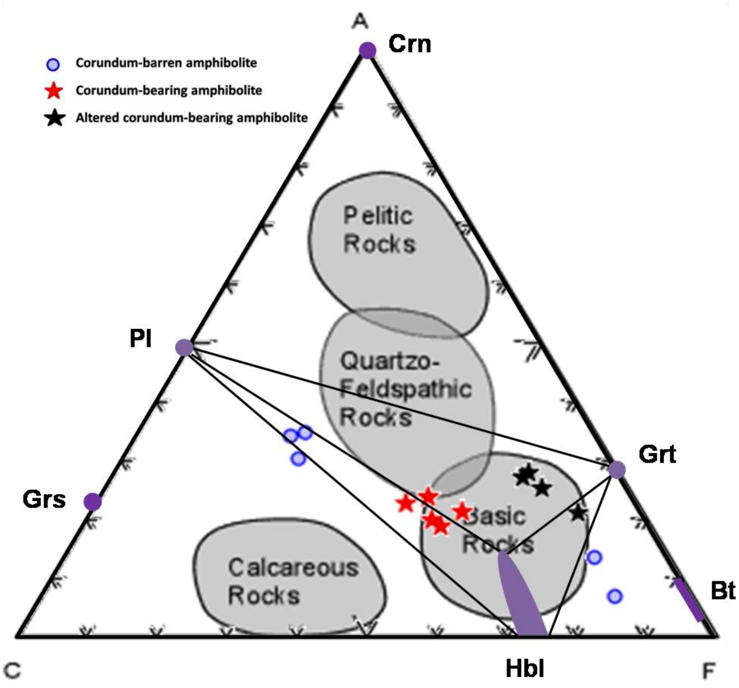

Figure 5.1 ACF diagram (Eskola, 1915) showing compositions of different amphibolites from Montepuez, Mozambique.

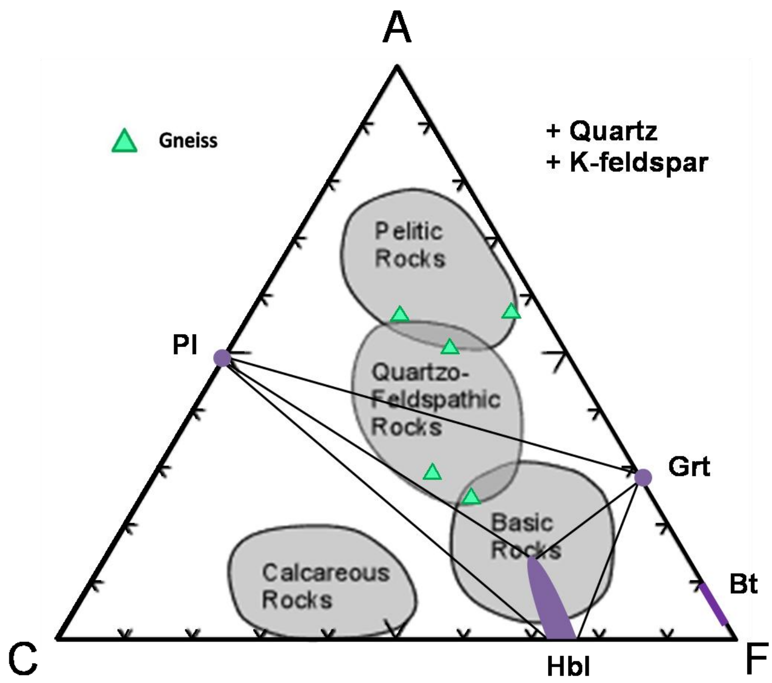

Figure 5.2 ACF diagram (modified after Eskola, 1915) showing various compositions of gneiss from Montepuez, Mozambique.

Moreover, initial compositions of these amphibolites can be distinguished graphically using variation diagrams including discrimination diagrams and tectono diagrams which indicate similar original geological environment.

Total alkali-silica diagram (TAS) (suggested by Le Bas et al., 1986) (Figure 5.3) shows that corundum-barren amphibolite, corundum-bearing amphibolite and altered corundum-bearing amphibolite fall obviously in the field of basaltic composition. MgO-FeO-Alkali plots (after Irvine and Baragar, 1971) (Figure 5.4) indicate signature of the calc-alkali magma series rather than tholeiite series for all types of amphibolite. Plots of Ti/1000 versus V (designed by Jian et al., 2009) (Figure 5.5) suggest that most of compositions of amphibolite samples appear to have related to a provenance of Island Arc Tholeiite (IAT) and Mid Oceanic Ridge Basalt (MORB). In addition, Th-Zr-Nb diagram (Wood, 1980) shows most amphibolite samples are associated with composition of arc-basalt (Figure 5.6).

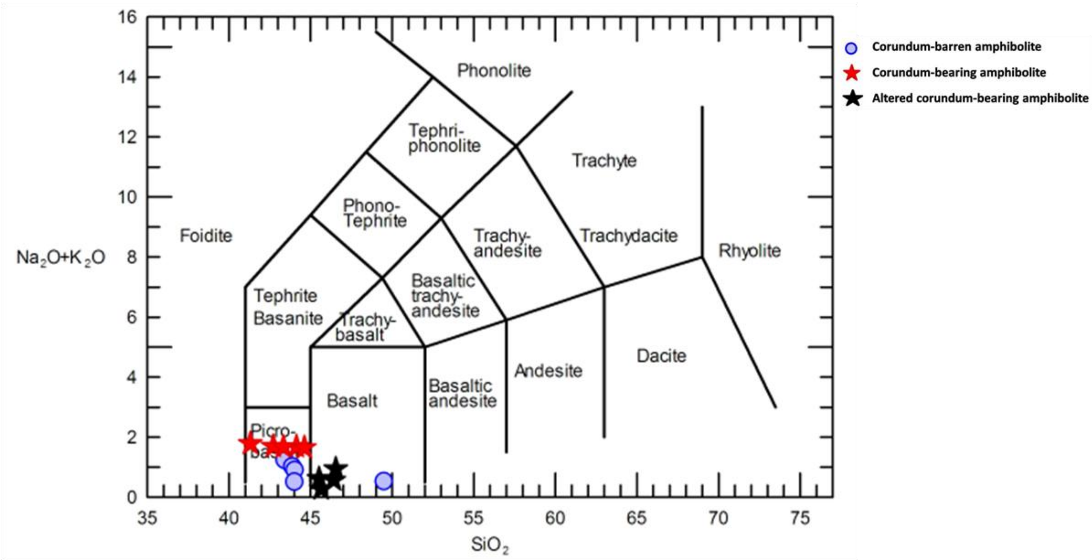

Figure 5.3 TAS diagram (Le Bas et al., 1986) showing compositional plots of whole-rock geochemistry of amphibolites from Montepuez, Mozambique.

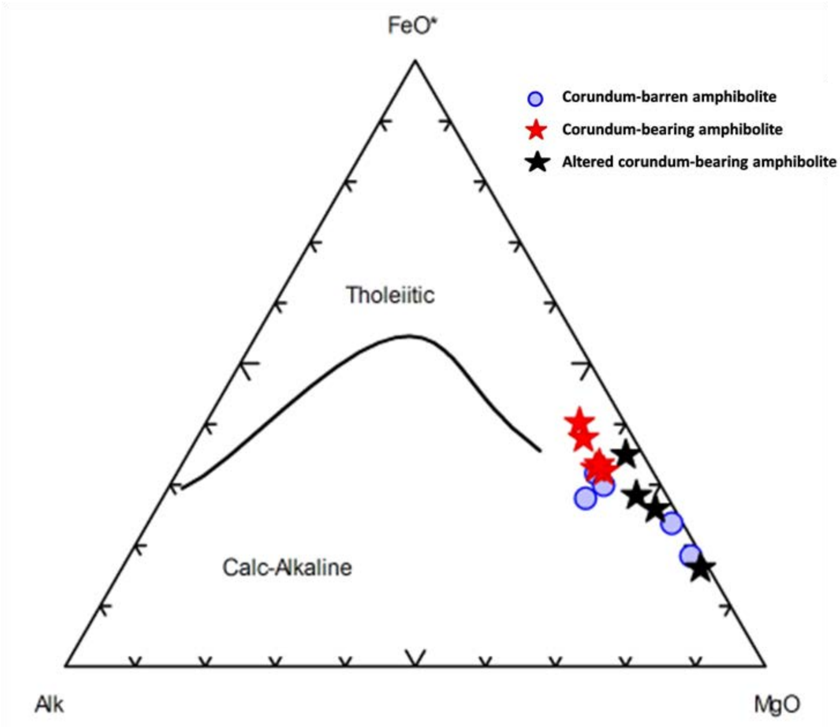

Figure 5.4 Ternary MgO-FeO-Alkali plots (after Irvine and Baragar, 1971) indicate initial magma series of amphibolites from Montepuez, Mozambique.

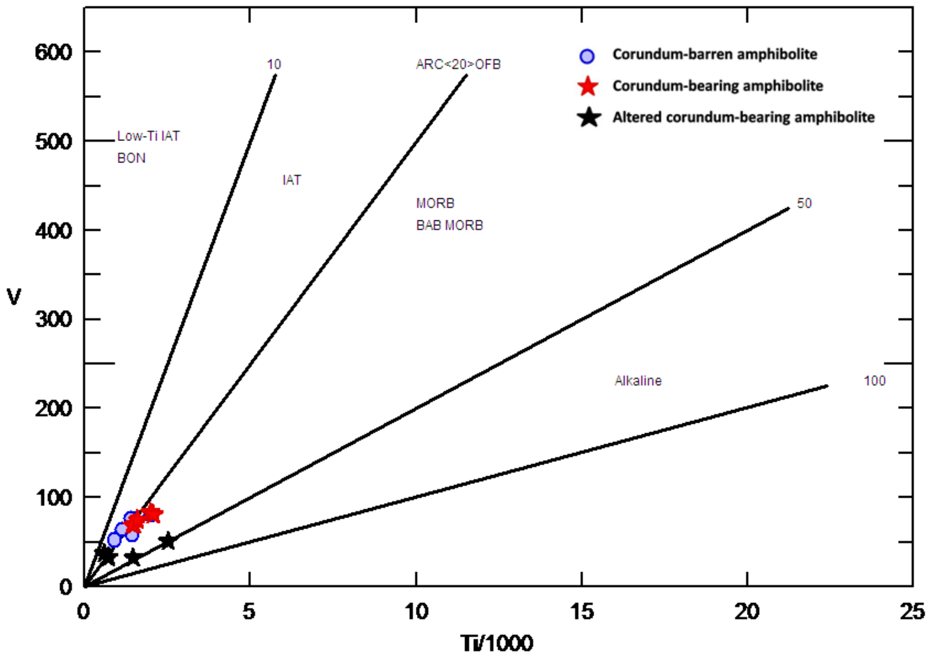

Figure 5.5 Ti-V plots of tectono-diagram (after Jian et al., 2009) indicating potentially initial magma series of amphibolites from Montepuez, Mozambique.

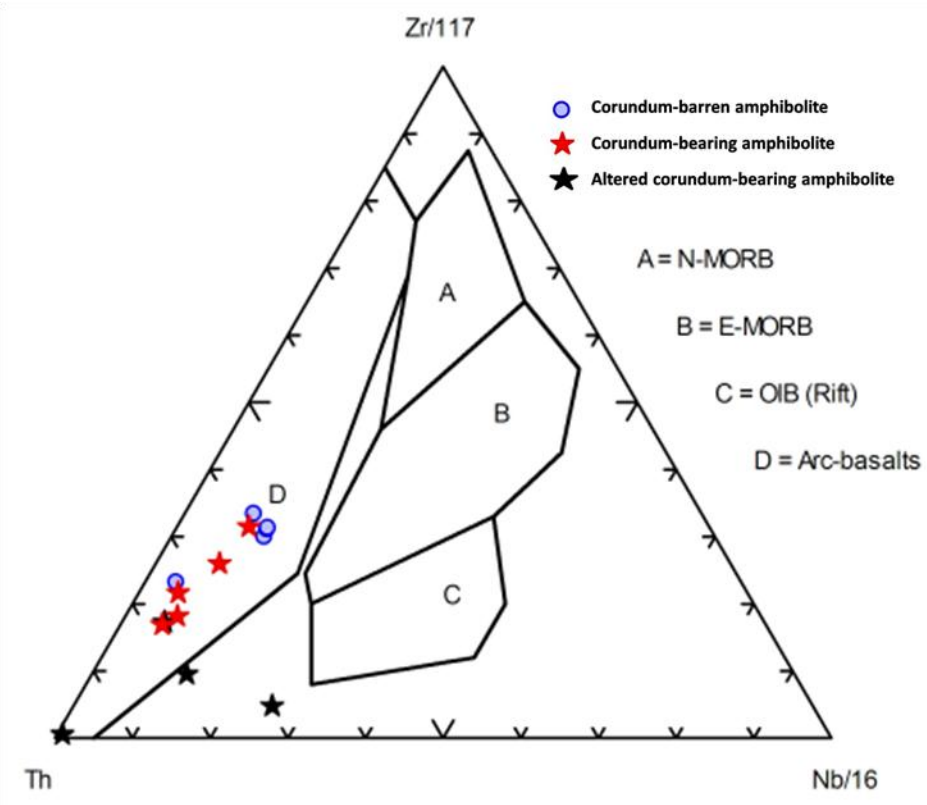

Figure 5.6 Th-Zr-Nb tectono-diagram (after Wood, 1980) indicating most whole-rock analyses of amphibolites associated with composition of arc-basalt.

According to geochemistry analyses, they may indicate, on the basis of isochemical metamorphic process, that the initial compositions of amphibolites, both corundum-barren amphibolite and corundum-bearing amphibolite may have originated from calc-alkali basaltic magmas within an ancient region involving island arc and mid oceanic ridge.

In addition, chondrite-normalized REE patterns (chondrite composition after Sun and McDonaugh, 1989) (Figures 5.7 to 5.10) of all amphibolites and gneiss are compared to patterns of the same types of rocks found in Mozambique Belt from Tanzania (reported by Tenczer et al., 2006; Hauernhofer et al., 2009) and Kenya (Hauernhofer et al., 2009) as presented in the color shaded patterns. Most corundum-bearing amphibolites (Figure 5.7) altered corundum-bearing amphibolites (Figure 5.8), and corundum-barren amphibolites (Figure 5.9), show slightly decreasing from LREE to HREE which La/Lu ratios range from about 2.95-10.12 for corundum-bearing amphibolites, 4.18-11.39 for altered corundum-bearing amphibolites and 2.57-6.43 for corundum-barren amphibolites. These ratios suggest a rifting, MORB to subduction magmatism (Hauernhofer et al., 2009). Gneiss samples show steeper slope of decreasing trend from LREE to HREE with wide La/Lu ratios from 2.30-26.02 (see Figure 5.10). The higher concentrations of whole REE range indicate low-degrees of partial melting of subduction-related arc material (Hauernhofer et al., 2009). Subsequently, magma differentiation may lead to various felsic compositions of gneiss in this area.

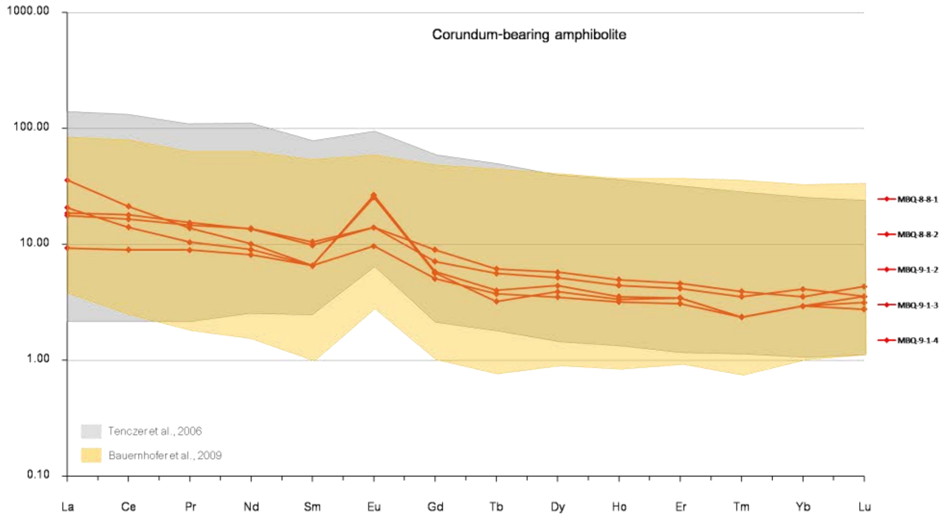

Figure 5.7 Chondrite-normalized REE pattern (chondrite composition after Sun and McDonaugh, 1989) of corundum-bearing amphibolites from Montepuez, Mozambique compared to color shaded pattern of amphibolite in Tanzania (data from Tenczer et al., 2006; Hauernhofer et al., 2009) and Kenya (data from Hauernhofer et al., 2009), Mozambique Belt.

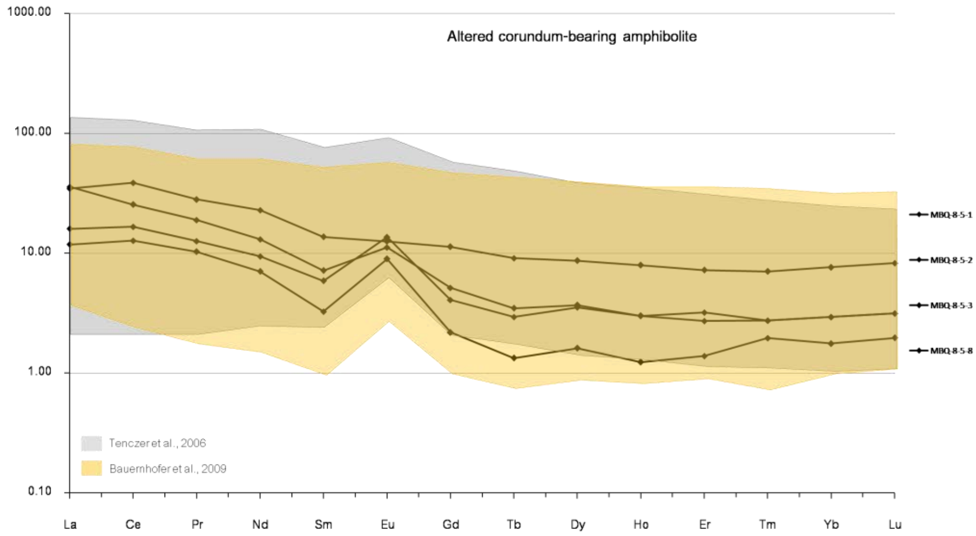

Figure 5.8 Chondrite-normalized REE pattern (chondrite composition after Sun and McDonaugh, 1989) of altered corundum-bearing amphibolites from Montepuez, Mozambique compared to shaded pattern of amphibolite in Tanzania (data from Tenczer et al., 2006; Hauernhofer et al., 2009) and Kenya (data from Hauernhofer et al., 2009), Mozambique Belt.

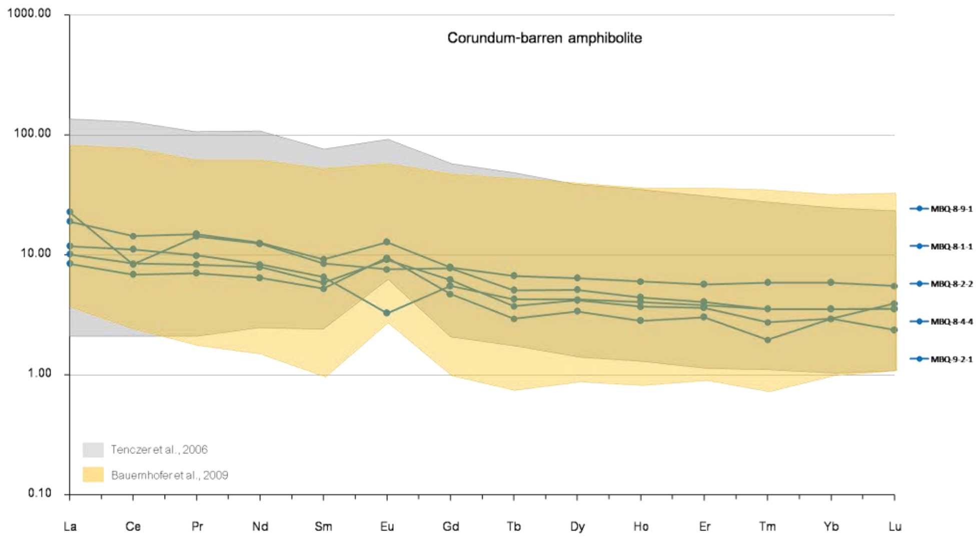

Figure 5.9 Chondrite-normalized REE patterns (chondrite composition after Sun and McDonaugh, 1989) of corundum-barren amphibolites from Montepuez, Mozambique compared to color shaded pattern of amphibolite in Tanzania (reported by Tenczer et al., 2006; Hauernhofer et al., 2009) and Kenya (reported by Hauernhofer et al., 2009), Mozambique Belt.

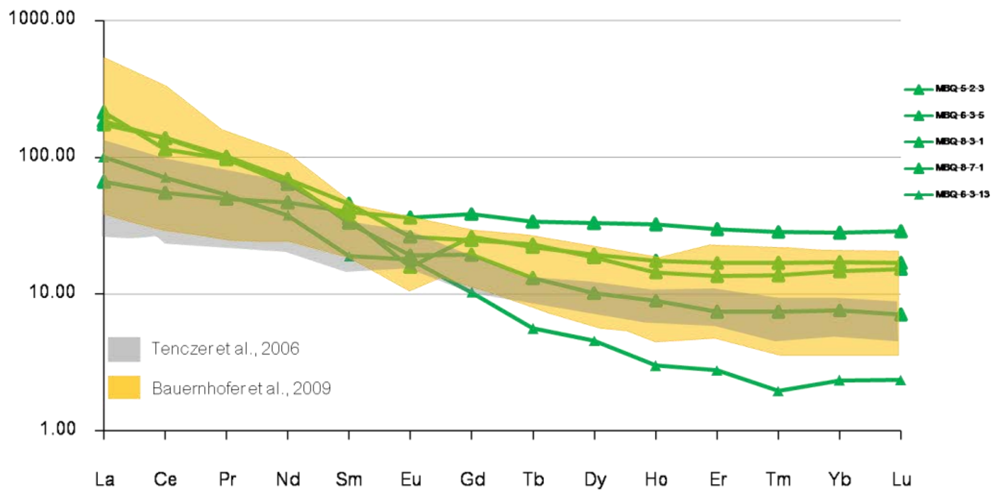

Figure 5.10 Chondrite-normalized REE pattern (chondrite composition after Sun and McDonaugh, 1989) of gneiss from Montepuez, Mozambique compared to shaded pattern of gneiss in Tanzania (data from Tenczer et al., 2006; Hauernhofer et al., 2009) and Kenya (data from Hauernhofer et al., 2009), Mozambique Belt.

Geochemically, high grade metamorphic rocks in Motepuez Deposits represented by amphibolites and gneiss are originated from different protoliths with a tectonic setting environment which has been related to tectonic evolution of the East African Orogen (Figure 5.11) suggested by stern (1994).

During Neoproterozoic, seafloor spreading, formation of volcanic arcs and back-arc basins, and terrane accretion had taken place 870-690 Ma (see Figure 5.11) (Stern, 1994) that originated all types of protoliths. Amphibolites' protoliths are indicated by basic rocks which is calc-alkali basaltic magmas within an ancient region involving island arc and mid oceanic ridge within MORB to subduction magmatism region (Hauernhofer et al., 2009). Gneiss protolith can be indicated by quartzo-feldspartic rocks and pelitic rocks referring to subduction-related arc material (Hauernhofer et al., 2009).

Then continental collision of East and West Gondwana led to crustal thickening, uplift and formation of granulite as 750-650 Ma (see Figure 5.11) (Stern, 1994).

Orogenic collapse and escape tectonic during 650-550 Ma may effect granulite formation (see Figure 5.11) (Stern, 1994) that can be related to Mozambique Belt formation (Figure 5.12) (Fritz et al, 2005). Mozambique Belt formation has been devided into 2 stages, Western Granulite and Eastern Granulite, respectively (Fritz et al, 2005). REE pattern analyses also present most of metamorphic rocks in Montepuez Deposits relate to Eastern Granulite in which amphibolite may be related to metaanorthosite (Figure 5.12) and gneiss may be related to metamagmatic rocks (Figure 5.12).

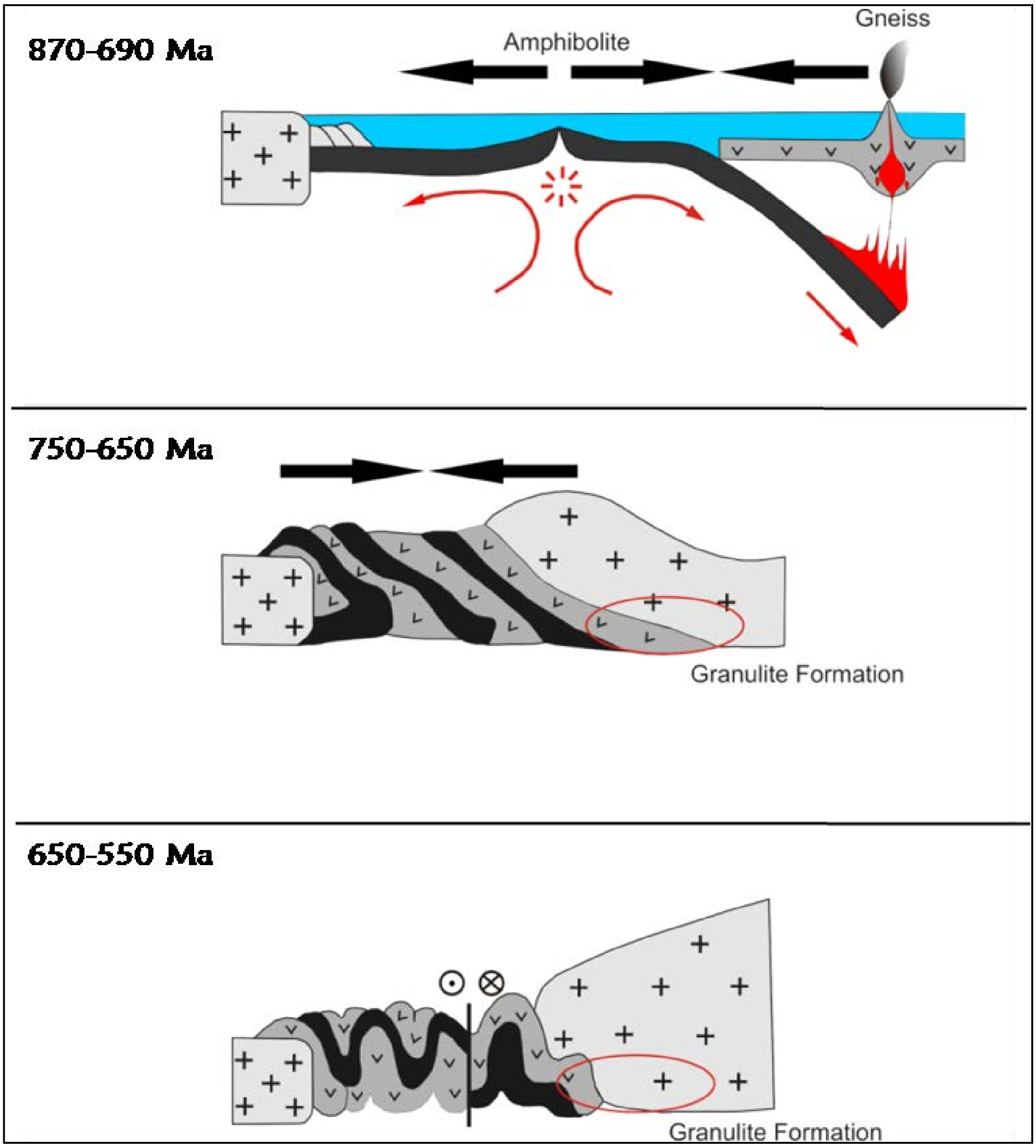

Figure 5.11 Tectonic evolution of East Africa Orogen (modified after Stern, 1994).

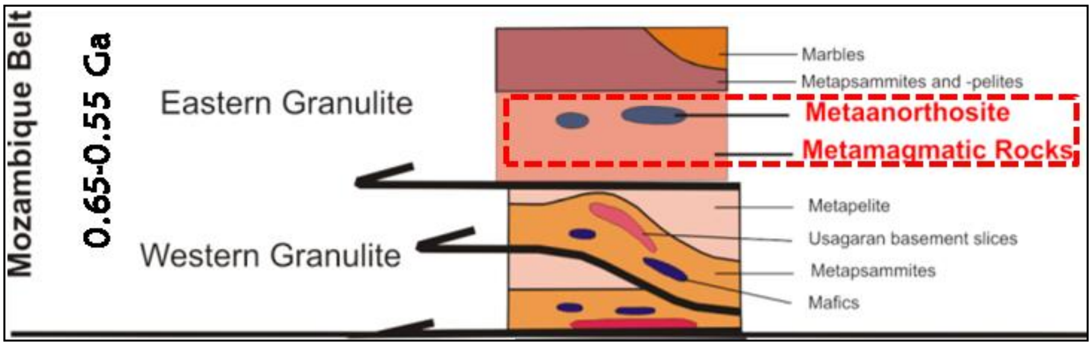

Figure 5.12 Tectono-stratigraphy of Mozambique Belt and main lithologies, amphibolite appears to have related to meta-anorthosite whereas gneiss appears to have related to metamagmatic rocks of Eastern Granulite from central Tanzania (after Fritz et al., 2005).

5.2 P-T Estimation for Metamorphism

ACF diagram, plots of mole proportion between A (Al_2O_3+FeO-(Na_2O+K_2O)), C (CaO+3.33P_2O_5) and F (FeO+MgO+MnO), were selected for presentation of metamorphic facies amphibolite (Figure 5.1) and gneiss (Figure 5.2) in this study. Therefore, both of amphibolite and gneiss are significantly corresponding to amphibolites facies, based on their mineral assemblages (Nelson, 2001).

P–T conditions of metamorphism were determined by combination methods. Calibrations of geothermobarometer were selected according to mineral assemblage of each selective sample. Moreover, thermodynamic equilibrium calculations, pseudosections, were calculated to constrain P–T condition of metamorphism. Thermodynamic modeling was performed by Perplex (Connolly, 1995; 2005).

Three samples were selected including MBQ-9-1-4 of corundum-bearing amphibolite, MBQ-8-9-1 of corundum-barren amphibolite and MBQ-5-2-3 of gneiss.

Al in hornblende calibrated for barometer (Schmidt, 1992) was applied for pressure estimating by Mathematica package PET (Dachs, 1998; 2004).

Pseudosections yielded by Perplex (Connolly, 2005) were constructed by internally consistent thermodynamic dataset (hp04ver.dat) from Holland and Powell (1998). The chemical system Na_2O–MgO-MnO–Al_2O_3–SiO_2–CaO–FeO–H_2O was used for amphibolite samples and Na_2O–MgO-MnO–Al_2O_3–SiO_2–K_2O-CaO–FeO–H_2O was used for gneiss sample.

The results of P-T estimation from combination of psudosection and Al in hornblende barometry calculation are described below.

Regarding to corundum-bearing amphibolite (MBQ-9-1-4), its pseudosection shows a series of mineral assemblages (Figure 5.13). The stability field which contains the assemblage of Pl-Gt-di-parg-clin-q-cor (di-clin-q are absent phases) is stable in a narrow P–T field. In order to restrict the P–T conditions, mineral isopleths of plagioclase (Xan) and Al in hornblende barometry were taken into account. Consequently, P–T conditions can be limited as about10.5-11 kbar and~550– 600 ^{o}C.

Corundum-barren amphibolite (MBQ-8-9-1) shows mineral assemblages of Pl-Gt-di-parg-clin-q (di-clin-q are absent phases) (Figure 5.14). Psudosection, mineral isopleths of plagioclase (Xan) and Al in hornblende barometry show P-T range of about 10.5-11.5 kbar and 450-550 ^{o}C.

Gneiss (MBQ-5-2-3) shows the stability field of the mineral assemblage Bio-Pl-Gt-Cpx-parg-q-H_2O (Cpx is absent phase) (Figure 5.15). P-T psudosection and Al in hornblende barometry indicate P-T range of about 9-9.5 kbar and ~550-600 ^{o}C.

Regarding to psudosections, some absent phases in amphibolites have also been distinguished. Quartz may be absent caused by low melting point of silica and low content in amphibolites. Diopside may be transferred to amphibole whereas clinochlore may appear in mica. Moreover, clinopyroxene in gneiss is absent due to amphibole formation.

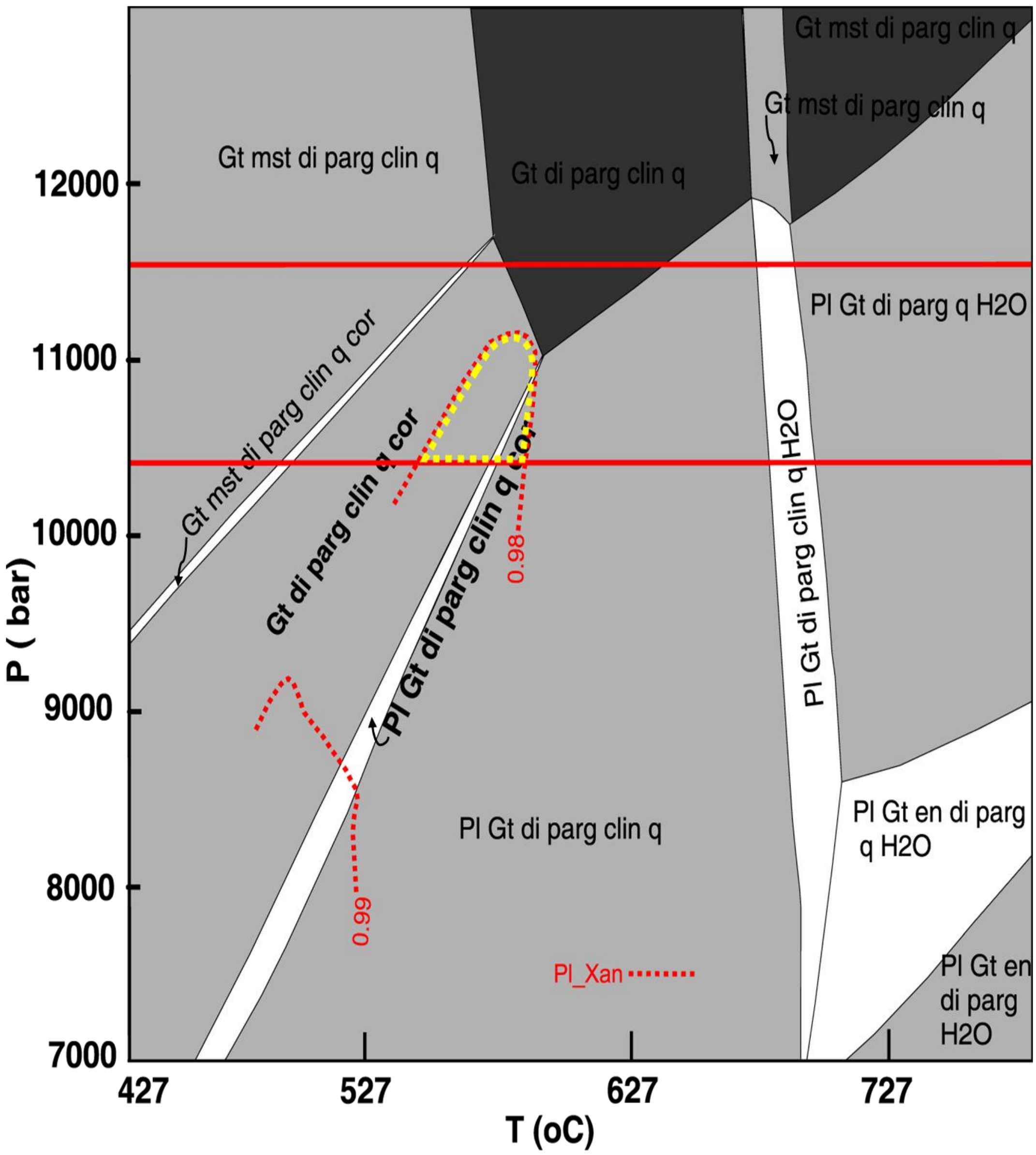

Figure 5.13 Intersections of P-T psudosection, anortite isopleths and amphibole barometry (red lines) of representative corundum-bearing amphibolite (MBQ-9-1-4).

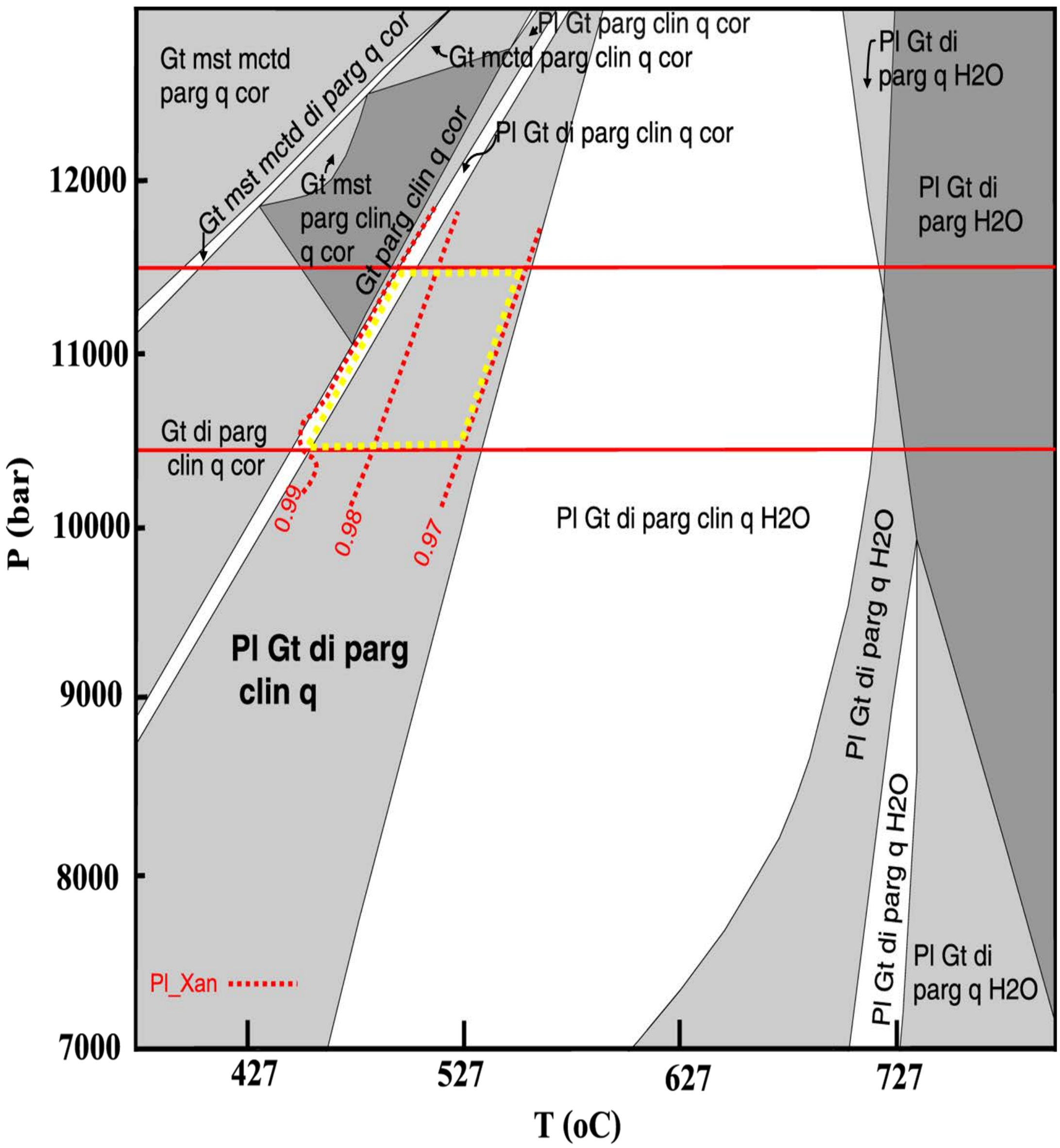

Figure 5.14 Intersections of P-T psudosection, anortite isopleths and amphibole barometry (red lines) of representative corundum-barren amphibolite (MBQ-8-9-1).

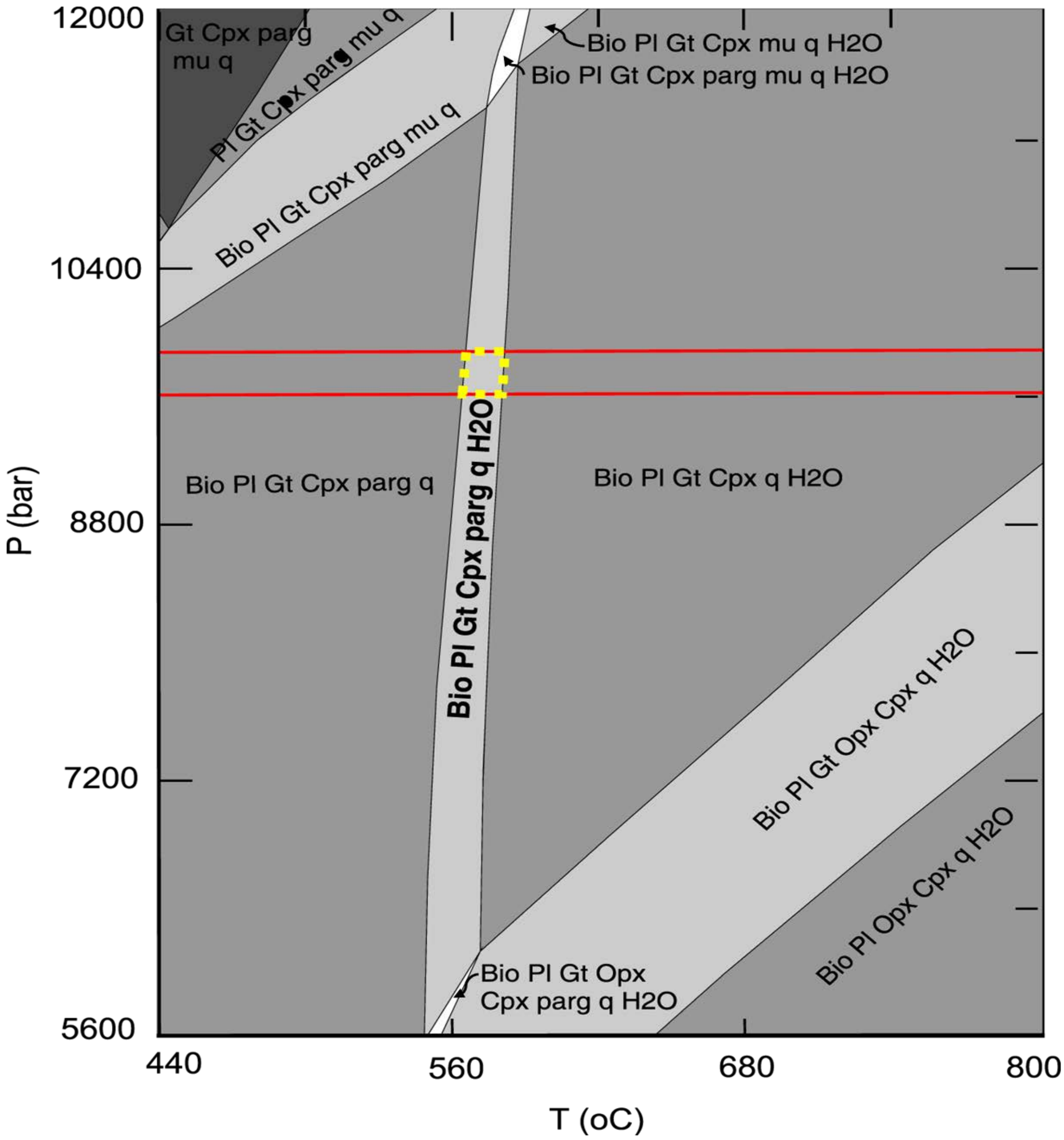

Figure 5.15 Intersections of P-T psudosection and amphibole barometry (red lines) of representative gneiss (MBQ-5-2-3).

All of temperature and pressure ranges calculated from P-T psudosections, amphibole barometry and mineral isopleths are also plotted together in Figure 5.16. They mainly belong to amphibolite facies that are similar to previous reports from Montepuez Complex Metamorphism (Boyd et al., 2010). These metamorphic conditions are related to Eastern Granulite of Mozambique Belt northward to Tanzania and SE-Kenya. Their peak of metamorphism was reported to be granulite facies (Hauzenberger et al., 2004; Fritz et al., 2009) before eastern granulite appear to have been cooling down to amphibolite facies (Fritz et al., 2009; Muhongo et al., 1999).

Pressure and temperature (P-T) plots of amphibolites and gneiss from Montepuez, Northeastern Mozambique (Figure 5.16) show P-T ranges close to melting curve of basalt (dashed line) at higher temperature. Migmatite found in the study area clearly indicates patial melting process of gneiss which may relate to pegmatite formation that probably led to alteration of corundum-bearing amphibolite.

Aluminosilicate equilibriums (black lines) show show all PT ranges of Montepuez metamorphic rocks falling within kyanite field (Figure 5.16) that indicate high pressure condition.

PT conditions of all metamorphic rocks range from ~9.5-11.5 kbar and ~450-600 ^{o}C in amphibolite facies (Figure 5.16) that can be comparable to metamorphism of Easrtern Granulite in Tanzania (about 10-12 kbar and 850^{o}C) (reported by Fritz et al., 2005).

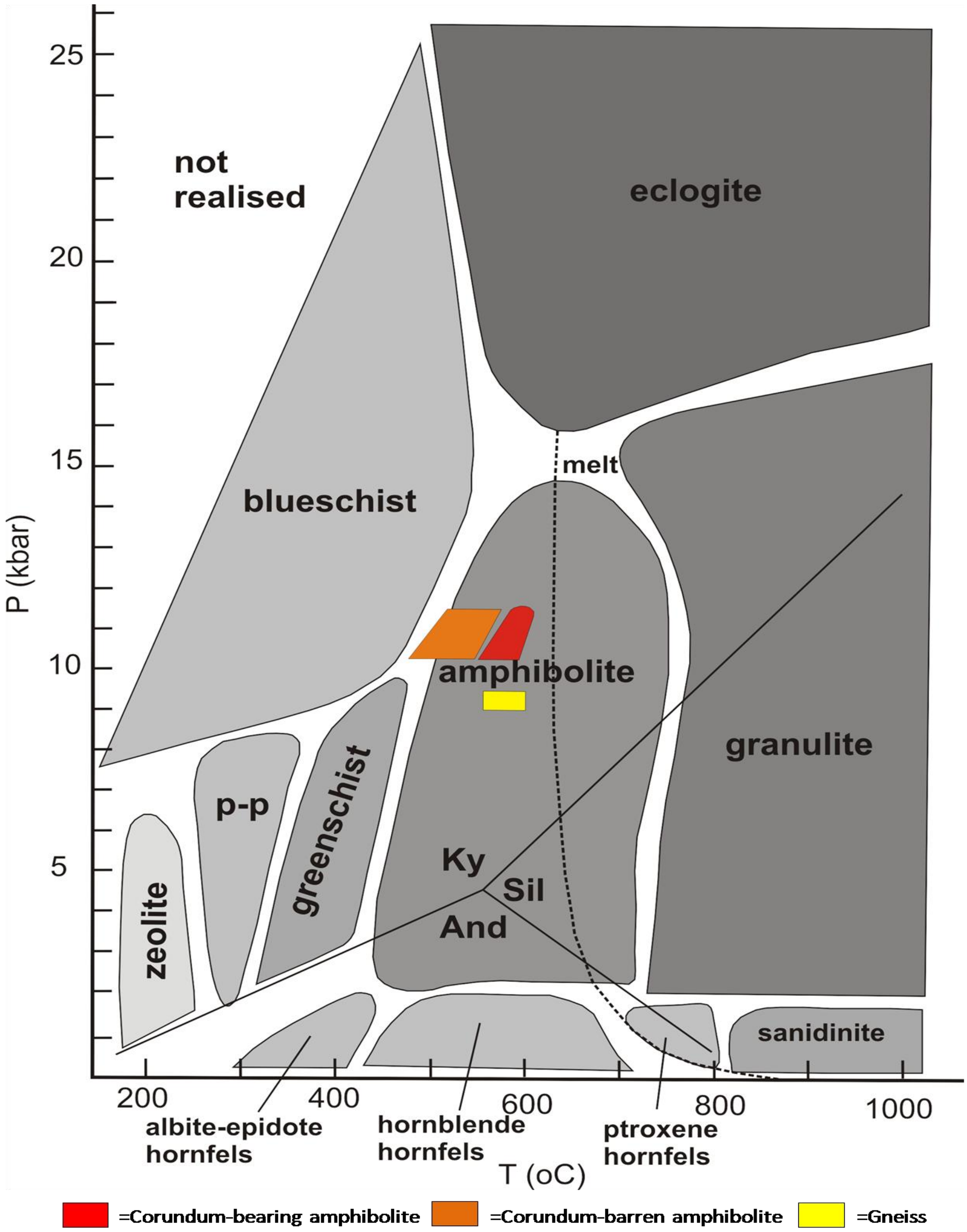

Figure 5.16 Plots of pressure and temperature (P-T) ranges of amphibolites and gneiss from Montepuez, Northeastern Mozambique under this study in correlation with metamorphic facies after Vernon and Clarke (2008).

5.3 Corundum Formation

Montepuez corundum deposits in Northeastern Mozambique have been considered as an important source of corundum especially ruby and pink sapphire (GIT-GTL, 2010, Atichat et al., 2011). They have been mainly discovered in primary deposits; however, some secondary deposits also occur along the primary rocks. Based on previous works, primary corundum deposits can be divided into many geological environments (Figure 5.17). Montepuez corundum deposits are significantly related to metamorphic sources which is corundum-bearing amphibolite and altered corundum-bearing amphibolite.

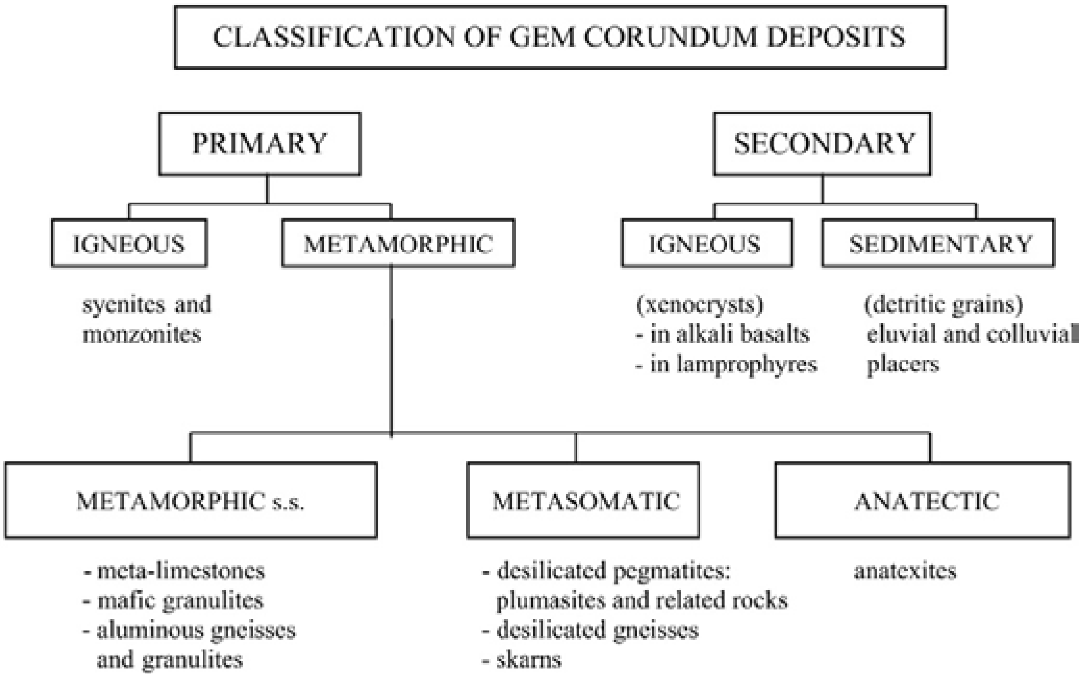

Figure 5.17 Classification scheme for gem corundum deposits (Simonet et al., 2008).

Based on petrographic study, crucial mineral assemblages, including corundum, amphibole, plagioclase, spinel, mica and garnet of corundum-bearing amphibolite may indicate corundum origin as described by the following reactions.

2Hornblende + 9Corumdum = 8Spinel + 4Plagioclase + 4Silica + 2 Water + 1/2Oxigen ....(1)

$(2Ca_2Mg_4Al_3Si_6O_{22}(OH)_2 + 9Al_2O_3 = 8MgAl_2O_4 + 4CaAl_2Si_2O_8 + 4SiO_2 + 2H_2O + 1/2O_2)$

3Plagioclase = Garnet + 2Corumdum + 3Silica ....(2)

$(3CaAl_2Si_2O_8 = Ca_3Al_2Si_3O_{12} + 2Al_2O_3 + 3SiO_2)$

PT estimation of corundum-bearing amphibolite shows temperature of about 550 – 600 ^oC and pressure of 10.5-11 kbar. These PT ranges are similar to those previously reported at T= 650 ^OC and P=9.5 kbar for metamorphic ruby from Montepuez (SSEF Swiss Gemmological Institute, 2010) (Figure 5.18). Moreover, this condition can be compared to PT data summarized for gem corundum deposits reported by Simonet et al. (2008) (Figure 5.18).

Corundum should have originated within high grade metamorphism under condition of amphibolite facies (Rakotondrazafy et al., 2008, Simonet et al., 2008). Their protolith should contain high alumina and low silica contents (Simonet et al., 2008) which may be close to basic rocks such as basaltic magma.

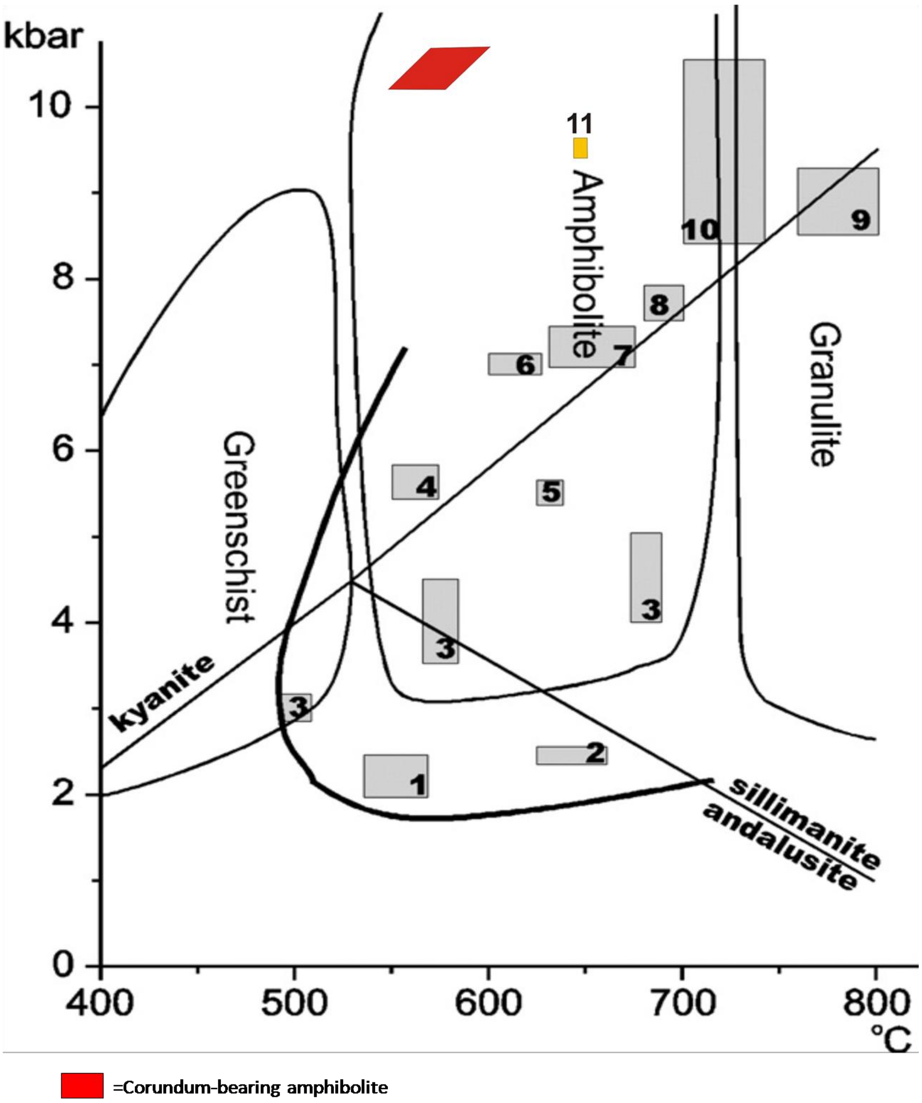

Figure 5.18 Plots of P–T conditions of corundum-bearing amphibolite available under this study in correlation with formation of metamorphic gem corundum after Simonet et al. (2008). The thick black line outlines the “gem corundum domain”, Boxes indicate P–T fields of known deposits. Key: 1.Mong Hsu rubies; 2. Ural rubies in marbles; 3. Kashmir sapphires; 4.Greenlandmetasomatic rubies; 5. Sri Lanka sapphires from granulites; 6. Pakistan rubies in marbles; 7. Metasomatic rubies fromsouthern Kenya; 8. Corundum-bearing anatexites of Morogoro; 9. Rubies from mafic granulites, North Carolina; 10. Metasomatic rubies from Southern Kenya (Simonet et al., 2008) and 11. Metamorphic rubies from Montepuez, Mozambique (SSEF Swiss Gemmological Institute, 2010)

5.4 Conclusions

1.) Montepuez corundum deposits in Northeast Mozambique are closely associated with amphibolite. However, four groups of rocks in the area can be distinguished according to corundum occurrence, physical properties, petrographic description, whole-rock geochemistry and mineral chemistry. They are corundum-bearing amphibolite, altered corundum-bearing amphibolite, corundum-barren amphibolite and gneiss.

2.) Corundum-bearing amphibolite is composed of essential corundum, amphibole, spinel and plagioclase with minor composts of garnet and mica. Moreover, some corundum-bearing amphibolites have been altered to contain significant mica and clay minerals. These altered rocks are crucially associated with pegmatite. Geochemically, their protolith should be close to basic rocks which undertook metamorphism under amphibolite facies condition.

3.) Corundum-barren amphibolite contains amphibole, plagioclase, spinel and garnet. They may have originated from similar protolith of corundum-bearing amphibolite. However, they may have undertaken metamorphism of lower temperature of amphibolite facies.

4.) Gneiss is composed of plagioclase, microcline, biotite, quartz, amphibole and garnet. Geochemically, quartzo-feldspathic rocks and pelitic rocks appear to be protolith before undertaking metamorphism and reaching amphibolite facies.

5.) Corundum should have originated from high grade metamorphism under condition of amphibolite facies as indicated by P-T condition with close reaction related to amphibole, plagioclase, spinel and garnet.

6.) Corundum (ruby) is closely associated with corundum-bearing amphibolite which contains abundant amphibole. On the other hand, corundum-barren amphibolite presents more abundance of plagioclase with less amount of spinel. However, both of them appear to occur as lens in gneiss basement.

REFERENCES

Accommodation Mozambique. 2013. Northern, Central and Southern Mozambique Maps [online]. Available from: http://www.accommodationmozambique.co.za/mozambique-map.html. [2013, Febuary 12]

Andreoli, M. A. G. 1984. Petrochemistry, Tectonic Evolution and Metasomatic Mineralisations of Mozambique Belt Granulites from S Malawi and Tete (Mozambique). Precambian Research 25: 161-186.

Appel, P. 1998. High-pressure granulite facies metamorphism in the Pan-African belt of eastern Tanzania: P-T-t evidence against granulite formation by continent collision. J. metamorphic Geol. 16: 491-509.

Atichat, W., Sutthirat, C., Pisutha-Arnond, V., Wathanakul, P., Sriprasert, B., and Leelawatanasuk, T. 2011. "Mozambique" Ruby-An African Shining Star. [online]. Available from: www.gemstone.org.

Bingen, B., et al. 2009. Geochronology of the Precambrian crust in the Mozambique belt in NE Mozambique, and implication for Gondwana assembly. Precambrian Research 170: 231-255.

Boyd, R., et al. 2010. The Geology and Geochemistry of the East African Orogen in Northeastern Mozambique. South African Journal of Geology 113(1): 87-129.

Chen, T. 2001. Mozambique Belt: The Link Between East and West Gondwana in the Neoproterozoic and Possible Connection with the Trans-Antarctic Mountains. Gondwana Research 4(4): 594-595.

Collins, A. S., and Pisarevsky, S. A. 2005. Amalgamating eastern Gondwana: The evolution of gthe Circum-Indian Orogens. Earth-Science Reviews 71: 229-270.

Condie, K. C. 2003. Supercontinents, superplumes and continental growth: the Neoproterozoic record. Geological Society of London, Spacial publications 206: 1-25.

Connolly, J.A.D. 1995. Phase–diagram methods for graphitic rocks and application to the system C-O–H–FeO–TiO2–SiO2. Contribution to Mineralogy and Petrology 119: 94–116.

Connolly, J.A.D. 1995. Phase–diagram methods for graphitic rocks and application to the system C-O–H–FeO–TiO2–SiO2. Contribution to Mineralogy and Petrology 119: 94–116.

Dachs, E. 1998. PET: Petrological Elementary Tools for Mathematica. Computers & Geosciences 24: 219–235.

Dachs, E. 2004. PET: Petrological Elementary Tools for Mathematica: an update. Computers & Geosciences 30: 173–182.

Dalet, D. Mozambique. 2007. [online]. Available from: http://d-maps.com/pays.php?num_pay=41&lang=en. [2013, Febuary 12]

Droop, G. T. R. 1987. A general equation for estimating Fe3+ concentrations in ferromagnesian silicates and Oxides from microprobe analyses, using stoichiometric criteria. Mineral Magazine 51: 431-435.

Engvik, A. K., Tveten, E., Viola, G. Erambert, M., Feito, P. and de Azavedo, S. 2007. P-T-t evolution and textural evidence for decompression of Pan-African high-pressure granulites, Lurio Belt, north-eastern Mozambique. Journal of metamorphic Geoleology 25: 935-952.

Eskola, P. 1915. On the relations between the chemical and mineralogical composition in the metamorphic rocks of the Orijarvi region. Comm. geol. Finlande Bull. 44: 1-107.

Fritz, H., Tenczer, V., Hauzenberger, C. A., Wallbrecher, E. and Hoinkesn, G. 2005. Central Tanzanian tectonic map: A step forward to decipher Proterozoic structural event in the East African Orogen. Tectonics 24: 1-26.

Fritz, H., Tenczer, V., Hauzenberger, C., Wallbrecher, E. and Muhongo, S. 2009. Hot Granulite nappes-Tectonic styles and thermal evolution of the Proterozoic granulite belts in East Africa. Tectonophysics 477: 160-173.

GIT Gem Testing Laboratory. 2010. New ruby deposits in Mozambique [online]. Available from: http://www.git.or.th. [2013, Febuary 26].

Grantham, G.H., et al. 2008. Terrane correlation between Antarctica, Mozambique and Sri Lanka; comparisons of geochronology, lithology, structure and metamorphism and possible implications for the geology of southern Africa and Antarctica. Geological society of London, spacial Publications 308: 91-119.

Grantham, G.H., Thomas, R. J., and Mendonidis, P. 1994. Contrasting P-T-t loops from southern East Africa, Natal and East Antarctica. Journal of African Earth Sciences 19(3): 225-235.

Hauernhofer, A.H., et al. 2009. Geochemistry of basement rocks from SE Kenya and NE Tanzania: indications for rifting and early Pan-African subduction. Int J Earth Sci (Geol Rundsch) 98: 1809-1834.

Hauzenberger, C. A., Bauernhofer, A. H., Hoinkes, G., Wallbrecher, E., and Mathu, E. M. 2004. Pan-African high pressure granulites from SE-Kenya: Petrological and geothemobarometric evidence for a polycyclic evolution in the Mozambique belt. Journal of African Earth Sciences 40: 245-268.

Holland, T.J.B., and Powell, R. 1998. An internally consistent thermodynamic data set for phase of petrological interest. Journal of Metamorphic Geology 16: 309–343.

Irvine, T.N., and Baragar, W.R.A. 1971. A guide to the chemical classification of the common volcanic rocks. Can. J. Earth Sci.: 523-548.

Jacobs, J., and Thomas, R. J. 2004. Himalayan-type indenter-escape tectonics model for the southern part of the late Neoproterozoic-early Paleozoic East African-Antarctic orogen. Geological Society of America 32 (8): 721-724.

Jian, P., et al. 2009. Devonian to Permian plate tectonic cycle of the Paleo-Tethys Orogen in southwest China (I): Geochemistry of ophiolites, arc/back-arc assemblages and within-plate igneous rocks. Lithos 113: 748-765.

Johnson, S. P., Cutten, H. N. C., Muhongo, S., and De Waele, B., 2003. Neoarchean magmatism and metamorphism of the western granulites in the central domain of the Mozambique belt, Tanzania: U-Pb shrimp geochronology and PT estimates. Tectonophyssics 375: 125-145.

Kartz, M. B. 1974. Paired Metamorphic Belts in Precambrian Granulite Rocks in Gondwanaland. Geology: 237-241.

Klein, C., and Hurlbut, C.S. 1993. Manual of Mineralogy 21st edition. United State of America.

Kriegsman, L. M. 1994. The Pan-African event in East Antarctica: a view from Sri Lanka and the Mozambique Belt. Precambrian Research 75: 263-277.

Kroner, A., Sacchi, R., Jaeckel, P., and Coata, M. 1997. Kibaran magmatism and Pan-African granulite metamorphism in northern Mozambique: single zircon ages and regional implications. Journal of African Earth Sciences 25(3): 467-484.

Kroner, A., Willner, A. P., Hegner, E., Kaeckel, P., and Nemchin, A. 2001. Single zircon ages, PT evolution and Nd isotopic systematics of high-grade gneisses in southern Malawi and their bearing on the evolution of the Mozambique belt in sotheastern Africa. Precambrian Research 109: 257-291.

Le Bas, M.J., LeMaitre, R.W., Streckeisen, A., and Zanettin, B.A. 1986. Chemical classification of volcanic rocks based on the total alkali silica diagram. J. Pet. 27: 745-750.

Leake, B.E. 1997. Nomenclature of amphibole: report of the subcommittee amphiboles of the international mineralogy association, commission on new minerals and mineral names. The Canadian Mineralogist 35: 219-246.

Lehto, T., and Goncalves, R. 2008. Mineral resources potential in Mozambique. Geological Survey of Finland, Special Paper 48: 307–321.

Maboko, M. A. H. 1997. P-T conditions of metamorphism in the Wami River granulite complex, central coastal Tanzania: implications for Pan-African geotectonics in the Mozambique Belt of eastern Africa. Journal of African Earth Sciences 24(1/2): 51-64.

Maboko, M. A. H. 2000. Nd and Sr isotopic investigation of the Archean-Proterozoic boundary in north eastern Tanzania: constraints on the nature of Neoproterozoic tectonism in the Mozambique Belt. Precambrian Research 102: 87-98.

Maboko, M. A. H. 2000. Preliminary Evidence for a second ~525-545 Ma OLD event of granulite facies metamorphism in the Mozambique belt of Tanzania and its implications for a two-stage model for Gondwana assembly. Tanz. J. Sci. 26: 16p.

Maboko, M. A. H. 2001. Dating Post-Metamorphic Cooling of the Eastern Granulites in the Mozambique Belt of Northern Tanzania Using the Garnet Sm-Nd Method. Gondwana Research 4(3): 329-336.

Maboko, M. A. H., and Nkamura, E. 2002. Isotopic dating of Neoproterozoic crustal growth in the Usambara Mountains of Northeastern Tanzania: evidence for coeval crust formation in the Mozambique Belt and the Arabian-Nubian Shield. Precambrian Research 113: 227-242.

Macey, P. H., et al. 2010, Mesoproterozoic geology of the Nampula Block, northern Mozambique: Tracing Fragments of Mesoproterozoic crust in the heart of Gondwana. Precambrian Research 182: 124-148.

Malisa, E., and Muhongo, S. 1990. Tectonic Setting of Gemstone Mineralization in the Proterozoic Metamorphic Terrane of the Mozambique Belt in Tanzania. Precambrian Research. 46: 167-176.

Marcos, E.O.J. 2011. Mozambique [online]. Available from: http://en.wikipedia.org/wiki/Mozambique. [2013, Febuary 12]

Meert, J. G. 2003. A synopsis of events related to the assembly of eastern Gondwana. Tectonophysics 362: 1-40.

Mercier, A., Debat P., and Saul J. M. 1999. Exotic origin of the ruby deposits of the Mangari area in SE Kenya. Ore Geology Reviews 14: 83-104.

Ministry of Mineral Resources of Mozambique. 2005. Geological map 1:250000. Sheet 1239.

Ministry of Mineral Resources of Mozambique. 2005. Geological map 1:250000. Sheet 1339.

Muhongo, A. 1999. Anatomy of the Mozambique Belt of Eastern and Southern Africa: Evidence from Tanzania. Gondwana Research 2(3): 369-375.

Muhongo, S., Kroner, A., Wallbrecher, E., Tuisku, P., Hauzenberger, C., and Sommer, H. 2001. Crosss-Section Through the Mozambique Belt of East Africa and Implications for Gondwana Assembly. Gondwana Research 4(4): 709-780.

Muhongo, S., Tuisku, P., and Mtoni, Y. 1999. Pan-African pressure-temperature evolution of the Merelani area in the Mozambique Belt in northeast Tanzania. Journal of African Earth Sciences 29(2): 353-365.

Munyanyiwa, H., Hanson, R. E., Blenkinsop, T. G., and Treloar, P. J. 1997. Geochemistry of amphibolites and quartzofeldapathic gneisses in the Pan-African Zambezi belt, northweat Zimbabwe: evidence for bimodal magmatism in a continental rift setting. Precambrian Research 81: 179-196.

Murphy, J. B., and Nance, R. D. 1991. Supercontinent model for the contrasting character of Late Proterozoic orogenic belts. Geology 12: 469-472.

Nelson, S.A. 2004. Metamorphic facies & metamorphism and plate tectonics. Earth Materials [online]. Available from: http://www.tulane.edu/metamorphic_facies. [2013, Febuary 26].

Nelson, S.A. 2004. Metamorphic facies & metamorphism and plate tectonics. Earth Materials [online]. Available from: http://www.tulane.edu/metamorphic_facies. [2013, Febuary 26]

NordNordWest. 2012. Pemba, Mozambique [online]. Available from: http://en.wikipedia.org/wiki/Pemba,_Mozambique. [2013, Febuary 12]

Nyamai, C. M., Opiyo-Akech, N., Gaciri, S. J., and Fujimaki, H. 1999. Geochemistry and Tectonomagmatic Affinities of the Mozambique Belt Intrusive Rocks in Matuu-Masinga Area, Central Kenya. Gondwana Research 2 (3): 387-399.

Oliveira, P. 2005. Climate of Mozambique [online]. Available from: http://en.wikipedia.org/wiki/Mozambique#Climate. [2013, Febuary 12]

Pearce, J.A. 1983. The role of subcontinental lithosphere in magma genesis at destructive plate margins. In Continental basalts and mantle xenoliths: 230-249.

Pinna, P. 1995. Short Communication on the dual nature of the Mozambique Belt, Mozambique to Kenya. Journal of African Earth Sciences 21(3): 477-480.

Pinna, P., Jourde, G., Calvez, J. Y., Mroz, J. P., and Marques, J. M. 1993. The Mozambique Belt in Northern Mozambique: Neo-proterozoic (1100-850 Ma) crustal growth and tectogenesis, and superimposed Pan-African (800-550 Ma) tectonism. Precambrian research 62: 1-59.

Powell, C., Mc, A., And Pisarevsky, S. A. 2002. Late Neoproterozoic assembly of East Gondwana. Geological Society of American 30(1): 3-6.

Rakotondrazafy, A. F. M., et al. 2008. Gem corundum deposites of Madagascar: A review. Ore Geology Reviews 34: 134-154.

Reddy, S. M., Collins A.S., and Mruma A. 2003. Complex high-strain deformation in the Usagaran Orogen, Tanzania: structural setting of Palaeoproterozoic eclogites. Techtonophysics 375: 101-123.

Reeves, C., and Wit, D. M. 2000. Making ends meet in Gondwana: retracing the transforms of the Indian Ocean and reconnecting continental shear zones. Terra Nova 12(6): 272-280

Rollinson, H.R. 1993. Using geochemical data: evaluation, presentation and interpretation. Longman Scientific and Technical Ltd.: Harlow, UK.

Sacchi, R., Cadoppi, P., and Costa, M. 2000. Pan-African reactivation of the Lurio segment of the Kibaran Belt system: a reappraisal from recent age determinations in northern Mozambique. Journal of African Earth Sciences 30(3): 629-639.

Sacchi, R., Marques, J., Costa, M., and Casati, C. 1984. Kibaran Events in The Southernmost Mozambique Belt. Precambrian Research 25: 141-159.

Schwarz, D., et al. 2008. Rubies and Sapphires from Winza, Central Tanzania. Gem&Gemology: 322-347.

Shackleton, R. M. 1996. The final collision zone between East and West Gondwana: where is it?. Journal of African Earth Sciences 23(3): 271-287.

Shapiro, L. 1975. Rapid Analysis of Silicate, Carbonate, and Phosphate Rocks-Revised Edition. Geological Survey Bulletin 1401.

Shibata, K., Suwa, K., Uchiumi, S., and Agata, T. 1996. Excess Ar in biotites from the Broderick Falls (Webuye) western Kenya: implications for the Mozambique Belt and its Archaean foreland. Journal of African Earth Sciences 23: 433-441.

Simonet, C., Fritsch, E., and Lasnier, B. 2008. A classification of gem corundum deposits aimed towards gem exploration. Ore Geology Reviews 34: 127-133.

SSEF Swiss Gemmological Institute. 2010. New rubies from Montepuez, Mozambique. SSEF Facette 17: 24.

Stern, R. J. 1994. Arc Assembly and Continental Collision in the Neoproterozoic East African Orogen: Impications for the Consolidation of Gondwanaland. Earth Planet. Sci. 22: 319-351.

Sun, S., and McDonough, W. F. 1989. Chemical and isotopic sysbtematics of oceanic basalts: implications for mantle composition and processes. Geological Society of London. Spacial Publications 42: 313-345.

Suwa, K., Suzuki, K., and Agata, T. 1996. Vanadium grossular from the Mozambique metamorphic rocks, south Kenya. Journal of Southeast Asian Earth Science 14: 299-308.

Tenczer, V., et al. 2006. Anorthosites in the Eastern Granulites of Tanzania-New SIMS zircon U-Pb age data, petrography and geochemistry. Precambian Research 148: 85-114.

Tenczer, V., Fritz, H., Bauernhofer, A., and Hauzenberger, C. 2007. Two orogens- One shear belt: 1 Ga of repeated deformation along the Central Tanzanian Shear Belt. Journal of structural Geology 29: 1632-1649.

Thomas, R. J., Jacobs, J., Horstwood, M. S. A., Ueda, K., Bingen, B., and Matola, R. 2010. The Mecuburi and Alto Benfica Groups, NE Mozambique: Aids to unravelling ca. 1 and 0.5 Ga events in the East African Orogen. Precambrian Research 178: 72-90.

Thompson, R.N. 1982. British Tertiary volcanic province. Journal of Geology 18: 49-107.

Torsvik, T. H., Dietmar, M.R., DerVoo, R. V., Steinberger, B., and Gaina, C. 2008. Global Plate Motion Frames: Toward A Unified Model. Reviews of Geophysics 46: 1-44.

Ueda, K., Jacobs, J., Thomas, R. J., Kosler, J., Jourdan, F., and Matola, R. 2012. Delamination-induced late-tectonic deformation and high-grade metamorphism of the Proterozoic Nampula Complex, northern Mozambique. Precambrian Research 196-197: 275-294.

Vall, J. R. 1989. Ring complexes and related rocks in Africa. Journal of African Earth Sciences 8(1): 19-40.

Veevers, J. J. 2003. Pan-African is Pan-Gondwanaland: Oblique convergence drives rotation during 650-500 Ma assembly. Geological society of American 31: 501-504.

Vernon, R.H., and Clarke, G.L. 2008. Principles of Metamorphic Petrology. United State of America.

Viola, G., Henderson, I. H. C., Bingen, B., Thomas, R. J., Smethurst, M. A., and de Azavedo, S. 2008. Growth and collapse of a deeply eroded oroded: Insights from structural, geological, and geochronological constraints on the Pan-African evolution of NE Mozambique. Tectonics 27: 1-31.

Vogt, M., Kroner, A., Poller, U., Sommer, H., Muhongo, S., and Wingate, M. T. D. 2006. Archaean and Paleoproterozoic gneisses reworked during a Neoproterozoic (Pan-African) high-grade event in the Mozambique belt of East Africa: Structural relationships and zircon ages from the Kidatu area, central Tanzania. Journal of African Earth Sciences 45: 139-155.

Wilson, M. 1989. Igneous petrogenesis: a global tectonic approach. Unwin Hyman, Winchester.

Wood, D. A. 1980. The application of a Th-Hf-Ta diagram to problems of tectonomagnetic classification and to estrablishing the nature of crustal contamination of basaltic lavas of the Bitish Tertiary volcanic province. Earth Planet Sc. Lett 50: 11-30.

Yoshida, M., Jacobs, J., Santosh, M., and Rajesh, H. M. 2003. Role of Pan-African events in the Circum-East Antarctic Orogen of East Gondwana: a Critical overview. Geological Society of London, spacial publications 26: 57-75.

APPENDICES

APPENDIX A

List of Samples Analysis

Rock type	Samples no.	XRF	Titration	ICP-OES,	XRD	Thin section	EPMA	
							Polish thin section	Polish section
Altered Corundum-bearing amphibolite	MBQ-8-5-1	MBQ-8-5-1	MBQ-8-5-1	MBQ-8-5-1	MBQ-8-5-1	-	-	MBQ-8-5-1 (1)
Altered Corundum-bearing amphibolite	MBQ-8-5-2	MBQ-8-5-2	MBQ-8-5-2	MBQ-8-5-2	MBQ-8-5-2	-	-	MBQ-8-5-2 (1)
Altered Corundum-bearing amphibolite	MBQ-8-5-3	MBQ-8-5-3	MBQ-8-5-3	MBQ-8-5-3	MBQ-8-5-3	-	-	MBQ-8-5-3 (1,2)
Altered Corundum-bearing amphibolite	MBQ-8-5-4	-	-	-	-	-	-	MBQ-8-5-4 (1,2,3,4)
Altered Corundum-bearing amphibolite	MBQ-8-5-5	-	-	-	-	-	-	MBQ-8-5-5 (1,2)
Altered Corundum-bearing amphibolite	MBQ-8-5-6	-	-	-	-	-	-	MBQ-8-5-6 (1,2)
Altered Corundum-bearing amphibolite	MBQ-8-5-7	-	-	-	-	-	-	MBQ-8-5-7 (1,2)
Altered Corundum-bearing amphibolite	MBQ-8-5-8	MBQ-8-5-8	MBQ-8-5-8	MBQ-8-5-8	MBQ-8-5-8	-	-	MBQ-8-5-8 (1,2)
Altered Corundum-bearing amphibolite	MBQ-8-5-9	-	-	-	-	-	-	MBQ-8-5-9 (1,2)

Rock type	Samples no.	XRF	Titration	ICP-OES,	XRD	Thin section	EPMA	
							Polish thin section	Polish section
Altered Corundum-bearing amphibolite	MBQ-8-5-10	-	-	-	-	-	-	MBQ-8-5-10 (1,2)
Altered Corundum-bearing amphibolite	MBQ-8-5-11	-	-	-	-	-	-	MBQ-8-5-11 (1,2)
Altered Corundum-bearing amphibolite	MBQ-8-5-12	-	-	-	-	-	-	MBQ-8-5-12 (1,2)
Altered Corundum-bearing amphibolite	MBQ-8-5-13	-	-	-	-	-	-	MBQ-8-5-13 (1)
Altered Corundum-bearing amphibolite	MBQ-8-5-14	-	-	-	-	-	-	MBQ-8-5-14 (1)
Altered Corundum-bearing amphibolite	MBQ-8-5-15	-	-	-	-	-	-	MBQ-8-5-15 (1)
Altered Corundum-bearing amphibolite	MBQ-8-5-16	-	-	-	-	-	-	MBQ-8-5-16 (1,2)
Corundum-bearing amphibolite	MBQ-8-8-1	MBQ-8-8-1	MBQ-8-8-1	MBQ-8-8-1	MBQ-8-8-1	MBQ-8-8-1	MBQ-8-8-1 (1,2,3,4,5,6,7,8,9,10,11,12)	MBQ-8-8-1 (13,14,15,16)
Corundum-bearing amphibolite	MBQ-8-8-2	MBQ-8-8-2	MBQ-8-8-2	MBQ-8-8-2	MBQ-8-8-2	MBQ-8-8-2	MBQ-8-8-2 (1,2,3,4,5,6,7,8,9,10)	-

Rock type	Samples no.	XRF	Titration	ICP-OES,	XRD	Thin section	EPMA	
							Polish thin section	Polish section
Corundum-bearing amphibolite	MBQ-9-1-2	MBQ-9-1-2	MBQ-9-1-2	MBQ-9-1-2	MBQ-9-1-2	-	MBQ-9-1-2 (1,2,3,4,5,6,7,8)	-
Corundum-bearing amphibolite	MBQ-9-1-3	MBQ-9-1-3	MBQ-9-1-3	MBQ-9-1-3	MBQ-9-1-3	MBQ-9-1-3	MBQ-9-1-3 (1,2,3,4,5,6,7,8,9)	-
Corundum-bearing amphibolite	MBQ-9-1-4	MBQ-9-1-4	MBQ-9-1-4	MBQ-9-1-4	MBQ-9-1-4	MBQ-9-1-4	MBQ-9-1-4 (1,2,3,4,5,6,7,8)	-
Corundum-barren amphibolite	MBQ-8-1-1	MBQ-8-1-1	MBQ-8-1-1	MBQ-8-1-1	MBQ-8-1-1	MBQ-8-1-1_1		-
						MBQ-8-1-1_2		-
Corundum-barren amphibolite	MBQ-8-2-2	MBQ-8-2-2	MBQ-8-2-2	MBQ-8-2-2	MBQ-8-2-2	MBQ-8-2-2_1	MBQ-8-2-2 (1)	-
						MBQ-8-2-2_2		-
Corundum-barren amphibolite	MBQ-8-4-4	MBQ-8-4-4	MBQ-8-4-4	MBQ-8-4-4	MBQ-8-4-4	MBQ-8-4-4_1	MBQ-8-4-4 (1)	-
						MBQ-8-4-4_2		-
Corundum-barren amphibolite	MBQ-8-9-1	MBQ-8-9-1	MBQ-8-9-1	MBQ-8-9-1	MBQ-8-9-1	MBQ-8-9-1_1	MBQ-8-9-1	-
						MBQ-8-9-1_2		-
Corundum-barren amphibolite	MBQ-8-9-2	-	-	-	-	-	-	-

Rock type	Samples no.	XRF	Titration	ICP-OES,	XRD	Thin section	EPMA	
							Polish thin section	Polish section
Corundum-barren amphibolite	MBQ-8-9-3	-	-	-	-	MBQ-8-9-3_1	MBQ-8-9-3 (1,2)	-
						MBQ-8-9-3_2		-
						MBQ-8-9-3_3		-
Corundum-barren amphibolite	MBQ-9-2-1	MBQ-9-2-1	MBQ-9-2-1	MBQ-9-2-1	MBQ-9-2-1	MBQ-9-2-1_1	MBQ-9-2-1	-
						MBQ-9-2-1_2		-
Gneiss	MBQ-5-2-3	MBQ-5-2-3	MBQ-5-2-3	MBQ-5-2-3	MBQ-5-2-3	MBQ-5-2-3_1	MBQ-5-2-3	-
						MBQ-5-2-3_2		-
						MBQ-5-2-3_3		-
						MBQ-5-2-3_4		-
Gneiss	MBQ-8-7-1	MBQ-8-7-1	MBQ-8-7-1	MBQ-8-7-1	MBQ-8-7-1	MBQ-8-7-1	-	-
Gneiss	MBQ-8-3-1	MBQ-8-3-1	MBQ-8-3-1	MBQ-8-3-1	MBQ-8-3-1	MBQ-8-3-1_1	MBQ-8-3-1 (1)	-
						MBQ-8-3-1_2		-
						MBQ-8-3-1_3		-

Rock type	Samples no.	XRF	Titration	ICP-OES,	XRD	Thin section	EPMA	
							Polish thin section	Polish section
Gneiss	MBQ-6-3-14	-	-	-	-	MBQ-6-3-14_1	MBQ-6-3-14 (1,2)	-
						MBQ-6-3-14_2		-
Gneiss	MBQ-6-3-13	MBQ-6-3-13	MBQ-6-3-13	MBQ-6-3-13	MBQ-6-3-13	MBQ-6-3-13	MBQ-6-3-13	-
Gneiss	MBQ-6-3-5	MBQ-6-3-5	MBQ-6-3-5	MBQ-6-3-5	MBQ-6-3-5	MBQ-6-3-5_1	-	-
						MBQ-6-3-5_2	-	-
Green mica in altered amphibolite	MBQ-8-9-4	MBQ-8-9-4	MBQ-8-9-4	MBQ-8-9-4	MBQ-8-9-4	-	-	MBQ-8-9-4
Green mica in altered amphibolite	MBQ-8-9-5	-	-	-	-	-	-	MBQ-8-9-5

APPENDIX B

Petrographic Data

Sample No. : MBQ-5-2-3	
Thin Section No.: 5-2-3_2	
Photomicrograph No. : 3 (A/P)	
Rock Type : Metamorphic rock	
Rock Name : biotite gneiss	
Average Grain Size: 0.5-1 mm.; **Porphyroblast** : 2-3 mm. ; **Matrix** : 0.25-0.5 mm.	
Metamorphic Texture:	
- Granoblastic texture (K-feldspar, plagioclase,quartz) - Lepidoblastic texture (biotite) - Nematoblastic texture (amphibole) - Porphyroblastic texture (garnet) - Triple junction	
Mineral Compositions :	
Mineral Name	Abundance %
K-feldspar (microcline, orthoclase)	30
Plagioclase	30
Biotite	10
Amphibole	10
Quartz	10
Garnet	10

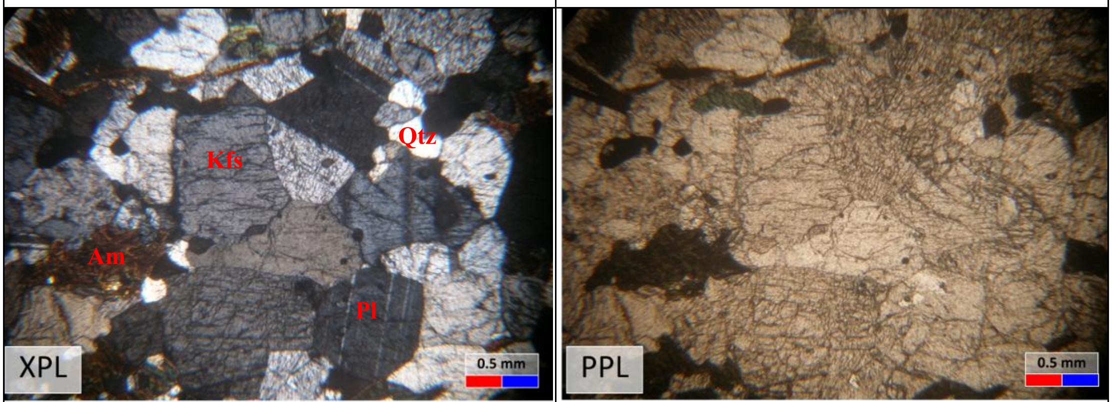

Petromicrograph Remark: Triple junction, granoblastic texture nematoblastic texture and lepidoblastic texture.

Sample No. : MBQ-6-3-5

Thin Section No.: 6-3-5_2

Photomicrograph No. : 4 (A/P)

Rock Type : Metamorphic rock

Rock Name : granitic gneiss

Average Grain Size: 0.5-1 mm.; **Porphyroblast** : - mm. ; **Matrix** : - mm.

Metamorphic Texture:

- Granoblastic texture (K-feldspar, plagioclase,quartz)
- Lepidoblastic texture (biotite)
- Nematoblastic texture (amphibole)
- Triple junction

Mineral Compositions :

Mineral Name	Abundance %
K-feldspar (microcline, orthoclase)	40
Plagioclase	30
Biotite	20
Amphibole	5
Quartz	5
-	-
-	-

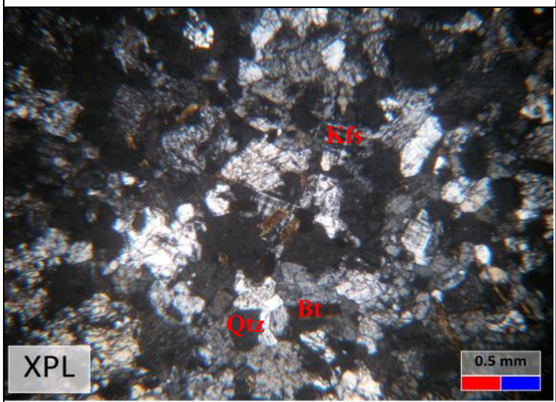

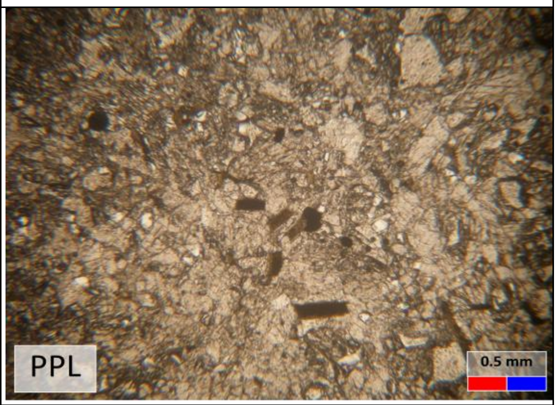

Petromicrograph Remark: Triple junction, granoblastic texture and lepidoblastic texture.

Sample No. : MBQ-6-3-14	
Thin Section No.: 6-3-14_1	
Photomicrograph No. : 1 (A/P)	
Rock Type : Metamorphic rock	
Rock Name : granitic gneiss	
Average Grain Size: 0.5-1 mm.; **Porphyroblast** : - mm. ; **Matrix** : - mm.	
Metamorphic Texture:	
- Granoblastic texture (K-feldspar, plagioclase,quartz) - Lepidoblastic texture (biotite) - Nematoblastic texture (amphibole) - Triple junction	
Mineral Compositions :	
Mineral Name	Abundance %
K-feldspar (microcline, orthoclase)	40
Plagioclase	30
Biotite	20
Amphibole	5
Quartz	5
-	-

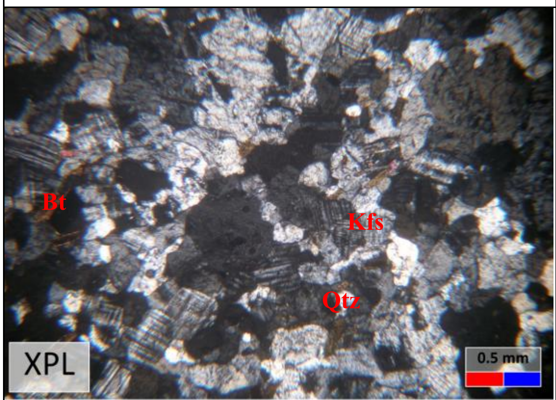

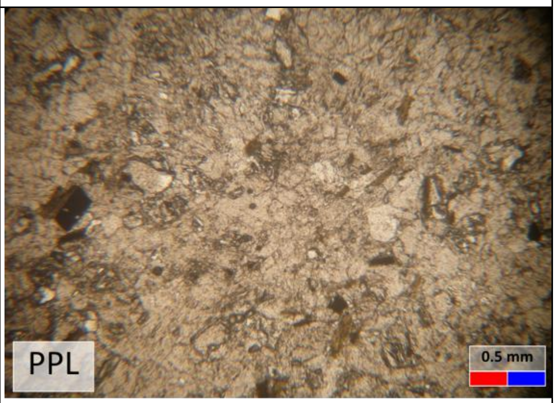

Petromicrograph Remark: Triple junction, granoblastic texture and lepidoblastic texture.

Sample No. : MBQ-8-3-1
Thin Section No.: 8-3-1_1
Photomicrograph No. : 3 (A/P)
Rock Type : Metamorphic rock
Rock Name : quartzitic gneiss
Average Grain Size: 1-2 mm.; **Porphyroblast** : - mm. ; **Matrix** : - mm.
Metamorphic Texture:
- Granoblastic texture (K-feldspar, plagioclase, quartz) - Lepidoblastic texture (biotite) - Triple junction
Mineral Compositions :

Mineral Name	Abundance %
K-feldspar (microcline, orthoclase)	50
Plagioclase	30
Quartz	10
Biotite	10
-	-
-	-
-	-

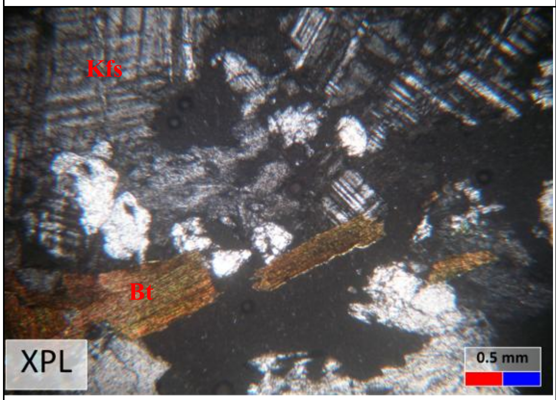

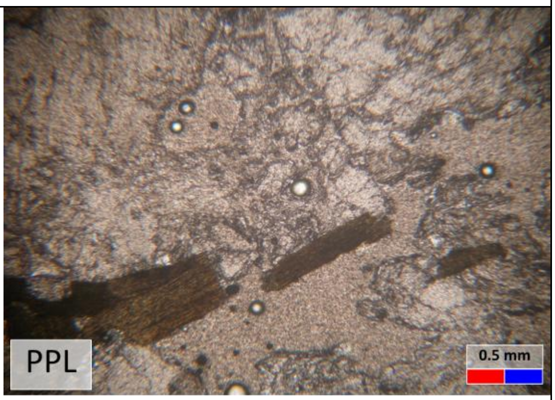

Petromicrograph Remark: Triple junction, granoblastic texture and lepidoblastic texture.

Sample No. : MBQ-8-1-1	
Thin Section No.: 8-1-1_2	
Photomicrograph No. : 1 (A/P)	
Rock Type : Metamorphic rock	
Rock Name : Amphibolite (Corundum-barren amphibolite)	
Average Grain Size: 0.5-1 mm.; **Porphyroblast** : - mm. ; **Matrix** : - mm.	
Metamorphic Texture:	
- Granoblastic texture (amphibole, plagioclase, spinel) - Nematoblastic texture (amphibole) - Triple junction	
Mineral Compositions :	
Mineral Name	Abundance %
Amphibole	50
Plagioclase	40
Spinel	10
-	-
-	-
-	-

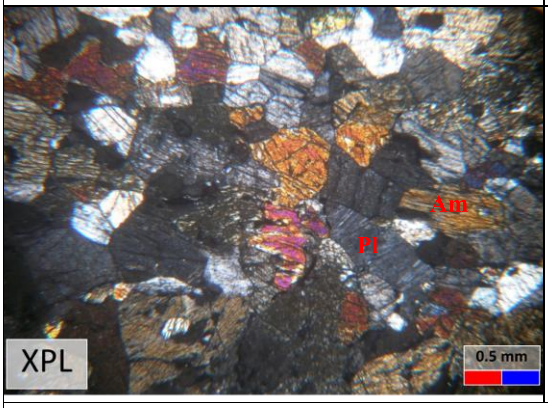

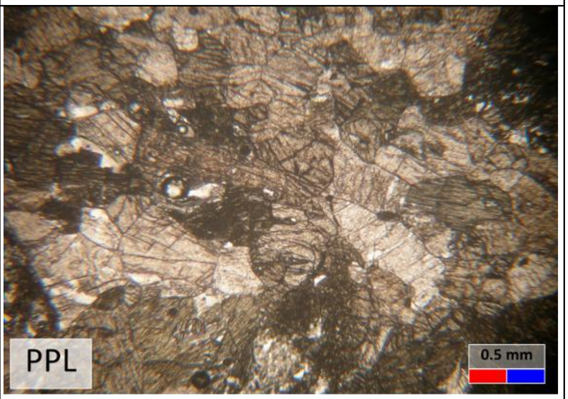

Petromicrograph Remark: Triple junction, granoblastic texture and nematoblastic texture.

Sample No. : MBQ-8-2-2	
Thin Section No.: 8-2-2_1	
Photomicrograph No. : 3 (A/P)	
Rock Type : Metamorphic rock	
Rock Name : Amphibolite (Corundum-barren amphibolite)	
Average Grain Size: 0.5-1.5 mm.; **Porphyroblast :** - mm. ; **Matrix :** - mm.	
Metamorphic Texture:	
- Granoblastic texture (amphibole, plagioclase, spinel) - Nematoblastic texture (amphibole) - Triple junction	
Mineral Compositions :	
Mineral Name	Abundance %
Amphibole	60
Plagioclase	30
Spinel	10
-	-
-	-
-	-

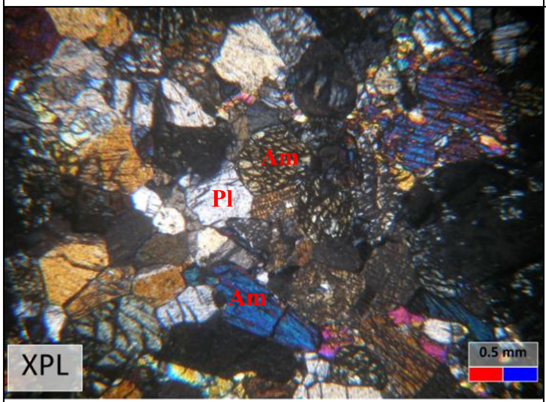

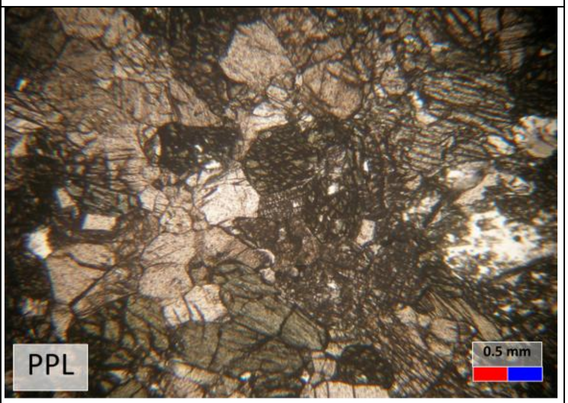

Petromicrograph Remark: Triple junction, granoblastic texture and nematoblastic texture.

Sample No. : MBQ-8-9-1	
Thin Section No.: 8-9-1_1	
Photomicrograph No. : 4 (A/P)	
Rock Type : Metamorphic rock	
Rock Name : Amphibolite (Corundum-barren amphibolite)	
Average Grain Size: 0.5-1 mm.; **Porphyroblast** : - mm. ; **Matrix** : - mm.	
Metamorphic Texture:	
- Granoblastic texture (amphibole, plagioclase, spinel) - Nematoblastic texture (amphibole) - Triple junction	
Mineral Compositions :	
Mineral Name	Abundance %
Amphibole	50
Plagioclase	40
Spinel	10
-	-
-	-
-	-

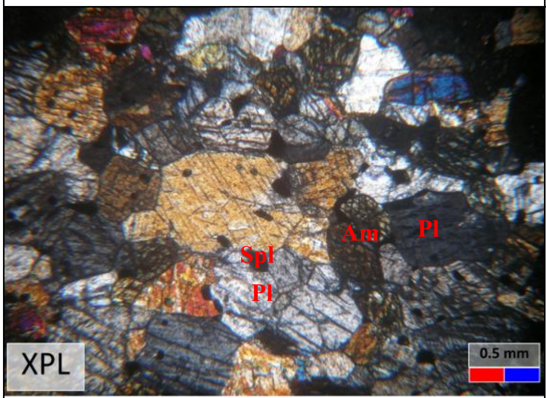

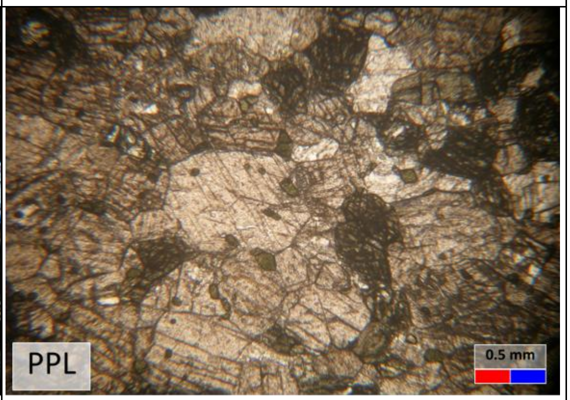

Petromicrograph Remark: Triple junction, granoblastic texture and nematoblastic texture.

Sample No. : MBQ-8-9-3

Thin Section No.: 8-9-3_1

Photomicrograph No. : 1 (A/P)

Rock Type : Metamorphic rock

Rock Name : Amphibolite (Corundum-barren amphibolite)

Average Grain Size: 0.5-1 mm.; **Porphyroblast** : - mm. ; **Matrix** : - mm.

Metamorphic Texture:

- Granoblastic texture (amphibole, plagioclase, spinel)
- Nematoblastic texture (amphibole)
- Triple junction

Mineral Compositions :

Mineral Name	Abundance %
Amphibole	55
Plagioclase	35
Spinel	10
-	
-	-
-	-

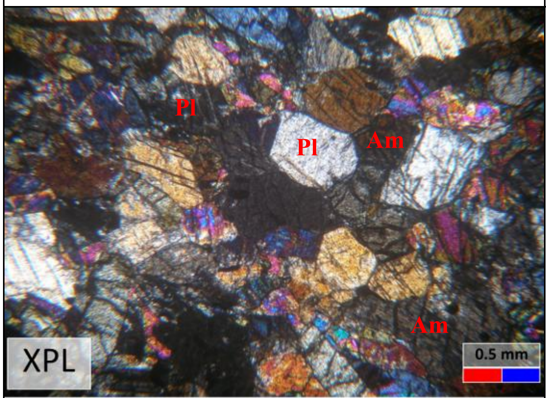

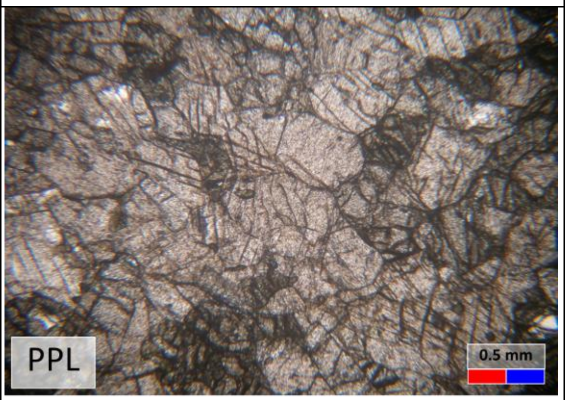

Petromicrograph Remark: Triple junction, granoblastic texture and nematoblastic texture.

Sample No. : MBQ-8-8-1

Thin Section No.: 8-8-1

Photomicrograph No. : 1 (A/P)

Rock Type : Metamorphic rock

Rock Name : Amphibolite (Corundum-bearing amphibolite)

Average Grain Size: 0.5-1.5 mm.; **Porphyroblast** : - mm. ; **Matrix** : - mm.

Metamorphic Texture:

- Granoblastic texture (amphibole, plagioclase, spinel)
- Nematoblastic texture (amphibole)
- Porphyroblastic texture (corumdum)
- Triple junction

Mineral Compositions :

Mineral Name	Abundance %
Amphibole	75
Spinel	10
Plagioclase	10
Corundum	5
-	-
-	-

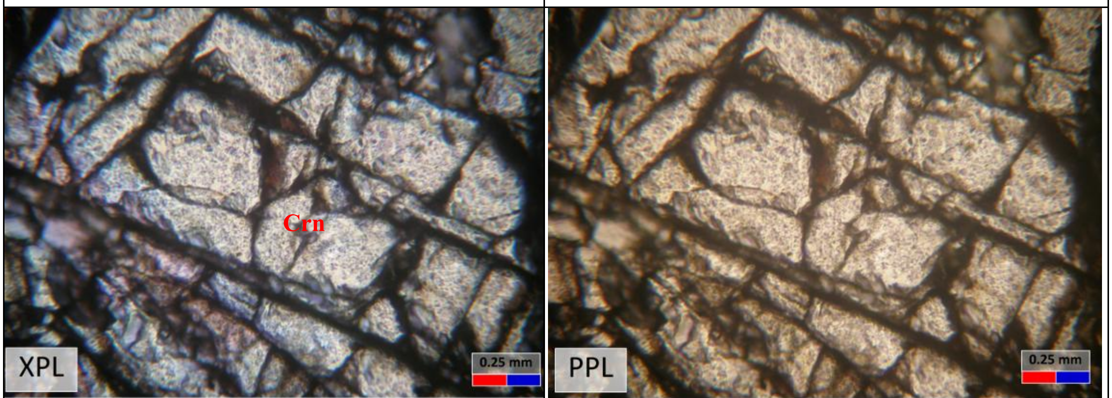

Petromicrograph Remark: Triple junction, granoblastic texture and nematoblastic texture.

Sample No. : MBQ-8-8-1

Thin Section No.: 8-8-1

Photomicrograph No. : 2 (A/P)

Rock Type : Metamorphic rock

Rock Name : Amphibolite (Corundum-bearing amphibolite)

Average Grain Size: 0.5-1.5 mm.; **Porphyroblast** : - mm. ; **Matrix** : - mm.

Metamorphic Texture:

- Granoblastic texture (amphibole, plagioclase, spinel)
- Nematoblastic texture (amphibole)
- Porphyroblastic texture (corumdum)
- Triple junction

Mineral Compositions :

Mineral Name	Abundance %
Amphibole	75
Spinel	10
Plagioclase	10
Corundum	5
-	-
-	-

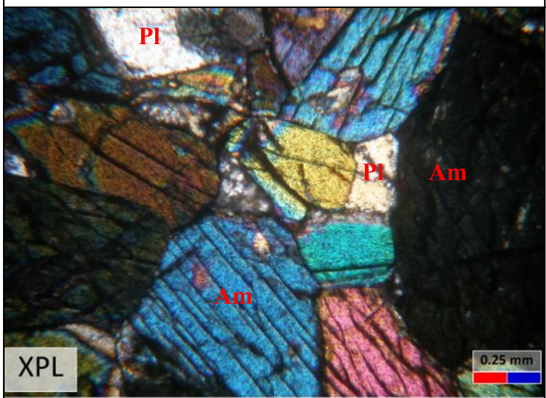

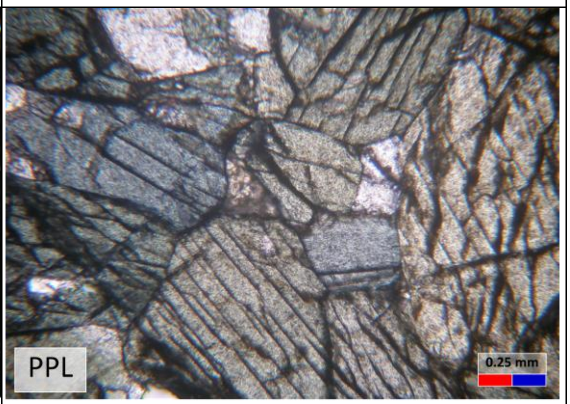

Petromicrograph Remark: Triple junction, granoblastic texture and nematoblastic texture.

Sample No. : MBQ-8-8-2	
Thin Section No.: 8-8-2	
Photomicrograph No. : 2 (A/P)	
Rock Type : Metamorphic rock	
Rock Name : Amphibolite (Corundum-bearing amphibolite)	
Average Grain Size: 0.5-1.5 mm.; **Porphyroblast** : - mm. ; **Matrix** : - mm.	
Metamorphic Texture:	
- Granoblastic texture (amphibole, plagioclase, spinel) - Nematoblastic texture (amphibole) - Porphyroblastic texture (corumdum) - Triple junction	
Mineral Compositions :	
Mineral Name	Abundance %
Amphibole	75
Spinel	10
Plagioclase	10
Corundum	5
-	-
-	-

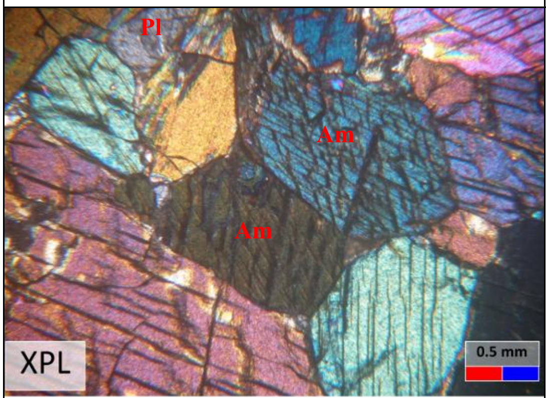

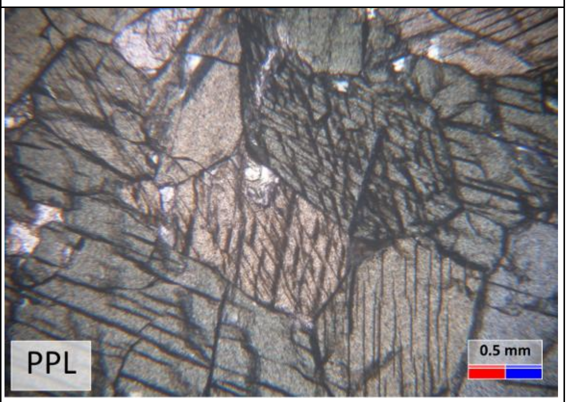

Petromicrograph Remark: Triple junction, granoblastic texture and nematoblastic texture.

Sample No. : MBQ-8-8-2

Thin Section No.: 8-8-2

Photomicrograph No. : 4 (A/P)

Rock Type : Metamorphic rock

Rock Name : Amphibolite (Corundum-bearing amphibolite)

Average Grain Size: 0.5-1.5 mm.; **Porphyroblast** : - mm. ; **Matrix** : - mm.

Metamorphic Texture:

- Granoblastic texture (amphibole, plagioclase, spinel)
- Nematoblastic texture (amphibole)
- Porphyroblastic texture (corumdum)
- Triple junction

Mineral Compositions :

Mineral Name	Abundance %
Amphibole	75
Spinel	10
Plagioclase	10
Corundum	5
-	-
-	-

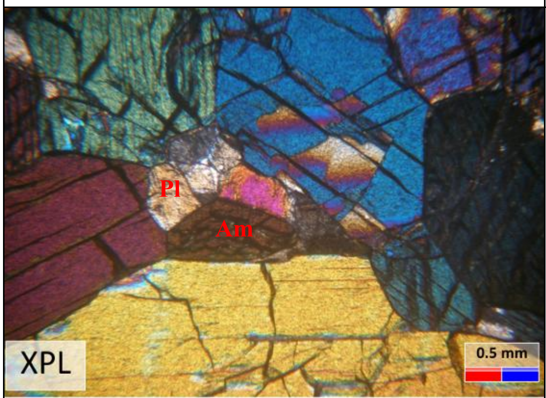

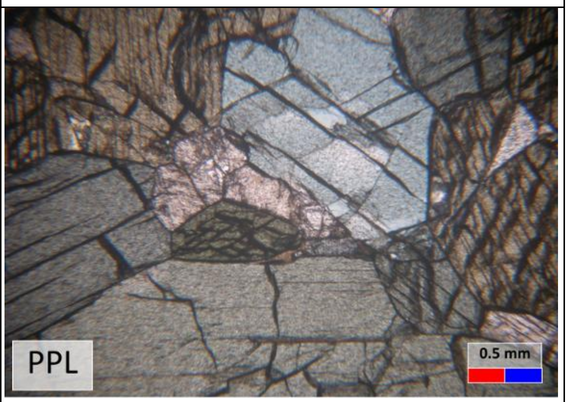

Petromicrograph Remark: Triple junction, granoblastic texture and nematoblastic texture.

Sample No. : MBQ-9-1-3

Thin Section No.: 9-1-3

Photomicrograph No. : 4 (A/P)

Rock Type : Metamorphic rock

Rock Name : Amphibolite (Corundum-bearing amphibolite)

Average Grain Size: 0.5-1.5 mm.; **Porphyroblast** : - mm. ; **Matrix** : - mm.

Metamorphic Texture:

- Granoblastic texture (amphibole, plagioclase, spinel)
- Nematoblastic texture (amphibole)
- Porphyroblastic texture (corumdum)
- Triple junction

Mineral Compositions :

Mineral Name	Abundance %
Amphibole	75
Plagioclase	15
Spinel	5
Corundum	5
-	-
-	-

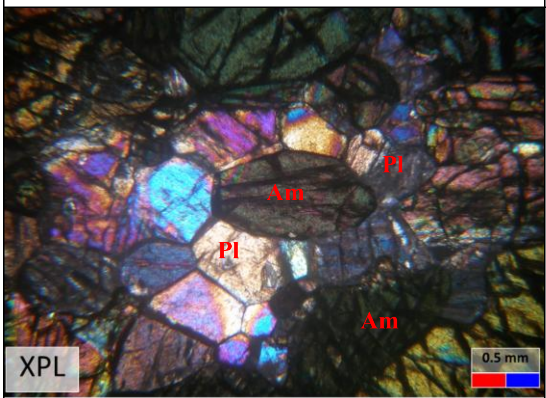

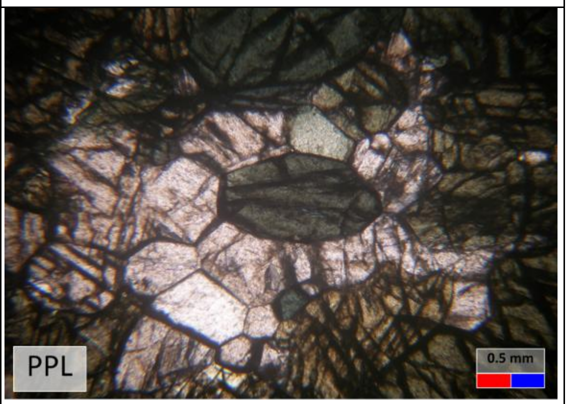

Petromicrograph Remark: Triple junction, granoblastic texture and nematoblastic texture.

Sample No. : MBQ-9-1-4

Thin Section No.: 9-1-4

Photomicrograph No. : 2 (A/P)

Rock Type : Metamorphic rock

Rock Name : Amphibolite (Corundum-bearing amphibolite)

Average Grain Size: 0.5-1.5 mm.; **Porphyroblast** : - mm. ; **Matrix** : - mm.

Metamorphic Texture:

- Granoblastic texture (amphibole, plagioclase, spinel)
- Nematoblastic texture (amphibole)
- Porphyroblastic texture (corumdum)
- Triple junction

Mineral Compositions :

Mineral Name	Abundance %
Amphibole	70
Plagioclase	13
Spinel	10
Corundum	5
Mica	2
-	-

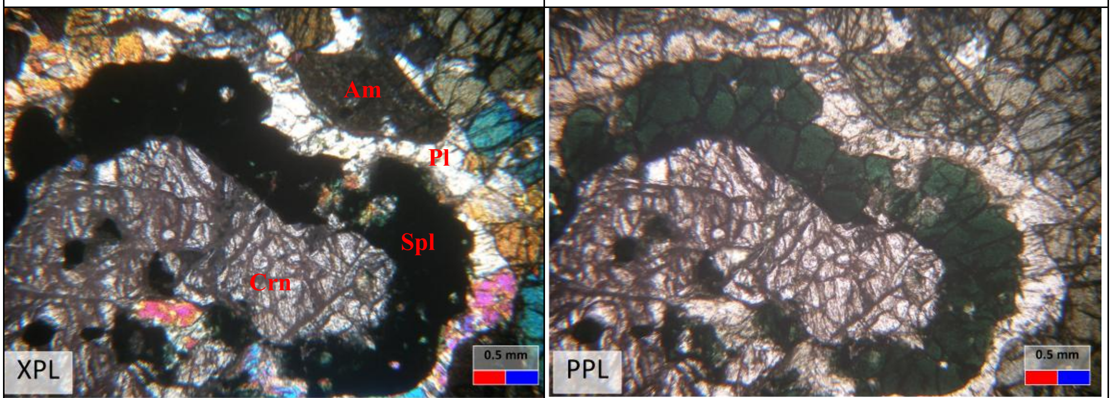

Petromicrograph Remark: Triple junction, granoblastic texture, nematoblastic texture and porphyroblastic texture.

Sample No. : MBQ-9-1-4	
Thin Section No.: 9-1-4	
Photomicrograph No. : 3 (A/P)	
Rock Type : Metamorphic rock	
Rock Name : Amphibolite (Corundum-bearing amphibolite)	
Average Grain Size: 0.5-1.5 mm.; **Porphyroblast :** - mm. ; **Matrix :** - mm.	
Metamorphic Texture:	
- Granoblastic texture (amphibole, plagioclase, spinel) - Nematoblastic texture (amphibole) - Porphyroblastic texture (corumdum) - Triple junction	
Mineral Compositions :	
Mineral Name	Abundance %
Amphibole	70
Plagioclase	13
Spinel	10
Corundum	5
Mica	2
-	-

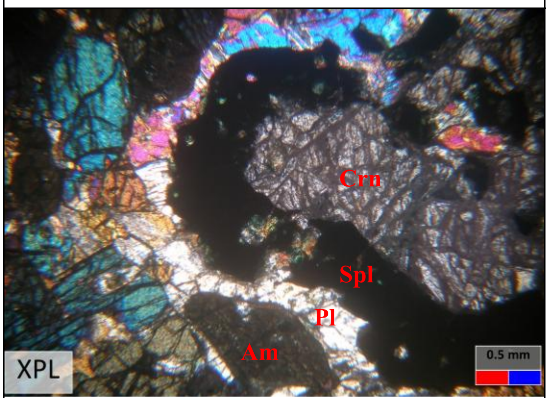

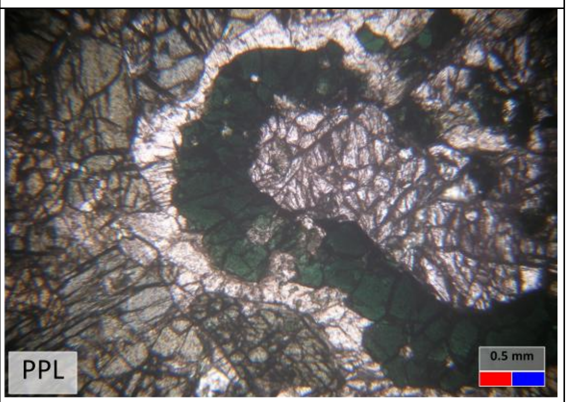

Petromicrograph Remark: Triple junction, granoblastic texture, nematoblastic texture and porphyroblastic texture.

Sample No. : MBQ-9-1-4

Thin Section No.: 9-1-4

Photomicrograph No. : 5 (A/P)

Rock Type : Metamorphic rock

Rock Name : Amphibolite (Corundum-bearing amphibolite)

Average Grain Size: 0.5-1.5 mm.; **Porphyroblast** : - mm. ; **Matrix** : - mm.

Metamorphic Texture:

- Granoblastic texture (amphibole, plagioclase, spinel)
- Nematoblastic texture (amphibole)
- Porphyroblastic texture (corumdum)
- Triple junction

Mineral Compositions :

Mineral Name	Abundance %
Amphibole	70
Plagioclase	13
Spinel	10
Corundum	5
Mica	2
-	-

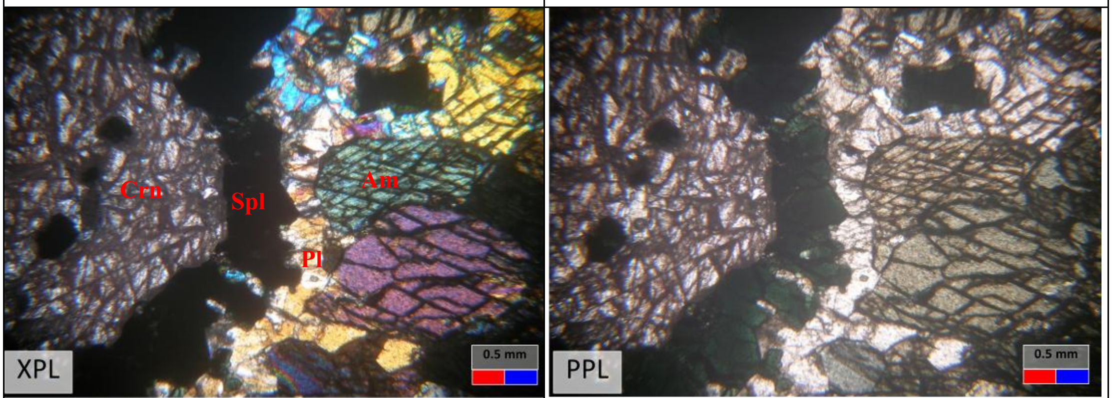

Petromicrograph Remark: Triple junction, granoblastic texture, nematoblastic texture and porphyroblastic texture

Sample No. : MBQ-9-1-4	
Thin Section No.: 9-1-4	
Photomicrograph No. : 5 (A/P)	
Rock Type : Metamorphic rock	
Rock Name : Amphibolite (Corundum-bearing amphibolite)	
Average Grain Size: 0.5-1.5 mm.; **Porphyroblast** : - mm. ; **Matrix** : - mm.	
Metamorphic Texture:	
- Granoblastic texture (amphibole, plagioclase, spinel) - Nematoblastic texture (amphibole) - Porphyroblastic texture (corumdum) - Triple junction	
Mineral Compositions :	
Mineral Name	Abundance %
Amphibole	70
Plagioclase	13
Spinel	10
Corundum	5
Mica	2
-	-
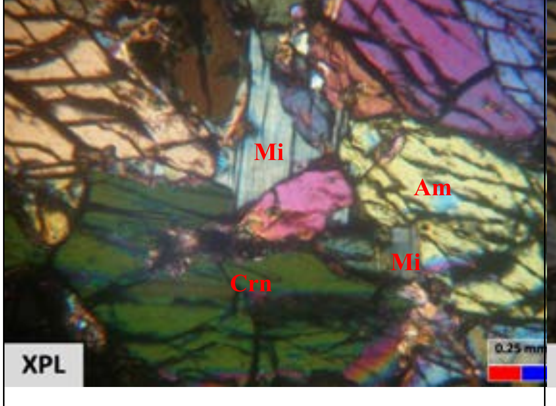	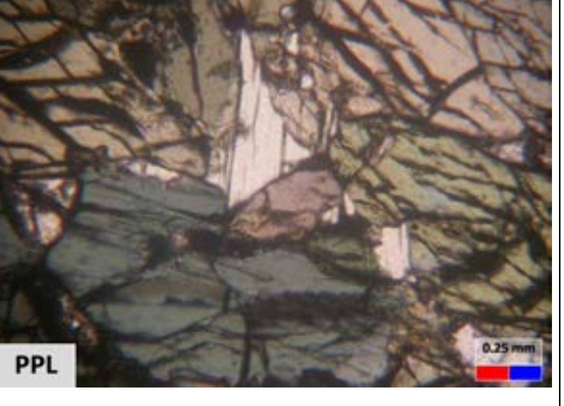
Petromicrograph Remark: Triple junction, granoblastic texture, nematoblastic texture	

Sample No. : MBQ-9-1-4	
Thin Section No.: 9-1-4	
Photomicrograph No. : 7 (A/P)	
Rock Type : Metamorphic rock	
Rock Name : Amphibolite (Corundum-bearing amphibolite)	
Average Grain Size: 0.5-1.5 mm.; **Porphyroblast** : - mm. ; **Matrix** : - mm.	
Metamorphic Texture:	
- Granoblastic texture (amphibole, plagioclase, spinel) - Nematoblastic texture (amphibole) - Porphyroblastic texture (corumdum) - Triple junction	
Mineral Compositions :	
Mineral Name	Abundance %
Amphibole	70
Plagioclase	13
Spinel	10
Corundum	5
Mica	2
-	-

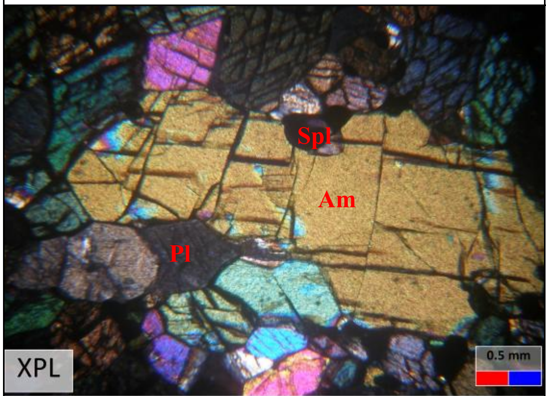

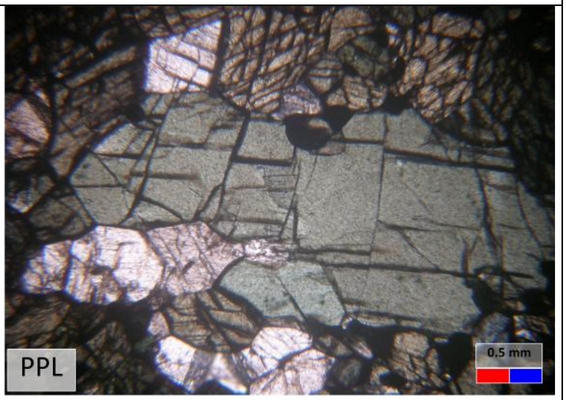

Petromicrograph Remark: Triple junction, granoblastic texture and nematoblastic texture.

APPENDIX C

EPMA Analysis Data

EPMA analysis of amphibole.

Oxide	Gneiss									
	5-2-3_Bt2-1b	5-2-3_Bt2-2b	5-2-3_Bt2-3b	5-2-3_Un2-1	5-2-3_Un2-2	5-2-3_Un2-3	5-2-3_Un3-1	5-2-3_Un3-2	5-2-3_Un3-3	5-2-3_Bt2-1b
SiO2	38.64	38.59	38.64	29.48	28.10	30.38	28.36	28.77	28.80	38.64
TiO2	1.00	0.97	0.98	0.67	0.66	0.73	0.65	0.74	0.76	1.00
Al2O3	14.51	15.00	14.93	11.91	11.84	12.05	11.29	11.20	11.35	14.51
Cr2O3	0.01	0.03	0.01	0.01	0.00	0.00	0.00	0.00	0.00	0.01
FeO *	19.74	20.10	19.64	14.71	15.16	14.47	12.48	13.12	12.96	19.74
MnO	0.08	0.07	0.11	0.12	0.10	0.11	0.12	0.07	0.06	0.08
MgO	8.34	8.16	8.28	7.35	7.42	7.56	7.39	7.22	7.33	8.34
CaO	12.59	12.46	12.78	8.52	8.34	8.64	8.09	7.98	8.00	12.59
Na2O	3.77	3.82	3.79	0.32	0.32	0.34	0.36	0.39	0.35	3.77
K2O	0.70	0.70	0.70	0.50	0.57	0.53	0.52	0.55	0.53	0.70
P2O5	0.00	0.02	0.02	0.00	0.01	0.01	0.04	0.01	0.00	0.00
F	0.00	0.00	0.00	0.00	0.00	0.00	0.00	0.00	0.00	0.00
Cl	0.02	0.00	0.04	0.00	0.00	0.02	0.01	0.00	0.00	0.02
Total	99.71	100.03	100.01	73.63	72.61	74.89	69.38	70.17	70.35	99.71
Formula 23(O)										
Si	5.874	5.845	5.849	5.938	5.787	5.991	5.999	6.033	6.019	5.874
Ti	0.114	0.111	0.112	0.101	0.102	0.108	0.104	0.117	0.119	0.114
Al	2.601	2.678	2.663	2.829	2.876	2.802	2.816	2.769	2.797	2.601
Cr	0.001	0.003	0.001	0.002	0.000	0.000	0.000	0.000	0.000	0.001
Fe3+	2.510	2.546	2.486	2.335	1.846	1.825	1.789	1.731	1.396	2.546
Fe2+	0.000	0.000	0.000	0.277	0.542	0.383	0.512	0.534	0.000	0.000
Mn	0.010	0.009	0.014	0.021	0.018	0.019	0.021	0.012	0.011	0.010
Mg	1.889	1.843	1.867	2.207	2.278	2.221	2.330	2.256	2.283	1.889
Ca	2.051	2.022	2.073	1.840	1.840	1.825	1.835	1.794	1.791	2.051
Na	1.112	1.123	1.113	0.124	0.126	0.132	0.149	0.160	0.140	1.112
K	0.135	0.136	0.135	0.129	0.150	0.132	0.141	0.146	0.141	0.135
P	0.000	0.002	0.002	0.000	0.001	0.001	0.007	0.002	0.000	0.000
F	0.000	0.000	0.000	0.000	0.000	0.000	0.000	0.000	0.000	0.000
Cl	0.005	0.001	0.009	0.000	0.000	0.006	0.004	0.000	0.000	0.005
Total (S)	16.322	16.325	16.324	15.670	15.802	15.627	15.620	15.607	15.587	16.322
Atomic%										
Fe	0.000	0.000	0.000	6.401	11.626	8.646	10.953	11.643	0.000	0.000
Mg	47.951	47.682	47.386	51.050	48.895	50.144	49.814	49.225	56.042	47.951
Ca	52.049	52.318	52.614	42.549	39.479	41.211	39.232	39.132	43.958	52.049

EPMA analysis of amphibole.

	Corundum-barren amphibolite									
Oxide	8-4-4_Am1-1c	8-4-4_Am1-2c	8-4-4_Am1-3c	8-4-4_Am2-1c	8-4-4_Am2-2c	8-4-4_Mi3-1c	8-4-4_Mi3-2c	8-4-4_Mi3-3c	8-4-4_Am3-2c	8-4-4_Am3-3c
SiO2	46.20	46.86	46.95	46.94	46.72	47.14	47.11	46.57	46.46	46.12
TiO2	0.42	0.44	0.42	0.39	0.37	0.36	0.43	0.38	0.43	0.37
Al2O3	13.55	13.43	13.23	13.45	13.65	13.17	13.33	13.36	13.55	13.44
Cr2O3	0.16	0.15	0.12	0.06	0.02	0.07	0.09	0.08	0.12	0.14
FeO *	5.79	5.82	5.74	5.67	5.84	5.90	5.85	5.98	5.71	5.95
MnO	0.07	0.07	0.06	0.03	0.04	0.07	0.02	0.07	0.07	0.06
MgO	19.18	18.71	18.77	18.99	18.71	18.94	18.68	18.75	19.11	19.16
CaO	12.04	12.18	12.16	12.16	12.12	12.14	11.97	12.09	12.10	12.13
Na2O	1.32	1.32	1.39	1.33	1.38	1.36	1.39	1.58	1.35	1.39
K2O	0.13	0.14	0.14	0.13	0.14	0.12	0.14	0.14	0.13	0.14
P2O5	0.01	0.01	0.01	0.02	0.00	0.02	0.00	0.01	0.02	0.02
F	0.00	0.00	0.00	0.00	0.00	0.00	0.00	0.00	0.00	0.00
Cl	0.01	0.00	0.00	0.00	0.02	0.00	0.00	0.00	0.01	0.03
Total	99.04	99.17	99.23	99.25	99.18	99.46	99.19	99.17	99.15	99.20
Formula 23(O)										
Si	6.437	6.509	6.522	6.507	6.494	6.533	6.538	6.485	6.458	6.430
Ti	0.044	0.046	0.044	0.040	0.038	0.038	0.045	0.040	0.045	0.039
Al	2.226	2.199	2.166	2.199	2.236	2.152	2.180	2.193	2.221	2.210
Cr	0.018	0.017	0.013	0.006	0.002	0.007	0.009	0.009	0.013	0.015
Fe3+	0.676	0.667	0.658	0.679	0.695	0.679	0.696	0.664	0.694	0.680
Fe2+	0.000	0.000	0.000	0.000	0.000	0.000	0.000	0.000	0.000	0.000
Mn	0.008	0.008	0.007	0.003	0.004	0.008	0.002	0.008	0.008	0.007
Mg	3.982	3.873	3.886	3.923	3.876	3.912	3.864	3.890	3.959	3.981
Ca	1.797	1.813	1.811	1.807	1.806	1.803	1.779	1.804	1.802	1.812
Na	0.357	0.357	0.373	0.356	0.371	0.365	0.373	0.425	0.364	0.375
K	0.023	0.024	0.026	0.022	0.025	0.022	0.025	0.025	0.023	0.025
P	0.001	0.001	0.002	0.002	0.000	0.003	0.000	0.001	0.002	0.003
F	0.000	0.000	0.000	0.000	0.000	0.000	0.000	0.000	0.000	0.000
Cl	0.003	0.000	0.000	0.000	0.005	0.000	0.000	0.000	0.003	0.006
Total (S)	15.581	15.524	15.533	15.532	15.539	15.532	15.512	15.590	15.565	15.608
Atomic%										
Fe	0.000	0.000	0.000	0.000	0.000	0.000	0.000	0.000	0.000	0.000
Mg	68.908	68.119	68.214	68.465	68.219	68.454	68.468	68.318	68.718	68.717
Ca	31.092	31.881	31.786	31.535	31.781	31.546	31.532	31.682	31.282	31.283

EPMA analysis of amphibole.

	Corundum-barren amphibolite									
Oxide	8-9-1_Am1-3b	8-9-1_Am4-1b	8-9-1_Am4-2b	8-9-1_Am4-3b	8-9-1_Am4-3b	8-9-1_Am1-1b	8-9-1_Am1-2b	8-9-1_Am1-3b	8-9-1_Am4-1b	8-9-1_Am1-1b
SiO2	39.00	38.32	39.17	39.24	39.24	38.77	38.91	39.00	38.32	38.77
TiO2	0.42	0.37	0.41	0.38	0.38	0.39	0.44	0.42	0.37	0.39
Al2O3	17.42	18.24	18.13	18.56	18.56	17.21	17.54	17.42	18.24	17.21
Cr2O3	0.20	0.25	0.26	0.23	0.23	0.28	0.23	0.20	0.25	0.28
FeO *	10.07	10.91	10.55	10.45	10.45	10.73	10.85	10.07	10.91	10.73
MnO	0.06	0.07	0.08	0.00	0.00	0.06	0.08	0.06	0.07	0.06
MgO	14.73	14.84	14.80	14.68	14.68	14.78	14.87	14.73	14.84	14.78
CaO	13.08	13.07	12.86	13.06	13.06	13.07	13.25	13.08	13.07	13.07
Na2O	2.08	2.02	2.06	2.07	2.07	2.02	2.00	2.08	2.02	2.02
K2O	1.16	1.17	1.17	1.19	1.19	1.12	1.15	1.16	1.17	1.12
P2O5	0.00	0.02	0.00	0.02	0.02	0.00	0.00	0.00	0.02	0.00
F	0.00	0.00	0.00	0.00	0.00	0.00	0.00	0.00	0.00	0.00
Cl	0.03	0.01	0.01	0.00	0.00	0.00	0.01	0.03	0.01	0.00
Total	98.27	99.43	99.65	100.03	100.03	98.62	99.37	98.27	99.43	98.62
Formula 23(O)										
Si	5.717	5.581	5.671	5.651	5.651	5.690	5.666	5.717	5.581	5.690
Ti	0.046	0.041	0.045	0.041	0.041	0.043	0.049	0.046	0.041	0.043
Al	3.011	3.131	3.094	3.150	3.150	2.978	3.010	3.011	3.131	2.978
Cr	0.023	0.029	0.029	0.026	0.026	0.032	0.027	0.023	0.029	0.032
Fe3+	1.234	1.329	1.277	1.258	0.305	1.322	1.234	1.329	1.277	1.316
Fe2+	0.000	0.000	0.000	0.000	0.000	0.000	0.000	0.000	0.000	0.000
Mn	0.007	0.009	0.010	0.000	0.000	0.008	0.009	0.007	0.009	0.008
Mg	3.218	3.222	3.192	3.150	3.150	3.233	3.226	3.218	3.222	3.233
Ca	2.055	2.040	1.995	2.015	2.015	2.056	2.067	2.055	2.040	2.056
Na	0.590	0.569	0.578	0.577	0.577	0.573	0.565	0.590	0.569	0.573
K	0.216	0.217	0.216	0.219	0.219	0.210	0.213	0.216	0.217	0.210
P	0.000	0.002	0.000	0.002	0.002	0.000	0.000	0.000	0.002	0.000
F	0.000	0.000	0.000	0.000	0.000	0.000	0.000	0.000	0.000	0.000
Cl	0.007	0.002	0.001	0.000	0.000	0.000	0.003	0.007	0.002	0.000
Total (S)	16.120	16.181	16.117	16.106	16.106	16.151	16.155	16.120	16.181	16.151
Atomic%										
Fe	0.000	0.000	0.000	0.000	0.000	0.000	0.000	0.000	0.000	0.000
Mg	61.025	61.239	61.543	60.981	60.981	61.131	60.944	61.025	61.239	61.131
Ca	38.975	38.761	38.457	39.019	39.019	38.869	39.056	38.975	38.761	38.869

EPMA analysis of amphibole.

Oxide	Corundum-bearing amphibolite									
	8-8-1_pl1-3c	8-8-1_Am1-1c	8-8-1_Am1-2c	8-8-1_Am1-3c	8-8-1_Bi1-1c	8-8-1_Bi1-2c	8-8-1_Bi1-3c	8-8-1_Fel1-1c	8-8-1_Fel1-2c	8-8-1_Fel1-3c
SiO2	42.07	37.21	35.58	35.45	31.57	31.32	32.19	31.88	31.98	32.20
TiO2	0.09	0.19	0.23	0.27	0.17	0.14	0.17	0.23	0.20	0.21
Al2O3	22.01	21.35	21.55	21.89	23.11	23.32	23.44	22.38	22.62	22.30
Cr2O3	0.06	0.05	0.08	0.05	0.05	0.07	0.08	0.04	0.11	0.05
FeO *	2.67	10.66	10.82	11.00	9.28	10.17	10.40	11.11	10.69	10.47
MnO	0.00	0.15	0.22	0.13	0.01	0.00	0.12	0.00	0.14	0.15
MgO	18.93	14.10	14.54	14.07	15.98	14.94	15.07	15.25	15.93	15.26
CaO	10.64	12.96	14.08	13.71	15.26	15.23	14.28	15.15	14.03	15.26
Na2O	3.10	2.45	2.58	2.53	3.37	3.19	3.22	3.08	3.33	3.01
K2O	0.00	0.56	0.01	0.61	0.68	0.58	0.59	0.55	0.56	0.62
P2O5	0.00	0.00	0.02	0.02	0.00	0.01	0.02	0.01	0.01	0.01
F	0.00	0.00	0.00	0.00	0.00	0.00	0.00	0.00	0.00	0.00
Cl	0.07	0.16	0.12	0.10	0.10	0.14	0.12	0.13	0.12	0.17
Total	99.65	99.92	99.89	99.90	99.75	99.73	99.78	99.82	99.82	99.79
Formula 23(O)										
Si	5.756	5.373	5.169	5.161	4.651	4.641	4.736	4.719	4.719	4.760
Ti	0.009	0.020	0.025	0.030	0.019	0.016	0.019	0.025	0.022	0.023
Al	3.549	3.635	3.691	3.757	4.014	4.073	4.066	3.906	3.935	3.887
Cr	0.006	0.005	0.009	0.006	0.006	0.009	0.010	0.005	0.013	0.005
Fe3+	0.305	1.288	1.315	1.339	1.143	1.261	1.280	1.376	1.319	1.294
Fe2+	0.000	0.000	0.000	0.000	0.000	0.000	0.000	0.000	0.000	0.000
Mn	0.000	0.018	0.027	0.016	0.001	0.000	0.015	0.000	0.017	0.019
Mg	3.860	3.034	3.147	3.052	3.508	3.299	3.303	3.365	3.502	3.362
Ca	1.559	2.005	2.191	2.138	2.410	2.418	2.252	2.403	2.218	2.417
Na	0.822	0.685	0.726	0.713	0.964	0.915	0.918	0.885	0.954	0.863
K	0.000	0.104	0.002	0.113	0.127	0.110	0.111	0.104	0.105	0.117
P	0.000	0.000	0.002	0.003	0.000	0.001	0.003	0.002	0.001	0.001
F	0.000	0.000	0.000	0.000	0.000	0.000	0.000	0.000	0.000	0.000
Cl	0.017	0.039	0.030	0.025	0.026	0.035	0.031	0.032	0.030	0.044
Total (S)	15.868	16.177	16.311	16.333	16.858	16.783	16.718	16.791	16.810	16.754
Atomic%										
Fe	0.000	0.000	0.000	0.000	0.000	0.000	0.000	0.000	0.000	0.000
Mg	71.224	60.209	58.951	58.804	59.284	57.701	59.465	58.339	61.225	58.171
Ca	28.776	39.791	41.049	41.196	40.716	42.299	40.535	41.661	38.775	41.829

EPMA analysis of amphibole.

Oxide	Corundum-bearing amphibolite									
	8-8-2_Am1-2c	8-8-2_Am1-3c	8-8-2_Am2-1c	8-8-2_Am2-2c	8-8-2_Am2-3c	8-8-2-1_Am3-3	8-8-2_Am1-1c	8-8-2_Am1-2c	8-8-2_Am1-3c	8-8-2_Am2-1c
SiO2	41.98	41.83	40.78	41.25	41.18	39.78	41.97	41.98	41.83	40.78
TiO2	0.35	0.31	0.28	0.31	0.31	0.43	0.33	0.35	0.31	0.28
Al2O3	18.01	17.94	18.47	18.27	18.24	16.67	18.17	18.01	17.94	18.47
Cr2O3	0.07	0.03	0.04	0.01	0.01	0.10	0.04	0.07	0.03	0.04
FeO *	7.91	8.35	8.78	8.62	8.76	9.32	8.03	7.91	8.35	8.78
MnO	0.16	0.18	0.14	0.18	0.14	0.19	0.14	0.16	0.18	0.14
MgO	15.28	15.16	15.22	15.17	15.20	13.84	15.20	15.28	15.16	15.22
CaO	12.62	12.65	12.86	12.97	12.91	12.14	12.50	12.62	12.65	12.86
Na2O	2.05	2.03	2.00	2.08	2.08	0.41	2.05	2.05	2.03	2.00
K2O	0.28	0.29	0.29	0.29	0.29	0.48	0.27	0.28	0.29	0.29
P2O5	0.00	0.01	0.02	0.01	0.00	0.00	0.02	0.00	0.01	0.02
F	0.00	0.00	0.00	0.00	0.00	0.00	0.00	0.00	0.00	0.00
Cl	0.00	0.01	0.03	0.01	0.05	0.01	0.03	0.00	0.01	0.03
Total	98.90	99.02	99.09	99.16	99.26	93.49	98.79	98.90	99.02	99.09
Formula 23(O)										
Si	5.969	5.958	5.829	5.880	5.871	6.011	5.969	5.969	5.958	5.829
Ti	0.037	0.033	0.030	0.033	0.033	0.049	0.035	0.037	0.033	0.030
Al	3.019	3.012	3.112	3.070	3.067	2.969	3.046	3.019	3.012	3.112
Cr	0.008	0.003	0.005	0.001	0.001	0.012	0.004	0.008	0.003	0.005
Fe3+	0.941	0.995	1.049	1.028	1.045	1.059	0.941	0.995	1.049	1.028
Fe2+	0.000	0.000	0.000	0.000	0.000	0.000	0.000	0.000	0.000	0.000
Mn	0.019	0.021	0.017	0.022	0.016	0.024	0.017	0.019	0.021	0.017
Mg	3.238	3.218	3.242	3.223	3.229	3.116	3.220	3.238	3.218	3.242
Ca	1.922	1.930	1.970	1.981	1.972	1.966	1.905	1.922	1.930	1.970
Na	0.565	0.560	0.555	0.574	0.574	0.120	0.565	0.565	0.560	0.555
K	0.052	0.053	0.054	0.052	0.052	0.092	0.048	0.052	0.053	0.054
P	0.000	0.001	0.003	0.001	0.000	0.000	0.002	0.000	0.001	0.003
F	0.000	0.000	0.000	0.000	0.000	0.000	0.000	0.000	0.000	0.000
Cl	0.000	0.002	0.007	0.003	0.013	0.002	0.006	0.000	0.002	0.007
Total (S)	15.784	15.800	15.876	15.864	15.870	15.548	15.772	15.784	15.800	15.876
Atomic%										
Fe	0.000	0.000	0.000	0.000	0.000	0.000	0.000	0.000	0.000	0.000
Mg	62.751	62.509	62.207	61.933	62.079	61.321	62.828	62.751	62.509	62.207
Ca	37.249	37.491	37.793	38.067	37.921	38.679	37.172	37.249	37.491	37.793

EPMA analysis of amphibole.

	Corundum-bearing amphibolite									
Oxide	9-1-2-8_Am1-3	9-1-2-8_Am2-1	9-1-2-8_Am2-2	9-1-2-8_Am2-3	9-1-2-8_Am3-1	9-1-2-8_Am3-2	9-1-2-8_Am3-3	9-1-2-8_Am4-1	9-1-2-8_Am4-2	9-1-2-8_Am4-3
SiO2	44.55	44.28	44.28	44.16	44.61	44.41	44.46	44.16	44.19	45.00
TiO2	0.33	0.33	0.34	0.33	0.38	0.35	0.38	0.38	0.34	0.31
Al2O3	16.64	16.91	16.87	17.00	16.61	16.54	16.94	17.01	17.18	16.91
Cr2O3	0.12	0.02	0.01	0.06	0.06	0.09	0.09	0.05	0.05	0.06
FeO *	9.46	9.65	9.48	9.81	9.65	9.95	9.50	9.75	9.73	9.96
MnO	0.22	0.21	0.22	0.22	0.21	0.22	0.23	0.24	0.26	0.25
MgO	13.65	13.81	13.72	13.75	13.94	13.94	13.71	13.47	13.71	13.66
CaO	12.60	12.58	12.53	12.54	12.62	12.34	12.50	12.53	12.43	12.31
Na2O	0.47	0.45	0.45	0.49	0.47	0.47	0.45	0.48	0.48	0.45
K2O	0.44	0.47	0.46	0.45	0.44	0.43	0.43	0.50	0.48	0.46
P2O5	0.00	0.03	0.01	0.00	0.00	0.03	0.02	0.00	0.00	0.00
F	0.00	0.00	0.00	0.00	0.00	0.00	0.00	0.00	0.00	0.00
Cl	0.00	0.00	0.00	0.00	0.01	0.00	0.01	0.00	0.00	0.00
Total	98.60	98.83	98.47	98.98	99.13	98.87	98.76	98.69	99.06	99.43
Formula 23(O)										
Si	6.328	6.280	6.298	6.262	6.309	6.302	6.300	6.278	6.259	6.338
Ti	0.035	0.036	0.036	0.036	0.040	0.037	0.041	0.041	0.036	0.032
Al	2.787	2.828	2.829	2.841	2.769	2.768	2.829	2.852	2.869	2.807
Cr	0.014	0.003	0.001	0.006	0.007	0.010	0.010	0.005	0.006	0.007
Fe3+	1.018	1.092	1.050	1.125	1.079	1.102	1.006	1.078	1.110	0.96
Fe2+	0.105	0.052	0.077	0.039	0.062	0.078	0.120	0.081	0.042	0.21
Mn	0.027	0.025	0.026	0.026	0.025	0.026	0.027	0.029	0.031	0.030
Mg	2.889	2.919	2.907	2.905	2.938	2.948	2.895	2.855	2.894	2.867
Ca	1.917	1.911	1.910	1.905	1.913	1.876	1.898	1.909	1.886	1.858
Na	0.131	0.125	0.125	0.134	0.128	0.129	0.123	0.131	0.132	0.122
K	0.080	0.086	0.084	0.081	0.079	0.078	0.078	0.091	0.087	0.082
P	0.000	0.003	0.001	0.000	0.000	0.003	0.003	0.000	0.000	0.000
F	0.000	0.000	0.000	0.000	0.000	0.000	0.000	0.000	0.000	0.000
Cl	0.000	0.000	0.000	0.000	0.003	0.000	0.001	0.000	0.000	0.000
Total (S)	15.340	15.365	15.350	15.376	15.360	15.368	15.335	15.360	15.371	15.321
Atomic%										
Fe	2.148	1.070	1.581	0.798	1.261	1.591	2.437	1.668	0.875	4.236
Mg	58.821	59.786	59.401	59.914	59.807	60.134	58.929	58.925	60.014	58.111
Ca	39.031	39.144	39.018	39.288	38.931	38.275	38.634	39.407	39.111	37.654

EPMA analysis of amphibole.

Oxide	Corundum-bearing amphibolite									
	9-1-3_Fel5-1c	9-1-3_Fel5-2c	9-1-3_Fel5-3c	9-1-3-5_Am1-1	9-1-3-5_Am1-2	9-1-3-5_Am1-3	9-1-3-5_Am2-1	9-1-3-5_Am2-2	9-1-3-5_Am2-3	9-1-3-5_Am3-1
SiO2	40.53	40.82	40.92	38.16	37.93	38.04	36.66	37.10	37.24	38.70
TiO2	0.41	0.45	0.38	0.36	0.31	0.32	0.27	0.30	0.25	0.34
Al2O3	17.27	17.21	17.56	16.72	16.60	16.43	15.45	15.83	15.71	16.72
Cr2O3	0.11	0.08	0.10	0.05	0.04	0.05	0.06	0.04	0.06	0.08
FeO *	9.06	8.76	8.72	8.12	7.97	7.94	7.30	7.66	7.24	8.35
MnO	0.15	0.17	0.14	0.20	0.19	0.21	0.20	0.23	0.16	0.26
MgO	15.42	15.28	15.30	13.49	13.65	13.35	13.42	13.20	13.12	13.57
CaO	14.15	14.22	14.04	12.10	11.98	12.07	11.73	11.59	11.55	12.32
Na2O	2.34	2.37	2.33	0.48	0.46	0.45	0.49	0.47	0.44	0.45
K2O	0.34	0.33	0.32	0.44	0.47	0.43	0.43	0.45	0.44	0.50
P2O5	0.01	0.00	0.00	0.01	0.01	0.02	0.01	0.00	0.02	0.01
F	0.00	0.00	0.00	0.00	0.00	0.00	0.00	0.00	0.00	0.00
Cl	0.00	0.00	0.01	0.00	0.01	0.00	0.00	0.01	0.00	0.00
Total	99.94	99.94	99.95	90.22	89.60	89.33	86.20	86.98	86.40	91.47
Formula 23(O)										
Si	5.796	5.832	5.830	5.956	5.955	5.988	5.984	6.000	6.044	5.969
Ti	0.044	0.048	0.041	0.042	0.036	0.038	0.034	0.036	0.031	0.040
Al	2.911	2.899	2.949	3.076	3.072	3.049	2.974	3.019	3.005	3.041
Cr	0.013	0.009	0.012	0.006	0.005	0.006	0.007	0.006	0.008	0.009
Fe3+	1.084	1.047	1.039	1.046	1.045	0.997	1.037	0.983	1.077	1.066
Fe2+	0.000	0.000	0.000	0.000	0.000	0.000	0.000	0.000	0.000	0.000
Mn	0.019	0.021	0.017	0.027	0.025	0.029	0.027	0.031	0.022	0.033
Mg	3.287	3.253	3.249	3.137	3.195	3.133	3.264	3.182	3.174	3.118
Ca	2.168	2.176	2.143	2.023	2.016	2.036	2.051	2.009	2.008	2.036
Na	0.649	0.656	0.642	0.144	0.139	0.136	0.156	0.148	0.137	0.133
K	0.062	0.060	0.057	0.087	0.094	0.086	0.089	0.092	0.091	0.099
P	0.001	0.000	0.000	0.001	0.001	0.002	0.001	0.000	0.003	0.001
F	0.000	0.000	0.000	0.000	0.000	0.000	0.000	0.000	0.000	0.000
Cl	0.000	0.000	0.003	0.000	0.002	0.000	0.000	0.003	0.000	0.000
Total (S)	16.046	16.020	15.994	15.572	15.584	15.552	15.606	15.571	15.521	15.569
Atomic%										
Fe	0.000	0.000	0.000	0.000	0.000	0.000	0.000	0.000	0.000	0.000
Mg	60.258	59.915	60.253	60.801	61.315	60.610	61.404	61.297	61.257	60.500
Ca	39.742	40.085	39.747	39.199	38.685	39.390	38.596	38.703	38.743	39.500

EPMA analysis of amphibole.

Oxide	Corundum-bearing amphibolite									
	9-1-4_Qtz1-2c	9-1-4_Qtz1-3c	9-1-4_Am4-1c	9-1-4_Am4-2c	9-1-4_Am4-3c	9-1-4_Pl5-1c	9-1-4_Pl5-2c	9-1-4_Pl5-3c	9-1-4_Am6-1c	9-1-4_Am6-2c
SiO2	43.45	42.63	41.29	43.13	43.17	42.55	40.66	42.39	42.60	44.48
TiO2	0.26	0.32	0.25	0.28	0.32	0.25	0.23	0.30	0.11	0.20
Al2O3	18.51	18.12	17.64	17.48	17.39	17.75	17.76	17.60	20.29	19.61
Cr2O3	0.03	0.05	0.05	0.03	0.05	0.06	0.08	0.06	0.00	0.04
FeO *	7.62	8.00	8.54	8.13	8.44	7.45	8.39	8.02	5.71	5.81
MnO	0.15	0.09	0.17	0.14	0.16	0.12	0.11	0.11	0.08	0.06
MgO	15.13	14.96	15.77	15.24	15.35	16.20	16.03	15.86	16.38	15.71
CaO	11.98	12.64	12.97	12.27	11.76	11.94	13.44	12.28	11.74	11.06
Na2O	2.41	2.40	2.67	2.59	2.58	2.95	2.79	2.54	2.74	2.42
K2O	0.33	0.33	0.30	0.33	0.32	0.32	0.30	0.33	0.24	0.27
P2O5	0.00	0.02	0.01	0.02	0.04	0.01	0.00	0.00	0.01	0.00
F	0.00	0.00	0.00	0.00	0.00	0.00	0.00	0.00	0.00	0.00
Cl	0.04	0.04	0.07	0.06	0.07	0.03	0.03	0.05	0.01	0.05
Total	99.93	99.90	99.88	99.89	99.88	99.81	99.87	99.87	99.92	99.85
Formula 23(O)										
Si	6.075	6.005	5.868	6.074	6.082	5.989	5.791	5.981	5.906	6.135
Ti	0.027	0.034	0.027	0.030	0.034	0.026	0.025	0.031	0.011	0.021
Al	3.051	3.010	2.955	2.902	2.889	2.946	2.981	2.928	3.315	3.188
Cr	0.003	0.006	0.006	0.004	0.006	0.007	0.009	0.007	0.000	0.004
Fe3+	0.942	1.015	0.957	0.995	0.877	0.999	0.946	0.662	0.670	0.717
Fe2+	0.000	0.000	0.000	0.000	0.000	0.000	0.000	0.000	0.000	0.000
Mn	0.018	0.011	0.020	0.016	0.019	0.014	0.013	0.013	0.009	0.007
Mg	3.152	3.141	3.341	3.199	3.224	3.399	3.401	3.336	3.384	3.230
Ca	1.794	1.909	1.975	1.852	1.776	1.801	2.051	1.857	1.743	1.634
Na	0.654	0.655	0.736	0.708	0.704	0.806	0.771	0.695	0.736	0.647
K	0.058	0.059	0.053	0.059	0.058	0.057	0.054	0.060	0.043	0.048
P	0.000	0.002	0.002	0.002	0.004	0.001	0.000	0.000	0.001	0.000
F	0.000	0.000	0.000	0.000	0.000	0.000	0.000	0.000	0.000	0.000
Cl	0.010	0.009	0.017	0.013	0.016	0.008	0.008	0.012	0.002	0.012
Total (S)	15.727	15.799	16.012	15.818	15.807	15.934	16.101	15.880	15.814	15.595
Atomic%										
Fe	0.000	0.000	0.000	0.000	0.000	0.000	0.000	0.000	0.000	0.000
Mg	63.725	62.204	62.851	63.337	64.484	65.359	62.385	64.242	66.000	66.404
Ca	36.275	37.796	37.149	36.663	35.516	34.641	37.615	35.758	34.000	33.596

EPMA analysis of amphibole.

Oxide	Altered corundum-bearing amphibolite									
	8-5-11-1_Am1-1	8-5-11-1_Am1-2	8-5-11-1_Am1-3	8-5-11-1_Am2-1	8-5-11-1_Am2-3	8-5-11-1_Am3-1	8-5-11-1_Am3-2	8-5-11-1_Am3-3	8-5-11-2_Am1-2	8-5-11-2_Am1-3
SiO2	45.22	45.79	45.98	44.07	44.46	45.67	45.63	44.12	44.42	44.44
TiO2	0.11	0.07	0.13	0.05	0.08	0.14	0.11	0.12	0.13	0.19
Al2O3	16.45	16.55	16.54	16.70	15.61	16.78	16.95	16.99	17.04	17.19
Cr2O3	0.44	0.41	0.46	0.48	0.43	0.40	0.40	0.49	0.53	0.55
FeO *	9.87	9.08	9.08	9.80	8.04	8.48	8.53	8.45	9.78	9.73
MnO	0.22	0.19	0.25	0.21	0.19	0.17	0.21	0.14	0.19	0.18
MgO	14.66	14.86	14.94	16.19	15.86	15.25	15.20	15.20	14.56	14.58
CaO	11.43	11.59	11.62	11.66	11.66	11.11	11.23	11.27	11.45	11.42
Na2O	0.48	0.45	0.49	0.46	0.46	0.48	0.49	0.50	0.50	0.49
K2O	0.32	0.36	0.36	0.26	0.36	0.37	0.38	0.36	0.34	0.37
P2O5	0.02	0.01	0.01	0.04	0.01	0.00	0.01	0.03	0.03	0.01
F	0.00	0.00	0.00	0.00	0.00	0.00	0.00	0.00	0.00	0.00
Cl	0.00	0.02	0.00	0.01	0.02	0.00	0.00	0.00	0.01	0.00
Total	99.31	99.60	99.92	100.14	97.28	99.03	99.28	98.00	99.05	99.23
Formula 23(O)										
Si	6.360	6.398	6.400	6.175	6.353	6.388	6.371	6.266	6.270	6.260
Ti	0.011	0.007	0.013	0.005	0.009	0.015	0.012	0.013	0.014	0.020
Al	2.727	2.726	2.713	2.759	2.630	2.767	2.790	2.844	2.836	2.855
Cr	0.049	0.046	0.051	0.053	0.048	0.044	0.044	0.055	0.059	0.061
Fe3+	0.994	0.890	0.903	1.148	0.961	0.851	0.894	1.003	1.08	1.08
Fe2+	0.168	0.172	0.154	0.000	0.000	0.141	0.102	0.000	0.07	0.07
Mn	0.026	0.023	0.030	0.025	0.023	0.020	0.024	0.017	0.023	0.021
Mg	3.073	3.094	3.099	3.380	3.377	3.179	3.163	3.216	3.063	3.061
Ca	1.723	1.735	1.733	1.751	1.785	1.666	1.680	1.715	1.732	1.724
Na	0.131	0.123	0.133	0.125	0.128	0.130	0.132	0.138	0.138	0.134
K	0.058	0.064	0.064	0.047	0.066	0.066	0.068	0.065	0.061	0.066
P	0.003	0.002	0.002	0.004	0.002	0.000	0.001	0.004	0.003	0.001
F	0.000	0.000	0.000	0.000	0.000	0.000	0.000	0.000	0.000	0.000
Cl	0.000	0.005	0.000	0.002	0.004	0.001	0.000	0.000	0.003	0.000
Total (S)	15.331	15.296	15.300	15.490	15.389	15.283	15.297	15.357	15.361	15.360
Atomic%										
Fe	3.378	3.433	3.083	0.000	0.000	2.833	2.060	0.000	1.480	1.415
Mg	61.917	61.874	62.157	65.878	65.420	63.757	63.967	65.220	62.931	63.063
Ca	34.705	34.692	34.759	34.122	34.580	33.410	33.973	34.780	35.588	35.522

EPMA analysis of amphibole.

	Altered corundum-bearing amphibolite									
Oxide	8-5-12-1_Am1-1	8-5-12-1_Am1-3	8-5-13-1_Am1-1	8-5-13-1_Am1-2	8-5-13-1_Am1-3	8-5-16-2_Am1-1	8-5-16-2_Am1-2	8-5-16-2_Am1-3	8-5-16-2_Am2-1	8-5-16-2_Am2-2
SiO2	44.68	44.61	44.90	44.35	44.22	43.20	42.34	42.44	45.61	44.79
TiO2	0.10	0.07	0.06	0.12	0.07	0.10	0.13	0.11	0.10	0.10
Al2O3	17.61	17.38	17.46	17.24	17.96	16.12	16.78	16.97	16.84	16.73
Cr2O3	0.41	0.42	0.54	0.61	0.53	0.47	0.52	0.50	0.44	0.48
FeO *	6.99	6.75	8.74	8.67	8.96	9.07	9.64	9.69	9.99	9.88
MnO	0.21	0.17	0.17	0.15	0.21	0.18	0.17	0.20	0.16	0.16
MgO	16.42	16.36	15.16	16.00	15.48	15.24	15.03	14.98	14.02	14.55
CaO	11.43	11.36	11.67	11.61	11.86	12.84	12.75	12.35	12.12	13.00
Na2O	0.37	0.34	0.43	0.39	0.43	0.45	0.43	0.43	0.45	0.46
K2O	0.27	0.26	0.34	0.31	0.33	0.26	0.32	0.30	0.26	0.24
P2O5	0.04	0.02	0.02	0.04	0.04	0.02	0.00	0.03	0.03	0.05
F	0.00	0.00	0.00	0.00	0.00	0.00	0.00	0.00	0.00	0.00
Cl	0.00	0.00	0.00	0.01	0.00	0.01	0.01	0.00	0.00	0.00
Total	98.67	97.91	99.66	99.61	100.24	98.01	98.32	98.10	100.13	100.59
Formula 23(O)										
Si	6.242	6.272	6.267	6.201	6.156	6.191	6.079	6.091	6.365	6.255
Ti	0.011	0.007	0.006	0.013	0.008	0.011	0.014	0.012	0.011	0.011
Al	2.900	2.881	2.873	2.842	2.947	2.723	2.840	2.872	2.770	2.754
Cr	0.046	0.047	0.060	0.067	0.058	0.053	0.059	0.056	0.049	0.053
Fe3+	0.82	0.79	1.02	1.01	1.04	1.087	1.157	1.164	0.870	1.153
Fe2+	0.00	0.00	0.00	0.00	0.00	0.000	0.000	0.000	0.296	0.000
Mn	0.025	0.021	0.020	0.018	0.025	0.022	0.020	0.024	0.019	0.018
Mg	3.419	3.428	3.153	3.333	3.211	3.254	3.217	3.205	2.916	3.028
Ca	1.711	1.712	1.746	1.739	1.769	1.971	1.962	1.899	1.813	1.945
Na	0.099	0.094	0.116	0.107	0.117	0.124	0.120	0.119	0.121	0.124
K	0.048	0.047	0.061	0.055	0.059	0.048	0.059	0.055	0.045	0.043
P	0.005	0.002	0.002	0.005	0.005	0.002	0.000	0.003	0.004	0.006
F	0.000	0.000	0.000	0.000	0.000	0.000	0.000	0.000	0.000	0.000
Cl	0.000	0.000	0.001	0.002	0.000	0.002	0.001	0.000	0.000	0.000
Total (S)	15.336	15.319	15.339	15.404	15.410	15.492	15.544	15.513	15.289	15.402
Atomic%										
Fe	0.000	0.000	0.045	0.000	0.000	0.000	0.000	0.000	5.891	0.000
Mg	66.645	66.693	64.332	65.723	64.480	62.278	62.117	62.795	58.034	60.896
Ca	33.355	33.307	35.623	34.277	35.520	37.722	37.883	37.205	36.076	39.104

EPMA analysis of amphibole.

Oxide	Altered corundum-bearing amphibolite									
	8-5-14-1_Am1-2	8-5-14-1_Am1-3	8-5-14-1_Am2-2	8-5-14-1_Am2-3	8-5-14-1_rCor2-1	8-5-14-1_rCor2-2	8-5-14-1_rCor2-3	8-5-14-1_rCor2-1	8-5-14-1_rCor2-2	8-5-14-1_rCor2-3
SiO2	45.09	44.78	44.16	44.63	44.73	45.47	44.38	44.73	45.47	44.38
TiO2	0.10	0.12	0.10	0.13	0.08	0.12	0.10	0.08	0.12	0.10
Al2O3	15.76	16.27	15.58	15.83	15.28	15.59	15.68	15.28	15.59	15.68
Cr2O3	0.45	0.44	0.45	0.45	0.57	0.54	0.51	0.57	0.54	0.51
FeO *	9.89	9.99	9.92	9.30	9.02	9.37	9.26	9.02	9.37	9.26
MnO	0.21	0.20	0.18	0.17	0.16	0.17	0.22	0.16	0.17	0.22
MgO	14.74	14.71	14.71	14.89	14.96	15.01	15.11	14.96	15.01	15.11
CaO	11.12	11.12	11.36	11.52	11.48	11.41	11.54	11.48	11.41	11.54
Na2O	0.49	0.46	0.49	0.48	0.46	0.47	0.44	0.46	0.47	0.44
K2O	0.36	0.35	0.33	0.34	0.29	0.35	0.37	0.29	0.35	0.37
P2O5	0.01	0.04	0.03	0.01	0.01	0.03	0.00	0.01	0.03	0.00
F	0.00	0.00	0.00	0.00	0.00	0.00	0.00	0.00	0.00	0.00
Cl	0.00	0.00	0.00	0.00	0.01	0.00	0.00	0.01	0.00	0.00
Total	98.36	98.58	97.41	97.88	97.11	98.61	97.83	97.11	98.61	97.83
Formula 23(O)										
Si	6.405	6.348	6.351	6.367	6.419	6.427	6.343	6.419	6.427	6.343
Ti	0.011	0.013	0.010	0.013	0.009	0.013	0.011	0.009	0.013	0.011
Al	2.639	2.719	2.641	2.663	2.586	2.598	2.642	2.586	2.598	2.642
Cr	0.051	0.050	0.051	0.050	0.065	0.061	0.058	0.065	0.061	0.058
Fe3+	1.001	1.018	1.147	1.075	1.00	0.964	1.107	0.964	1.107	1.968
Fe2+	0.174	0.167	0.046	0.035	0.09	0.144	0.000	0.144	0.000	0.510
Mn	0.025	0.024	0.021	0.021	0.019	0.021	0.026	0.019	0.021	0.026
Mg	3.120	3.107	3.153	3.165	3.200	3.162	3.219	3.200	3.162	3.219
Ca	1.693	1.689	1.750	1.761	1.766	1.728	1.768	1.766	1.728	1.768
Na	0.134	0.125	0.136	0.134	0.127	0.129	0.121	0.127	0.129	0.121
K	0.065	0.063	0.061	0.062	0.053	0.063	0.068	0.053	0.063	0.068
P	0.001	0.005	0.004	0.001	0.001	0.003	0.000	0.001	0.003	0.000
F	0.000	0.000	0.000	0.000	0.000	0.000	0.000	0.000	0.000	0.000
Cl	0.000	0.000	0.000	0.000	0.001	0.000	0.000	0.001	0.000	0.000
Total (S)	15.334	15.339	15.384	15.359	15.332	15.321	15.382	15.332	15.321	15.382
Atomic%										
Fe	3.485	3.356	0.927	0.704	1.684	2.858	0.000	2.816	0.000	9.283
Mg	62.562	62.611	63.716	63.798	63.359	62.809	64.547	62.629	64.657	58.555
Ca	33.953	34.033	35.357	35.499	34.957	34.333	35.453	34.555	35.343	32.162

EPMA analysis of feldspar.

Oxide	Gneiss									
	5-2-3_rGrt2-2	5-2-3_rGrt2-3	5-2-3_rGrt3-2	5-2-3_r2Grt2-1	5-2-3_Fel2-3b	5-2-3_Fel5-2b	6-3-14-2_Un2-1	6-3-14-2_Un2-2	6-3-14-2_Un3-1	6-3-14-2_Un3-2
SiO2	51.22	52.45	54.95	55.05	64.43	62.78	55.74	56.03	52.97	52.13
TiO2	0.00	0.00	0.02	0.03	0.02	0.01	0.00	0.00	0.01	0.01
Al2O3	21.78	18.89	18.80	18.10	22.50	23.12	20.49	19.87	21.71	21.58
FeO *	0.04	0.00	0.01	0.03	0.03	0.14	0.00	0.00	0.11	0.15
MnO	0.00	0.01	0.01	0.03	0.01	0.00	0.00	0.02	0.00	0.00
MgO	0.00	0.00	0.00	0.00	0.00	0.01	0.00	0.00	0.00	0.00
CaO	25.63	25.97	24.07	24.52	6.14	6.54	22.52	22.02	24.41	24.50
Na2O	1.62	1.58	1.67	1.67	7.29	7.98	1.03	1.30	0.92	1.16
K2O	0.14	0.14	0.11	0.11	0.17	0.14	0.07	0.08	0.18	0.20
P2O5	0.00	0.00	0.01	0.01	0.03	0.02	0.00	0.00	0.02	0.00
Total	100.57	99.07	99.66	99.75	100.93	100.99	100.02	99.46	100.34	99.91
Formula 8(O)										
Si	2.407	2.501	2.576	2.586	2.820	2.765	2.577	2.603	2.469	2.450
Ti	0.000	0.000	0.001	0.001	0.001	0.000	0.000	0.000	0.000	0.000
Al	1.207	1.062	1.039	1.002	1.161	1.200	1.117	1.088	1.193	1.196
Fe	0.001	0.000	0.000	0.001	0.001	0.005	0.000	0.000	0.004	0.006
Mn	0.000	0.000	0.000	0.001	0.000	0.000	0.000	0.001	0.000	0.000
Mg	0.000	0.000	0.000	0.000	0.000	0.000	0.000	0.000	0.000	0.000
Ca	1.291	1.327	1.209	1.234	0.288	0.309	1.116	1.096	1.219	1.234
Na	0.148	0.146	0.152	0.152	0.619	0.682	0.092	0.117	0.083	0.106
K	0.009	0.009	0.006	0.006	0.010	0.008	0.004	0.005	0.011	0.012
P	0.000	0.000	0.000	0.000	0.001	0.001	0.000	0.000	0.001	0.000
Total (S)	5.066	5.045	4.983	4.989	4.907	4.975	4.910	4.912	4.980	5.008
Atomic%										
An	89.21	89.57	88.44	88.63	31.40	30.93	92.03	90.00	92.83	91.26
Ab	10.20	9.84	11.10	10.90	67.55	68.28	7.62	9.60	6.34	7.84
Or	0.59	0.59	0.46	0.46	1.05	0.79	0.35	0.39	0.83	0.90

EPMA analysis of feldspar.

Oxide	Gneiss										
	6-3-14-2_Un6-1	6-3-14-2_Un6-2	6-3-14-2_Un6-3	6-3-14-2_Un7-1	6-3-14-2_Un7-2	6-3-14-2_Un7-3	6-3-14-2_Bt2-1b	6-3-14-2_Px1-2b	6-3-14-2_Am2-2b	6-3-14-2_Fel3-1b	6-3-14-2_Fel3-3b
SiO2	51.65	52.93	52.39	53.44	53.89	52.16	64.27	61.57	65.54	65.61	65.48
TiO2	0.02	0.01	0.00	0.02	0.02	0.01	0.01	0.00	0.01	0.04	0.01
Al2O3	20.41	20.56	20.03	21.64	21.52	21.06	21.82	20.50	20.90	20.58	19.54
FeO *	0.03	0.07	0.09	0.02	0.05	0.10	0.08	0.07	0.06	0.06	0.09
MnO	0.01	0.02	0.00	0.04	0.02	0.00	0.02	0.00	0.04	0.01	0.00
MgO	0.00	0.00	0.00	0.00	0.00	0.00	0.00	0.00	0.01	0.00	0.00
CaO	25.97	25.95	24.18	24.08	24.07	24.03	5.05	0.00	5.08	5.08	5.77
Na2O	0.98	0.91	1.04	0.88	0.84	1.90	7.51	0.45	7.99	7.92	7.82
K2O	0.18	0.16	0.17	0.19	0.18	0.20	0.21	15.96	0.20	0.22	0.17
P2O5	0.00	0.00	0.03	0.00	0.02	0.02	0.01	0.00	0.01	0.00	0.02
Total	99.35	100.68	98.13	100.45	100.72	99.58	99.21	99.00	99.90	99.76	99.02
Formula 8(O)											
Si	2.453	2.474	2.501	2.484	2.495	2.462	2.852	2.892	2.888	2.897	2.917
Ti	0.001	0.000	0.000	0.001	0.001	0.000	0.000	0.000	0.000	0.001	0.000
Al	1.143	1.133	1.128	1.186	1.175	1.172	1.142	1.136	1.086	1.071	1.026
Fe	0.001	0.003	0.004	0.001	0.002	0.004	0.003	0.003	0.002	0.002	0.003
Mn	0.001	0.001	0.000	0.002	0.001	0.000	0.001	0.000	0.001	0.001	0.000
Mg	0.000	0.000	0.000	0.000	0.000	0.000	0.000	0.000	0.001	0.000	0.000
Ca	1.321	1.300	1.237	1.199	1.194	1.215	0.240	0.000	0.240	0.240	0.275
Na	0.090	0.083	0.096	0.079	0.075	0.174	0.647	0.041	0.682	0.678	0.676
K	0.011	0.010	0.011	0.011	0.011	0.012	0.012	0.957	0.011	0.012	0.009
P	0.000	0.000	0.001	0.000	0.001	0.001	0.000	0.000	0.000	0.000	0.001
Total (S)	5.025	5.004	4.983	4.966	4.958	5.042	4.902	5.037	4.914	4.908	4.910
Atomic%											
An	92.87	93.37	92.05	93.00	93.26	86.76	26.72	0.00	25.69	25.82	28.67
Ab	6.36	5.94	7.16	6.14	5.90	12.39	71.96	4.13	73.13	72.86	70.35
Or	0.78	0.69	0.78	0.86	0.84	0.86	1.32	95.87	1.18	1.32	0.98

EPMA analysis of feldspar.

	Corundum-barren amphibolite										
Oxide	8-9-1_Px1-1b	8-9-1_Px1-2b	8-9-1_Px1-3b	8-9-1_Fel1-1b	8-9-1_Fel1-2b	8-9-1_Fel1-3b	8-9-1_Fel2-1b	8-9-1_Fel2-2b	8-9-1_Fel2-3b	8-9-1_Am2-1b	8-9-1_Px2-1b
SiO2	41.88	41.91	41.96	41.68	41.52	41.88	41.34	41.46	41.69	40.71	41.31
TiO2	0.01	0.00	0.01	0.00	0.00	0.03	0.03	0.01	0.05	0.04	0.00
Al2O3	36.92	36.36	36.76	36.74	36.81	36.24	36.17	36.48	36.09	36.32	36.77
FeO *	0.12	0.03	0.04	0.09	0.08	0.11	0.04	0.05	0.04	0.11	0.02
MnO	0.02	0.00	0.00	0.02	0.00	0.00	0.01	0.00	0.00	0.03	0.00
MgO	0.01	0.00	0.00	0.00	0.01	0.01	0.02	0.01	0.00	0.00	0.00
CaO	19.92	20.27	20.39	20.48	20.46	20.28	20.28	20.30	20.41	20.66	20.34
Na2O	0.04	0.06	0.04	0.05	0.06	0.05	0.05	0.06	0.05	0.58	0.06
K2O	0.00	0.00	0.00	0.01	0.00	0.01	0.00	0.00	0.00	0.00	0.00
P2O5	0.01	0.01	0.00	0.00	0.00	0.02	0.00	0.02	0.00	0.00	0.00
Total	99.17	98.77	99.39	99.06	98.99	98.68	98.20	98.51	98.45	98.51	98.64
Formula 8(O)											
Si	1.962	1.972	1.963	1.957	1.951	1.972	1.960	1.958	1.970	1.932	1.948
Ti	0.000	0.000	0.000	0.000	0.000	0.001	0.001	0.000	0.002	0.001	0.000
Al	2.039	2.017	2.027	2.033	2.039	2.012	2.021	2.031	2.010	2.032	2.044
Fe	0.005	0.001	0.001	0.003	0.003	0.004	0.002	0.002	0.002	0.004	0.001
Mn	0.001	0.000	0.000	0.001	0.000	0.000	0.000	0.000	0.000	0.001	0.000
Mg	0.001	0.000	0.000	0.000	0.001	0.000	0.001	0.001	0.000	0.000	0.000
Ca	1.000	1.022	1.022	1.030	1.030	1.023	1.030	1.027	1.033	1.050	1.028
Na	0.004	0.005	0.004	0.005	0.005	0.005	0.004	0.005	0.004	0.053	0.005
K	0.000	0.000	0.000	0.000	0.000	0.000	0.000	0.000	0.000	0.000	0.000
P	0.000	0.000	0.000	0.000	0.000	0.001	0.000	0.001	0.000	0.000	0.000
Total (S)	5.016	5.020	5.023	5.029	5.031	5.021	5.027	5.027	5.024	5.076	5.030
Atomic%											
An	99.64	99.48	99.62	99.51	99.49	99.50	99.57	99.47	99.59	95.20	99.49
Ab	0.36	0.52	0.38	0.45	0.50	0.45	0.43	0.52	0.41	4.80	0.50
Or	0.00	0.00	0.00	0.04	0.01	0.05	0.00	0.01	0.00	0.00	0.01

EPMA analysis of feldspar.

Oxide	Corundum-bearing amphibolite										
	8-8-1_pl1-1c	8-8-1_pl1-2c	8-8-1_Pl4-1c	8-8-1_Pl4-2c	8-8-1_Pl4-3c	8-8-1_Pl4-4c	8-8-1_Pl4-5c	8-8-1_Am3-1c	8-8-1_FeI5-1c	8-8-1_FeI5-3c	8-8-1_FeI5-2c
SiO2	39.53	44.58	43.67	43.78	42.97	43.98	44.15	43.60	40.68	43.28	42.79
TiO2	0.00	0.00	0.00	0.00	0.00	0.00	0.02	0.00	0.01	0.00	0.03
Al2O3	38.19	36.84	38.38	39.33	39.09	40.24	40.34	40.19	38.70	39.92	39.77
FeO *	0.35	0.05	0.01	0.06	0.13	0.05	0.08	0.09	0.00	0.08	0.04
MnO	0.00	0.01	0.00	0.00	0.00	0.00	0.01	0.02	0.00	0.00	0.02
MgO	0.23	0.04	0.00	0.01	0.06	0.04	0.00	0.07	0.00	0.02	0.04
CaO	19.84	17.82	17.58	16.48	17.45	15.02	14.76	15.55	20.28	16.19	16.70
Na2O	0.34	0.30	0.10	0.08	0.13	0.11	0.14	0.17	0.09	0.09	0.06
K2O	0.00	0.00	0.00	0.00	0.02	0.00	0.00	0.02	0.00	0.00	0.00
P2O5	0.00	0.00	0.00	0.00	0.08	0.04	0.03	0.00	0.00	0.01	0.02
Total	99.94	99.90	99.94	99.95	99.96	99.90	99.93	99.99	99.97	99.83	99.82
Formula 8(O)											
Si	1.868	2.050	2.004	2.001	1.972	2.003	2.007	1.987	1.895	1.979	1.965
Ti	0.000	0.000	0.000	0.000	0.000	0.000	0.001	0.000	0.000	0.000	0.001
Al	2.128	1.997	2.077	2.119	2.116	2.160	2.162	2.159	2.125	2.152	2.153
Fe	0.014	0.002	0.000	0.002	0.005	0.002	0.003	0.003	0.000	0.003	0.002
Mn	0.000	0.000	0.000	0.000	0.000	0.000	0.000	0.001	0.000	0.000	0.001
Mg	0.016	0.003	0.000	0.001	0.004	0.003	0.000	0.004	0.000	0.002	0.002
Ca	1.004	0.878	0.865	0.807	0.858	0.733	0.719	0.759	1.012	0.793	0.821
Na	0.031	0.027	0.009	0.007	0.012	0.010	0.012	0.015	0.008	0.008	0.006
K	0.000	0.000	0.000	0.000	0.001	0.000	0.000	0.001	0.000	0.000	0.000
P	0.000	0.000	0.000	0.000	0.003	0.001	0.001	0.000	0.000	0.000	0.001
Total (S)	5.073	4.961	4.960	4.941	4.972	4.917	4.911	4.936	5.043	4.945	4.957
Atomic%											
An	97.03	97.06	98.99	99.11	98.52	98.69	98.36	97.93	99.24	98.97	99.32
Ab	2.97	2.94	1.01	0.89	1.37	1.31	1.64	1.96	0.76	1.02	0.68
Or	0.00	0.00	0.00	0.00	0.11	0.00	0.00	0.11	0.00	0.01	0.00

EPMA analysis of feldspar.

Oxide	Corundum-bearing amphibolite										
	8-8-2_Pl1-1c	8-8-2_Pl1-2c	8-8-2_Pl1-3c	8-8-2_Pl2-1c	8-8-2_Pl2-2c	8-8-2_Pl2-3c	8-8-2_Fel2-1c	8-8-2_Fel2-2c	8-8-2_Fel2-3c	8-8-2_Pl4-1c	8-8-2_Pl4-2c
SiO2	42.59	42.03	41.97	40.35	41.05	40.75	42.77	42.58	41.98	42.45	42.34
TiO2	0.00	0.00	0.02	0.00	0.00	0.00	0.00	0.02	0.03	0.00	0.00
Al2O3	36.70	36.76	36.93	37.51	37.56	37.47	36.61	36.42	36.93	36.93	36.77
FeO *	0.06	0.06	0.05	0.08	0.06	0.11	0.11	0.16	0.10	0.03	0.00
MnO	0.01	0.01	0.00	0.02	0.02	0.02	0.02	0.00	0.00	0.02	0.00
MgO	0.00	0.00	0.00	0.00	0.00	0.01	0.00	0.00	0.01	0.00	0.00
CaO	20.37	20.43	20.48	20.05	20.04	20.18	19.30	19.66	19.45	19.45	19.61
Na2O	0.08	0.09	0.06	0.06	0.07	0.08	0.07	0.08	0.08	0.07	0.08
K2O	0.00	0.00	0.00	0.00	0.00	0.00	0.00	0.00	0.00	0.00	0.01
P2O5	0.00	0.02	0.00	0.00	0.00	0.00	0.00	0.01	0.02	0.01	0.01
Total	99.82	99.62	99.57	98.30	98.95	98.69	99.07	98.97	98.78	99.25	99.02
Formula 8(O)											
Si	1.980	1.963	1.959	1.912	1.930	1.922	1.998	1.993	1.970	1.982	1.982
Ti	0.000	0.000	0.001	0.000	0.000	0.000	0.000	0.001	0.001	0.000	0.000
Al	2.012	2.023	2.032	2.096	2.082	2.083	2.016	2.010	2.043	2.033	2.029
Fe	0.002	0.002	0.002	0.003	0.002	0.004	0.004	0.006	0.004	0.001	0.000
Mn	0.000	0.000	0.000	0.001	0.001	0.001	0.001	0.000	0.000	0.001	0.000
Mg	0.000	0.000	0.000	0.000	0.000	0.001	0.000	0.000	0.001	0.000	0.000
Ca	1.015	1.022	1.025	1.018	1.009	1.020	0.966	0.986	0.978	0.973	0.984
Na	0.007	0.008	0.005	0.005	0.006	0.008	0.006	0.007	0.007	0.006	0.007
K	0.000	0.000	0.000	0.000	0.000	0.000	0.000	0.000	0.000	0.000	0.000
P	0.000	0.001	0.000	0.000	0.000	0.000	0.000	0.000	0.001	0.000	0.000
Total (S)	5.017	5.024	5.026	5.039	5.032	5.040	4.995	5.004	5.008	5.002	5.006
Atomic%											
An	99.34	99.24	99.50	99.46	99.40	99.25	99.36	99.28	99.29	99.38	99.25
Ab	0.66	0.75	0.50	0.51	0.60	0.75	0.64	0.72	0.69	0.62	0.71
Or	0.00	0.01	0.00	0.02	0.00	0.00	0.00	0.00	0.02	0.00	0.04

EPMA analysis of feldspar.

Oxide	Corundum-bearing amphibolite										
	9-1-3_Pl1-1c	9-1-3_Pl1-2c	9-1-3_Pl1-3c	9-1-3_Fel1-1c	9-1-3_Fel1-2c	9-1-3_Fel1-3c	9-1-3_Fel2-1c	9-1-3_Fel2-2c	9-1-3_Fel2-3c	9-1-3_Fel3-1c	9-1-3_Fel3-2c
SiO2	40.52	40.50	40.63	40.77	40.61	40.73	40.71	41.00	40.58	40.65	40.82
TiO2	0.00	0.00	0.01	0.02	0.00	0.01	0.00	0.00	0.00	0.05	0.00
Al2O3	38.10	38.01	37.98	37.71	37.99	37.88	37.67	37.44	37.77	37.28	37.47
FeO *	0.05	0.18	0.05	0.09	0.07	0.07	0.03	0.04	0.07	0.08	0.07
MnO	0.00	0.00	0.01	0.03	0.00	0.00	0.00	0.00	0.01	0.01	0.01
MgO	0.00	0.00	0.00	0.00	0.00	0.00	0.00	0.00	0.00	0.01	0.00
CaO	21.03	21.09	21.14	21.10	21.11	21.19	21.13	21.25	21.30	21.68	21.42
Na2O	0.07	0.07	0.08	0.05	0.06	0.04	0.10	0.10	0.12	0.06	0.04
K2O	0.00	0.00	0.00	0.00	0.00	0.00	0.00	0.00	0.00	0.00	0.00
P2O5	0.02	0.02	0.00	0.01	0.01	0.02	0.00	0.00	0.00	0.00	0.01
Total	99.99	100.00	99.99	99.99	99.99	100.00	99.99	99.99	99.99	99.99	100.00
Formula 8(O)											
Si	1.893	1.893	1.898	1.906	1.897	1.901	1.905	1.915	1.897	1.904	1.909
Ti	0.000	0.000	0.000	0.001	0.000	0.000	0.000	0.000	0.000	0.002	0.000
Al	2.098	2.094	2.092	2.078	2.092	2.085	2.077	2.062	2.082	2.059	2.065
Fe	0.002	0.007	0.002	0.004	0.003	0.003	0.001	0.001	0.003	0.003	0.003
Mn	0.000	0.000	0.001	0.001	0.000	0.000	0.000	0.000	0.000	0.000	0.001
Mg	0.000	0.000	0.000	0.000	0.000	0.000	0.000	0.000	0.000	0.000	0.000
Ca	1.052	1.056	1.058	1.057	1.057	1.060	1.059	1.064	1.067	1.088	1.073
Na	0.006	0.006	0.007	0.005	0.005	0.004	0.009	0.009	0.011	0.006	0.004
K	0.000	0.000	0.000	0.000	0.000	0.000	0.000	0.000	0.000	0.000	0.000
P	0.001	0.001	0.000	0.000	0.000	0.001	0.000	0.000	0.000	0.000	0.000
Total (S)	5.057	5.060	5.060	5.056	5.058	5.056	5.059	5.056	5.065	5.066	5.058
Atomic%											
An	99.40	99.41	99.31	99.54	99.49	99.64	99.17	99.16	98.97	99.49	99.63
Ab	0.59	0.59	0.69	0.46	0.51	0.36	0.83	0.84	1.03	0.51	0.37
Or	0.01	0.00	0.01	0.00	0.00	0.00	0.00	0.00	0.00	0.01	0.00

EPMA analysis of feldspar.

Oxide	Corundum-bearing amphibolite								
	9-1-4_Pl1-1c	9-1-4_Pl1-2c	9-1-4_Pl1-3c	9-1-4_Pl2-1c	9-1-4_PL6-1c	9-1-4_PL6-2c	9-1-4_Spl6-1c	9-1-4_Spl6-2c	9-1-4_Spl6-3c
SiO2	41.15	44.43	40.76	38.26	43.73	38.37	44.83	43.81	45.20
TiO2	0.00	0.00	0.00	0.00	0.00	0.01	0.05	0.00	0.00
Al2O3	40.64	40.38	40.74	49.56	37.61	41.56	39.00	37.32	38.64
FeO *	0.20	0.13	0.04	0.06	0.05	0.37	0.09	0.10	0.32
MnO	0.00	0.01	0.04	0.00	0.00	0.00	0.02	0.01	0.02
MgO	0.14	0.17	0.01	0.14	0.00	0.28	0.05	0.00	0.30
CaO	16.76	14.50	18.11	11.09	18.28	18.84	15.65	18.47	14.96
Na2O	0.19	0.18	0.15	0.29	0.18	0.20	0.19	0.14	0.27
K2O	0.12	0.00	0.00	0.00	0.00	0.02	0.00	0.00	0.06
P2O5	0.01	0.02	0.00	0.00	0.02	0.07	0.01	0.00	0.07
Total	99.96	99.97	99.97	99.69	99.98	99.93	99.98	99.99	99.99
Formula 8(O)									
Si	1.900	2.014	1.882	1.732	2.012	1.788	2.039	2.017	2.054
Ti	0.000	0.000	0.000	0.000	0.000	0.000	0.002	0.000	0.000
Al	2.213	2.158	2.218	2.644	2.040	2.283	2.091	2.026	2.070
Fe	0.008	0.005	0.002	0.002	0.002	0.015	0.003	0.004	0.012
Mn	0.000	0.000	0.001	0.000	0.000	0.000	0.001	0.000	0.001
Mg	0.010	0.011	0.000	0.009	0.000	0.019	0.003	0.000	0.021
Ca	0.829	0.704	0.896	0.538	0.901	0.941	0.763	0.911	0.729
Na	0.017	0.016	0.014	0.025	0.016	0.018	0.017	0.013	0.024
K	0.007	0.000	0.000	0.000	0.000	0.001	0.000	0.000	0.003
P	0.000	0.001	0.000	0.000	0.001	0.003	0.000	0.000	0.003
Total (S)	4.995	4.912	5.015	4.955	4.974	5.073	4.921	4.975	4.918
Atomic%									
An	97.16	97.82	98.47	95.54	98.27	97.96	97.81	98.59	96.41
Ab	2.03	2.18	1.52	4.46	1.72	1.91	2.19	1.38	3.16
Or	0.81	0.00	0.02	0.00	0.01	0.13	0.00	0.03	0.43

EPMA analysis of spinel.

	Corundum-bearing amphibolite								
Oxide	9-1-4_6-Spl1-1	9-1-4_6-Spl1-2	9-1-4_6-Spl1-3	9-1-4_3-Spl1-1	9-1-4_3-Spl1-2	9-1-4_3-Spl1-3	9-1-4_2-Spl1-1	9-1-4_2-Spl1-2	9-1-4_2-Spl1-3
SiO2	0.00	0.00	0.00	0.00	0.00	0.07	0.00	0.00	0.00
TiO2	0.04	0.02	0.05	0.02	0.01	0.04	0.00	0.03	0.00
Al2O3	63.18	63.93	63.92	65.89	65.22	64.46	67.09	67.63	66.38
Cr2O3	0.04	0.07	0.04	0.01	0.01	0.00	0.06	0.06	0.07
FeO *	14.69	13.73	14.41	12.01	12.25	12.09	12.58	12.72	12.21
MnO	0.18	0.18	0.14	0.02	0.01	0.02	0.17	0.16	0.16
MgO	21.05	20.86	20.78	20.15	20.03	21.32	19.79	19.79	19.49
CaO	0.00	0.01	0.00	0.00	0.00	0.02	0.00	0.00	0.01
Na2O	0.04	0.06	0.04	0.02	0.03	0.02	0.05	0.06	0.03
K2O	0.00	0.00	0.00	0.02	0.00	0.80	0.02	0.01	0.00
P2O5	0.00	0.02	0.00	0.00	0.00	0.03	0.00	0.00	0.01
Total	99.35	99.02	99.54	98.30	97.67	99.04	99.95	100.53	98.57
Formula 4(O)									
Si	0.000	0.000	0.000	0.000	0.000	0.002	0.000	0.000	0.000
Ti	0.001	0.000	0.001	0.000	0.000	0.001	0.000	0.001	0.000
Al	1.913	1.931	1.926	1.982	1.977	1.939	1.989	1.992	1.993
Cr	0.001	0.001	0.001	0.000	0.000	0.000	0.001	0.001	0.001
Fe3+	0.113	0.087	0.093	0.021	0.030	0.104	0.014	0.010	0.008
Fe2+	0.202	0.208	0.215	0.235	0.233	0.153	0.251	0.256	0.253
Mn	0.004	0.004	0.003	0.000	0.000	0.000	0.004	0.003	0.003
Mg	0.806	0.797	0.792	0.766	0.768	0.810	0.742	0.737	0.740
Ca	0.000	0.000	0.000	0.000	0.000	0.000	0.000	0.000	0.000
Na	0.002	0.003	0.002	0.001	0.001	0.001	0.002	0.003	0.001
K	0.000	0.000	0.000	0.001	0.000	0.026	0.001	0.000	0.000
P	0.000	0.000	0.000	0.000	0.000	0.001	0.000	0.000	0.000
Total (S)	3.043	3.033	3.035	3.008	3.011	3.040	3.005	3.004	3.003
Atomic%									
Spinel	72.674	71.895	71.036	68.492	68.698	77.884	66.371	65.742	66.128
Hercynite	18.217	18.736	19.309	21.005	20.868	14.744	22.419	22.838	22.581
Magnetite	9.109	9.368	9.655	10.503	10.434	7.372	11.210	11.419	11.291

EPMA analysis of spinel.

Oxide	Corundum-bearing amphibolite					Corundum-barren amphibolite				
	9-1-4_6-Spl1-1	9-1-4_6-Spl1-2	9-1-4_6-Spl1-3	9-1-4_3-Spl1-3	9-1-4_2-Spl1-1	8-9-1_3-Spl1-1	8-9-1_3-Spl1-2	8-9-1_Spl1-1	8-9-1_Spl1-2	8-9-1_Spl1-3
SiO_2	0.00	0.00	0.00	0.07	0.00	0.00	0.00	0.02	0.00	0.00
TiO_2	0.04	0.02	0.05	0.04	0.00	0.02	0.01	0.00	0.01	0.01
Al_2O_3	63.18	63.93	63.92	64.46	67.09	65.89	65.22	56.97	56.31	56.74
Cr_2O_3	0.04	0.07	0.04	0.00	0.06	0.01	0.01	0.31	0.21	0.20
FeO *	14.69	13.73	14.41	12.09	12.58	12.01	12.25	25.74	25.78	25.60
MnO	0.18	0.18	0.14	0.02	0.17	0.02	0.01	0.50	0.52	0.51
MgO	21.05	20.86	20.78	21.32	19.79	20.15	20.03	10.79	10.83	10.60
CaO	0.00	0.01	0.00	0.02	0.00	0.00	0.00	0.00	0.00	0.00
Na_2O	0.04	0.06	0.04	0.02	0.05	0.02	0.03	0.27	0.28	0.27
K_2O	0.00	0.00	0.00	0.80	0.02	0.02	0.00	0.01	0.00	0.00
P_2O_5	0.00	0.02	0.00	0.03	0.00	0.00	0.00	0.00	0.01	0.02
Total	99.35	99.02	99.54	99.04	99.95	98.30	97.67	94.73	94.12	94.24
Formula 4(O)										
Si	0.000	0.000	0.000	0.002	0.000	0.000	0.000	0.001	0.000	0.000
Ti	0.001	0.000	0.001	0.001	0.000	0.000	0.000	0.000	0.000	0.000
Al	1.913	1.931	1.926	1.939	1.989	1.982	1.977	1.925	1.918	1.928
Cr	0.001	0.001	0.001	0.000	0.001	0.000	0.000	0.007	0.005	0.005
Fe3+	0.113	0.087	0.093	0.104	0.014	0.021	0.030	0.106	0.119	0.103
Fe2+	0.202	0.208	0.215	0.153	0.251	0.235	0.233	0.511	0.504	0.514
Mn	0.004	0.004	0.003	0.000	0.004	0.000	0.000	0.012	0.013	0.013
Mg	0.806	0.797	0.792	0.810	0.742	0.766	0.768	0.461	0.467	0.455
Ca	0.000	0.000	0.000	0.000	0.000	0.000	0.000	0.000	0.000	0.000
Na	0.002	0.003	0.002	0.001	0.002	0.001	0.001	0.015	0.016	0.015
K	0.000	0.000	0.000	0.026	0.001	0.001	0.000	0.000	0.000	0.000
P	0.000	0.000	0.000	0.001	0.000	0.000	0.000	0.000	0.000	0.000
Total (S)	3.043	3.033	3.035	3.040	3.005	3.008	3.011	3.040	3.045	3.039
Atomic%										
Spinel	72.67	71.90	71.04	77.88	66.37	68.49	68.70	37.56	38.16	37.12
Hercynite	18.22	18.74	19.31	14.74	22.42	21.01	20.87	41.63	41.23	41.92
Magnetite	9.11	9.37	9.65	7.37	11.21	10.50	10.43	20.81	20.61	20.96

EPMA analysis of garnet.

	Gneiss										
Oxide	5-2-3_Grt1-1	5-2-3_Grt1-2	5-2-3_Grt1-3	5-2-3_Grt2-1	5-2-3_Grt2-2	5-2-3_Grt2-3	5-2-3_Grt2-4	5-2-3_Grt2-5	5-2-3_Grt2-6	5-2-3_Grt2-7	5-2-3_Grt2-8
SiO2	41.17	40.98	41.25	44.54	44.74	44.79	43.05	44.19	44.06	44.52	44.90
TiO2	0.04	0.09	0.01	0.00	0.00	0.01	0.01	0.00	0.04	0.00	0.00
Al2O3	26.89	26.52	26.97	25.04	25.15	25.02	25.75	25.92	25.97	25.03	25.07
Cr2O3	0.00	0.00	0.00	0.01	0.00	0.00	0.00	0.00	0.00	0.00	0.00
FeO *	13.30	13.28	13.25	12.34	11.50	11.89	11.71	11.27	11.91	11.80	11.84
MnO	0.76	0.72	0.76	1.04	1.16	1.07	1.01	0.90	0.96	0.88	0.97
MgO	12.89	12.85	12.91	13.18	13.15	13.04	13.04	12.99	12.95	12.23	12.14
CaO	3.87	3.74	3.91	4.75	4.80	4.70	4.21	4.02	4.13	3.26	4.01
Na2O	0.00	0.00	0.01	0.00	0.02	0.00	0.03	0.00	0.02	0.00	0.00
K2O	0.00	0.00	0.00	0.00	0.02	0.01	0.01	0.02	0.00	0.00	0.01
P2O5	0.01	0.00	0.03	0.00	0.00	0.00	0.01	0.00	0.01	0.01	0.01
Total	99.06	98.26	99.22	101.07	100.54	100.71	98.93	99.35	100.19	97.79	99.17
Formula 12(O)											
Si	2.991	3.000	2.991	3.154	3.171	3.174	3.105	3.154	3.134	3.224	3.219
Ti	0.002	0.005	0.000	0.000	0.000	0.001	0.000	0.000	0.002	0.000	0.000
Al	2.303	2.289	2.305	2.091	2.102	2.091	2.189	2.181	2.177	2.137	2.119
Cr	0.000	0.000	0.000	0.000	0.000	0.000	0.000	0.000	0.000	0.000	0.000
Fe3+	0.000	0.000	0.000	0.000	0.000	0.000	0.000	0.000	0.000	0.000	0.000
Fe2+	0.808	0.813	0.803	0.731	0.682	0.705	0.706	0.673	0.708	0.714	0.710
Mn	0.047	0.044	0.047	0.062	0.070	0.064	0.062	0.054	0.058	0.054	0.059
Mg	1.396	1.402	1.395	1.391	1.389	1.378	1.402	1.382	1.372	1.319	1.297
Ca	0.301	0.294	0.304	0.360	0.364	0.357	0.325	0.308	0.315	0.253	0.308
Na	0.000	0.000	0.001	0.000	0.002	0.000	0.005	0.000	0.002	0.000	0.000
K	0.000	0.000	0.000	0.000	0.002	0.000	0.001	0.002	0.000	0.000	0.001
P	0.000	0.000	0.002	0.000	0.000	0.000	0.000	0.000	0.000	0.001	0.001
Total (S)	7.851	7.849	7.852	7.796	7.780	7.775	7.801	7.755	7.774	7.706	7.719
Atomic%											
Pyrope	55.731	55.884	55.751	56.043	57.039	56.474	57.612	58.489	57.287	57.693	56.031
Almandine	32.257	32.410	32.100	29.450	28.003	28.890	29.029	28.491	29.575	31.237	30.650
Grossular	12.012	11.707	12.149	14.506	14.958	14.636	13.359	13.020	13.138	11.070	13.319

EPMA analysis of garnet.

	Gneiss			Corundum-barren amphibolite			Corundum-bearing amphibolite		
Oxide	5-2-3_Grt1-1b	5-2-3_Grt1-2b	5-2-3_Grt1-3b	8-9-1_Am3-1b	8-9-1_Am3-2b	8-9-1_Am3-3b	9-1-3_inPl4-1c	9-1-3_inPl4-2c	9-1-3_inPl4-3c
SiO2	39.58	39.70	39.32	38.15	37.76	37.76	37.83	37.67	38.14
TiO2	0.01	0.05	0.00	0.06	0.05	0.03	0.02	0.12	0.07
Al2O3	22.06	22.10	22.97	36.61	36.04	36.24	29.09	29.14	28.82
Cr2O3	0.02	0.00	0.02	0.14	0.15	0.23	0.06	0.05	0.10
FeO *	12.49	12.56	12.86	2.14	2.06	1.99	6.83	6.78	6.65
MnO	1.75	1.66	1.37	0.02	0.04	0.01	0.10	0.04	0.04
MgO	17.75	17.69	17.74	0.10	0.10	0.08	0.23	0.23	0.27
CaO	5.57	5.13	4.38	23.99	23.85	23.71	25.52	25.72	25.55
Na2O	0.01	0.01	0.02	0.00	0.00	0.02	0.01	0.00	0.00
K2O	0.01	0.00	0.00	0.00	0.00	0.00	0.00	0.01	0.00
P2O5	0.01	0.01	0.01	0.06	0.06	0.08	0.04	0.04	0.05
Total	99.28	98.99	98.70	101.33	100.25	100.39	99.98	99.97	99.96
Formula 12(O)									
Si	2.921	2.934	2.906	2.707	2.710	2.706	2.819	2.808	2.841
Ti	0.000	0.003	0.000	0.003	0.003	0.002	0.001	0.007	0.004
Al	1.919	1.925	2.001	3.062	3.049	3.063	2.556	2.561	2.531
Cr	0.001	0.000	0.001	0.008	0.008	0.013	0.003	0.003	0.006
Fe3+	0.351	0.296	0.275	0.000	0.000	0.000	0.000	0.000	0.000
Fe2+	0.420	0.480	0.520	0.127	0.124	0.119	0.426	0.423	0.414
Mn	0.109	0.104	0.086	0.001	0.002	0.000	0.006	0.003	0.003
Mg	1.953	1.948	1.954	0.011	0.010	0.008	0.026	0.025	0.030
Ca	0.441	0.406	0.347	1.824	1.834	1.821	2.038	2.054	2.039
Na	0.002	0.001	0.002	0.000	0.001	0.003	0.002	0.000	0.000
K	0.001	0.000	0.000	0.000	0.000	0.000	0.000	0.001	0.000
P	0.000	0.001	0.001	0.004	0.004	0.005	0.002	0.002	0.003
Total (S)	8.119	8.100	8.093	7.748	7.750	7.746	7.891	7.897	7.879
Atomic%									
Pyrope	69.418	68.752	69.272	0.555	0.516	0.422	1.044	1.008	1.203
Almandine	14.917	16.924	18.423	6.462	6.285	6.114	17.106	16.893	16.681
Grossular	15.665	14.323	12.305	92.982	93.198	93.464	81.850	82.099	82.116

EPMA analysis of corundum.

	Corundum-bearing amphibolite										
Oxide	9-1-4_4-Cor1-1	9-1-4_4-Cor1-2	9-1-4_4-rCor1-1	9-1-4_4-rCor1-2	9-1-4_4-rCor1-3	9-1-4_5-Spl1-1	9-1-4_6-Cor1-1	9-1-4_6-Cor1-2	9-1-4_6-Cor1-3	9-1-4_3-Cor1-1	9-1-4_3-Cor1-2
SiO2	0.00	0.04	0.39	0.31	0.83	0.69	0.01	0.00	0.22	0.00	0.00
TiO2	0.01	0.01	0.00	0.07	0.01	0.00	0.01	0.02	0.01	0.00	0.03
Al2O3	98.67	98.66	99.37	99.71	99.54	97.21	100.29	99.24	98.93	98.68	98.83
Cr2O3	0.00	0.01	0.00	0.00	0.02	0.00	0.00	0.05	0.07	0.04	0.06
FeO *	0.00	0.00	0.17	0.00	0.37	0.00	0.07	0.13	0.19	0.11	0.07
MnO	0.00	0.01	0.00	0.05	0.00	0.00	0.03	0.00	0.00	0.00	0.00
MgO	0.00	0.02	0.90	0.25	0.11	0.00	0.00	0.00	0.00	0.00	0.01
CaO	0.01	0.01	0.01	0.54	0.01	0.00	0.01	0.01	0.00	0.00	0.02
Na2O	0.00	0.03	0.00	0.04	0.00	0.00	0.00	0.01	0.00	0.03	0.00
K2O	0.00	0.00	0.01	0.01	0.02	0.00	0.01	0.00	0.00	0.00	0.01
V2O3	0.01	0.00	0.01	0.00	0.01	0.01	0.00	0.01	0.00	0.00	0.02
ZrO2	0.00	0.01	0.07	0.01	0.02	0.00	0.00	0.00	0.02	0.02	0.02
P2O5	0.01	0.00	0.00	0.01	0.03	0.03	0.02	0.00	0.00	0.01	0.00
HfO2	0.01	0.00	0.01	0.00	0.01	0.01	0.00	0.02	0.00	0.00	0.03
Ga2O3	0.00	0.02	0.00	0.00	0.00	0.00	0.04	0.00	0.00	0.00	0.01
NiO	0.01	0.00	0.01	0.00	0.00	0.00	0.00	0.00	0.01	0.00	0.02
Total	98.77	98.82	100.95	101.09	101.03	98.07	100.49	99.49	99.45	98.90	99.11
Formula 3(O)											
Si	0.000	0.001	0.007	0.005	0.014	0.012	0.000	0.000	0.004	0.000	0.000
Ti	0.000	0.000	0.000	0.001	0.000	0.000	0.000	0.000	0.000	0.000	0.000
Al	1.999	1.998	1.973	1.980	1.974	1.983	1.998	1.997	1.992	1.998	1.997
Cr	0.000	0.000	0.000	0.000	0.000	0.000	0.000	0.001	0.001	0.000	0.001
Fe	0.000	0.000	0.002	0.000	0.005	0.000	0.001	0.002	0.003	0.002	0.001
Mn	0.000	0.000	0.000	0.001	0.000	0.000	0.000	0.000	0.000	0.000	0.000
Mg	0.000	0.000	0.023	0.006	0.003	0.000	0.000	0.000	0.000	0.000	0.000
Ca	0.000	0.000	0.000	0.010	0.000	0.000	0.000	0.000	0.000	0.000	0.000
Na	0.000	0.001	0.000	0.001	0.000	0.000	0.000	0.000	0.000	0.001	0.000
K	0.000	0.000	0.000	0.000	0.000	0.000	0.000	0.000	0.000	0.000	0.000
V	0.000	0.000	0.000	0.000	0.000	0.000	0.000	0.000	0.000	0.000	0.000
Zr	0.000	0.000	0.001	0.000	0.000	0.000	0.000	0.000	0.000	0.000	0.000
P	0.000	0.000	0.000	0.000	0.000	0.000	0.000	0.000	0.000	0.000	0.000
Hf	0.000	0.000	0.000	0.000	0.000	0.000	0.000	0.000	0.000	0.000	0.000
Ga	0.000	0.000	0.000	0.000	0.000	0.000	0.000	0.000	0.000	0.000	0.000
Ni	0.000	0.000	0.000	0.000	0.000	0.000	0.000	0.000	0.000	0.000	0.000
Total(S)	2.000	2.001	2.006	2.005	1.998	1.996	2.000	2.001	2.000	2.001	2.001

EPMA analysis of corundum.

Oxide	Corundum-bearing amphibolite										
	8-8-1-14_Cor1-1	8-8-1-14_Cor1-2	8-8-1-14_Cor1-3	8-8-1-15_Cor1-1	8-8-1-15_Cor1-2	8-8-1-15_Cor1-3	8-8-1-16_Cor1-1	8-8-1-16_Cor1-3	8-8-1-16_Cor2-2	8-8-1-16_Cor2-3	8-8-1-1_Cor1-1
SiO2	0.00	0.00	0.00	0.00	0.01	0.00	0.01	0.00	0.00	0.00	0.00
TiO2	0.00	0.02	0.02	0.00	0.00	0.03	0.02	0.02	0.00	0.00	0.01
Al2O3	100.05	99.88	99.34	100.47	100.25	98.10	98.70	98.10	98.35	99.72	98.64
Cr2O3	0.17	0.16	0.17	0.05	0.11	0.07	0.02	0.06	0.03	0.00	0.22
FeO *	0.75	0.73	0.53	0.52	0.56	0.67	0.45	0.46	0.48	0.93	0.52
MnO	0.00	0.00	0.00	0.00	0.00	0.00	0.00	0.00	0.00	0.00	0.00
MgO	0.00	0.00	0.01	0.00	0.00	0.00	0.00	0.00	0.00	0.00	0.00
CaO	0.00	0.01	0.00	0.01	0.01	0.01	0.00	0.00	0.01	0.00	0.01
Na2O	0.02	0.00	0.00	0.00	0.00	0.00	0.01	0.00	0.00	0.00	0.00
K2O	0.00	0.02	0.00	0.01	0.01	0.01	0.01	0.00	0.00	0.01	0.00
V2O3	0.00	0.00	0.00	0.02	0.00	0.02	0.02	0.01	0.00	0.00	0.02
ZrO2	0.05	0.00	0.07	0.00	0.00	0.00	0.00	0.02	0.05	0.00	0.01
P2O5	0.00	0.00	0.00	0.00	0.01	0.00	0.00	0.00	0.01	0.00	0.02
HfO2	0.04	0.00	0.05	0.00	0.01	0.05	0.00	0.01	0.00	0.00	0.03
Ga2O3	0.00	0.03	0.03	0.00	0.00	0.00	0.09	0.06	0.01	0.13	0.00
NiO	0.00	0.00	0.00	0.00	0.00	0.00	0.00	0.00	0.03	0.01	0.00
Total	101.14	100.92	100.22	101.16	100.96	98.96	99.33	98.73	99.06	100.79	99.49
Formula 3(O)											
Si	0.000	0.000	0.000	0.000	0.000	0.000	0.000	0.000	0.000	0.000	0.000
Ti	0.000	0.000	0.000	0.000	0.000	0.000	0.000	0.000	0.000	0.000	0.000
Al	1.989	1.990	1.991	1.994	1.993	1.991	1.994	1.994	1.993	1.990	1.991
Cr	0.002	0.002	0.002	0.001	0.001	0.001	0.000	0.001	0.000	0.000	0.003
Fe	0.011	0.010	0.008	0.008	0.008	0.010	0.006	0.007	0.007	0.013	0.007
Mn	0.000	0.000	0.000	0.000	0.000	0.000	0.000	0.000	0.000	0.000	0.000
Mg	0.000	0.000	0.000	0.000	0.000	0.000	0.000	0.000	0.000	0.000	0.000
Ca	0.000	0.000	0.000	0.000	0.000	0.000	0.000	0.000	0.000	0.000	0.000
Na	0.001	0.000	0.000	0.000	0.000	0.000	0.000	0.000	0.000	0.000	0.000
K	0.000	0.000	0.000	0.000	0.000	0.000	0.000	0.000	0.000	0.000	0.000
V	0.000	0.000	0.000	0.000	0.000	0.000	0.000	0.000	0.000	0.000	0.000
Zr	0.000	0.000	0.001	0.000	0.000	0.000	0.000	0.000	0.000	0.000	0.000
P	0.000	0.000	0.000	0.000	0.000	0.000	0.000	0.000	0.000	0.000	0.000
Hf	0.000	0.000	0.000	0.000	0.000	0.000	0.000	0.000	0.000	0.000	0.000
Ga	0.000	0.000	0.000	0.000	0.000	0.000	0.001	0.001	0.000	0.001	0.000
Ni	0.000	0.000	0.000	0.000	0.000	0.000	0.000	0.000	0.000	0.000	0.000
Total(S)	2.004	2.004	2.002	2.004	2.003	2.003	2.003	2.002	2.002	2.004	2.002

EPMA analysis of corundum.

	Altered corundum-bearing amphibolite										
Oxide	8-5-16-1_Cor1-1	8-5-16-1_Mi1-2	8-5-16-1_Mi1-3	8-5-15-1_Cor1-1	8-5-15-1_Cor1-2	8-5-15-1_Cor1-3	8-5-15-1_inCor1-1	8-5-15-1_inCor1-2	8-5-15-1_inCor1-3	8-5-14--1_Cor1-1	8-5-14-1_Cor1-2
SiO2	0.00	0.00	0.00	0.00	0.01	0.00	0.02	0.01	0.00	0.01	0.00
TiO2	0.01	0.01	0.01	0.03	0.00	0.00	0.03	0.01	0.00	0.00	0.01
Al2O3	97.73	99.72	99.42	98.55	98.84	99.05	98.65	98.99	98.43	98.06	98.20
Cr2O3	0.68	0.67	0.77	0.19	0.14	0.21	0.20	0.18	0.20	0.54	0.55
FeO *	0.28	0.31	0.35	0.30	0.39	0.27	0.27	0.28	0.36	0.33	0.33
MnO	0.00	0.02	0.00	0.00	0.00	0.02	0.03	0.01	0.00	0.00	0.00
MgO	0.00	0.00	0.01	0.00	0.01	0.00	0.00	0.00	0.00	0.01	0.02
CaO	0.00	0.00	0.00	0.00	0.00	0.01	0.00	0.02	0.00	0.02	0.00
Na2O	0.01	0.00	0.00	0.00	0.01	0.00	0.00	0.00	0.00	0.00	0.01
K2O	0.01	0.01	0.00	0.00	0.00	0.00	0.01	0.00	0.00	0.00	0.00
V2O3	0.01	0.00	0.00	0.00	0.00	0.00	0.00	0.00	0.01	0.02	0.00
ZrO2	0.08	0.00	0.00	0.04	0.02	0.01	0.00	0.00	0.02	0.05	0.00
P2O5	0.00	0.00	0.00	0.00	0.00	0.00	0.00	0.00	0.00	0.02	0.01
HfO2	0.00	0.00	0.00	0.10	0.06	0.00	0.00	0.01	0.00	0.03	0.02
Ga2O3	0.06	0.02	0.03	0.05	0.06	0.00	0.04	0.09	0.00	0.04	0.00
NiO	0.02	0.02	0.00	0.00	0.00	0.02	0.00	0.01	0.03	0.00	0.00
Total	98.88	100.78	100.60	99.25	99.63	99.58	99.25	99.72	99.12	99.16	99.14
Formula 3(O)											
Si	0.000	0.000	0.000	0.000	0.000	0.000	0.000	0.000	0.000	0.000	0.000
Ti	0.000	0.000	0.000	0.000	0.000	0.000	0.000	0.000	0.000	0.000	0.000
Al	1.986	1.987	1.986	1.992	1.992	1.994	1.993	1.993	1.993	1.987	1.989
Cr	0.009	0.009	0.010	0.003	0.002	0.003	0.003	0.002	0.003	0.007	0.007
Fe	0.004	0.004	0.005	0.004	0.006	0.004	0.004	0.004	0.005	0.005	0.005
Mn	0.000	0.000	0.000	0.000	0.000	0.000	0.000	0.000	0.000	0.000	0.000
Mg	0.000	0.000	0.000	0.000	0.000	0.000	0.000	0.000	0.000	0.000	0.000
Ca	0.000	0.000	0.000	0.000	0.000	0.000	0.000	0.000	0.000	0.000	0.000
Na	0.000	0.000	0.000	0.000	0.000	0.000	0.000	0.000	0.000	0.000	0.000
K	0.000	0.000	0.000	0.000	0.000	0.000	0.000	0.000	0.000	0.000	0.000
V	0.000	0.000	0.000	0.000	0.000	0.000	0.000	0.000	0.000	0.000	0.000
Zr	0.001	0.000	0.000	0.000	0.000	0.000	0.000	0.000	0.000	0.000	0.000
P	0.000	0.000	0.000	0.000	0.000	0.000	0.000	0.000	0.000	0.000	0.000
Hf	0.000	0.000	0.000	0.000	0.000	0.000	0.000	0.000	0.000	0.000	0.000
Ga	0.001	0.000	0.000	0.001	0.001	0.000	0.000	0.001	0.000	0.000	0.000
Ni	0.000	0.000	0.000	0.000	0.000	0.000	0.000	0.000	0.000	0.000	0.000
Total(S)	2.001	2.002	2.002	2.001	2.002	2.001	2.001	2.002	2.002	2.001	2.002

EPMA analysis of corundum.

	Altered corundum-bearing amphibolite										
Oxide	8-5-14-1_Cor1-3	8-5-11-1_Cor1-1	8-5-11-1_Cor1-2	8-5-11-1_Cor1-3	8-5-11-2_Un1-1	8-5-11-2_Un1-3	8-5-12-1_Un1-1	8-5-12-1_Un1-2	8-5-12-1_Un1-3	8-5-8-2_Cor1-1	8-5-8-2_Cor1-2
SiO2	0.00	0.00	0.00	0.01	0.00	0.00	0.00	0.02	0.00	0.00	0.00
TiO2	0.01	0.02	0.00	0.00	0.00	0.00	0.00	0.00	0.02	0.01	0.04
Al2O3	97.54	98.36	98.97	98.43	97.55	97.59	98.51	98.88	99.46	98.95	98.42
Cr2O3	0.56	0.59	0.61	0.66	0.61	0.60	0.48	0.52	0.49	0.37	0.38
FeO *	0.37	0.28	0.37	0.26	0.24	0.29	0.32	0.29	0.28	0.31	0.22
MnO	0.01	0.00	0.02	0.00	0.00	0.00	0.02	0.00	0.00	0.00	0.02
MgO	0.00	0.00	0.00	0.02	0.00	0.01	0.01	0.00	0.00	0.00	0.00
CaO	0.00	0.02	0.00	0.01	0.01	0.00	0.00	0.01	0.00	0.00	0.02
Na2O	0.01	0.01	0.00	0.00	0.00	0.00	0.01	0.00	0.00	0.01	0.02
K2O	0.00	0.01	0.00	0.00	0.00	0.00	0.00	0.00	0.00	0.00	0.00
V2O3	0.03	0.00	0.00	0.00	0.00	0.02	0.00	0.02	0.01	0.00	0.00
ZrO2	0.02	0.02	0.00	0.00	0.02	0.02	0.06	0.00	0.03	0.00	0.00
P2O5	0.00	0.00	0.00	0.00	0.02	0.01	0.01	0.01	0.00	0.01	0.01
HfO2	0.00	0.00	0.00	0.00	0.00	0.00	0.00	0.00	0.00	0.02	0.00
Ga2O3	0.07	0.00	0.05	0.00	0.00	0.00	0.00	0.04	0.09	0.04	0.00
NiO	0.02	0.03	0.00	0.00	0.00	0.02	0.00	0.01	0.02	0.00	0.01
Total	98.75	99.33	100.03	99.40	98.55	98.58	99.41	99.80	100.39	99.72	99.13
Formula 3(O)											
Si	0.000	0.000	0.000	0.000	0.000	0.000	0.000	0.000	0.000	0.000	0.000
Ti	0.000	0.000	0.000	0.000	0.000	0.000	0.000	0.000	0.000	0.000	0.000
Al	1.987	1.988	1.987	1.988	1.988	1.988	1.989	1.989	1.989	1.991	1.991
Cr	0.008	0.008	0.008	0.009	0.008	0.008	0.006	0.007	0.007	0.005	0.005
Fe	0.005	0.004	0.005	0.004	0.003	0.004	0.005	0.004	0.004	0.004	0.003
Mn	0.000	0.000	0.000	0.000	0.000	0.000	0.000	0.000	0.000	0.000	0.000
Mg	0.000	0.000	0.000	0.000	0.000	0.000	0.000	0.000	0.000	0.000	0.000
Ca	0.000	0.000	0.000	0.000	0.000	0.000	0.000	0.000	0.000	0.000	0.000
Na	0.000	0.000	0.000	0.000	0.000	0.000	0.000	0.000	0.000	0.000	0.001
K	0.000	0.000	0.000	0.000	0.000	0.000	0.000	0.000	0.000	0.000	0.000
V	0.000	0.000	0.000	0.000	0.000	0.000	0.000	0.000	0.000	0.000	0.000
Zr	0.000	0.000	0.000	0.000	0.000	0.000	0.000	0.000	0.000	0.000	0.000
P	0.000	0.000	0.000	0.000	0.000	0.000	0.000	0.000	0.000	0.000	0.000
Hf	0.000	0.000	0.000	0.000	0.000	0.000	0.000	0.000	0.000	0.000	0.000
Ga	0.001	0.000	0.001	0.000	0.000	0.000	0.000	0.000	0.001	0.000	0.000
Ni	0.000	0.000	0.000	0.000	0.000	0.000	0.000	0.000	0.000	0.000	0.000
Total(S)	2.002	2.002	2.002	2.001	2.001	2.002	2.002	2.001	2.001	2.001	2.001

BIOGRAPHY

Mr. Alongkot Fanka was born in Nan, Thailand on 9th March 1986. He completed high school from Sa School, Nan in 2004. After finished the high school, he was studying at Department of Geology, Faculty of Science, Chulalongkorn University. He graduated his Bachelor's Degree (B.Sc) in geology in 2008 focused on petrography and geochemistry of igneous rocks. After completed the B.Sc., he got the Scholarship from the Human Resources Development in Science Project (Science Achievement Scholarship of Thailand, SAST) and start his Master's Degree Program in Geology at Chulalongkorn University. His research has been focused on petrochemistry of corundum-bearing rocks of Montepuez Deposits, Mozambique and published in Journal of The Gemmological Association of Hong Kong (ISSN2076-7412) Volume XXXIV in 2013.